Intestinal Epithelial Injury Induced by Cell Death and Altered Stemness During Cirrhosis Progression.

Den Daas, Stijn

Awarding institution:
King's College London

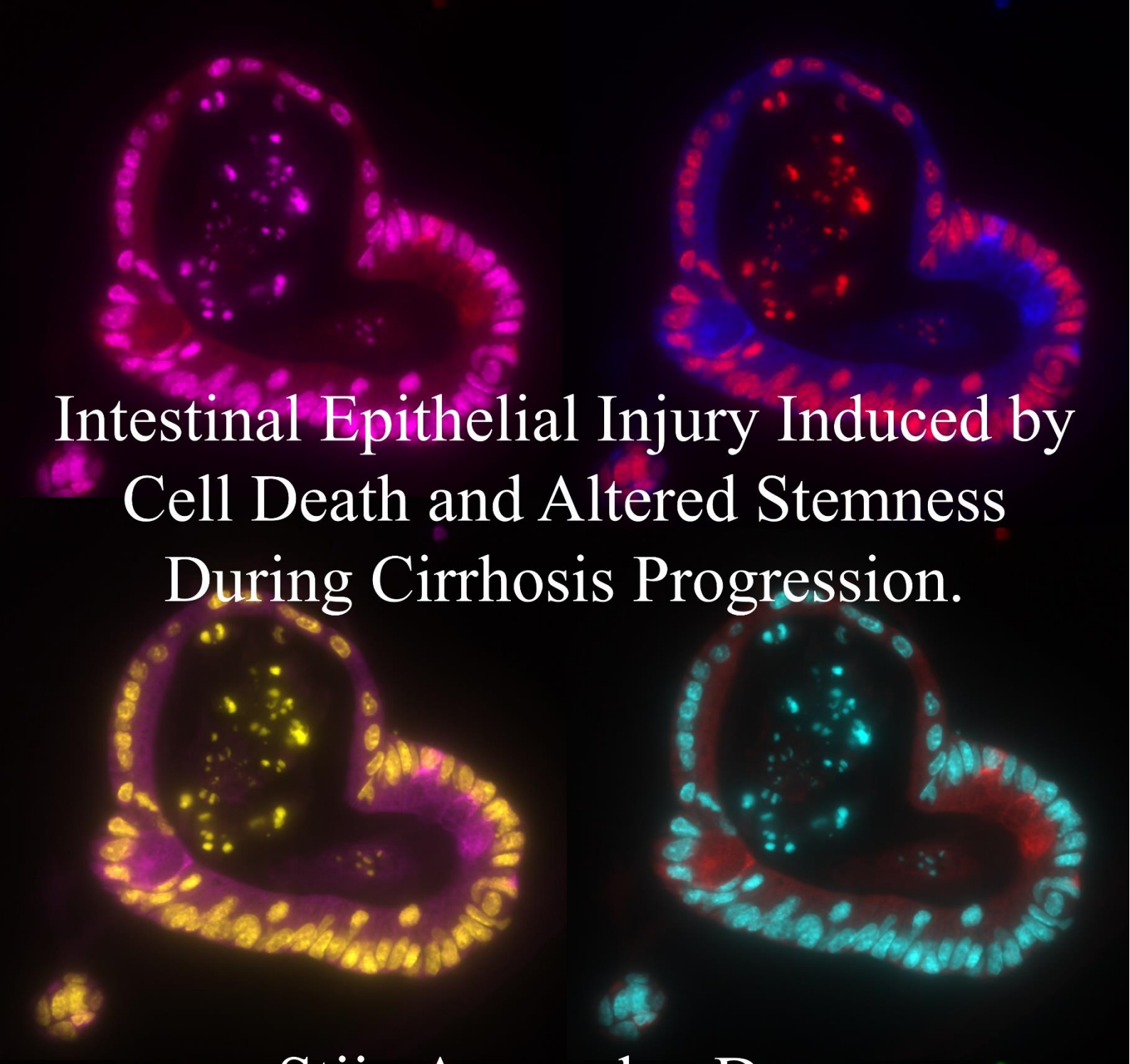

Intestinal Epithelial Injury Induced by Cell Death and Altered Stemness During Cirrhosis Progression.

Stijn Aaron den Daas

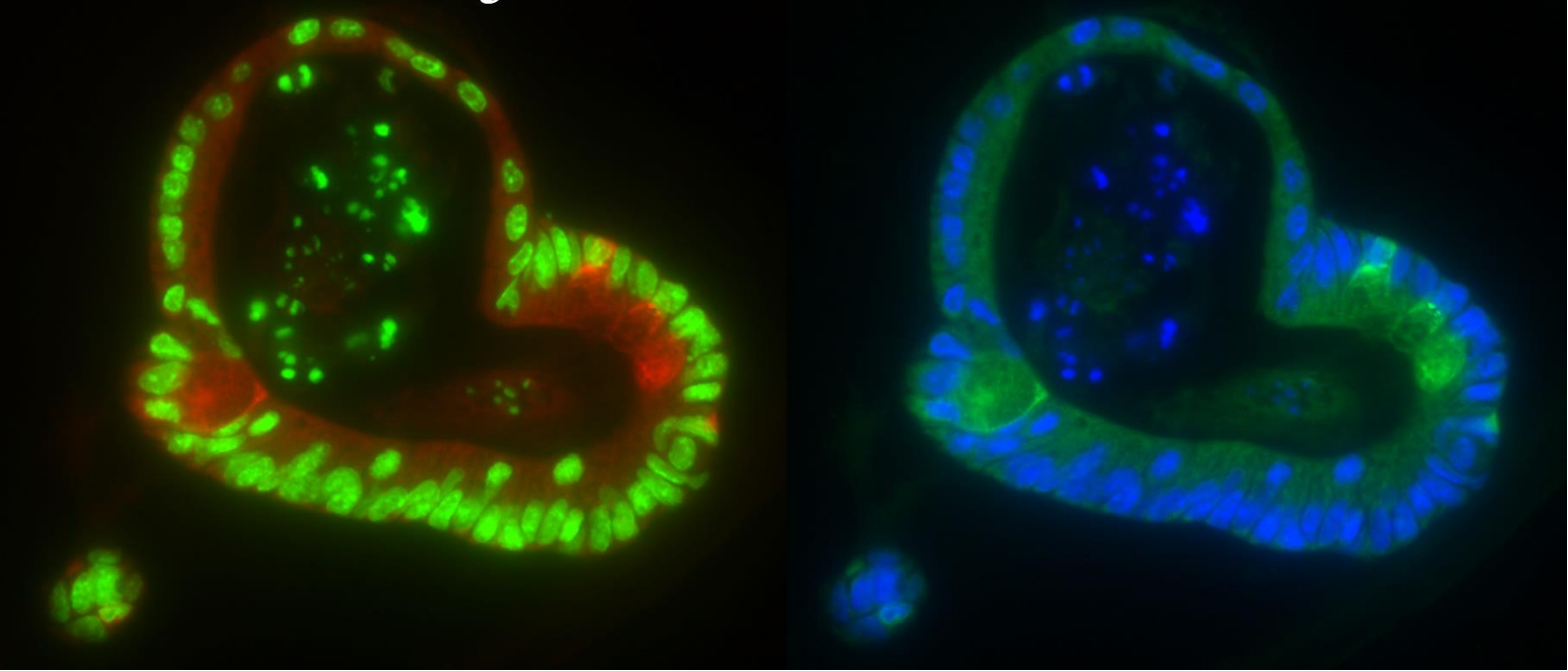

KING'S *College* LONDON

Doctor of Philosophy Thesis for Biomedical Sciences

Intestinal Epithelial Injury Induced by Cell Death and Altered Stemness During Cirrhosis Progression.

By

Stijn Aaron den Daas, M.Sc.

K19079521

06/January/2020 – 03/January/2023

The Foundation for Liver Research
Roger Williams Institute of Hepatology

Contents

Authorship declarations

I, Stijn Aaron den Daas, declare that the work conducted and presented is my own, unless stated otherwise by reference and or acknowledgements. I declare that this thesis is composed by myself and has not been submitted for any other degree.

Acknowledgements

Roger Williams Institute of Hepatology – KCL

Dr. Ugo Soffientini*, Dr. Anna Hadjihambi, Dr. Betsy Arefaine, Dr. Vishal Patel, Prof. Roger Williams, Prof. Shilpa Chokshi*.

Royal Free Hospital – UCL

Mr. Andrew Hall, Dr. Tu Vinh Luong.

Laboratory of Hepatology - KU Leuven

Ms. Lena Smets, Ms. Marie Wallays, Dr. Hannelie Korf, Prof. Schalk van der Merwe.

Institute for Liver and Digestive Health – UCL

Ms. Abeba Habtesion, Ms. Lama Almohamad, Ms. Andrea Krstevski, Ms. Alexandra Phillips, Prof. Rajiv Jalan, Dr. Gautam Mehta*.

Thesis Committee

*Supervisors, Prof. Richard Thompson, Prof. Julian Naglik, Dr. Bu Hayee.

I want to particularly thank all my family members and friends who have helped me during this time with laughter and support. Especially, my parents Mirjam Bunt & Jan den Daas, and brother Jan Hugo den Daas who have always encouraged me to pursue my dreams, even when it led to moving abroad. My grandmother Marianne Bunt-Sciarone†, my aunt Judith Bunt, sister-in-law Marissa Bastemeijer, and other family-members/friends. My long-time friends from Velp & Arnhem Jialun Hao, Max van den Berg, Elena Höppener, Yord Yedema & Sebastiaan Smits; friends I've made during my time in Amsterdam Stijn Emmelot, Marieke van Leeuwen, Winnie Vos, Raymond Pasman, Kim de Wit & Nina Frerichs; in New York Eli Ter Keurst; and in London Anna Hadjihambi, Christos Konstantinou, Ugo Soffientini, Marilena Stamouli, Panos Petridis, Kate Tourna, Gabriella Assante & Merianne Mohamad.

Publications and presentations

EASL, The International Liver Congress 2021.

Abstract: PO-2147 - Intestinal Epithelial Cell Signalling and Cell Death in Cirrhosis and Acute-on-Chronic Liver Failure.

Poster: PO-2147 - Intestinal Epithelial Cell Death in Cirrhosis and Acute-on-Chronic Liver Failure.

BASL, Basic Science Retreat 2021.

Presentation: Intestinal Inflammasome Activation in a Mouse Model of Cirrhosis

CellPress - STAR Protocols:

A permeability assay for mouse intestinal organoids [1].

Abbreviations

ACLF – Acute-on-Chronic Liver Failure

ALD – Alcoholic Liver Disease

ALT – Alanine Aminotransferase

ATF4 – Activating Transcription Factor 4

ATF6 – Activating Transcription Factor 6

Casp - Caspase

CCl4 – Carbon tetrachloride

cDNA – complementary DNA

CHOP – C/EBP Homologous Protein

cK18 – Caspase-cleaved Keratin 18

DAMP – Damage-Associated Molecular Pattern

eIF2alpha – Eukaryotic translation initiation factor 2 subunit 1

EDTA – Ethylenediaminetetraacetic acid

ER – Endoplasmic Reticulum

ERAD – Endoplasmic-Reticulum-Associated protein Degradation

GADD34 – Growth Arrest and DNA Damage Protein 34

GRP78 – Glucose Regulatory Protein 78

GSDMD – Gasdermin-D

H&E – Hematoxyline and Eosine

IBD – Inflammatory Bowel Disease

IL-18 – Interleukine-18

IL-1beta – Interleukine-1beta

IRE1 – Inositol-Requiring Enzyme 1

K18 – Keratin 18

LDH – Lactate Dehydrogenase

LGR5 – Leucine-rich repeat-containing G-protein coupled receptor 5

LPS - Lipopolysaccharides

mRNA – Messenger RNA

NAFLD – Non-Alcoholic Fatty Liver Disease

NASH – Non-Alcoholic Steatohepatitis

NLRP3 – NLR family pyrin domain containing 3

OLFM4 – Olfactomedin 4

PAMP – Pathogen-Associated Molecular Pattern

PBS – Phosphate Buffered Saline

PERK – Protein Kinase R-like ER Kinase

qPCR – quantitative PCR

RNA-Seq – RNA-sequencing

SubCut – Subcutaneous

TRAF2 – TNF Receptor Associated Factor 2

Tunel – Terminal deoxynucleotidyl transferase dUTP nick end labelling

UPR – Unfolded Protein Response

XBP1 – X-Box Binding Protein 1

Figures and Tables

0 Abstract

Persistent liver injury can drive asymptomatic stable cirrhosis to symptomatic acute decompensated cirrhosis (AD) or acute-on-chronic liver failure (ALCF). This progression to decompensated cirrhosis is defined by the development of ascites, gastrointestinal haemorrhage, hepatic encephalopathy, and/or bacterial infections, with acute hepatic and extrahepatic organ failure for ACLF. The progression to decompensated cirrhosis significantly increases the mortality rates, with a 28-day mortality rate of 33.9% for ACLF. Importantly, AD and ACLF remain clinically unmet needs with lack of targetable therapeutic options and there is an urgent need to understand the pathophysiology to identify and develop treatments. The progression from stable cirrhosis to AD and ACLF is multi-facted, complex and the molecular pathways responsible are not fully understood. However, clinically, progression to AD and ACLF is characterised under the umbrella of the PIRO definition, where predisposing factors (Predisposition) can contribute to precipitating events of AD and ACLF (Injury) and elicit a systemic inflammatory host response (Response), leading to multi-organ failure (Organ failure).

Many PIRO factors are associated with increased bacterial translocation from the intestine, due to the impaired intestinal barrier and gut dysbiosis associated with cirrhosis. Translocating bacteria from the intestine can induce hepatic inflammation and concomitant immunoparesis with an increased susceptibility to the bacterial infections, these not only drive progression, but also contribute directly to systemic inflammation that is a hallmark of AD and ACLF. However, the mechanisms that facilitate increased intestinal permeability and consequent bacterial translocation in these patients remains unknown.

The aim of this PhD project was to investigate the mechanisms underpinning intestinal epithelial injury and response that may contribute to increased permeability, bacterial translocation, and progression of cirrhosis. The chapters described herein delineate the role of intestinal endoplasmic reticulum (ER) stress mediated inflammasome activation on epithelial cell death in cirrhosis, report on the development of a permeability assay for mouse intestinal organoids and assess the impact of intestine epithelial stem cell and cell death disruption that promotes intestinal permeability in cirrhosis.

Firstly, I showed no ER stress or inflammasome activation in cirrhosis and no ER stress sensitised pyroptosis via the non-canonical inflammasome pathway in intestine epithelial cells. Secondly, I showed that luminal propidium iodide-stained dead cells in intestinal organoids can be analysed to measure intestinal organoid permeability. And lastly, I showed reduced stemness and increased intestine epithelial cell death in cirrhosis. Taken together this work contributes to our understanding

of the molecular mechanisms of barrier failure and identifies pathways that maybe modulated for better outcomes in patients with liver cirrhosis.

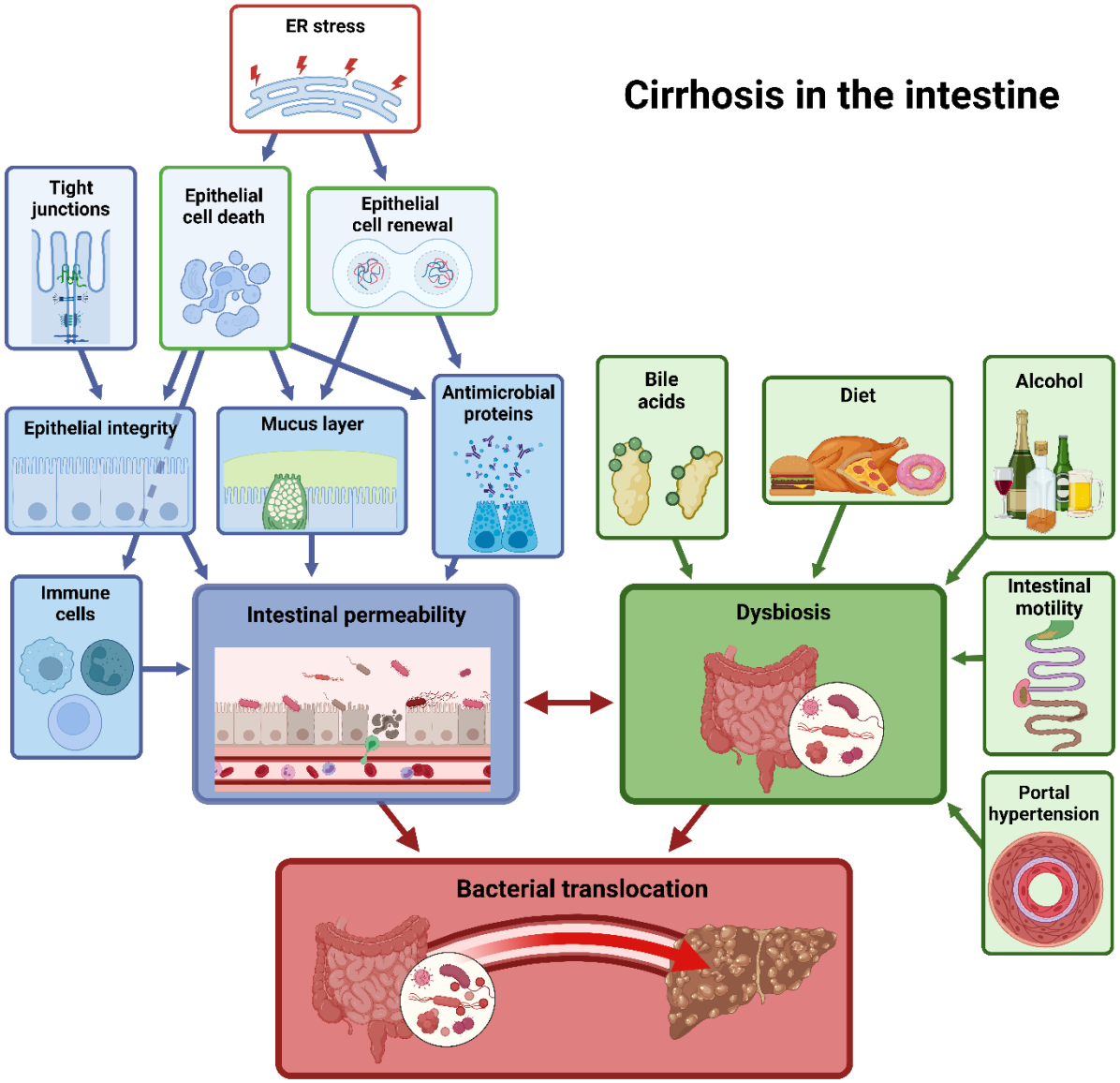

Figure 1: Graphical abstract summarising the themes discussed in the thesis.

Dysbiosis and intestinal permeability influence each other and contribute to bacterial translocation in cirrhosis. Intestinal permeability is regulated by immune cells, epithelial integrity, mucus layer, and antimicrobial proteins. Dysbiosis is affected by bile acids, diet, alcohol, intestinal motility, and portal hypertension.

1 Introduction

1.1 Cirrhosis:

1.1.1 Cirrhosis mortality

Cirrhosis leads to over 1 million deaths annually worldwide making cirrhosis the 11th leading cause of death in the world, causing 2.1% of all global deaths [2][3]. Morbidity and mortality from cirrhosis is thus a major worldwide issue, which will continue to increase in the absence of targeted therapeutics [4][5]. Epidemiologically, cirrhosis mortality rates vary per region, as well as between countries, driven by differences in lifestyle choices, alcohol consumption, the availability and participation of hepatitis A and B vaccines, obesity prevalence, socio-economic status, and access and quality of health care [2][4]. For instance, central Asia has the highest cirrhosis age-standardised death rate, while east Asia had the second lowest (20th globally) [4]. In Europe, eastern Europe has the highest cirrhosis age-standardised death rate (6th globally), and western Europe the lowest (18th globally). In western Europe, most countries decreased their age-standardised mortality rates between 1980 and 2010, such as Italy, France, Germany, and Spain, whereas it increased in Ireland, Finland, and the UK [2]. Cirrhosis leads to premature death, with two-thirds of patients dying before the age of 65 [6]. This is a bigger loss of working life than non-working life compared to most other chronic diseases [6]. In England, years of working life lost (between age 16 and 64) due to liver disease was second only to suicide, but the years of working life lost due to liver disease is increasing while it is decreasing for suicide [7]. Improving treatment options to prevent cirrhosis death and disability has thus potential to greatly reduce years of working life lost to liver disease.

1.1.2 Aetiologies of cirrhosis

Cirrhosis is a progressive liver disease resulting from prolonged liver injury caused by various aetiologies including alcoholic liver disease (ALD), non-alcoholic fatty liver disease (NAFLD), and viral hepatitis - hepatitis B and hepatitis C virus [4]. Alcohol is the biggest cause of liver disease, including cirrhosis, in Europe, which is caused by Europeans having the highest alcohol consumption worldwide [8]. Furthermore, obesity and insulin-resistance are risk factors for NAFLD, which has also been described as a metabolic associated fatty liver disease that is driven by metabolic dysfunction. Worldwide, the number of overweight and obese people are increasing, and in the EU more than 50% of adults are overweight or obese, which is putting them at increased risk for NAFLD [8]. Viral hepatitis is caused by hepatitis A-E virus, with hepatitis B virus and hepatitis C virus being the most prominent [3].

ALD is the most common cause of cirrhosis deaths in Europe (Western Europe 31.4% females, 47.9% males; Central Europe 44.8% females, 43.6% males; Eastern Europe 32.8% females, 40.3% males),

but the proportion varies greatly depending on the world region [4]. The lowest percentage of deaths due to ALD is in North Africa and Middle East, with ALD only accounting for 3.7% in females and 6.3% in males as shown in **Figure 2** [4].

Alcohol can increase the risk of liver disease when combined with other liver disease risk factors, e.g. obesity and viral infection, which increases the risks for liver disease [9]–[12]. Alcohol abuse in patients with hepatitis C virus increased the development fibrosis, cirrhosis, and hepatocellular cancer, which was linked to increased oxidative stress as the synergistic mechanism [9]. Additionally, alcohol consumption of 15 units or more a week synergistically increased liver disease mortality in overweight and obese patients, and alcohol consumption and obesity synergistically increased the development of hepatocellular cancer [10][12]. Obesity prevalence and population body mass index has increased in Europe and is projected to increase further, as well as the alcohol consumption in some European countries [6]. The increase in alcohol consumption and obesity, because of the synergistic affect, is projected to increase liver disease, including cirrhosis, even in European countries with historically low prevalence [6]. Therefore, it is important to study the different causes of cirrhosis development, as the liver injury can have multiple contributing factors.

1.1.3 Fibrosis development

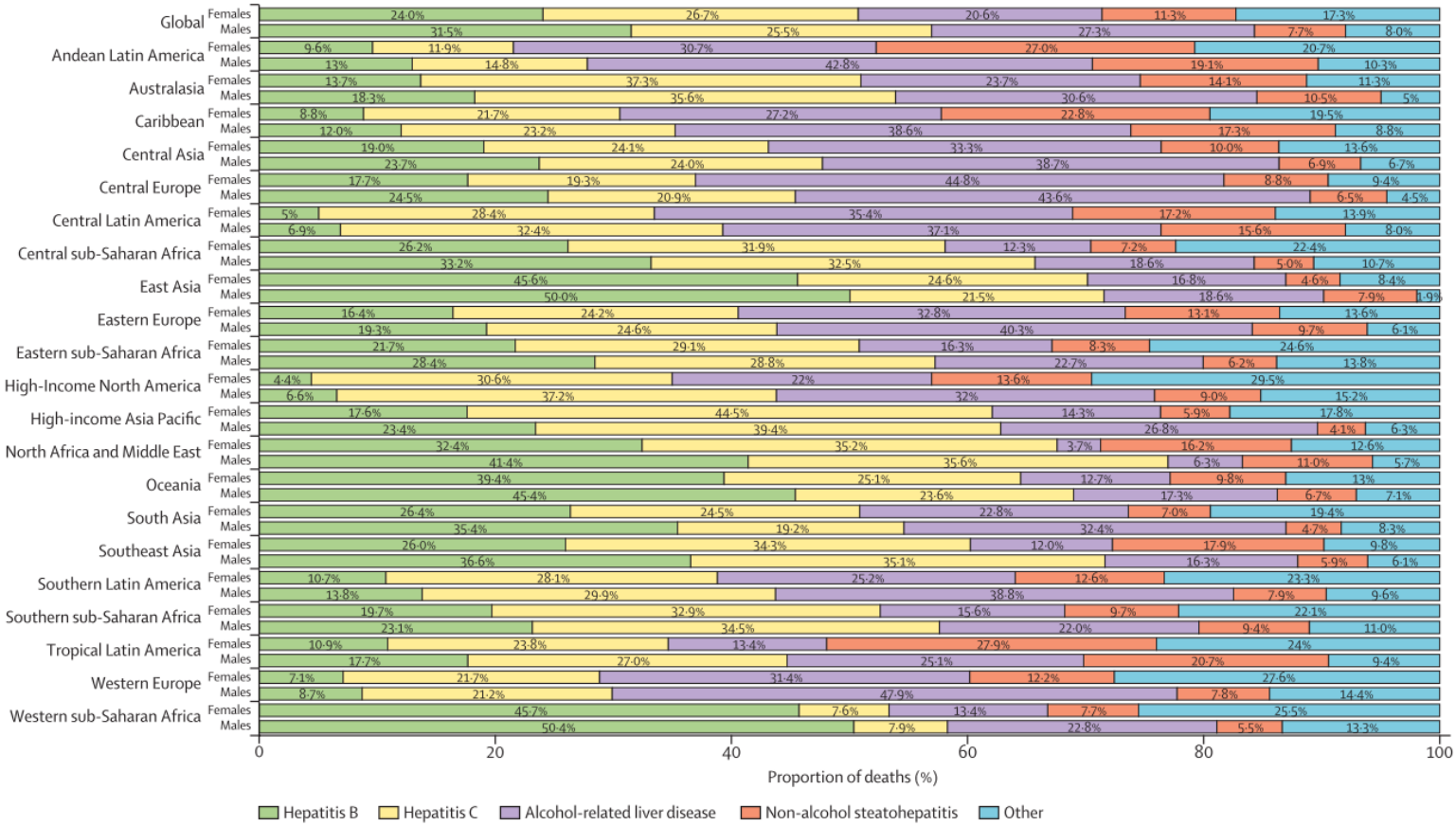

Figure 2: Proportion of deaths due to five causes of cirrhosis at global and regional levels by sex, 2017.
(Sepanlou et al., 2020). Bar graph showing proportion of cirrhosis deaths due to Hepatitis B (green), Hepatitis C (yellow), Alcohol-related liver disease (purple), Non-alcohol steatohepatitis (orange), and other (blue) for males and females per region.

Chronic hepatic injury from conditions such as: ALD, NAFLD, viral hepatitis, and others, can cause fibrosis which is due to the excessive production and accumulation of extracellular matrix (ECM) proteins, e.g. collagen [13]. Hepatoxicity and inflammation (DAMPs and pro-inflammatory cytokines) activate hepatic stellate cells, which migrate to the damaged sites and release ECM proteins [13][14]. This is a wound-healing response to liver injury, but excessive activation and ECM accumulation alters the liver stiffness, which leads to fibrosis and reduced liver function [14]. If the underlying cause of liver injury is removed such with abstinence from alcohol, weight loss, and/or viral suppression for ALD, NAFLD, and/or viral hepatitis respectively, disease progression can be reversed before cirrhosis develops [15]. However, continued chronic liver injury in a fibrotic liver irreversibly causes the progression to cirrhosis, which results in hepatocellular dysfunction and increased intrahepatic resistance that leads to hepatic insufficiency and portal hypertension [14].

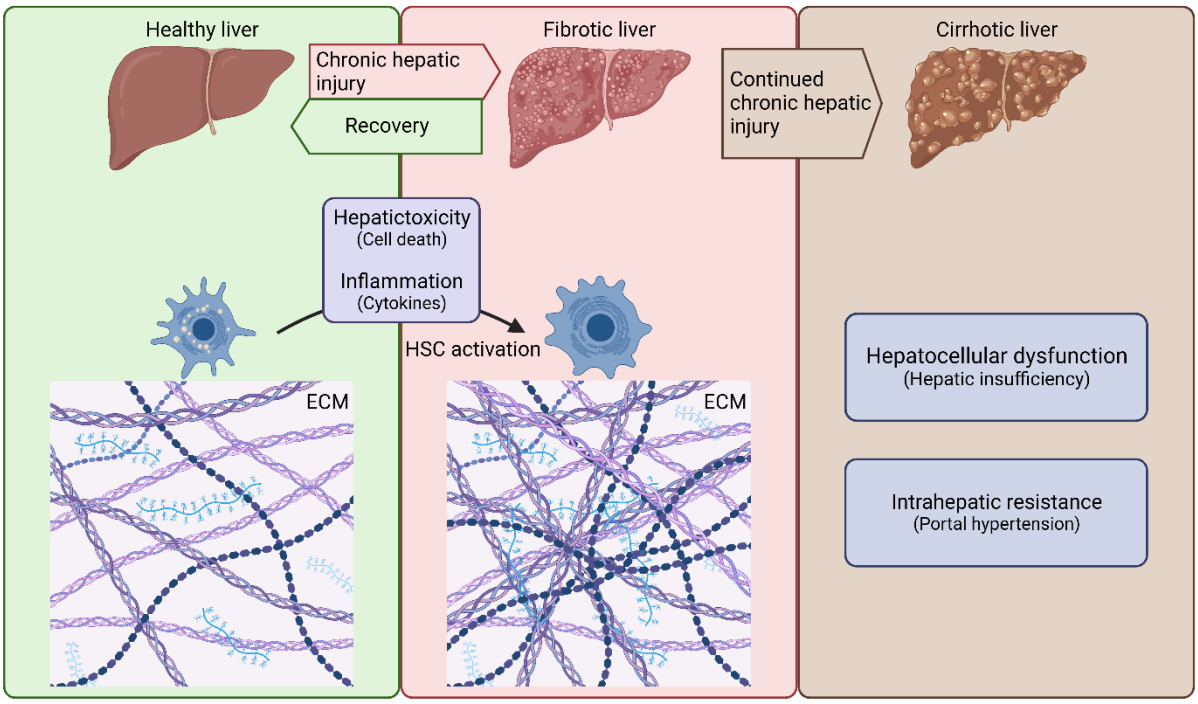

Figure 3: Fibrosis development to cirrhosis. *ECM accumulation by HSC activation during fibrosis development from healthy liver activated by hepatotoxicity and inflammation. Progression to cirrhosis causes hepatocellular dysfunction and increased intrahepatic resistance.*

1.1.4 Cirrhosis diagnosis

Cirrhosis develops by prolonged chronic liver injury, which steadily reduces liver function with late-stage liver scarring. Cirrhosis in its compensated stage is mostly asymptomatic or non-specific, and is only identified during medical screening for other causes [4][16]. These non-specific symptoms may include: fatigue, weakness, loss of appetite, discomfort in the right upper quadrant of the abdomen, and weight loss [17]. Physical examination findings can further indicate the presence of cirrhosis

[17]. The development of ascites, hepatic encephalopathy, gastrointestinal haemorrhage and/or jaundice symptoms distinguish the progression from mostly asymptomatic compensated cirrhosis to symptomatic decompensated cirrhosis [17][18].

Non-invasive tests, i.e. biochemical markers and radiological tests, are used to diagnose cirrhosis, but liver biopsy remains the gold standard to confirm the diagnosis and grade the fibrosis, **Table 1** [19]. However liver biopsies are subjected to sampling error by the pathological heterogeneity [17]. FibroTest score calculated with alpha2-macroglobulin, apolipoprotein A1, haptoglobin, GGT and bilirubin, and enhanced liver fibrosis score calculated with hyaluronic acid, PIIINP and TIMP-1 are used to assess liver fibrosis, and radiological tests, such as FibroScan, can measure abnormalities of the liver and other tissues. Furthermore, Child-Pugh score calculated with ascites assessment, bilirubin, albumin, PT/INR and encephalopathy grade, and MELD score calculated with dialysis history, creatinine, bilirubin, and PT/INR (and sodium for MELD-Na) are used to identify cirrhosis stage and estimate mortality in patients [17].

Table 1: Diagnosis tools and measurements identifying cirrhosis [19].

Cirrhosis diagnosis tools	**Measurement**
Biochemical markers	
Complete blood count (CBC)	Red and white blood cell and platelets count for overall health
Alanine transaminase (ALT)	Hepatic enzymes released upon hepatocellular death
Aspartate transaminase (AST)	Hepatic enzymes released upon hepatocellular death
Albumin	Protein synthesized exclusively in the liver
Alkaline phosphatase (ALP)	Liver (and bone) enzyme increased by cholestasis
Gamma-glutamyl transferase (GGT)	Predominately liver protein released by liver damage
Alpha2-macroglobulin	Liver produced plasma protein
Apolipoprotein A1	High-density lipoprotein (HDL)
Haptoglobin	Liver produced plasma protein
Hyaluronic acid	Extracellular matrix component
Amino-terminal propeptide-of-type-III-collagen (PIIINP)	Procollagen terminal peptide released during synthesis of type III collagen
Tissue-inhibitor of matrix-metaloproteinase-1 (TIMP-1)	Produced mainly by activated hepatic stellate cells and Kupffer cells in the liver
Bilirubin	Blood cell waste product removed by the liver

Creatinine	Muscle waste product removed by the kidneys
Prothrombin time/international normalised ratio (PT/INR)	Blood clotting capabilities by hepatic synthesized cascade proteins
Radiological tests (Ultrasound, CT, MRI, Fibroscan)	Abnormalities: liver stiffness, hepatomegaly, splenomegaly, hepatic nodularity, ascites, portal vein thrombosis, portal hypertension, varices, and hepatocellular carcinoma
Liver biopsy and histology	Grade and stage of fibrosis

1.1.5 Decompensated cirrhosis

The progression to decompensated cirrhosis is caused by the steady decline of liver function that leads to the associated complications, symptoms, and eventually death. As mentioned before, the continued chronic hepatic injury decreases hepatocellular function and disrupts hepatic structure, which leads to intrahepatic resistance to portal blood flow [14]. This causes hepatic insufficiency and portal hypertension, which contribute to an acute decompensation event [17][18]. The distinction between acute decompensation and acute-on-chronic liver failure has been historically difficult to untangle [20]–[22]. The CANONIC and PREDICT studies aimed to define and establish criteria that helped define and differentiate acute decompensation (AD) and acute-on-chronic liver failure (ACLF), summarised in **Figure 4** [21]–[26]. AD is defined by a sudden and rapid decline of liver function that develops ascites, gastrointestinal haemorrhage, hepatic encephalopathy and/or bacterial infections, whereas ACLF is characterised as AD with acute hepatic and extrahepatic organ failure(s) with a high short-term mortality [22]–[24].

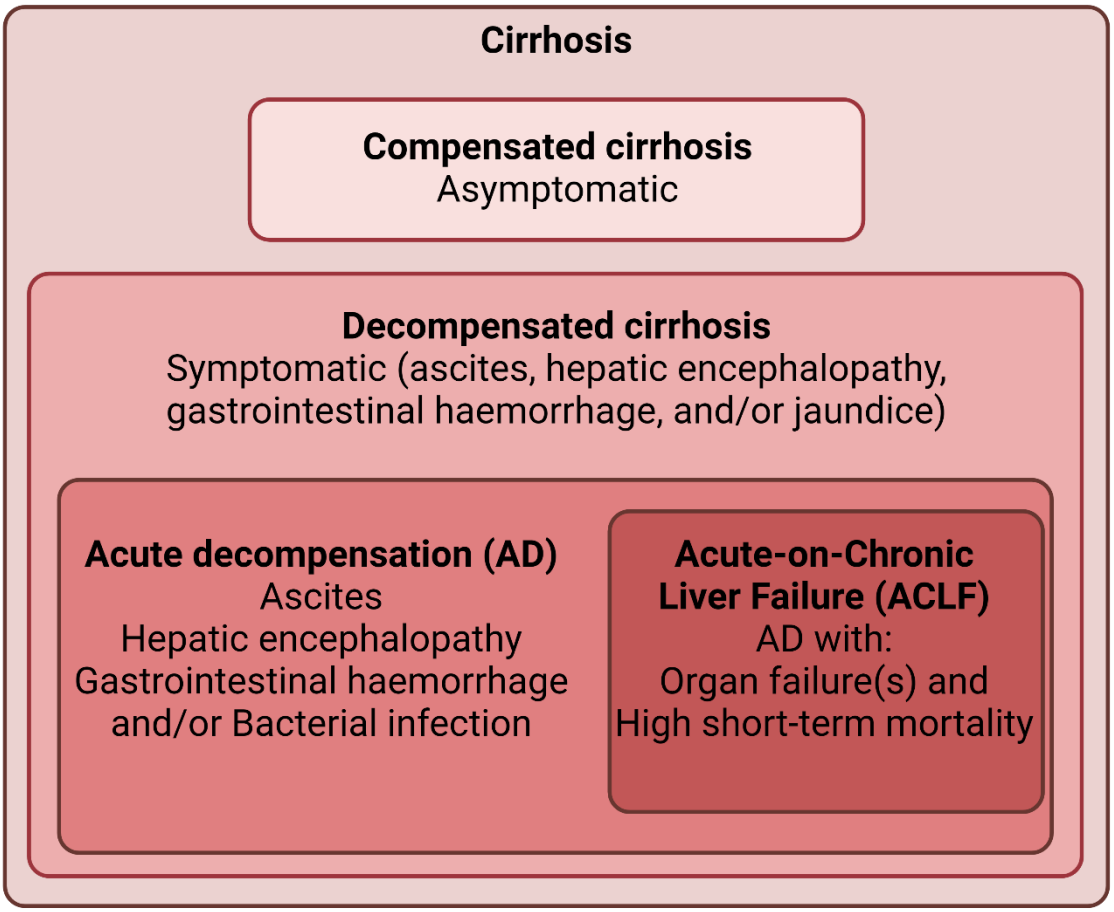

Figure 4: Grouping of compensated cirrhosis, decompensated cirrhosis, AD, and ACLF. *Complications of compensated cirrhosis, decompensated cirrhosis, AD, and ACLF.*

1.1.6 Decompensated cirrhosis mortality rates

Disease progression from compensated cirrhosis to AD and ACLF increases the mortality rate. Compensated cirrhosis has a low 5-year mortality rate of 1.5% without varices, and 10% with varices [16]. The development of decompensated cirrhosis increases this mortality rate and the requirement of frequent medical care and hospitalisations, but this various depending on the number of events and onset or not of ACLF. The 5-year mortality rate rises to 20% in decompensated cirrhosis with one event and up to 88% following a second decompensating event [16]. The development of ACLF increases the mortality rate even further to a 28-day mortality rate of 33.9%, from a 29-day mortality rate of 4.6% of AD without ACLF [21][22]. Disease progression thus increases hospitalisation and mortality rate with every event, as summarised in **Figure 5**. The increasing mortality rate with progression highlights the need for more treatment options, especially for late-stage cirrhosis.

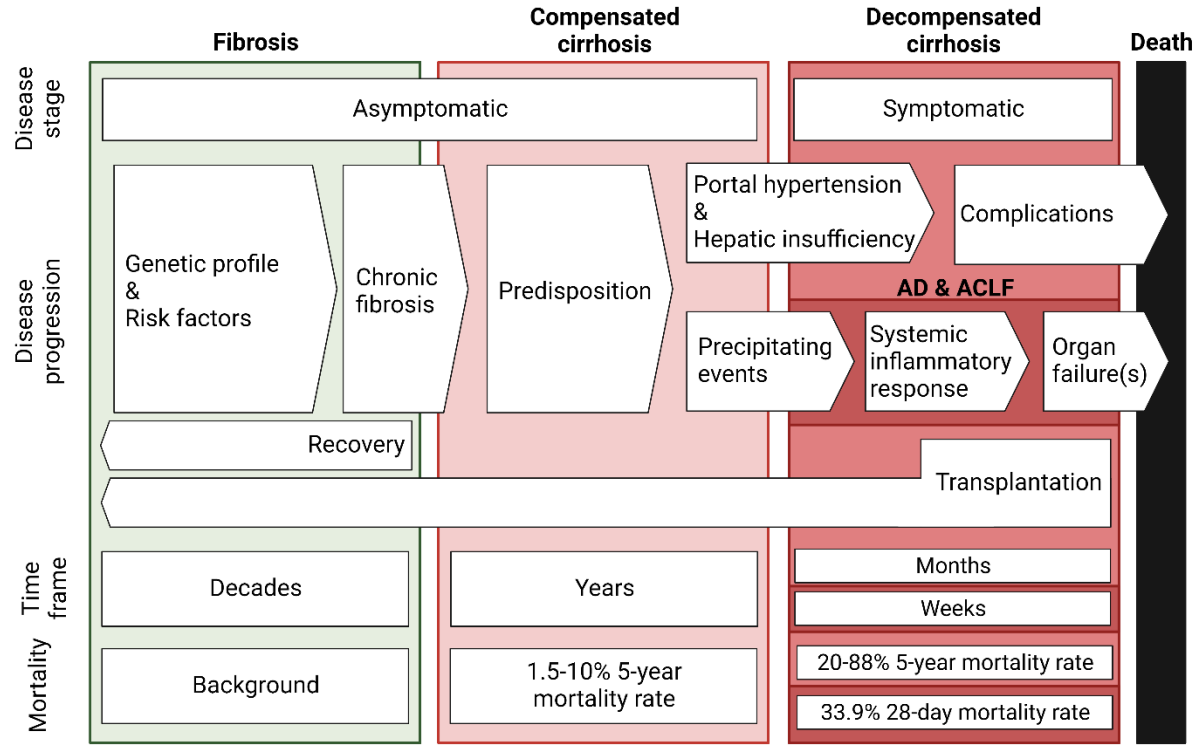

Figure 5: Schematic overview of cirrhosis progression showing stages of fibrosis, compensated cirrhosis, and decompensated cirrhosis. *Schematic showing disease stage, disease progression, time frame, and mortality of fibrosis, compensated cirrhosis, and decompensated cirrhosis.*

1.1.7 Predisposition, Injury, Response, Organ failure (PIRO)

The development of AD and ACLF during cirrhosis progression has been explained with the predisposition, injury, response, and organ failure (PIRO) concept [21]–[27].Predisposing factors and precipitating events play a key role in the progression to AD and ACLF. Predisposing factors (Predisposition) are underlying conditions that develop during the compensated cirrhosis stage that contribute to precipitating events (Injury) [25][27]. Injury from precipitating events causes severe systemic inflammation and infections (Response), which trigger progression to AD and ACLF (Organ failure(s)) [25][27].

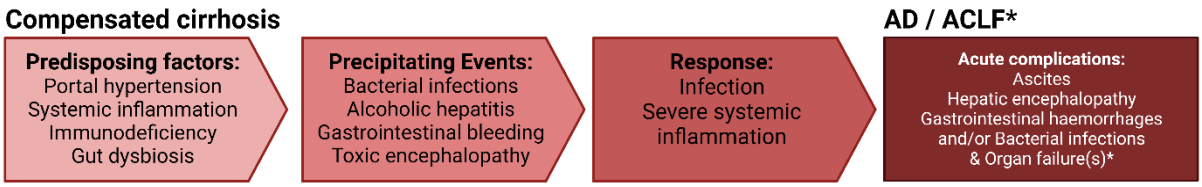

Figure 6: Graphic overview highlighting developments during progression from compensated cirrhosis to decompensated cirrhosis*. Predisposing factors, precipitating events, and complications associated with cirrhosis progression from compensated to decompensated cirrhosis, AD, and ACLF.*

1.1.8 Predisposing factors (Predisposition)

Predisposing factors including portal hypertension, systemic inflammation, immunodeficiency, and gut dysbiosis have been identified to contribute to cirrhosis progression and precipitating events, as shown in **Figure 6** [15].

Portal Hypertension

During the development of cirrhosis, an increase in intrahepatic resistance to portal blood flow caused by structural changes and vasoconstriction, leads to a permanently distorted liver architecture and portal hypertension [28][29]. Portal hypertension affects extrahepatic vascular beds, which lead to arterial vasodilation and formation of collateral vessels, causing increased portal inflow, and thereby creating a positive feedback loop worsening portal hypertension [29][30]. These architectural changes ultimately lead to increased blood flow in the gastro-oesophageal veins, resulting in enlarged abnormal gastro- oesophageal veins (varices), which in turn can leak or rupture leading to life-threatening bleeding (gastrointestinal haemorrhage) [31][32]. Additionally, portal hypertension contributes to the development of abdominal fluid build-up (ascites) by sodium retention [26], [32]–[34]. For these reasons, portal hypertension is an important therapeutic target, and reducing portal hypertension via beta-blockers and TIPS has been shown to decrease risk of variceal rebleeding, ascites, spontaneous bacterial peritonitis and hepatorenal syndrome, but conflicting results on hepatic encephalopathy [29], [30], [34], [35].

Gut dysbiosis

Gut microbiota overgrowth and microbial compositional changes (gut dysbiosis) are associated with cirrhosis, however whether causally related remains an important question [36]–[38]. The aetiology of cirrhosis plays an initial role in determining the nature of gut dysbiosis, with microbiota changes specific for ALD and NAFLD. However, as the disease progresses gut dysbiosis presents its own profile independent of aetiology [37]–[40]. Cirrhosis disrupts intestinal motility, which increases with severity independently of aetiology [41][42]. The intestinal motility disruption is associated with portal hypertension, but also with an altered microbiome, and small intestinal bacterial overgrowth [43]. As cirrhosis progresses, diversity of the microbiota decreases with the severity of the disease [37][44]. Importantly, prevalence of pathogenic bacteria increases and beneficial bacteria decreases during cirrhosis progression, which results in an increasingly pathogenic gut microbiome [37], [38], [44], [45]. The increased pathogenic gut microbiota in cirrhosis is associated with development of infections, hepatic encephalopathy, and ascites [36], [44], [46], [47]. The increase in microbiome overgrowth in addition to an increase of pathogenic bacteria facilitates an increase of PAMPs in the gut that can translocate out of the lumen, and circulate via the systemic circulation, thereby affecting other tissues [26][47]. Additionally, gut dysbiosis contributes to malnutrition with reduced

short chain fatty acid producing bacterial in cirrhosis patients, thereby affecting the gut metabolism [38], [48], [49]. Thus, gut dysbiosis contributes to the development of complications during cirrhosis progression via PAMPs, pathogenic bacteria, and a reduction of gut microbiome metabolism.

Systemic inflammation and immunodeficiency

During the development of compensated cirrhosis, patients develop low levels of systemic inflammation, which is an exaggerated immune response throughout the body caused by a loss of regulation of immune pathways [50]. This systemic inflammation is correlated with portal hypertension and associated with liver fibrogenesis in cirrhosis patients [50][51]. The low level of systemic inflammation in compensated cirrhosis patients is characterised by an increase of both pro and anti-inflammatory cytokines [23], [52], [53]. Inflammation is triggered by circulating DAMPs and PAMPs that lead to the production and release of pro-inflammatory cytokines [53]. Systemic inflammation fluctuates in cirrhosis patients, which indicates a contribution of transient episodes of PAMPs and DAMPs translocation from the intestine, overlayed to sustained levels of inflammation [25], [53]–[55]. The translocation from the gut is considered the main driving mechanisms of systemic inflammation in cirrhosis [50]. Moreover, cirrhosis patients also develop immunodeficiency, which is a decreased immune capability to combat bacterial infections [23][53]. Importantly, the increased systemic inflammation during cirrhosis is associated with increased susceptibility to bacterial infection in cirrhosis [56]. Thus, systemic inflammation in cirrhosis patients contributes to disease progression, while the immune response to bacteria is reduced thereby increasing infection susceptibility.

1.1.9 Precipitating events (Injury)

As mentioned before, the above-mentioned predisposing factors contribute to precipitating events that drive AD and ACLF. Severe alcoholic hepatitis, gastrointestinal bleeding with shock, toxic encephalopathy, and/or bacterial infection have been identified as precipitating events that drive AD and ACLF [22]–[24]. However, in approximately 60% of AD and 40% of ACLF cases no precipitating events is identified, which shows the complexity of identifying the cause of progression [22][24]. Bacterial infection and severe alcoholic hepatitis are the most common precipitating event for AD, followed by gastrointestinal haemorrhage and toxic encephalopathy [24]. Especially the number of precipitating events, rather than the specific event, determined the course and mortality of the disease with increased mortality in patients [24]. Multiple precipitating events increased the intensity of severe systemic inflammation and prevalence of organ failures compared to a single precipitating event or no identified event [24]. For ACLF, infection is the most common cause for

hospital admission divided between spontaneous bacterial peritonitis and other infections of the chest, urinary tract, leg ulcer, and others [27]. Second most common cause for hospital admission was active alcoholism, followed by gastrointestinal haemorrhage [27]. Furthermore, the type of precipitating event could not predict mortality in these patients [22][27].

1.1.10 Severe systemic inflammatory response and infection (Response)

The low levels of systemic inflammation in compensated cirrhosis is exacerbated to severe systemic inflammatory response and is usually caused by the precipitating events (independent of infections) during the progression to AD and ACLF [23], [27], [53]. Additionally, the level of systemic inflammation is increased in patients with progressive outcomes of decompensation at admission [53]. Systemic inflammation is associated with ascites development and mortality in alcohol hepatitis, decompensated and ACLF patients, and severity of systemic inflammation predicts bleeding and progression of ACLF in AD patients [22], [23], [52], [57], [58]. Furthermore, ACLF is associated with mostly pro-inflammatory cytokines, indicating a transition in the type of inflammation [52]. Reduced systemic inflammation or increased systemic inflammation a few days after admission with ACLF is indicative of improving or worsening ACLF, respectively [53]. Systemic inflammation is able to induce organ dysfunction/failure via decreased arterial blood volume and increased vasoconstriction, immune response mediated tissue damage, and via alterations in the metabolic pathways that inhibit energy production in cells in decompensated cirrhosis [53][59].

The antibacterial functions of circulating immune cells are reduced with progression. The ability of immune cells to migrate to the location of infection/site of bacteria is reduced in patients with AD [56]. Additionally, the ability of immune cells to recognise and kill bacteria is impaired in AD [56]. This further limits the ability of immune cells to combat infections, and approximately a quarter of admitted patients with ACLF develop new infections, which increases mortality [27]

1.1.11 AD / ACLF development (Organ failure)

The predisposing factors contributing to precipitating events, which drive severe systemic inflammation and infection culminates in AD/ACLF progression with the development of organ dysfunction/failure(s) [25][27]. ACLF is generally associated with organ failure(s), however patients with a degree of organ dysfunction that do not fulfil the criteria for ACLF are classified as AD [23][25]. Common organ dysfunction/failure(s) that are examined during cirrhosis progression are liver, kidney, brain, coagulation, cardiac, circulatory and respiratory system [23], [25], [27]. Development of organ dysfunction/failure(s) is associated with increased mortality in patients [23], [25], [27].

1.1.12 Treatments of cirrhosis complications

Treatment options for cirrhosis are available to reduce risk of progression, treat aetiologies, symptoms, and complications, but no targeted treatment option is available and the only curative option is liver transplantation [15]. The NHS in the UK lists lifestyle changes to reduce risk of cirrhosis progression and complications, which include avoiding alcohol, quitting smoking, losing weight (if overweight or obese), regular exercising, practising good hygiene, and speaking to a general practitioner about vaccinations and medicines [60]. Additionally dietary changes to combat malnutrition and treatments to help against the aetiology e.g., antiviral medicine against viral hepatitis, treatment program for alcohol addiction against ALD, medication against primary biliary cirrhosis, etc. can be prescribed [60][61]. Other treatments are prescribed for specific symptoms and complications, which include skin itching, varices, ascites, portal hypertension, encephalopathy, gastrointestinal bleeding, and infections [60][61].

Clinical trials have tested therapeutic options to reduce cirrhosis complications and increase survival in patients. Many of the different treatment options have shown promising results, although final outcomes vary across literature. These treatments focus on specific complications of cirrhosis e.g., immunodeficiency (GCSF), portal hypertension (beta-blockers and TIPS), dysbiosis (FMT), and systemic inflammation (albumin and emricasan).

Granulocyte colony-stimulating factor

Granulocyte colony-stimulating factor (GCSF) was tested in patients with cirrhosis, which showed increased survival and stability [62]–[65], however other trials showed no improvement [66]–[68]. GCSF increases immune cell production that can reduce infection risk, but thus GCSF treatment showed mixed results in cirrhosis trials [69].

Beta-blockers

Beta-blockers can have beneficial effect on portal hypertension in cirrhosis, however clinical trials showed contradicting results on survival, and varices and ascites development [70]. A post hoc analysis of three clinical trials showed no improvement in mortality of non-selective beta-blocker treated cirrhosis patients [71]. Furthermore, beta-blocker timolol did not reduce gastroesophageal varices or variceal haemorrhage in cirrhosis patients [72]. A clinical trial using propranolol or carvedilol treatment showed increased survival in cirrhosis patients due to reduced incidence of ascites, while a post hoc analysis of another trial showed reduced infection at hospitalisation, but no reduction in mortality [73][74]. A trial focussing on carvedilol showed improved survival and renal perfusion in cirrhosis [75]. Another trial focussing on propranolol showed decreased survival compared to endoscopic variceal ligation in cirrhosis [76]. A comprehensive review on beta blockers

in cirrhosis has highlighted their beneficial capabilities and their safety risks, but these clinical trials show inconclusive results regarding the effectiveness of beta-blockers on cirrhosis [77].

Transjugular intrahepatic portosystemic shunt

A transjugular intrahepatic portosystemic shunt (TIPS) connects the portal vein and the hepatic vein, which alleviates portal hypertension [78]. TIPS reduced rebleeding in cirrhosis, but conversely increased hepatic encephalopathy and did not improve mortality [79][80]. Other trials however, showed a decrease in bleeding, but no difference in hepatic encephalopathy or mortality [81][82]. While again other trials showed reduced bleeding and mortality in cirrhosis patients [83]–[86]. Furthermore, one trial showed that emergency portacaval shunt was more effective in reducing bleeding and increased survival compared to TIPS [87].

Faecal microbiota transplantation

Faecal microbiota transplantation (FMT) and other forms of microbiota manipulation treatments can restore gut microbial functions and potentially reverse negative effects of dysbiosis during cirrhosis progression [88]. FMT can be an alternative to antibiotics prescribed to cirrhosis patients even without infections, which has shown to be ineffective to reduce hospital acquired infections or improve mortality in these patients [89]. FMT was shown to be well-tolerated and reduced hospitalisation and hepatic encephalopathy episodes in cirrhosis patients [90]–[92]. However, larger clinical trials are needed to further indicate the effectiveness of FMT in cirrhosis [93].

Albumin

Albumin treatment normalises serum albumin levels and reduces systemic inflammation in cirrhosis [55]. Albumin treatment showed decreased infections and increased resolution from ACLF, beneficial effect on survival in cirrhosis, while one trial showed some beneficial effects from albumin treatment in cirrhosis but no effect on mortality [94]–[96]. Furthermore, another trial showed no difference in infection, kidney dysfunction, mortality, or inflammatory markers by albumin treatment in cirrhosis, and even more severe events by albumin treatment [97]–[99].

Emricasan

Another experimental therapeutic intervention targeting systemic inflammation and portal hypertension in cirrhosis is Emricasan. Emricasan is a pan-caspase inhibitor that inhibits caspase-mediated cell death and thereby has potential to affect inflammation and has been shown to lower portal hypertension. In cirrhosis rodent models, Emricasan decreased portal hypertension, which was associated with increased liver function, decreased hepatocellular cell death, reduced inflammation, and improved survival [100][101]. Clinical studies consistently showed Emricasan to be well tolerated in cirrhosis patients, but less effective in beneficial effects on cirrhosis. Emricasan

decreased portal hypertension in compensated cirrhosis patients with severe portal hypertension, and decreased AST and ALT levels as well as circulating cell death markers [102]. Another clinical trial also showed decreased cell death in AD patients, but did not show beneficial effects on MELD score [103]. However, in a different study, Emricasan reduced MELD and Child-Pugh score in cirrhosis patients with a MELD score ≥ 15 and well tolerated [104]. Furthermore, Emricasan treatment was not associated with reduced portal hypertension or improved clinical outcomes in cirrhosis patients [105] [106].

1.2 Gut-liver axis:

1.2.1 Gut-liver axis connections

The gut and liver act together as a physiological unit linked by a bidirectional connection termed the gut-liver axis, as illustrated in **Figure 7**. The primary role of the gastrointestinal tract and the microbiome within is to digest food and absorb the macronutrients, whereas the main function of the liver is to metabolise of the macronutrients from the gut in addition to creating bile [107]–[109]. Liver cells convert macronutrients into energy rich substances and store excess energy [107]–[109]. Additionally, the liver has an important immunological function, producing antibodies and detecting foreign material (including food antigens, viruses, bacteria, etc.) from the gut [110]. Immune cells in the liver capture and clear toxins, while staying immunotolerant to foreign non-pathogenic molecules, thereby regulating the access of gut derived materials [110][111]. The bidirectional communication between the two organs is facilitated by the biliary tract, portal vein, and systemic circulation as shown in **Figure 8**. Signalling molecules, including primary bile acids, and antibodies from the liver facilitate the interaction between the liver and the gut, which can affect the function of the gut and composition of the microbiome [30], [112], [113]. Conversely, the gut microbiome is essential to the gut-liver axis, and can generate metabolites that can impact liver function and influence the development of liver diseases [108], [113]–[115]. The gut-liver axis is a dynamic and intricate connection between the two organs that is crucial for regulating general health and wellbeing.

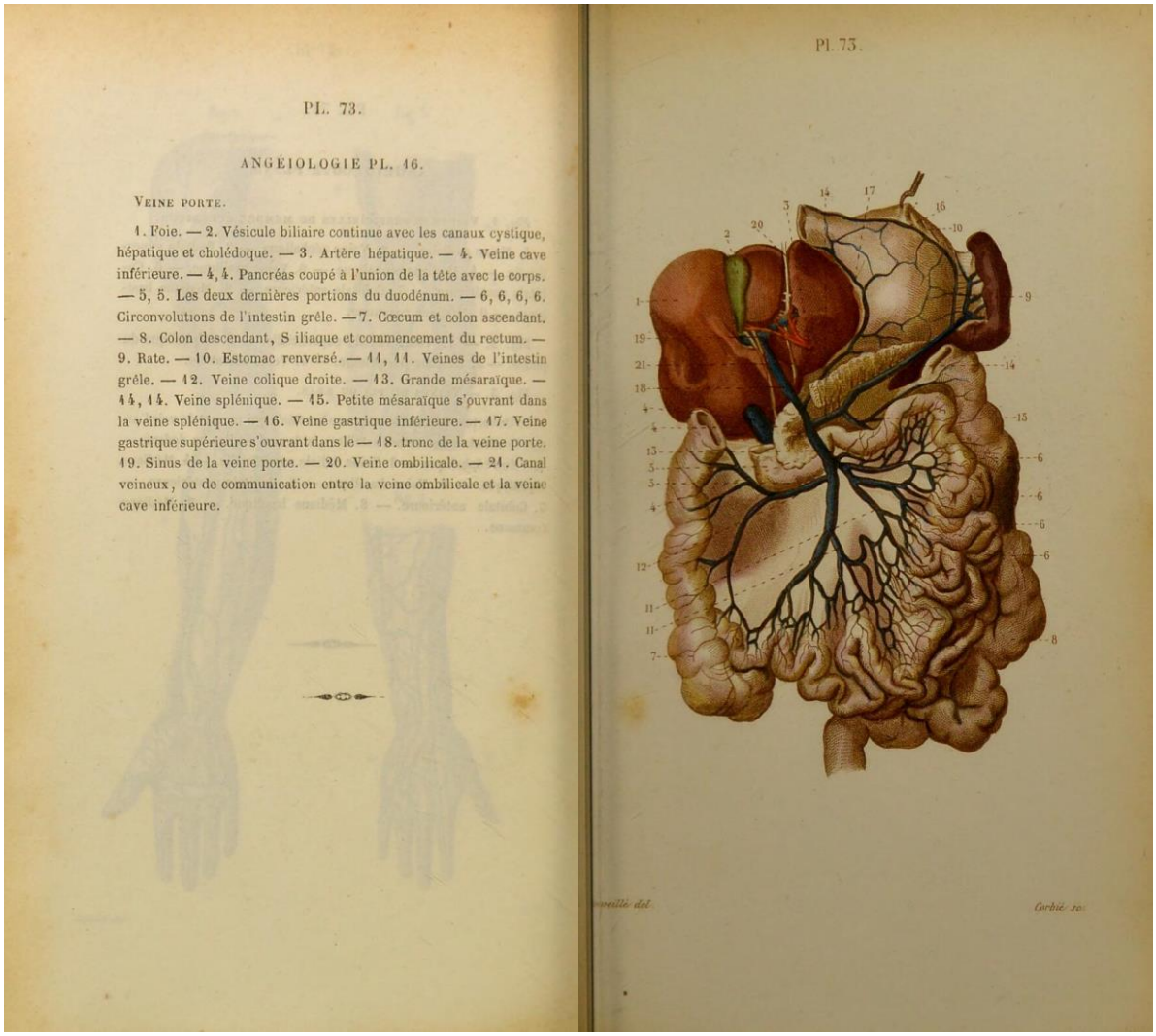

PL. 73.

ANGÉIOLOGIE PL. 16.

VEINE PORTE.

1. Foie. — 2. Vésicule biliaire continue avec les canaux cystique, hépatique et cholédoque. — 3. Artère hépatique. — 4. Veine cave inférieure. — 4, 4. Pancréas coupé à l'union de la tête avec le corps. — 5, 5. Les deux dernières portions du duodénum. — 6, 6, 6, 6. Circonvolutions de l'intestin grêle. — 7. Cœcum et colon ascendant. — 8. Colon descendant, S iliaque et commencement du rectum. — 9. Rate. — 10. Estomac renversé. — 11, 11. Veines de l'intestin grêle. — 12. Veine colique droite. — 13. Grande mésaraïque. — 14, 14. Veine splénique. — 15. Petite mésaraïque s'ouvrant dans la veine splénique. — 16. Veine gastrique inférieure. — 17. Veine gastrique supérieure s'ouvrant dans le — 18. tronc de la veine porte. 19. Sinus de la veine porte. — 20. Veine ombilicale. — 21. Canal veineux, ou de communication entre la veine ombilicale et la veine cave inférieure.

Pl. 73.

Figure 7: Illustration from Dr. Joseph Nicolas Masse in Petit Atlas complet d'Anatomie descriptive du Corps Humain from 1848. *Human anatomy illustration showing the connection between the gut and liver* [116].

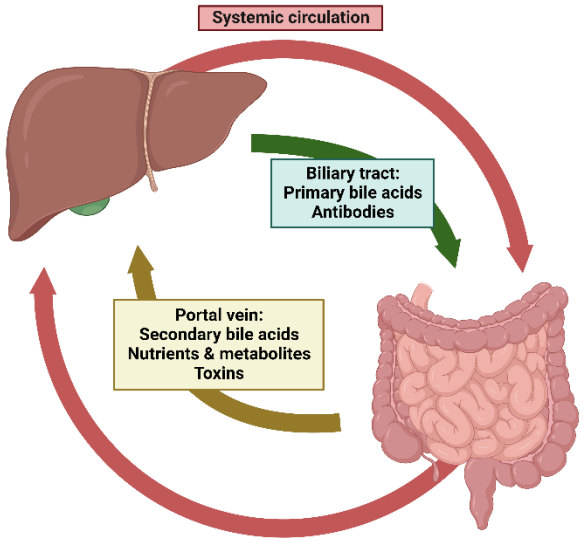

Figure 8: Schematic gut-liver axis showing bidirectional connection. *The bidirectional between the gut and liver by the portal vein, biliary tract, and systemic circulation.*

1.2.2 Portal vein transport and systemic circulation

Macronutrients and metabolites that are ingested by the gut are transported to the liver via the portal vein [108]. These macronutrients and metabolites are incorporated, metabolised, stored, and secreted by the liver [117]. The nutrients, glucose, vitamins and minerals secreted by the liver are transported to the other organs (including the gastrointestinal tract) via the systemic circulation [117]. Furthermore, toxins and bacterial metabolites from the gut can translocate through the intestinal barriers and are transported to the liver via the portal vein [115]. These toxins can include live bacteria, viruses, PAMPs, DAMPs, ethanol, acetaldehyde, trimethylamine, short chain fatty acids, and free fatty acids [113][115]. The increased portal hypertension in cirrhosis disrupts the microcirculation of the intestine, which could lead to neo-angiogenesis (blood vessel formation), and increased permeability in the splanchnic vasculature (blood supply of the gastrointestinal tract, liver, spleen, and pancreas) [30][118]. These changes contribute to intestinal permeability, which leads to translocation of bacteria and toxins from the gut [30][118]. Toxic compounds are absorbed and broken down by the liver, while immune cells in the liver detect and clear PAMPs, bacteria and viruses, thereby limiting access of gut derived toxins to the systemic circulation [110][111]. However, an immune response in the liver leads to a release of pro-inflammatory products into the systemic circulation, and excess of toxins from the gut can (further) damage the liver and other organs, contributing to liver disease, **Figure 9** [113][119].

1.2.3 Bile acid communication

Bile acid circulation from the liver to the intestines, and reabsorption from the intestines back to the liver, is termed the enterohepatic circulation [120]. The secretion of primary bile acids from the liver

to the gut plays a key role in regulating the homeostasis inside the intestinal lumen [113]. Bile acids facilitate the digestion of dietary fats and oils by forming micelles, which are transported by the portal vein. Additionally, bile acids regulate the microbiota composition by their antimicrobial interactions [30]. The microbiota in turn converts some primary bile acids into secondary bile acids, which enter the systemic circulation and interact with other tissues [30]. Cirrhosis development with disrupted synthesis and secretion of bile acids (cholestasis), leads to a reduction of bile acids in the gut [112]. This reduction of bile acid levels in the gut is associated with bacterial overgrowth and inflammation [121]. The changes in microbiota composition during cirrhosis and disrupted primary bile acids lead to changes in secondary bile acids, which in turn affects other tissues including the liver [114]. Thus, disrupted bile acid production and altered enterohepatic circulation during cirrhosis development can negatively affect the intestine and the liver.

1.2.4 "Leaky gut"

The development of the described gut dysbiosis and disrupted gut-liver axis signalling during cirrhosis intersect in what is described as a "leaky gut", which is described as increased intestinal permeability resulting in bacterial translocation, as illustrated in **Figure 9**. Intestinal permeability is required to absorb and transport nutrients from the gut, while toxins from the gut are prevented from entering [122]. However, during cirrhosis development intestinal permeability increases, which leads to increased translocation of bacteria, metabolites, and toxins from the intestinal lumen to the portal vein [123]–[126]. In patients with cirrhosis, both portal hypertension and liver insufficiency contribute to bacterial translocation [127][128]. However, studies with rat models showed that portal hypertension without liver insufficiency did not increase bacterial translocation, whereas liver insufficiency solely did increase bacterial translocation [127][128]. The increased bacterial translocation can lead to inflammation and exacerbate portal hypertension [118]. Additionally, small intestinal bacterial overgrowth is associated with increasing cirrhosis severity and with ascites development [129][130]. This bacterial overgrowth and increased intestinal permeability can drive bacterial translocation in cirrhosis [38], [117], [131]. Cirrhosis patients with ascites often show increased intestinal permeability, pathological systemic endotoxin levels, and high bacterial translocation to the mesenteric lymph nodes, which are associated with inflammation and the progression of cirrhosis [46], [132]–[137]. Live bacteria from the gut have been identified in mesenteric lymph nodes and ascites in cirrhosis mice models, thereby providing direct evidence of bacterial translocation [138]. Furthermore, bacterial translocation in cirrhosis can lead to spontaneous bacterial peritonitis, which often originates from gut bacteria and is a lethal condition associated with high mortality [47].

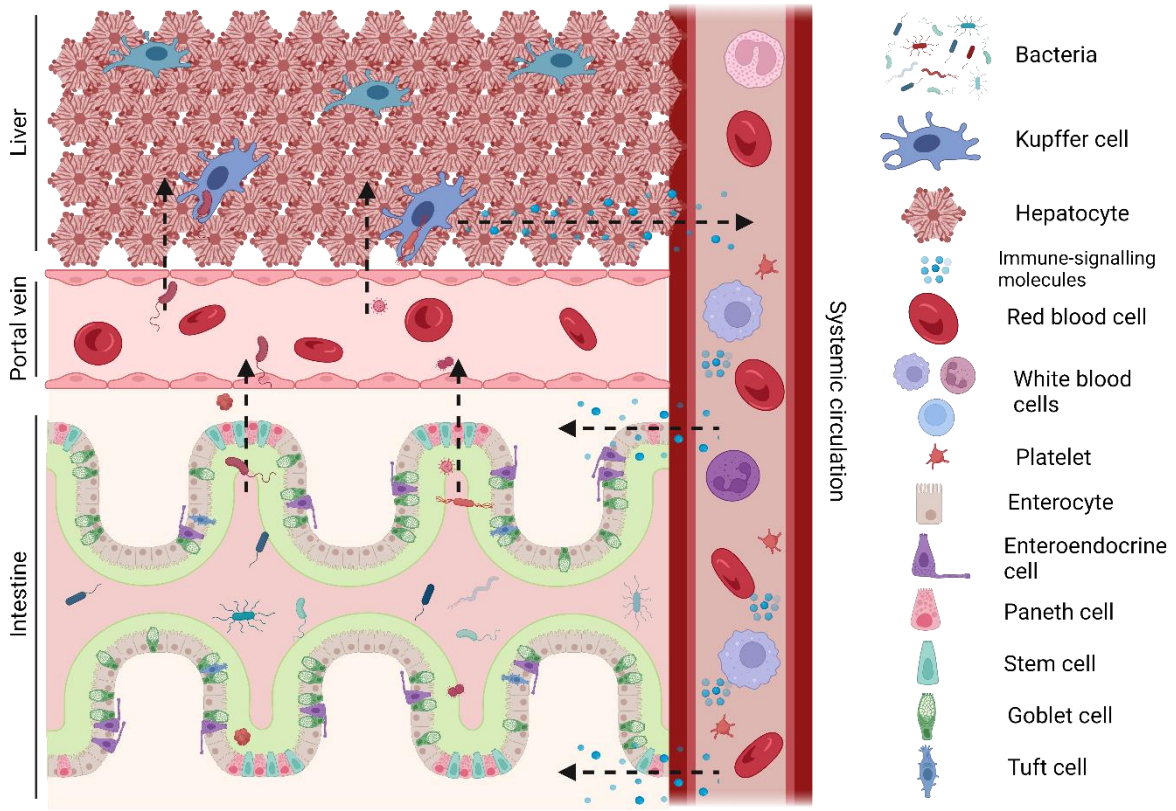

Figure 9: Leaky gut connection with the liver by the gut-liver axis. *Illustration showing bacterial translocation from the intestine to the liver via the portal vein, where it induced an immune response by liver immune cells, which in turn can influence the intestine.*

1.3 Intestine:

1.3.1 Intestinal homeostasis

The intestinal barriers regulate permeability and protects the systemic circulation from exposure of the microbiome and microbial products in the intestinal lumen. In healthy conditions, the intestinal barrier selectively allows for absorption and transportation of nutrients and metabolites across the epithelium to the liver and systemic circulation, while impeding the absorption and transportation of toxins and live bacteria [139]. A healthy microbiome contributes to the defence of toxins by out-competing pathogenic bacteria, and signals via the gut-liver axis with secondary bile acids [140][141]. The microbiome and the intestinal epithelium maintain homeostasis in the intestine lumen, thereby facilitating food digestion [122]. Therefore, a healthy microbiome and intact intestinal barriers are required for facilitating nutrient and metabolite absorption and transportation, while limiting toxins and live bacteria from accessing the systemic circulation, illustrated in **Figure 10** [139].

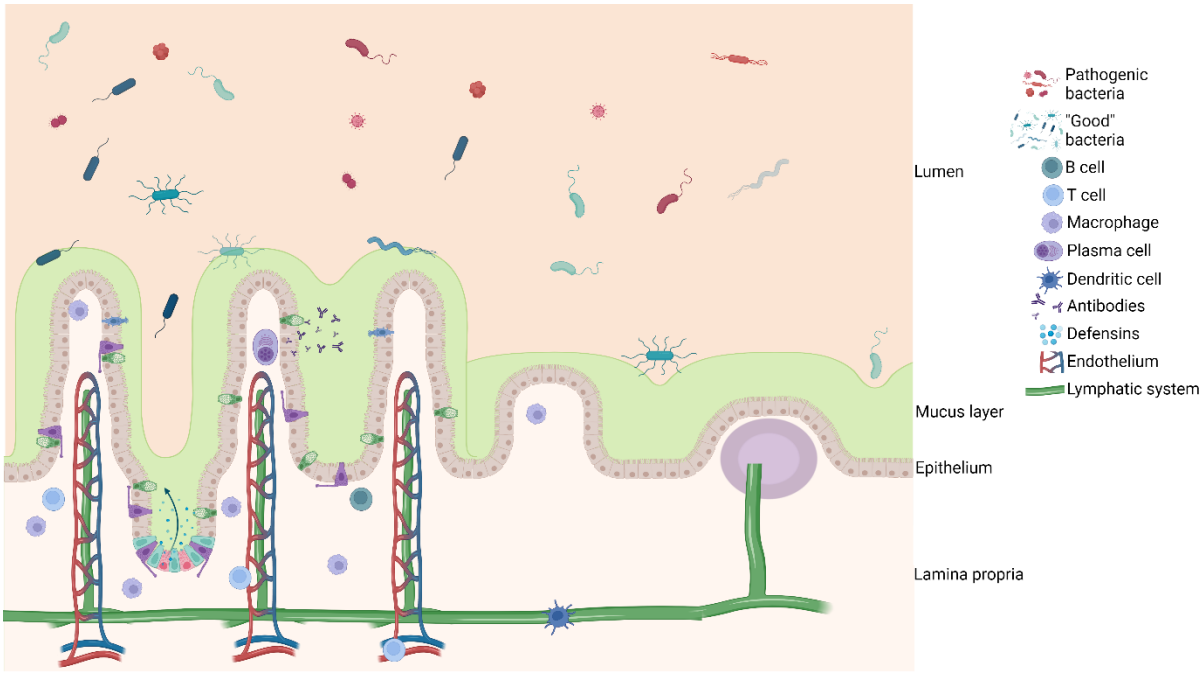

Figure 10: Schematic overview of the intestinal barriers. *Overview showing a healthy microbiome limiting pathogenic bacteria in the lumen, mucus layer inhibiting infiltration, intact epithelial monolayer, and immune cell compartment.*

1.3.2 Intestinal barriers

As mentioned, beneficial bacteria in the microbiome can limit pathogenic bacteria by out-competing them for nutrients in the lumen [140]. Additionally, beneficial bacteria limit pathogenic bacteria by producing inhibitory compounds, secondary bile acids, and short-chain fatty acids [140]. Pathogenic bacteria in the intestinal lumen are inhibited from spreading from disseminating to other tissues by several mechanisms:

1. The mucus layer, mainly produced by Goblet cells and consisting of mucin 2, limit exposure of bacterial cells and bacterial products from accessing the epithelium [122]. This mucus layer also contains immune regulators, which creates a gradient of the microbiota within the mucus layer [122]. The mucus layer covers the lumen side of the intestinal epithelial layer.

2. The epithelial barrier is a monolayer consisting mainly of enterocytes, goblet cells, enteroendocrine cells, Paneth cells, and stem cells formed into crypts and villi [122]. An intact epithelial monolayer, allows for selective transport of nutrients from the lumen to the lamina propria, which is strictly regulated by tight junctions, adherens junctions, and desmosomes [122].

3. The immune cells in the lamina propria comprise the last barrier [139]. These immune cells, especially gut-resident macrophages contribute to the host defence and barrier maintenance with high phagocytic activity and the secretion of cytokines that promote cell maintenance [142]. Additionally, the gut-associated lymphoid tissue, a network of lymphatic system, immune cells

(including macrophages, B cells, T cells, Plasma cells, and dendritic cells), Peyer's patches (small intestine), and mesenteric lymph nodes [143]. The components of the gut-associated lymphoid tissue allows for rapid migration of immune cells to detect and combat bacterial translocating toxins and bacteria [143]. Disruption of any of these barriers can contribute to increased gut permeability and bacterial translocation, and impaired barrier functions has been shown to contribute to systemic immune activation [139].

1.3.3 Epithelial cell types and function

The epithelial barrier is a monolayer consisting mainly of enterocytes, goblet cells, enteroendocrine cells, Paneth cells, and stem cells formed into crypts and villi, as shown in **Figure 11** [122][144].

Enterocytes are the predominant cell type of the intestinal epithelial monolayer. The main function of enterocytes is the absorption and transportation of nutrients and metabolites from the lumen [139].

Goblet cells as well as Paneth and enteroendocrine cells belong to the secretory intestinal epithelial cells [139]. Goblet cell's primary function is the production and secretion of the mucus layer, which main component is mucin 2 [122]. The mucus layer covers the lumen side of the intestinal epithelial layer [122]. Goblet cells are more abundant in the colon compared to the small intestine, which leads to two mucus layers in the colon compared to one in the small intestine [145]. The mucus layer prevents infiltrating bacteria from accessing host cells [122]. This mucus layer also contains immune regulators, which creates a gradient of the microbiota within the mucus layer [122].

Additionally, Goblet and Paneth cells, and in limited capacity enterocytes, secrete immune regulators that are released into the mucus layer [139]. Paneth cells, unlike other differentiated cells remain in the small intestinal crypt and do not migrate up the villi [139]. In the colon, deep secretory/Goblet-like cells populate the crypt instead of Paneth cells [146][147]. Paneth cells and deep secretory/Goblet-like cells are specialised for secreting antimicrobial proteins, including defensins, cathelicidins, and lysozymes [148]. These secreted antimicrobial proteins predominately target pathogenic bacteria to regulate the microbiome.

Enteroendocrine cells secrete gut hormones in response from stimuli in the lumen. Enteroendocrine cells link the neuroendocrine systems in the gastrointestinal tract and is thereby able to regulate digestion e.g., via insulin release [149].

Pluripotent stem cells reside in the crypt of the intestine from where they replenish the intestinal epithelial cells [150]. The crypt stem cells proliferate and differentiate into the above-mentioned cells, while maintaining their pluripotency [150]. These new cells created in the intestinal crypt

migrate upward on the villi. Paneth cells and stem cells, differ from the other epithelial cells, as they remain in the crypt. Two distinct stem cell types have been identified in the intestinal crypt. Potten's stem cells, label-retaining cells (LRC), are located on average at the +4 position (counted from crypt bottom), while LeBlond's stem cells, crypt base columnar (CBC) cells, are located at the crypt bottom interlaced with Paneth cells in the small intestine, and interlaced with deep secretory cells/Goblet-like cells in the ascending/descending colon [147], [151]–[153]. The CBC cells are actively proliferating to replenish intestinal epithelial cells, while the LRC are quiescent, which serve as reserve pluripotent stem cells that can replenish CBC cells.

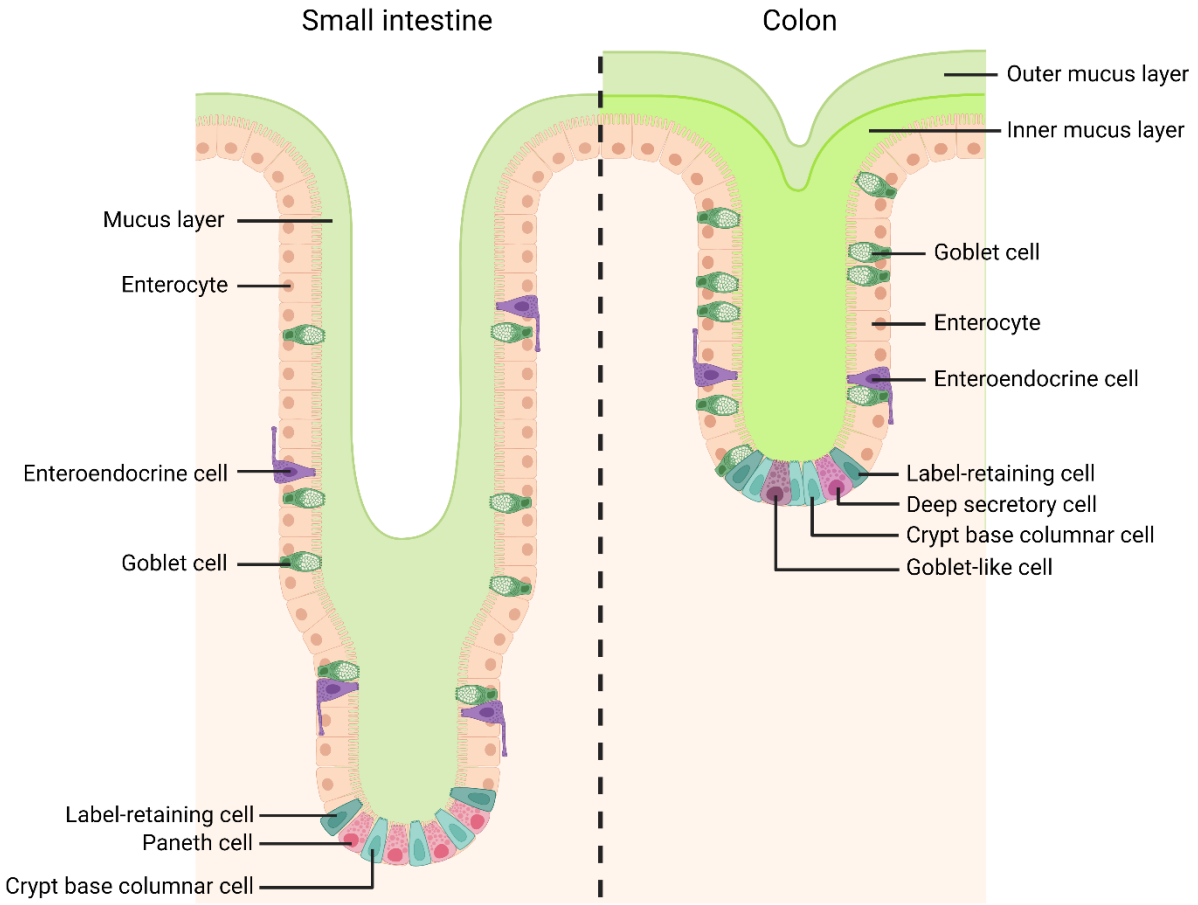

Figure 11: Small intestine epithelium (left) vs colon epithelium (right). *The small intestinal structure on the left showing a single mucus layer and cell types in the epithelium vs the colon structure on the right showing double mucus layer and cell types in the epithelium.*

1.3.4 Intestinal barrier dysfunction

As described before, the microbiome is disrupted during cirrhosis and beneficial bacteria are reduced while pathogenic bacteria are increased, which causes an imbalance in the intestine [37], [38], [44], [45].

There is conflicting data on the expression of intestinal tight junctions during cirrhosis development [124], [154], [155]. Intestinal staining in the duodenum of cirrhosis patients showed decreasing Occludin and Claudin-1 with cirrhosis severity, however in a different study intestinal Claudin-3 and Claudin-4 expression was decreased and Occludin was increased in cirrhosis [124][155]. Another study showed increased Claudin-2 levels in the intestine of decompensated cirrhosis, but no difference in Occludin or Claudin-1 [154]. These junctions regulate paracellular permeability facilitating selective absorption and transport of nutrients, and thus dysregulation of these junctions during cirrhosis progression can contribute to bacterial translocation [122].

Additionally, intestinal immune cells in the lamina propria are activated in cirrhosis [154]. During cirrhosis development intestinal macrophages are activated, which is part of the immune response to bacteria to regulate intestinal inflammation [154]. An intestinal pro-inflammatory immune response was increased in a rat model of cirrhosis with ascites, which was associated with epithelial junction disruption and bacterial translocation [156]. Decontamination of the intestine reduced the pro-inflammatory increase, as well as reduced bacterial translocation [156]. In a mice model of cirrhosis intestinal microbiome activated macrophages contributed to intestinal cell death, permeability and inflammation [157]. These studies thus show that in cirrhosis activation of intestinal macrophages can contribute to bacterial translocation and disease progression [154], [156], [157].

Furthermore, important intestinal epithelial cells that help regulate intestinal barriers with mucus and antimicrobial proteins are reduced in cirrhosis [138][158]. Importantly, a reduction of intestinal Paneth was shown to be associated with bacterial translocation in a cirrhosis rat model [138]. Besides a reduction in Paneth cells, reduced Goblet cells and mucus layer was found in the intestine of cirrhosis mice, which associated with bacterial overgrowth and bacterial translocation [158]. These studies show alterations of the intestinal epithelium that occurs during cirrhosis, which contributes to bacterial translocation, as summarised in **Figure 12**. However, the driving mechanisms that causes a reduction in Paneth cells and Goblet cells, i.e. increased cell death, decreased proliferation, decreased differentiation, remains unknown.

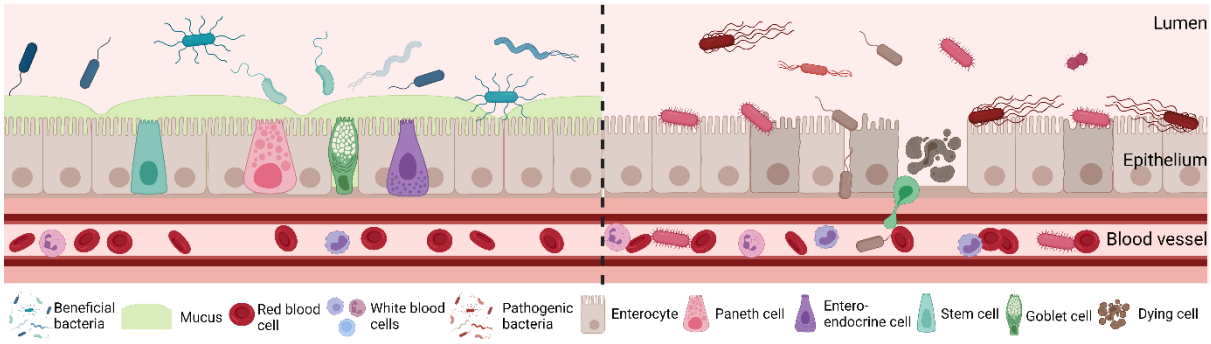

Figure 12: Healthy intestinal barriers vs disrupted intestinal barriers. *A healthy intestine on the left with a "good" microbiome, mucus layer, diverse epithelial cell monolayer, and on the right a disrupted intestine with dysbiosis, reduced mucus layer, reduced epithelial cell monolayer diversity facilitating bacterial translocation.*

1.4 Cell death:

1.4.1 Intestinal cell death mechanisms

Regulation of cell death in the intestinal epithelium is required to maintain epithelial homeostasis, with an estimated 300 new cells being generated from stem cells in the intestinal crypt every day [159][150]. These newly generated cells differentiate and migrate upward on the villi, where they are extruded at the top. Apoptosis, necroptosis, anoikis, and pyroptosis of intestinal epithelial cells control the turn-over of cells to maintain an consistent number of cells in the monolayer, and the extrusion of these dying cells together with the remodelling of microtubules maintains the monolayer integrity, **Figure 13** [150]. While apoptosis and anoikis do not elicit an immune response, pyroptosis and necrosis cause DAMP release, which elicits an immune response. Apoptosis typically occurs in cells at the top of the villi, which are differentiated epithelial cells at the end of their life. Apoptosis creates apoptotic bodies, which encapsulate the intracellular contents, so they are not released in the environment [160]. Anoikis is caused by mechanical or pathogen-induced pathways leading to extrusion of the epithelial cell from the monolayer [161]. This extrusion from the monolayer in turn causes apoptosis in the cell, resulting in an immune silent removal of the cell. Necroptosis is a lytic form of cell death, where intracellular contents are released, causing a pro-inflammatory immune response [160]. Necroptosis is considered to substitute for apoptosis when effector caspases facilitating apoptosis are dysregulated. Pyroptosis is also a lytic pro-inflammatory cell death. Pyroptotic cell death is activated in response to PAMPs and DAMPs and contributes to the defence against infiltrating bacteria, and therefor will be further discussed below [162]. Pyroptosis causes the release of intracellular contents including pro-inflammatory cytokines that help elicit an immune response and combat bacteria. Disruption of these cell death pathways contribute to inflammation in the gut and is associated with inflammatory bowel disease in patients and animal models [150], [163]–[165].

Regulating cell death and stemness to balance turnover and cell renewal in the intestinal epithelium is required to maintain the intestinal barrier's integrity, **Figure 14** [150][166]. Disruption of stemness and cell death pathways can impair the mucus layer by a reduction in Goblet cells, decrease antimicrobial protein secretion by a reduction in Paneth cells, and increase inflammation by lytic cell death upregulation [167]–[169]. Investigating cell death pathways and cell renewal during cirrhosis can thus help elucidate underlying causes of a leaky gut.

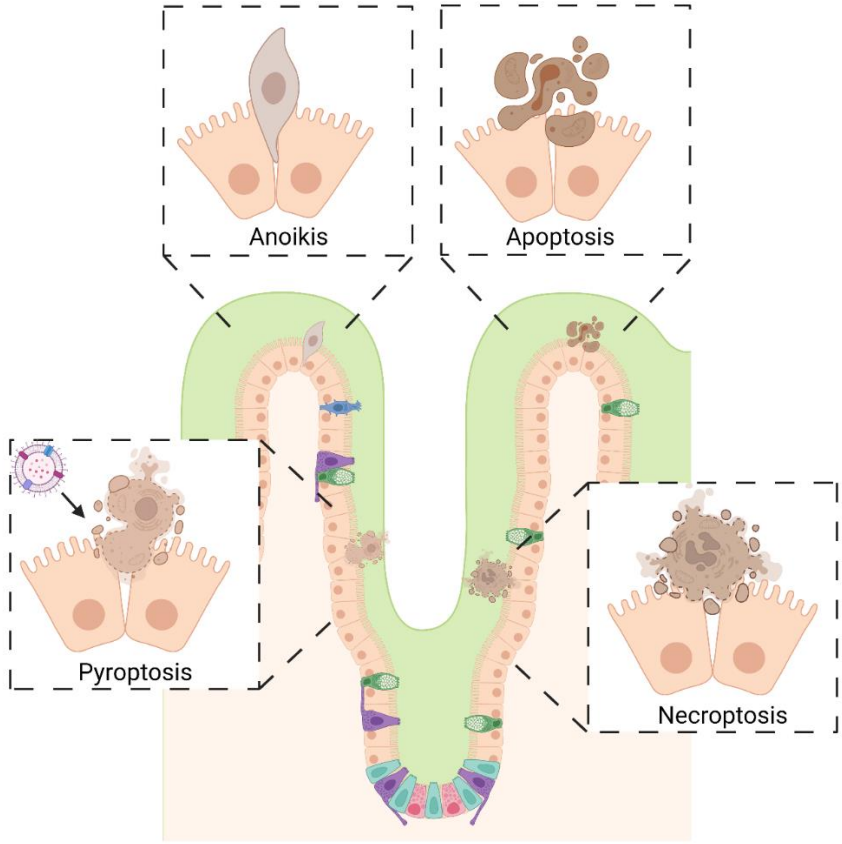

Figure 13: Four modes of cell death/extrusion regulating intestinal cell turnover. *Cell turnover in the intestinal epithelium is regulated by apoptosis, anoikis, necroptosis, and pyroptosis to maintain epithelial homeostasis.*

Figure 14: Graphic representing the balance of cell renewal and removal in the intestinal epithelium. *Cell renewal by crypt stem cells and removal by apoptosis, anoikis, necroptosis, and pyroptosis needs to be balanced to maintain epithelial monolayer homeostasis.*

1.4.2 Pyroptosis

As mentioned before, pyroptosis is a pro-inflammatory lytic cell death in response to PAMPs and DAMPs. Pyroptosis causes the release of cellular contents and cytokines, including mature IL-1β and IL-18, which is mediated by the Gasdermin family of proteins [170]. The cleaved N-terminal part of GSDMD can form pores in the membrane cells (including bacterial membranes, through which cytokines and cellular contents are released, leading to lytic cell death [170]–[172]. GSDMD can be cleaved via two pathways, the canonical inflammasome pathway via caspase-1, or the non-canonical inflammasome pathway via caspase-4/5, as shown in **Figure 15**.

Canonical inflammasome pathway

The canonical inflammasome pathway is activated by the recognition of PAMPs and DAMPs by pattern recognition receptors (PRRs) [173]. Members of the inflammasome PRRs, such as the NLRP complexes are specialised to recognise different PAMPs and DAMPs. NLRP3, together with mitochondria, is suggested to monitor K^+ efflux, mitochondrial Ca^{2+} uptake, reactive oxygen species, mitochondrial DNA, and lysosomal cathepsins to recognise PAMPs and DAMPs, pore-forming toxins, crystals, UV radiation, and protein aggregates. NLRP1 recognises *Bacillus anthracis* (also known as Anthrax) and lethal toxins via it's receptor binding, NLRC4 recognises Flagellin, T3SS and T4SS, and

AIM2 receptor binds to virus DNA, *Francisella tularensis* and *Listeria monocytogenes* [173][174]. These PRR bind with apoptosis-associated speck-like protein containing a CARD (ASC) to form ASC specks, which cleave caspase-1 into its active form [173][175]. NLRP1 and NLRC4 can activate caspase-1 independent of ASC, but the activation is enhanced by ASC. Active caspase-1 in turn cleaves IL-1β, IL-18 and GSDMD into its active form [174].

Non-canonical inflammasome pathway

In the non-canonical inflammasome pathway LPS can activate caspase-4/5 in humans (caspase-11 in mice) directly without an intermediate PRR [170]. Active caspase-4/5 in turn can cleave and activate GSDMD [170]. Although caspase-4/5 cannot cleave IL-1β and IL-18, caspase-1 has been shown to indirectly be activated via NLRP3 during non-canonical inflammasome activation [176].

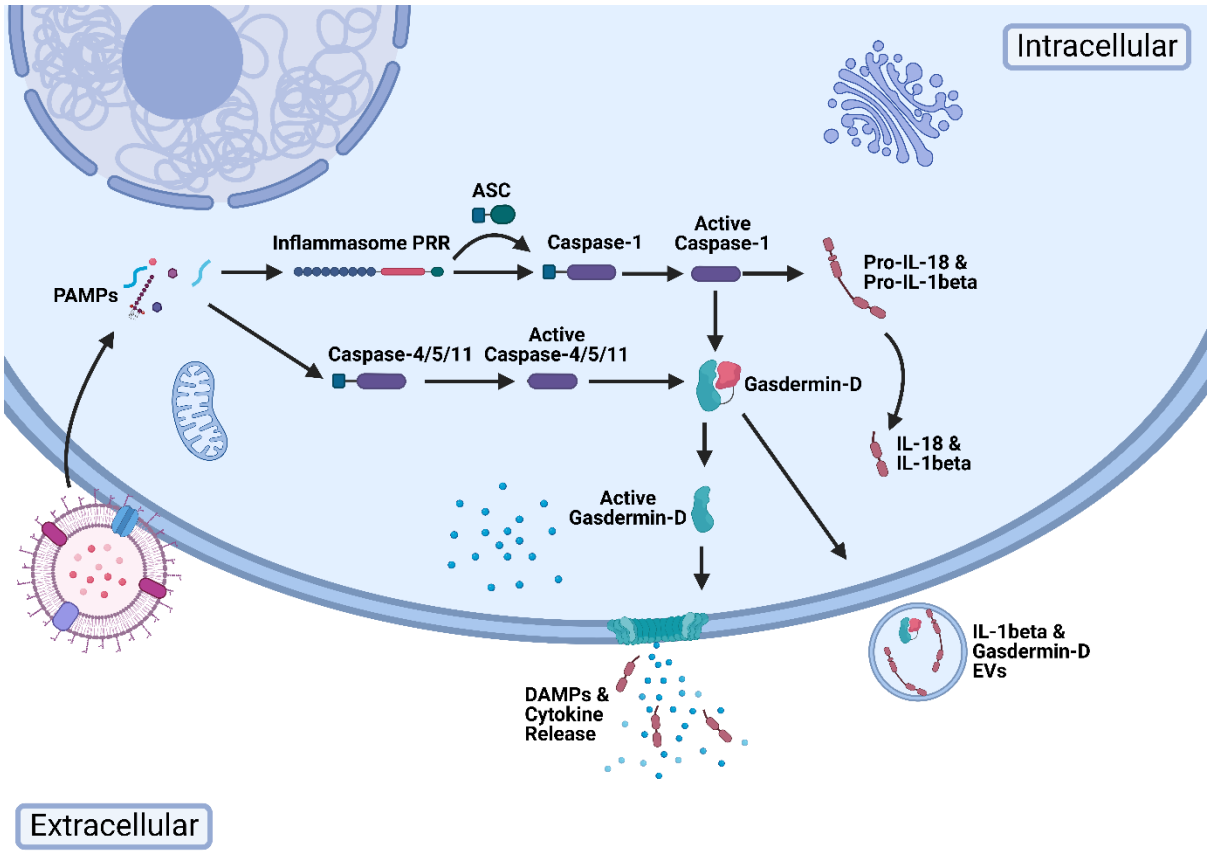

Figure 15: Overview of pyroptosis showing canonical and non-canonical inflammasome pathway activation. *Pathway activation of the canonical inflammasome (top) via caspase-1 leading to IL-1β and IL-18 maturation and Gasdermin-D activation, and pathway activation of the non-canonical inflammasome (bottom) via caspase-4/5/11 leading to Gasdermin-D activation.*

Pyroptosis induced inflammation

Infiltrating bacteria can directly induce pyroptosis in intestinal epithelial cells, which contributes to the bacterial defence via the cytokines and DAMPs release [177]. Additionally, the non-canonical

inflammasome activation contributes to the antimicrobial defence in the intestinal epithelium, with caspase-4 deficiency resulting in decreased pyroptosis and increased bacterial colonization [178]. However, caspase-1 mediated intestinal epithelial cell extrusion leads to an increase in permeability [164]. Thus, intestinal pyroptosis contributes to the antimicrobial defence, but over-activation can disrupt the barrier integrity. The pro-inflammatory cytokines IL-1β and IL-18 play a key role for regulating inflammation. Experimental sepsis mice with IL-1β and IL-18 deficiency showed reduced mortality, which indicates that inflammasome activation contributes to inflammation [179]. Similarly, in the intestine canonical inflammasome and non-canonical inflammasome activation contribute to regulate inflammation. There are conflicting results whether inflammasome contributes to or protects against inflammation. Caspase-1 deficiency protected against colitis in mice [180]. However, in a different study NLRP3 or ASC and caspase-1 deficient mice had increased susceptibility to colitis [181]. Similarly, caspase-11 deficient mice had increased susceptibility to colitis [182]. Furthermore, GSDMD has been shown to mediate pyroptosis-independent release of GSDMD and IL-1β extracellular vesicles in intestinal epithelial cells during IBD with GSDMD deficiency attenuating disease severity [183]. Thus, regulating inflammasome activation and pyroptosis in the intestine is important for proper antimicrobial defence, while maintaining barrier integrity.

Inflammasome activation during liver disease

Inflammasome activation has been shown during liver disease and contribute to disease progression. Canonical and non-canonical inflammasome have increased expression in livers of NASH patients, as well as increased *CHOP* expression [184]. Increased UPR and canonical and non-canonical inflammasome activation is found in NASH mice model, with similar results in obese mice treated with an ER stress inducer, showing the link with ER stress and inflammasome activation in liver disease. The NLRP3 inflammasome is also increased in a NASH rat model, with degree of gut dysbiosis correlating with IL-1β [185]. Furthermore, NLRP3 deficiency causes increased liver injury, gut immune dysregulation, intestinal permeability, dysbiosis, and bacterial translocation [186]. Antibiotic treatment, which is often prescribed to cirrhosis patients, has been shown to disrupt intestinal barriers with increased intestinal permeability, decreased tight junctions and increased activation of NLRP3 inflammasome and autophagy [187]. Lastly, non-canonical inflammasome activation is associated with disease progression in cirrhosis [188]. These studies show that inflammasome activation and potential ER stress sensitisation contributes to liver disease and disease progression, but their role in the intestine during cirrhosis remains unknown.

1.4.3 ER stress

ER stress is caused by extrinsic or intrinsic factors that disrupt protein folding leading to the accumulation of unfolded/misfolded proteins, which has been shown to affect intestinal stemness and induce cell death [189][190]. In response to ER stress ER-associated degradation (ERAD) and the unfolded protein response (UPR) pathways are activated, as summarised in **Figure 16** [191]. The ERAD pathway degrades incorrectly folded proteins by transporting these proteins to the proteasome, and the UPR alleviates ER stress by decreasing protein synthesis, and increasing proteins involved in protein folding and protein degradation [191][192]. Increased ER stress is associated with intestinal barrier disruption in inflammatory bowel disease and has been indicated in the intestine during liver disease [190], [193], [194].

Unfolded protein response

The key initiator protein of the UPR is GRP78, also known as BIP or HSP5a [191]. The accumulation of unfolded and misfolded proteins causes GRP78 to release from the three key transmembrane receptors of the UPR (IRE1, PERK and ATF6), and GRP78 instead binds to the unfolded and misfolded proteins, which facilitates protein folding [191].

IRE1 oligomerizes and phosphorylates by the disassociation of GRP78 and/or direct interaction with unfolded [195]–[200]. Activated IRE1 splices *XBP1* mRNA, which switches XBP1 protein production from unspliced XBP1 (XBP1u), to spliced XBP1 (XBP1s) [201] [202]. XBP1u inhibits transcription of UPR target genes, e.g. lipid biosynthesis enzymes, ERAD proteins, chaperones, etc., whereas XBP1s activates these genes [201] [203].

PERK oligomerizes and phosphorylates by the release of GRP78, which in turn phosphorylates and inhibits eIF2α [191], [204]–[206]. Activated eIF2α is involved in initiating translation, so PERK inhibiting eIF2α thereby reduces protein synthesis. Conversely, eIF2α inhibition induces ATF4, which increases amino acid transport proteins, XBP1, chaperones, CHOP (cell death transcription factor), etc. [207] [208].

ATF6 is transported to the Golgi apparatus via membrane vesicles by the disassociation of GRP78 and/or unfolded protein signalling [209]. ATF6 is cleaved in the Golgi apparatus by Golgi proteases, whereafter the active N-terminal fragment of ATF6 can activate UPR target genes, including GRP78 and XBP1, but further remains largely unknown [201][210].

The activation of these three arms of the UPR will lead to an increase in chaperone proteins for protein folding, an increase in ERAD proteins for protein degradation, and a decrease in transcription to reduce protein synthesis, in an attempt to alleviate ER stress. However if these processes are not sufficient to re-establish ER protein homeostasis, prolonged UPR activation initiates apoptosis via CHOP [189][211].

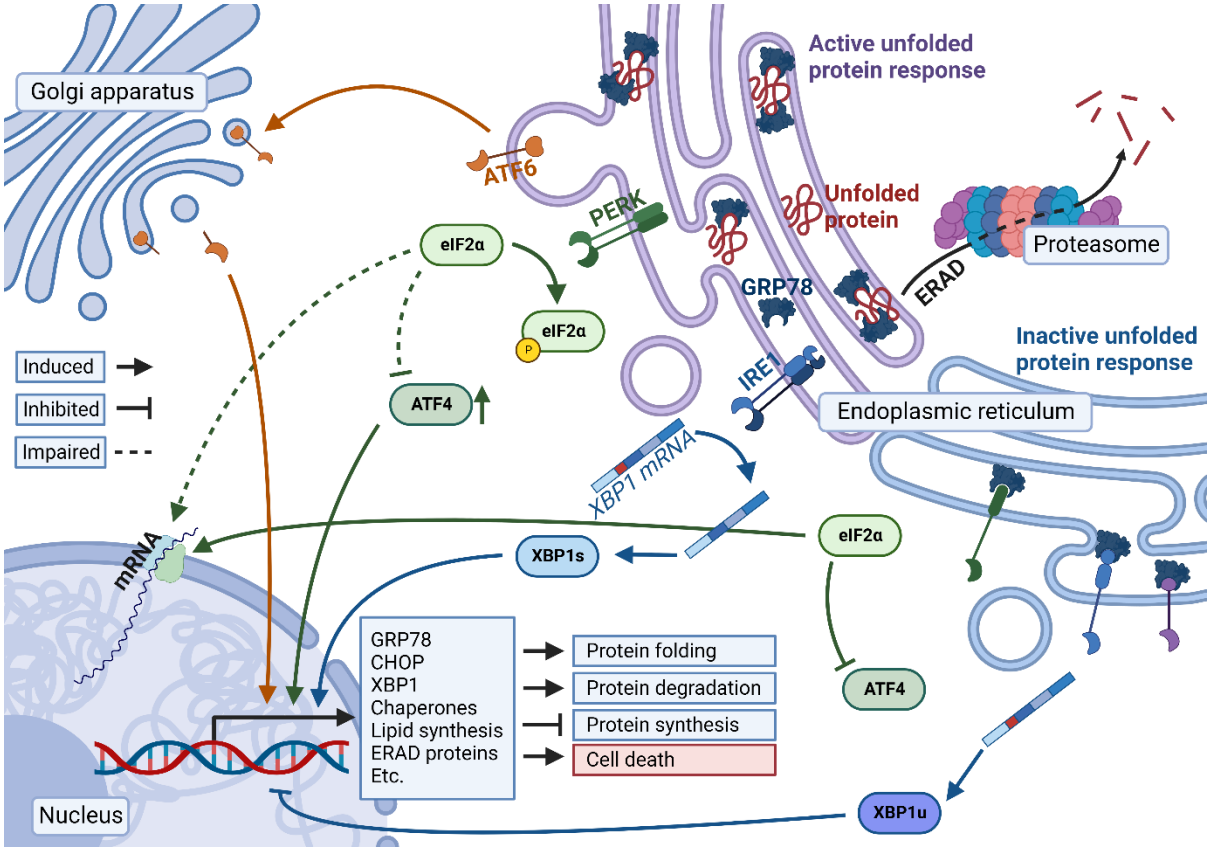

Figure 16: A representation of the unfolded protein response. *Transmembrane receptors are activated directly by mis/unfolded proteins, and/or indirectly by the disassociation of GRP78. ATF6 is transported to the Golgi apparatus, where it is cleaved into its active form. This N-terminal fragment induces UPR target genes. Release of GRP78 causes PERK to oligomerize, phosphorylate, and activate, which phosphorylate and inactivate eIF2α, thereby reducing mRNA translation. Phosphorylation of eIF2α also increases ATF4, which induces UPR target genes. GRP78 disassociation and/or unfolded protein signalling activates IRE1. This splices XBP1 mRNA, which translates into XBP1s. This decreases the unspliced XBP1u from inhibiting UPR target genes, which is then induced by XBP1s. Together the UPR arms facilitate protein folding, increase protein degradation, inhibit protein synthesis, and can eventually lead to cell death.*

ER stress in liver disease

ER stress has been shown to contribute to liver disease, including NAFLD, hepatitis, paracetamol overdose, hepatic ischemia-reperfusion and ALD, and disease progression [212]–[220]. However, the role of ER stress in the intestine during liver disease remains largely unknown.

Cirrhosis rodent models showed increased ER stress and UPR activation in the liver [221] [222]–[224]. The ER stress lead to a sensitised cell death response to LPS, with reduced TRAF2 (anti-apoptotic protein) expression in the liver [221]. However, CHOP deficiency did not protect against liver damage, which indicated that UPR-CHOP induced cell death does not play a significant role in liver injury during cirrhosis development [222][223].

One study showed increased intestinal ER stress and decreased stemness in cirrhosis patients as well as in bile duct ligated mice [194]. In the model CHOP deficiency reduced liver injury, liver cytokine expression, and apoptotic liver cells. In the intestine of the model, CHOP deficiency inhibited the increase in immune response and cell death and inhibited the decrease of crypt and villi length from the cholestatic liver injury mice model. CHOP deficiency mostly did not affect tight junctions or adherens junctions in the small intestine but did inhibit the decrease of tight junctions and adherens junctions in the colon, and reduced permeability and translocation in the model. This is only one paper and the increased of intestinal ER stress and decreased stemness expression in cirrhosis patients is shown in the supplementary data with relative mRNA levels, however it does indicate a potential role of intestinal ER stress, cell death, and stemness in cirrhosis.

ER stress induced intestinal disruption

Activation of the UPR in stem cells reduce intestinal stem cell marker genes *Lgr5* and *Olfm4* and self-renewal properties [190]. The loss of stemness causes these cells to differentiate and migrate upwards on the villi [190]. ER stress induced loss of stem cells is dependent on the PERK arm [190]. Particularly, the inhibited translation caused by eIF2α phosphorylation, resulted in reduced short half-life stem cell proteins (e.g. MYC) that are important for the self-renewal properties [225] [226]. XBP1 and/or ATF6 overexpression in colon cells decreased WNT dependent LGR5 and OLFM4, which decreased proliferation [227]. Co-overexpression of GADD34 (protein opposing the PERK arm) rescued the stem cell markers, protein synthesis, and proliferation of the XBP1 overexpressing cells. Deficiency of XBP1, which leads to perpetual activation of the unfolded protein response, in mice leads to an absence of Paneth cells, a decrease of Goblet cells, and an increase in stem cells migration upward on the villi in the intestine [228]. These XBP1 deficient mice have increased susceptibility to colitis induction, and the UPR is induced in the colon of IBD patients [193][228]. These studies show that ER stress and UPR dysregulation can reduce intestinal stemness and disrupt intestinal barrier integrity by reducing Paneth cells and Goblet cells, which leads to reduced antimicrobial protein secretion and a reduced mucus layer.

ER stress sensitised cell death

ER stress can lead to apoptosis via CHOP by prolonged UPR activation when the UPR is not able to resolve the ER stress. During liver disease progression of NAFLD, NASH patients show increased liver *CHOP* expression, but also pyroptosis markers [184], [229], [230]. ER stress and UPR has been shown to sensitise cells for cell death independent of CHOP induced apoptosis, specifically pyroptosis is sensitised by ER stress [231]–[233]. In IBD UPR markers are upregulated, but *CHOP* expression is downregulated, which could indicate that ER stress sensitised, CHOP independent, cell death is

involved in the disruption of the intestinal barrier during IBD [234]–[236]. The effect of ER stress on intestinal epithelial cell death and barrier integrity during cirrhosis remains unknown.

1.5 Hypothesis and Aims

The above-mentioned changes in the gut during cirrhosis e.g., gut dysbiosis, epithelial barrier dysfunction, immune cell activation, etc., may indicate that intestinal epithelial injury is associated with cirrhosis, which can contribute to increased intestinal permeability. Therefore, I hypothesize that intestinal epithelial injury, and inflammatory and cell death responses contribute to gut barrier dysfunction during cirrhosis progression. Intestinal epithelial injury may cause an increase of PAMPs and DAMPs in the systemic circulation, which may contribute to the systemic inflammation and progression to decompensated cirrhosis.

Are ER stress mediated intestinal inflammasome activation and pyroptotic cell death associated with cirrhosis?

Hypothesis: ER stress mediated intestinal inflammasome activation and pyroptotic cell death are associated with cirrhosis.

Aim 1: Characterise intestinal inflammasome activation in cirrhosis mouse models.

Aim 2: Characterise intestinal ER stress induction (UPR) in cirrhosis mouse models.

Aim 3: Determine synergy between ER stress and non-canonical inflammasome activation on intestinal cell death.

Aim 4: Characterise intestinal ER stress induction (UPR) in cirrhosis patients.

Development of a permeability assay for mouse intestinal organoids.

Hypothesis: Mouse intestinal organoids can be used to quantify intestinal epithelial permeability.

Aim 1: Measure intestinal organoid permeability using established protocols.

Aim 2: Develop a permeability assay for mouse intestinal organoids.

Are increased intestinal cell death and reduced stemness associated with cirrhosis?

Hypothesis: Increased intestinal cell death and reduced stemness are associated with cirrhosis.

Aim 1: Characterise intestinal cell death in cirrhosis patients.

Aim 2: Characterise intestinal cell death in cirrhosis rodent model.

Aim 3: Characterise intestinal stemness in cirrhosis rodent models.

Aim 4: Determine effect of reduced stemness on intestinal cell death, permeability, and proliferation.

Aim 5: Characterise cell death, permeability, and proliferation in intestinal organoids derived from cirrhosis rodent models.

Aim:6 Therapeutically target cell death and stemness for beneficial effects on cell death, permeability, and proliferation in intestinal organoids derived from cirrhosis rodent models.

2 Methods

2.1 In vivo

2.1.1 Human patient intestinal biopsy ethics

We received approval for the acquisition of UCL-RFH Biobank formalin fixed and paraffin embedded intestinal biopsy samples from the Royal Free London NHS Foundation Trust Biobank (National Research Ethics Service, NRES, approved Research Tissue Bank). Project Title: Intestinal cell death and inflammasome activation in cirrhosis, Reference number: NC2021.18, NRES number: 16/WA/0289. I received a certificate of achievement in Good Clinical Practice (GCP) from the NIHR, and a research passport and letter of access for research from the Royal Free Hospital – NHS Foundation trust to collect data and documentation of NHS patient information for "Intestinal Cell Death and Inflammasome Activation in Cirrhosis" in compliance with NHS Confidentiality Code of Practice and the Data Protection Act 2018.

2.1.2 Animal experiment approval and housing

All rodent animal experiments were performed according to the Home Office guidelines under the UK Animals in Scientific Procedures Act of 1986 (updated in 2012). The animals were maintained per the principle, guidelines, and study approval from the Ethical Review Board (AWERB) and conducted with a United Kingdom Home Office project license from Prof. Nathan Davies. The animals were housed and treated for experiments at the Biological Support Unit of Royal Free and University College Medical School, University College London. Sprague-Dawley rats and C57BL/5 (wild type, Caspase-11 KO, Caspase-1+11 KO) mice were housed in a temperature (19C-23C), light (12/12 hours light/dark cycle) and humidity (~50%) controlled facility and received standard chow and water *ad libitum*.

2.1.3 Mouse subcutaneous CCl4

To better understand liver disease and liver fibrosis in particular, *in vivo* models (mainly mice and rat models) have been created and utilised. The induction of liver injury can be subdivided into 6 groups: immune damage-induced liver fibrosis model, transgenic animal liver fibrosis model, alcohol-induced liver fibrosis model, diet metabolism-induced liver fibrosis model, chemical drug-induced liver fibrosis model, and surgery-induced liver fibrosis model [237]. The immune damage-induced liver fibrosis model is mainly a model for autoimmune hepatitis; transgenic animal liver fibrosis model to study hepatitis virus with a narrow host range, which requires human liver cells, or to identify the role of a specific gene; alcohol-induced liver fibrosis model to study alcoholic liver disease; diet metabolism-induced liver fibrosis model for NAFLD/NASH; chemical drug-induced liver fibrosis model for liver fibrosis/cirrhosis; and surgery-induced liver fibrosis model for cholestatic liver

fibrosis/cirrhosis [237]. For this study, I utilised a chemical drug-induced liver fibrosis model and a surgery-induced liver fibrosis model to induce cirrhosis in rodents, which best suited the focus of this project.

We subcutaneously administered CCl4 (chemical drug-induced liver fibrosis model) for 12 weeks to induce cirrhosis and examine the effect of cirrhosis on the intestine. CCl4 is a compound that can directly damage liver cells. Domenicali *et al.* showed that subcutaneous administration of CCl4 successfully induced cirrhosis, albeit at 13 weeks [238]. The more conventional intraperitoneal injection of CCl4 causes extensive abdominal adhesions and evidence of enhanced hepatic inflammation, which is a potential confounding effect when investigating the role of the gut-liver axis in cirrhosis [238]. Subcutaneous administration of CCl4 reduces this potential confounding effect, but subcutaneous administration of CCl4 can cause the formation of granulomas at the site of injection [238]. The reduced confounding effect on subcutaneous administration of CCl4 on the abdomen makes this treatment the better option compared to intraperitoneal to model cirrhosis for this project focussing on the intestine.

Figure 17: Representing image showing subcutaneous injection. *Subcutaneous injection in mice for chemical drug-induced liver fibrosis mice model.*

Olive oil (control) and carbon tetrachloride (CCl4) was administered to mice subcutaneously twice every week for 12 weeks (cirrhosis). After 12 weeks of treatment mice were injected with water or 2mg/kg LPS *Klebsiella pneumoniae* 4 hours before sacrifice (cirrhosis + precipitating event). The mice model was performed by Ms. Abeba Habtesion at the Royal Free BSU. Liver, kidney, and colon tissues from the animal model was split between flash frozen for molecular analysis and fixed for histology. Serum was collected at sacrifice for ALT and creatinine analysis, measured with Cobas

Integra 400 automated analyzer (Roche Diagnostics, Burgess Hill, UK) using relevant kits according to manufacturer's instructions.

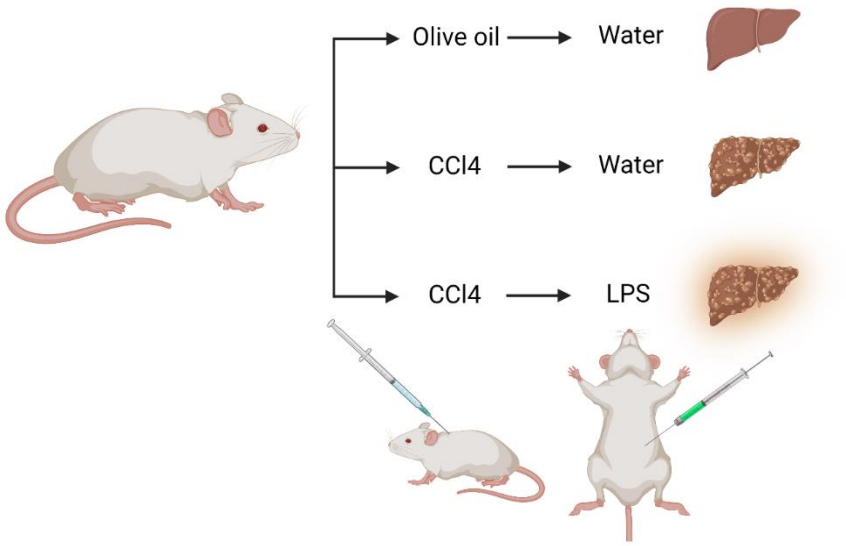

Figure 18: Mouse subcutaneous CCl4 model.

Additionally, Schalk van der Merwe utilised an extended subcutaneous CCl4 model with subcutaneous administration of CCl4 twice every week for 14 weeks followed by three times CCl4 subcutaneous administration every week, with phenobarbital added to ad libitum drinking water. From 14, 17 and 20 week treated mice, they collected liver and colon tissue split between flash frozen for molecular analysis and fixed for histology. They collected serum at 14 weeks and 19 weeks into CCl4 administration for ALP, AST, ALT, albumin, and creatinine analysis. The mice model from the group of Schalk van der Merwe (Laboratory of Hepatology) will be referenced as 14, 17 and 20 weeks.

2.1.4 Rat bile duct ligation

The other *in vivo* model I utilised was a surgery-induced liver fibrosis rat model, which induces cholestatic cirrhosis by bile duct ligation. Cholestatic liver diseases show a reduction of bile flow, which can lead to chronic inflammation, which in turn can cause further injury in the bile duct and liver [112]. Cholestasis can occur by extrahepatic factors e.g. bile duct tumours, cysts, pancreatitis, etc. but also by intrahepatic factors e.g. alcoholic liver disease, viral hepatitis, etc. [112]. Bile duct ligation models induce cholestatic liver fibrosis/cirrhosis by restricting the bile flow in the bile duct [237]. Bile duct ligation causes bile duct stenosis and increased bile duct pressure, and liver cirrhosis after 2 to 4 weeks [239]. This bile duct ligation therefore complements the subcutaneous CCl4 cirrhosis model with a cirrhosis cholestasis model.

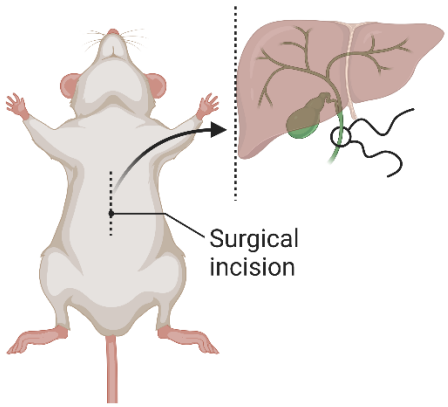

Figure 19: Representing image showing bile duct ligation. *Bile duct ligation in mice for surgery-induced liver fibrosis model.*

Rats were sham operated (control) and double bile duct ligated for 2 weeks (cholestatic cirrhosis). BDL rats were additionally gavaged with 1% DMSO in corn oil 23 hours and 5 hours before sacrifice and injected with 0.03mg/kg LPS *Klebsiella pneumoniae* 3 hours before sacrifice (cholestatic cirrhosis + precipitating event), or 100mg/kg Disulfiram (DFF) dissolved in 1% DMSO in corn oil 23 hours and 5 hours before sacrifice, and injected with 0.03mg/kg LPS *Klebsiella pneumoniae* 3 hours before sacrifice (cholestatic cirrhosis + treatment + precipitating event). The rat model was performed by Ms. Abeba Habtesion and Ms. Andrea Krstevski at the Royal Free BSU. Liver, kidney, and intestine tissue from the animal models is split between flash frozen for molecular analysis and fixed for histology. Duodenum, jejunum, ileum, caecum, and colon of the intestinal tract is dissected as shown in **Figure 21**, with cut marks separating the parts with a black line. Serum was collected at sacrifice for creatinine, ALT, ammonia, GGT, GLUC, and AST analysis, measured with Cobas Integra 400 automated analyzer (Roche Diagnostics, Burgess Hill, UK) using relevant kits according to manufacturer's instructions.

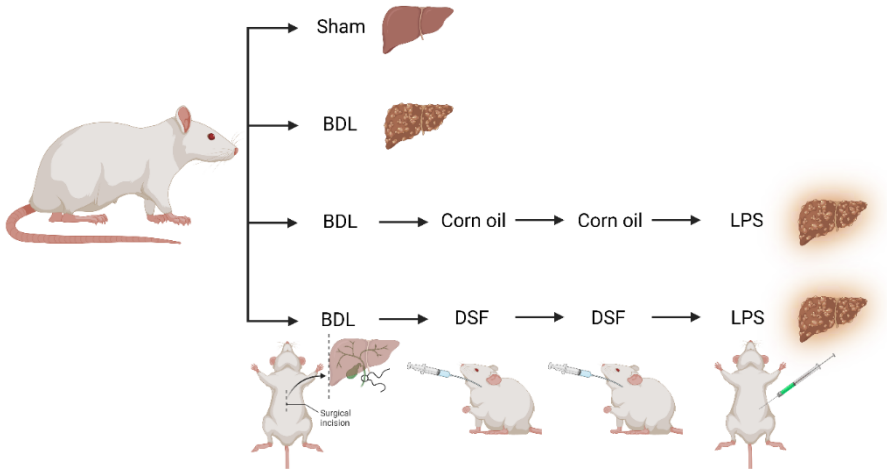

Figure 20: Rat bile duct ligation model.

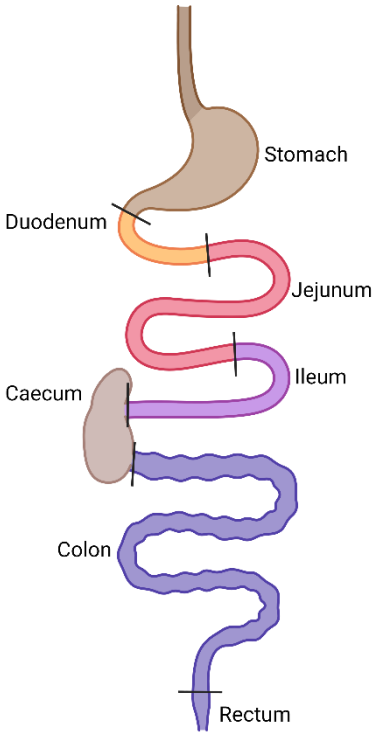

Figure 21: Proximal (stomach) to distal (rectum) anatomy drawing of a rodent intestine.

2.1.5 Mouse bile duct ligation

Mice were sham operated (control) and double bile duct ligated for 2 weeks (cholestatic cirrhosis). Mice were additionally gavaged with 10% DMSO in corn oil every day for 4 days leading up to sacrifice or 40mg/kg Disulfiram dissolved in 10% DMSO in corn oil (treatment) every day for 4 days leading up to sacrifice. The mice model was performed by Ms. Abeba Habtesion, Ms. Andrea Krstevski, and Dr. Ugo soffientini at the Royal Free BSU.

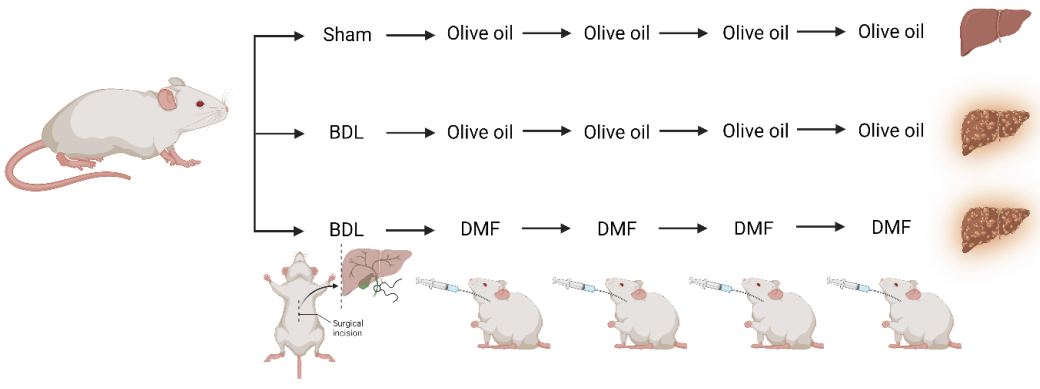

Figure 22: Mouse bile duct ligation model.

2.2 In vitro

2.2.1 Cell culture

The subcutaneous CCl4 cirrhosis mice and BDL cholestatic cirrhosis rat *in vivo* models of liver cirrhosis and cholestatic liver cirrhosis were used to analyse pathways in the intestinal epithelium, however *in vitro* models of the intestine are better suited to analyse the effect of specific insults/treatments on the epithelium and/or determine the causality of pathway activation/inhibition on the epithelium. Commonly, caco-2 and HCT-116 cell lines are used as an *in vitro* model for the intestine [240][241]. These cell lines are intestinal epithelial cells derived from a colorectal adenocarcinoma (caco-2) and colorectal carcinoma (HCT-116). These cell lines can be used for high-throughput screening of compounds/insults, for instance caco-2 cells are commonly used to investigate permeability via a Transwell grown caco-2 monolayer, and cell death is easily assessable on 2D cell cultures[242]. However, these cell lines do not model some key aspects of the intestine epithelium. Caco-2 and HCT-116 cell lines lack the various other cell types present in the intestinal epithelium, i.e. Goblet cells, Paneth cells, Enteroendocrine cells, Stem cells, and Tuft cells, as well the crypt and villi structure of the intestine [243].

Caco-2 and HCT-116 cells were cultured with standard culture methods. Cells were cultured in sterile tissue culture treated flask for cell passaging and maintenance, with 20% FBS for Caco-2 and 10% FBS for HCT-116 in DMEM, 100/100U/ml Penicillin/Streptomycin at 37C with 5% CO_2. Passage cells after reaching confluency ~80-90%. Discard media, disassociate cells by adding pre-warmed Trypsin solution (0.25% Trypsin & 1mM EDTA in Hank's balanced salt solution) to cover the cells, incubate at 37C with 5% CO_2 for 5 minutes and resuspend cells with pre-warmed complete growth media. Centrifuge cells at 500g for 5 minutes, remove supernatant and resuspend cells in fresh pre-warmed complete growth media, and plate in flasks for passaging or in cell culture treated well plates for experiments at ~20-40% confluency.

2.2.2 Organoid derivation and culture

Organoids derived from intestinal crypts do contain the various cell types that are present in the intestine epithelium and form into a 3D budding spheroid that organises into crypt and villi –like structures, as shown in **Figure 23** [244]. Intestinal stem cells inside the isolated intestine crypts proliferate and differentiate, similarly to the intestine, to form the intestinal organoid, while maintaining stemness [244]. These cells form an intact monolayer with the apical side inward and basolateral side outward, creating the lumen inside the intestinal organoid. Cells proliferated from the stem cells are pushed up the villi and dying cells at the top of the villi are extruded out into the lumen of the organoid, while maintaining an intact monolayer [245]. Small intestinal derived

organoids with intestinal organoid media and colon derived organoids with colon organoid media differ in phenotype with intestinal organoids forming a budding spheroid whereas colon organoids balloon [244]. The characteristic of an intact monolayer, morphology, and cell composition similar to the intestine makes intestinal organoids a suitable model to study the intestinal epithelium *in vitro*. Although this project has a focus on the colon, intestinal organoids with their budding structure more similar to villi and crypts, as well as the larger sample length of the small intestine compared to the colon made intestinal organoids better suited for this project.

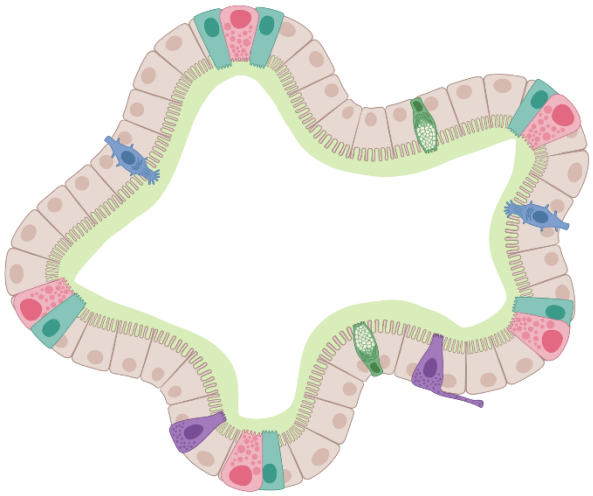

Figure 23: Illustration showing the structure and cell variety of an intestinal organoid.

I used intestinal organoids to study the effect of inflammasome, UPR, and stem-ness inducers/inhibitors on permeability, cell death, and growth. Permeability was determined with a permeability assay that I developed specifically for this project [1], cell death with LDH release and/or propidium iodide staining [246], and growth by the size of the organoids after incubation [247]. By measuring permeability in intestinal organoids, the direct effect of inflammasome, UPR, and stem-ness activation/inhibition on intercellular junctions can be examined. Additionally, the effect on intestinal epithelial cell viability of these pathways can be determined with LDH release and propidium iodide staining. Lastly, by analysing organoid growth the cell renewal capabilities of stem cells are examined, which is needed to replenish the epithelium. Intracellular junctions, cell viability, and cell renewal are key factors in order to maintain the homeostasis of an intact epithelial monolayer [139], [150], [166]. Thus, by measuring the effect of inflammasome, UPR, and stemness activation/inhibition on intestinal organoid permeability, cell death, and growth the intestinal epithelial integrity can be examined.

Derive mouse intestinal organoids from small intestine [244]. Dissect and isolate mouse small intestine (minimal 5cm) and remove binding tissue. Flush the small intestine tube with ice cold PBS.

Cut open the intestine longitudinally and scrape off left over stool and villi with a glass superfrost slide. Cut the intestine into one-centimetre pieces into a 50ml falcon tube with ice cold PBS. Gently wash the intestinal pieces 5 times with fresh ice cold PBS and replace PBS with 30ml of 2mM EDTA in PBS and incubate rotating at 4C for 30 minutes. Replace 2mM EDTA in PBS with fresh ice cold PBS. Vigorously shake for 5 seconds and strain supernatant through 70µm cell strainer into a falcon tube. Analyse droplet of the strained supernatant for high crypt to debris ratio, add fresh PBS to intestinal pieces and repeat shaking and straining step to create 2nd fraction, repeat until high crypt to debris ratio is obtained. Centrifuge best fraction at 500g for 3 minutes and discard supernatant. Resuspend crypt cell pellet in Matrigel to plate 30µl domes at roughly 100 crypt cell clumps per dome, 1 dome in 24 well plate, 4 domes in 12 well plate, or 8 domes in 6 well plate per well. Incubate the plate at 37C with 5% CO_2 for 15 minutes to stiffen the Matrigel. Afterwards add intestinal organoids medium with Y-27632 (500µl for 24 well plate, 1ml for 12 well plate, and 2ml for 6 well plate) for 7-10 days with fresh medium every 3-4 days to grow the organoids. Afterwards passage organoids every week. Remove media from well and disrupt organoid dome by resuspending vigorously with ice cold PBS. Transfer suspension to falcon tube and rinse the well once with fresh ice cold PBS and transfer to the falcon tube to collect stuck organoids. Centrifuge falcon tube at 500g for 3 minutes and discard supernatant. Resuspend crypt cell pellet in Matrigel to plate 30µl domes at roughly 100 crypt cell clumps per dome, 1 dome in 24 well plate, 4 domes in 12 well plate, or 8 domes in 6 well plate per well. Incubate the plate at 37C with 5% CO_2 for 15 minutes to stiffen the Matrigel. Afterwards add intestinal organoids medium (with Y-27632 for initial couple passages) (500µl for 24 well plate, 1ml for 12 well plate, and 2ml for 6 well plate) for 7 days with fresh medium every 3-4 days to grow the organoids.

Mouse intestinal organoid medium: DMEM/F12 (1:1) + L-Glutamine + 15mM HEPES (Gibco 11330-032), 100/100 U/ml Penicillin/Streptomycin, 1x N2 supplement (ThermoFisher 17502-048), 1x B27 supplement (17504-044), 1mM N-Acetylcysteine (Sigma-Aldrich A9165-5G), 50ng/ml mEGF (Peprotech 315-09), 100ng/ml mNoggin (Peprotech 250-38), 1µg/ml hR-Spondin-1 (Peprotech 120-38). For the initial culture and first few passes of mouse derived intestinal organoids add Rock inhibitor Y-27632 (Peprotech 1293823) to the medium at a final 10µM concentration.

Alternative intestinal organoid medium: 1:2:7 ratio of Noggin CM: R-Spondin-1 CM: DMEM/F12 with final concentration of 100/100 U/ml Penicillin/Streptomycin, 1x N2 supplement, 1x B27 supplement, 1mM N-Acetylcysteine, and 50ng/ml mEGF. Compare this alternative mouse intestinal organoid medium to the mouse intestinal organoid medium with recombinant R-Spondin-1 and Noggin on intestinal organoids for organoid growth and health.

Create R-Spondon-1 and Noggin conditioned medium [248]. Culture 293T-HA-RSpo1-Fc and HEK293-mNoggin-Fc cells in 10% FBS in DMEM (P/S) with selection antibiotic, 300µg/ml Zeocin for R-Spondin and 500µg/ml G418 for Noggin producing cells. Plate cells in a T-175 flask with 50ml 10% DMEM (P/S) media (without selection antibiotic) until roughly 60% confluency. Replace media with 50ml DMEM/F12 (P/S). After 5-7 days collect conditioned media. Centrifuge to pellet cells and filter supernatant through a 0.2µm filter and store conditioned media at -20C.

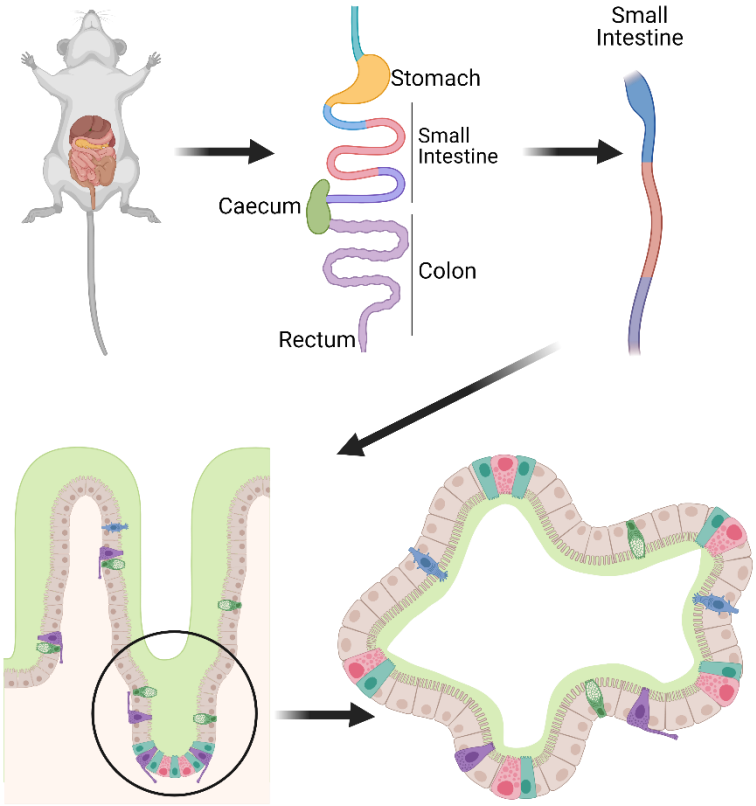

Figure 24: Method to derive intestinal organoids from mouse small intestine crypts.

2.2.3 Organoid cell death, permeability, and size assay

After treatment on plated mouse intestinal organoids in Matrigel, add HOECHST and Propidium Iodide to the media at 5µg/ml final concentration of both HOECHST and Propidium Iodide. Incubate for 30-60 minutes at 37C with 5% CO_2. Set Cytation 5 temperature to 37C and image organoids at fluorescent DAPI (HOECHST), GFP (green background autofluorescence), and RFP (Propidium Iodide) channels as a Z stack. Open fluorescence images in Fiji/Image J (with SCF plug-in, segmentation, interactive wand tool 2D). Z-project image stacks (Max intensity) of DAPI, GFP, and RFP channels. In the Z projected DAPI channel select the organoid with the wand tool and measure pixel area for the size of the organoid. In the Z projected RFP channel paste the organoid selected region (Control+Shift+E) and measure the intensity (Mean gray value) for the cell death in the organoid. In the Z projected GFP channel select the organoid green fluorescent lumen with the wand tool, paste

the lumen selected region in the Z projected RFP channel and measure the intensity for the stained dead cells in the organoid lumen as a marker for permeability.

2.3 Protein

2.3.1 Protein isolation tissue and cell culture

Protein was isolated from tissue with RIPA. Add beads, ~5mm tissue, and 500µl PBS to screw cap Eppendorf tubes. Homogenize sample with a bead-base homogenizer. Centrifuge for 15 minutes at 16,000g at 4C to pellet beads and non-homogenised tissue and collect supernatant. Transfer 200µl supernatant to new tube and resuspend with 100µl 3 times concentrated RIPA with proteinase inhibitor. Aliquot and store protein mixture at -80C.

Protein was isolated from cell culture with RIPA. Collect supernatant cell media from cell culture plate, centrifuge for 5 minutes at 500g, store supernatant, and resuspend cell pellet (floating and dead cells) with RIPA (same volume as media). Collect RIPA mixture and resuspend adherent cells in the cell culture plate with RIPA mixture. Aliquot and store protein mixture at -80C.

2.3.2 Western blot

BCA assay cell lysate to measure protein concentration. Add 12.5µl BSA standard (2000, 1000, 500, 250, 125, 0µg/ml) and 5x diluted sample to 96 wells plate. Add 200µl reaction mix to standard and samples (50:1 Bicinchonic acid: 4% cupric sulphate) and incubate for 1 hour at 37C or 2 hours at RT. Measure wavelength at 562nm to measure concentration and 450nm to remove background. Calculate concentration according to standard curve.

Prepare samples for western blot by mixing sample, ddH2O, DTT, loading buffer for equal protein concentration per sample, 200mM DTT, 1x loading buffer. Incubate at 95C for 5 minutes, centrifuge, and load ladder and samples in the gel according to manufactures gel loading volume. Run gel at 140 Volts for 1 hour at 500 milliamps maximum.

Transfer proteins to PVDF membrane. Place cassette, sponge, blotting paper (wetted in transfer buffer), gel, wetted PVDF membrane (wetted in methanol then transfer buffer), blotting paper (wetted in transfer buffer), sponge, and cassette into tank with transfer buffer. Run at 90 Volts for 90 minutes at 500 milliamps maximum. Wash membrane with PBS-T, block in 5% milk in PBS-T, incubate primary antibody in 5% milk in PBS-T overnight at 4C, wash membrane with PBS-T at RT (3x 5 minutes), incubate secondary antibody in 5% milk in PBS-T for 1 hour at RT, wash membrane with PBS-T at RT (3x 5 minutes), add western blot substrate and image blot with Bio-Rad ChemiDoc. Analyse bands with Image Lab, Densitometry tools.

Table 2: Western blot antibodies. *Target species mus musculus.*

Antibody	Company	Cat#	Dilution
Tubulin	Cell Signaling	2144S	1:3000
GAPDH	Biorbyt	Orb555879	1:5000
PPIB	Biorbyt	Orb252737	1:5000
TBP	Biorbyt	Orb128814	1:3000
Histone H3	Biorbyt	Orb256595	1:1000
COX IV	Biorbyt	Orb382539	1:2000
ACTB	Protein tech	66009-1-Ig	1:2000
Casp-1	Fisher	15278187	1:2000
Cleaved Casp-1	Novus	NBP1-45433	1:1000
Casp-11	Abcam	Ab180673	1:2000
Cleaved Casp-11	Abcam	Ab180673	1:2000
GSDMD	Abcam	Ab219800	1:2000
Cleaved GSDMD	Abcam	Ab219800	1:2000
IL-1beta	Novus	NB600-633	1:1000
Cleaved IL-1beta	Novus	NB600-633	1:1000
IL-18	Novus	NBP3-03699	1:1000
Cleaved IL-18	Novus	NBP3-03699	1:1000

2.3.3 Promega LDH-Glo cytotoxicity assay

Use Promega LDH-Glo cytotoxicity assay according to Promega's instructions. Dilute lactate dehydrogenase standard (1000 U/ml stock). 2.5µl stock in 778.75 buffer (200mM Tris-HCl pH7.3 + 10% glycerol + 1% BSA) to 3.2 U/ml. 10µl 3.2 U/ml in 490µl buffer to 64 mU/ml. Use 250µl buffer to dilute to 32, 16, 8, 4, 2, 1, 0.5, 0 mU/ml.

Add 40µl of standard and 40µl of diluted sample (pre-test dilution) to 96 well plate. Add 40µl of reaction solution (40µl detection mix + 0.2µl substrate) per well. Read at 520 nm after 1 hour incubation at RT.

2.3.4 Invivogen HEK-Blue IL-1beta reporter cells

Use HEK-Blue IL-1beta reporter cells according to Inivogen's instructions to mease IL-1beta. Prepare a cell suspension of HEK-Blue IL-1beta reporter cells at $3x10^5$ cells/ml in test media (DMEM, 4.5g/l glucose, 2mM L-glutamine, 10% FBS, 100/100 U/ml Penicillin/Streptomycin). Add 50µl test sample (conditioned media) and 150µl HEK-Blue IL-1beta reporter cell suspension to a cell culture treated flat-bottom 96-well plate and incubate overnight at 37C with 5% CO_2. Prepare QUANTI-Blue solution

(1ml QB reagent, 1ml QB buffer, 98ml ddH_2O). Add 180µl of QUANTI-Blue solution and 20µl conditioned media from treated HEK-Blue IL-1beta reporter cells in a flat-bottom 96-well plate, incubate at 37C for 30min – 3 hours. Determine SEAP levels using a spectrophotometer at 620-655nM and analyse IL-1beta in conditioned media.

2.4 RNA

2.4.1 RNA isolation tissue and cell culture

RNA from tissue was isolated with TRIzol. Add beads, ~5mm tissue, and 1ml TRIzol to screw cap Eppendorf tubes. Homogenize sample with a bead-base homogenizer. Centrifuge to pellet beads and non-homogenised tissue and collect supernatant. Incubate for 5 minutes at RT, add 100µl bromo-3-chloropropane per 1 ml TRIzol used, and vigorously shake for 15 seconds. Incubate sample for 2-15 minutes at RT and centrifuge 15 minutes at 16,000g at 4C, which creates 3 layers: a bottom red organic layer (protein), an interlayer (DNA), and an upper colourless aqueous layer (RNA). Collect the RNA layer and transfer ~450µl to a new tube, resuspended with 500µl 2-propanol (per 1ml TRIzol), and incubated for 5-10 minutes at RT. Centrifuge at 16,000g for 10 minutes at 4C, discard the supernatant, and wash the RNA pellet with 1ml 75% ethanol. Centrifuge at 7,500g for 5 minutes at 4C and discard supernatant. Dry RNA pellet for 5-10 minutes, and resuspend RNA pellet in 50µl ddH2O, and store at -80C.

RNA from cell and organoid culture was isolated with Monarch Total RNA Miniprep Kit according to manufacturer's instructions. Resuspend cell/organoid pellet with 400µl RNA lysis buffer and transfer to gDNA removal columns. Centrifuge for 30 seconds at 16,000g and resuspend the flow through with 400µl ethanol. Transfer mixture to RNA purification column, centrifuge for 30 seconds at 16,000g, and discard flow through. Add 500µl RNA wash to column, centrifuge for 30 seconds at 16,000g, and discard flow through. Add 80µl DNase mixture (5µl DNase I with 75µl DNase I reaction buffer) on column and incubate for 15 minutes at RT. Add 500µl RNA priming buffer, centrifuge for 30 seconds at 16,000g, and discard flow through. Add 500µl RNA wash buffer, centrifuge for 30 seconds at 16,000g, and discard flow through. Add 500µl RNA wash buffer, centrifuge for 120 seconds at 16,000g, and discard flow through. Add column to a new tRNase-free tube, add 80µl nuclease -free water to the column, and centrifuge for 30 seconds at 16,000g.

Analyse RNA concentration using Nanodrop and normalise samples for cDNA synthesis for equal concentrations in experiments.

2.4.2 cDNA synthesis

Use Qiagen cDNA synthesis kit according to Qiagen's instructions to synthesise cDNA. Add 10µl first trand master mix (2x), 3µl oligo dT primer / random hexamer primer (0.1µg/µl), 1µl AffinityScript RT / RNase block enzyme mix, and 6µl of RNA sample (0.3pg – 3µg) in ddH2O to PCR reaction tubes. Incubate 15 minutes at 25C, 15 minutes at 42C, 5 minute at 95C, and store on ice (short term) or -20C.

Alternatively, use Thermo Scientific RevertAid First Strand cDNA Synthesis kit according to Thermo Scientific instructions. Add 1µl Oligo dT primer / random hexamer primer, 4µl 5x reaction buffer, 1µl RiboLock RNase inhibitor (20U/µl), 2µl dNTP mix (10mM), 1µl RevertAid M-MuLV RT (200U/µl), and 11µl of RNA sample (0.1ng – 5µg) in ddH2O to PCR reaction tubes. Incubate for 60 minutes at 42C, 5 minutes at 70C, and store on ice (short term) or -20C.

2.4.3 qPCR

Analyse gene expression with qPCR. Add 5µl SYBR green qPCR master mix, 0.5µl Fw primer (4µM), 0.5µl Rv primer (4µM), and 4µl of cDNA in ddH2O (1:10 – 1:100 diluted) in qPCR plate. Centrifuge for 1 minute at 1000rpm, and run qPCR program on AriaMX qPCR: Hot start 3 minutes at 95C, Amplification 50x 5 seconds at 95C followed by 10 seconds at 60C, and Melt 30 seconds at 95C, 30 seconds at 65C, 30 seconds at 95C. Analyse qPCR data with Agilent AriaMx software according to software instructions.

Table 3: qPCR primers. *Target species mus musculus (m) and human (h).*

Target:	Forward primer:	Reverse primer:
mACTB	CATTGCTGACAGGATGCAGAAGG	TGCTGGAAGGTGGACAGTGAGG
mCOX	TCATTGGCTTCACTGCGCTCGT	TCCAGCATTCGCTTGGTCTGCA
mH3	ACAAAAGCCGCTCGCAAGAGTG	TTCTCGCACCAGACGCTGAAAG
mTBP	CTACCGTGAATCTTGGCTGTAAAC	AATCAACGCAGTTGTCCGTGGC
mGAPDH	CTTAAGAGGGATGCTGCCCTTACCC	GCGCCCAATACGGCCAAATCC
mPPIB	AGGACTTCATGATCCAGGGTGGAGA	TGGTGTCTTTGCCTGCATTGGC
mNRLP12	GGGACAAGGGAGGCTTGGCT	CAAAGGGCACGCTGATTGGCT
mNLRP3	ACAATGCCCTGGGGGACTTTGG	TGGAGCTCAGAACCAATGCGAGA
mCasp-1	ACCTGGCAGGAATTCTGGAGCTT	AGGGTCCCAGTCAGTCCTGGAAA
mCasp-11	CCTACCGAGACAAAACAGGAGGCT	GCCCGATCAATGGTGGGCATC
mIL-1b	AGCTGAAAGCTCTCCACCTCAATGG	CAGGGTGGGTGTGCCGTCTT
mIL-18	GCCGACTTCACTGTACAACCGC	CAGTCTGGTCTGGGGTTCACTGG

mGSDMD	TGCTCCCGGGTTGAGCAGAC	ATCGCCTCTGCTGCCGCTTA
mGRP78	TTGGAGGTGGGCAAACCAAGACA	TTGGTTGCTTGTCGCTGGGC
mXBP1s	GGTCTGCTGAGTCCGCAGCAGG	CTGGGTAGACCTCTGGGAGTTCCTC
mXBP1u	AGAAAGCCCGGATGAGCGAGC	CCTGCTGCAGAGGTGCACATAGT
mCHOP	ATGTTGAAGATGAGCGGGTGGCA	GCAGGGACTCAGCTGCCATGA
mLyz1	GGAATGGATGGCTACCGTGGTGT	TGCCATCATTACACCAGTATCGGCT
mSI	TGGGGAGGACACTGGTTGGGA	CATCCAACGAGCACAGAGGTGGT
mKrt20	ACCTACCGCCGCCTTCTGGA	ACACGACCTTGCCGTCTACCAC
mMuc2	AGGCACCACAAAGTTTGCCCCT	TTCCACCCTCCCGGCAAACA
mCHGA	AGACAGTGTGGAGGCCCGAAG	TCATCCCCGCCGCAAAGCC
mKi67	CCTGTGAGGCTGAGACATGGAGAC	ACCTTCCCCATCAGGGTCAGCA
mLgr5	GATGCGATACCGCGGGGCT	AGGAGACTGGCGGGTAGCTGA
mOLFM4	GCTCTGCCTCCCGGACAACT	GCAGGTCCCATGGCTGTCCA
mAHR	CTGGTTGTCACAGCAGATGCCT	CGGTCTTCTGTATGGATGAGCTC
mCYP1A1	CATCACAGACAGCCTCATTGAGC	CTCCACGAGATAGCAGTTGTGAC
mCYP1B1	GCCACTATTACGGACATCTTCGG	ACAACCTGGTCCAACTCAGCCT
mOCL	TGGCAAGCGATCATACCCAGAG	CTGCCTGAAGTCATCCACACTC
mCLA	GGACTGTGGATGTCCTGCGTTT	GCCAATTACCATCAAGGCTCGG
mTJP	GTTGGTACGGTGCCCTGAAAGA	GCTGACAGGTAGGACAGACGAT
hGRP78	TCATCGGCCGCACGTGGAAT	AGCAAATGTCTTTGTTTGCCCACCT
hXBP1s	GGTCTGCTGAGTCCGCAGCAGG	GGGCTTGGTATATATGTGG
hXBP1u	AGTGAGCTGGAACAGCAAGTGGT	TGCTGCAGAGGTGCACGTAGT
hCHOP	GGTGGCAGCGACAGAGCCAAA	CAGCTGCCATCTCTGCAGTTGGA
hRPLP0	GCCGTGATGCCCAGGGAAGA	TTCCCGCGAAGGGACATGCG

2.5 Histology

2.5.1 Whole organoid staining

Fix whole organoids in Matrigel domes by adding 4% formaldehyde to fully cover the organoids without dislocating them. Incubate for 15-30 minutes at RT, discard 4% formaldehyde, wash organoids twice with PBS (without dislocating them), and incubate organoids in PBS-T (0.5% Tween-20 in PBS) for 1 hour at RT. Discard PBS and incubate with HOECHST and Phalloidin in PBS (5µg/ml HOECHST + 1:1000 Phalloidin-iFluor 647 in PBS) for 2 hours at RT. Replace HOECHST and Phalloidin in

PBS with PBS and image organoids with Cytation 5, fluorescence channel DAPI (HOECHST) and Texas-Red (Phalloidin-iFluor 647).

2.5.2 Organoid embedding

Embed and section intestinal organoids for antibody staining [249]. Fix whole organoids in Matrigel domes by adding 4% formaldehyde to fully cover the organoids without dislocating them. Incubate for 15-30 minutes at RT, discard 4% formaldehyde was organoids twice with PBS (without dislocating them). Dislocate organoids with cold PBS and transfer organoids to 50ml falcon tube. Centrifuge organoids at 500g for 5 minutes and discard supernatant. Resuspend organoids in 2% agarose in water (melted with microwave), centrifuge at 500g for 5 minutes, and cool on ice to harden the agarose. Collect agarose embedded organoids from tube. Agarose embedded organoids, can now be used as tissue for formalin fixation and paraffin embedding.

2.5.3 Tissue formalin fixation, paraffin-embedding, and sectioning

Add freshly dissected tissue to 10% formalin pots for 1-7 days at RT. Wash tissue three times with PBS, and dehydrate tissue through 70%, 80%, 95%, and 3 changes of 100% ethanol incubations for 1 hour each at RT. Clear tissue through 2 changes of xylene incubations for 1 hour each at RT. Immerse tissue in paraffin, for 1 hour at 37C, and embed tissue in paraffin blocks. Store paraffin embedded tissue blocks at RT.

Section formalin fixed, paraffin-embedded (FFPE) tissue with microtome at 5-8µm thickness. Float 5-8µm thick paraffin slice on 40C ddH_2O and transfer paraffin slice onto SuperFrost glass slides for staining.

2.5.4 Antibody staining

Remove paraffin by immersing in HistoClear 2 times 5 minutes at RT. Rehydrate by immersing 2 times in 100% ethanol 3 minutes, 95% 3 minutes, 80% 3 minutes, 70% 3 minutes, 50% 3 minutes, 0.85% NaCl 5 minutes, and PBS 5 minutes. Antigen retrieve and permeabilise in 95C Tris-EDTA buffer (10mM Tris, 1mM EDTA, 0.1% Tween-20, pH9), EDTA buffer (1mM EDTA, 0.1% Tween-20, pH8), or sodium citrate buffer (10mM sodium citrate, 0.1% Tween-20, pH6) for 30 minutes. Wash 3 times with PBS for 5 minutes. Remove excess liquid and cover section with 100µl blocking solution (5% BSA in PBS) with coverslip and incubate for 1 hour at RT in a humidified chamber. Remove coverslip and wash with PBS for 5 minutes. Remove excess liquid and cover section with 100µl primary antibody solution (primary antibody in 5% BSA in PBS) with coverslip and incubate for 1 hour at RT in a humidified chamber. Remove coverslip and wash with PBS for 5 minutes. Remove excess liquid and cover section with 100µl secondary antibody solution (secondary antibody in 5% BSA in PBS) with coverslip and incubate for 1 hour at RT in a dark humidified chamber (keep dark from now on to

prevent bleaching). Remove coverslip and wash with PBS for 5 minutes. Remove excess liquid, add mounting solution, seal slide with coverslip, and let dry at RT in the dark overnight.

Table 4: Immunohistochemistry antibodies. *Target species mus musculus.*

Antibody	Company	Cat#	Dilution
Ki67	R&D systems Biotechne	AF7649	10µg/ml
Lysozyme	Novus	NBP2-61118	2µg/ml
CHGA	Novus	NB120-15160	1:100
Villin	Novus	NBP2-75707	1:500
Muc2	Novus	NBP1-31231	1:500
Phalloidin-iFluor 647	Abcam	Ab176759	1:1000
HOECHST 33342	Fisher	H3570	5µg/ml
GT anti RB 488	Biorbyt	Orb347687	1:1000
DK anti SH Texas-Red	Biorbyt	Orb347956	1:1000

2.5.5 Abcam TUNEL Assay Kit – BrdU-Red

Remove paraffin by immersing in HistoClear 2 times 5 minutes at RT. Rehydrate by immersing 2 times in 100% ethanol 3 minutes, 95% 3 minutes, 80% 3 minutes, 70% 3 minutes, 50% 3 minutes, 0.85% NaCl 5 minutes, and PBS 5 minutes. Antigen retrieve and permeabilise in 95C Tris-EDTA buffer (10mM Tris, 1mM EDTA, 0.1% Tween-20, pH9) for 30 minutes. Wash 3 times in PBS for 5 minutes. Remove excess liquid and cover section with 100µl wash buffer with coverslip and incubate for 5 minutes at RT, remove coverslip and repeat once. Remove coverslip and excess liquid and cover slide with 50µl DNA labelling solution (TdT reaction buffer 10µl, TdT Enzyme 0.75µl , Br-dUTP 8µl, ddH2O 32.25µl) with coverslip and incubate at 37C in a dark humidified chamber for 1 hour. Remove coverslip and wash 3 times with PBS for 5 minutes. Remove excess liquid and cover slide with 100µl antibody solution (anti-BrdU-Red antibody 5µl, rinse buffer 95µl) with coverslip and incubate at RT in the dark for 30 minutes. Remove coverslip and wash with PBS for 5 minutes. Remove excess liquid and cover slide with 100µl counterstain (HOECHST (5mg/ml) 1µl, ddH2O 99µl) with coverslip and incubate for at RT in the dark for 30 minutes. Remove coverslip and wash with PBS for 5 minutes. Remove excess liquid, add mounting solution, seal slide with coverslip, and let dry at RT in the dark overnight.

2.5.6 Promega DeadEnd Fluorometric TUNEL system

Remove paraffin by immersing in HistoClear 2 times 5 minutes at RT. Rehydrate by immersing 2 times in 100% ethanol 3 minutes, 95% 3 minutes, 80% 3 minutes, 70% 3 minutes, 50% 3 minutes, 0.85% NaCl 5 minutes, and PBS 5 minutes. Antigen retrieve and permeabilise in 95C Tris-EDTA buffer

(10mM Tris, 1mM EDTA, 0.1% Tween-20, pH9) for 30 minutes. Wash 3 times in PBS for 5 minutes. Remove excess liquid and cover section with 100µl equilibration buffer with coverslip and incubate for 5-10 minutes at RT. Remove coverslip and excess liquid and cover slide with 50µl TdT reaction mix (equilibration buffer 45µl, nucleotide mix 5µl, rTdT enzyme 1µl, HOECHST (5mg/ml) 1µl) with coverslip and incubate at 37C in a dark humidified chamber for 1 hour. Remove coverslip stop reaction by immersing in 2x SSC at RT for 15 minutes. Wash 3 times with PBS for 5 minutes. Remove excess liquid, add mounting solution, seal slide with coverslip, and let dry at RT in the dark overnight.

2.5.7 Polysciences Picrosirius Red Stain Kit

Remove paraffin by immersing in HistoClear 2 times 5 minutes at RT. Rehydrate by immersing 2 times in 100% ethanol 3 minutes, 95% 3 minutes, 80% 3 minutes, 70% 3 minutes, 50% 3 minutes, 0.85% NaCl 5 minutes, and PBS 5 minutes. Immerse in Solution A for 2 minutes, wash in ddH2O for 5 minutes, immerse in Solution B for 60 minutes, immerse in Solution C for 2 minutes, and immerse in 70% ethanol for 45 seconds. Remove excess liquid, add mounting solution, seal slide with coverslip, and let dry at RT overnight. Image slides with bright field setting on Olympus microscope, and analyse images with FIJI/Image J for collagen stained area.

3 Are ER stress mediated intestinal inflammasome activation and pyroptotic cell death associated with cirrhosis?

3.1 Introduction

Cirrhosis can progress to acute decompensated cirrhosis (AD) and acute-on-chronic liver failure (ACLF), which are associated with increased mortality [21][22]. AD and ACLF are defined by the development of ascites, hepatic encephalopathy, gastrointestinal haemorrhages and/or bacterial infections, with additionally multi-organ injury and high 28-day mortality rate for ACLF, which leads to hospitalisation [22]–[24].

Cirrhosis progression has been explained with the PIRO (Predisposition, Injury, Response, Organ failure) concept [27]. The intestine has been identified as a source of PAMPs and DAMPs that can translocate to the portal vein and contribute to disease progression [118], [123]–[126].

Dysbiosis with overgrowth of prevalence of pathogenic bacteria, and reduced population of beneficial bacteria is associated with cirrhosis progression, leading to an increasingly pathogenic intestinal lumen [37], [38], [44], [45]. This is accompanied by a disruption of intestinal barriers in cirrhosis and a reduction in the number of intestinal Paneth cells and Goblet cells, which is associated with increased bacterial translocation [138][158]. Paneth cells and Goblet cells are key for the bacterial defence of the epithelial monolayer with antimicrobial protein secretion and mucus layer production respectively [122][148].

This intestinal pro-inflammatory immune response is recapitulated in the cirrhosis rat model, which is associated with epithelial junction disruption and bacterial translocation [156]. Decontamination of the intestine reduced this pro-inflammatory response and bacterial translocation, which shows the causality of the microbiome on these processes [156]. Furthermore, the intestinal microbiome in a cirrhosis mice model was shown to activate intestinal macrophages, which contributed to intestinal cell death, permeability and inflammation [157].

Bacteria and PAMPs from the pathogenic microbiome that translocate to the portal vein in cirrhosis cross the intestinal epithelial monolayer. Pyroptosis, driven by inflammasome activation, is an important innate immune response in intestinal epithelial cells in response to PAMPs and pathogenic bacteria. Expression of GSDMD, the pyroptosis executioner protein, is specifically localised epithelial cells, including the epithelium of the gastrointestinal tract [250]. GSDMD was shown to be increased in inflammatory bowel disease, while GSDMD deficiency showed beneficial effects in a colitis mice model [183]. Besides GSDMD mediated pyroptosis, GSDMD facilitated extracellular vesicle release containing GSDMD and IL-1beta in the colitis mice model [183].

Furthermore, our group has previously shown increased non-canonical inflammasome activation in livers from AD patients, which was correlated with MELD score and circulating markers of cell death [188]. Additionally, ER stress sensitised liver cells to pyroptosis, and caspase-11 deficiency protected cirrhotic mice from multi-organ [188]. However, our group did not study these processes in the intestine of cirrhosis patients or models.

ER stress has been shown to reduce stemness and self-renewal properties in the intestine [190]. Perpetual unfolded protein response increases susceptibility to colitis (condition with chronic inflamed intestine), and leads to an absence of Paneth cells and a decrease of Goblet cells, which is a feature of cirrhosis [138], [158], [228]. In cirrhosis, increased intestinal unfolded protein response (GRP78, ATF4, and CHOP expression), and decreased intestinal stemness (Lgr5, SOX-9, cMYC expression) and proliferation (Ki67 expression) were demonstrated by Liu *et al.* [194]. In their cirrhosis mice model (BDL) deficiency of CHOP (ER stress induced cell death transcription factor) reduced liver injury, inflammation, and IL-1beta and IL-18 expression [194]. Intestinal unfolded protein response was increased in cirrhosis mice, which is similar to their findings in cirrhosis patients [194]. Furthermore, CHOP deficiency in the cirrhosis model reduced intestinal permeability, IL-1beta expression, epithelial cell death, and normalised proliferating crypt cells, crypt length, and villi length [194].

The study from Liu *et al.*, thus indicates that intestinal ER stress leads to intestinal barrier disruption that could contribute to the disease in cirrhosis [194]. ER stress can sensitise cells for inflammasome activation and pyroptosis. The pro-inflammatory lytic cell death in response to PAMPs and DAMPs of pyroptosis makes it an attractive candidate for the cause of epithelial barrier injury [188]. However, activation of the inflammasome pathway and the effect of PAMPs on intestinal epithelial cells in cirrhosis remains unknown. Pyroptosis by inflammasome activation in intestinal epithelial cells could contribute to liver injury by exacerbating systemic inflammation by pro-inflammatory cytokine and DAMP release that can translocate to the liver. Therefore, I aimed to characterise intestinal inflammasome activation and ER stress sensitisation in cirrhosis.

3.2 Hypothesis and aims

Hypothesis: ER stress mediated intestinal inflammasome activation and pyroptotic cell death are associated with cirrhosis.

Aim 1: Characterise intestinal inflammasome activation in cirrhosis mouse models.
Aim 2: Characterise intestinal ER stress induction (UPR) in cirrhosis mouse models.
Aim 3: Determine synergy between ER stress and non-canonical inflammasome activation on

intestinal cell death.

Aim 4: Characterise intestinal ER stress induction (UPR) in cirrhosis patients.

3.3 Materials and Methods

I used two subcutaneous CCl4 cirrhosis mice models as previously described, **2.1.3 Mouse subcutaneous CCl4**. Our 12 week CCl4 administration model (olive oil, CCl4, CCl4 + LPS) was performed at the Institute for Liver and Digestive Health - UCL, whereas the 14,17 and 20 week CCl4 administration model was performed at the Laboratory of Hepatology – KU Leuven by the group of Schalk van der Merwe. Liver tissue from our 12 week model was formalin fixed, paraffin embedded, and sectioned according to **2.5.3 Tissue formalin fixation, paraffin-embedding, and sectioning.** Serum ALT, serum creatine, and liver collagen was determined as described **2.1.3 Mouse subcutaneous CCl4** and **2.5.7 Polysciences Picrosirius Red Stain Kit**. Liver collagen images, and serum ALP, AST, ALT, albumin and creatinine data from the 14, 17 and 20 week model, as well as colon tissue was shared by the group of Schalk van der Merwe, Laboratory of Hepatology – KU Leuven.

RNA was isolated from colon tissue of the mice models with TRIzol as previously described, **2.4.1 RNA isolation tissue and cell culture**. cDNA was synthesised according to **2.4.2 cDNA synthesis**, and quantified inflammasome pathway (NLRP12, NLRP3, Caspase-1, Caspase-11, IL-1beta, IL-18, and GSDMD), unfolded protein response (GRP78, XBP1s, XBP1u, and CHOP), and housekeeping (Beta-actin (ACTB), Cyclooxygenase (COX), Histone H3 (H3), TATA box binding protein (TBP), Glyceraldehyde-3-phosphate dehydrogenase (GAPDH), and Cyclophilin B (PPIB)) gene expressions with qPCR as described in **2.4.3 qPCR**.

Protein was isolated from colon tissue of the mice models with RIPA as previously described, **2.3.1 Protein isolation tissue and cell culture**. Inflammasome pathway (full length and cleaved Caspase-1, Caspase-11, GSDMD, IL-1beta, and IL-18) and housekeeping (alpha-Tubulin (Tub), GAPDH, PPIB, TBP, H3, and COX IV) protein levels were quantified with western blot, **2.3.2 Western blot**.

Caco-2 and HCT-116 cells were cultured, as previously described **2.2.1 Cell culture**, for tunicamycin / LPS treatments. Complete growth media was replaced from plated Caco-2 and HCT-116 cells in cell culture treated well plates when ~70% cell confluency was reached with serum free media with and without treatment of tunicamycin (ER stress inducer) and/or LPS (*Klebsiella pneumoniae*). For combination treatments, LPS was added to the serum free media at the final concentration for the treatment duration. Conditioned media was collected from treated Caco-2 and HCT-116 cells and quantified LDH release as previously described, **2.3.3 Promega LDH-Glo cytotoxicity assay**. Treated Caco-2 and HCT-116 cells were collected, RNA isolated, cDNA synthesised, and unfolded protein

response (GRP78, XBP1s, XBP1u, and CHOP) and housekeeping (RPLP0) gene expression quantified with qPCR, according to **2.4.1 RNA isolation tissue and cell culture**, **2.4.2 cDNA synthesis**, and **2.4.3 qPCR**.

Intestinal organoids were derived from mice, according to **2.2.2 Organoid derivation and culture**. Organoids were cultured for a week. RNA was isolated from the organoids and a part of the small intestine tissue, **2.4.1 RNA isolation tissue and cell culture**. cDNA was synthesised, **2.4.2 cDNA synthesis**, and intestinal epithelial cell markers (Lysozyme 1 (Lyz1), Sucrase-isomaltase (SI), Keratin 20 (Krt20), Mucin 2 (Muc2), Chromogranin A (CHGA), Ki-67, Leucine Rich Repeat Containing G Protein-Coupled Receptor 5 (Lgr5), Olfactomedin 4 (Olfm4)), and housekeeping (PPIB) genes were determined with qPCR, **2.4.3 qPCR**. Additionally, organoids were stained for polarity and cell types (Ki67, Villin, Lysozyme, Mucin 2, and CHGA). Whole organoids were stained as described in, **2.5.1 Whole organoid staining**, for polarity. Whole organoids were embedded, **2.5.2 Organoid embedding**, formalin fixed, paraffin embedded and sectioned, **2.5.3 Tissue formalin fixation, paraffin-embedding, and sectioning**, and stained with antibodies against Ki67, Villin, Lysozyme, Mucin 2, and CHGA, **2.5.4 Antibody staining**.

Mouse intestinal organoids from wild type (WT), Casp-11 KO, and Casp-1+11 KO mice were derived and cultured, as previously described **2.2.2 Organoid derivation and culture**, for tunicamycin / LPS. Mouse intestinal organoids were plated and cultured for 3 days, afterwards media was replaced with fresh mouse intestinal organoid media with or without tunicamycin / LPS. For some experiment media was replaced with fresh mouse intestinal organoid media with or without tunicamycin / LPS, incubated for the noted duration, and afterwards conditioned media collected (CM1) and replaced for another 24 hours with fresh mouse intestinal organoid media (CM2). Conditioned media were collected to quantify LDH with **2.3.3 Promega LDH-Glo cytotoxicity assay**, and IL-1beta with **2.3.4 Invivogen HEK-Blue IL-1beta reporter cells**. Organoid cell pellets were collected for RNA isolation, **2.4.1 RNA isolation tissue and cell culture**, cDNA synthesis, **2.4.2 cDNA synthesis**, and quantification of inflammasome pathway (caspase-1 and caspase-11), unfolded protein response (GRP78, XBP1s, XBP1u, and CHOP), and housekeeper (PPIB) gene expression with qPCR, **2.4.3 qPCR**.

Gene expression data from human healthy control and cirrhosis duodenum and colon biopsies was shared by the group of Schalk van der Merwe, Laboratory of Hepatology – KU Leuven. RNA was isolated, cDNA synthesised, and gene expression quantified with qPCR, as described in [154]. TaqMan probes for GRP78, XBP1s, XBP1u, CHOP and beta-Actin was used to quantify unfolded protein response in human intestinal biopsies.

3.4 Results

3.4.0 Characterise cirrhosis mouse models and housekeeping genes

To examine intestinal inflammasome activation and ER stress in cirrhosis I used a drug-induced liver cirrhosis model, with subcutaneous administration of CCl4 for 12 weeks [188][238]. LPS injection was administered to simulate a decompensation event [188]. To validate cirrhosis in our model, serum creatinine, serum ALT, and liver collagen were measured, **Figure 25**. Serum creatinine levels did not show a significant difference between any of the groups, **Figure 25**A. Serum ALT levels was increased in CCl4 and CCl4 + LPS treated mice compared to olive oil treated mice (control), **Figure 25**B. Furthermore, liver collagen was increased in CCl4 and CCl4 + LPS treated mice compared to control, **Figure 25**C,D. Additionally, colon samples from control and CCl4 subcutaneous CCl4 administrated mice for 14, 17 and 20 weeks were used. Liver collagen of control and 14 week CCl4 administered mice appeared similar to our control and 12 week CCl4 treated mice, respectively, with increasing collagen in 17 and 20 week CCl4 administration, **Figure 26**. Additionally, serum ALP, AST, ALT, albumin and creatinine were measured in 14 week and 19 week treated mice, **Figure 27**. At 14 week serum ALP was increased compared to control, but not serum AST, ALT, albumin or creatinine, **Figure 27**. Also at 19 weeks serum ALP was increased, while serum albumin was decreased. No differences were found in AST, ALT or creatinine at 14 or 19 weeks, **Figure 27**.

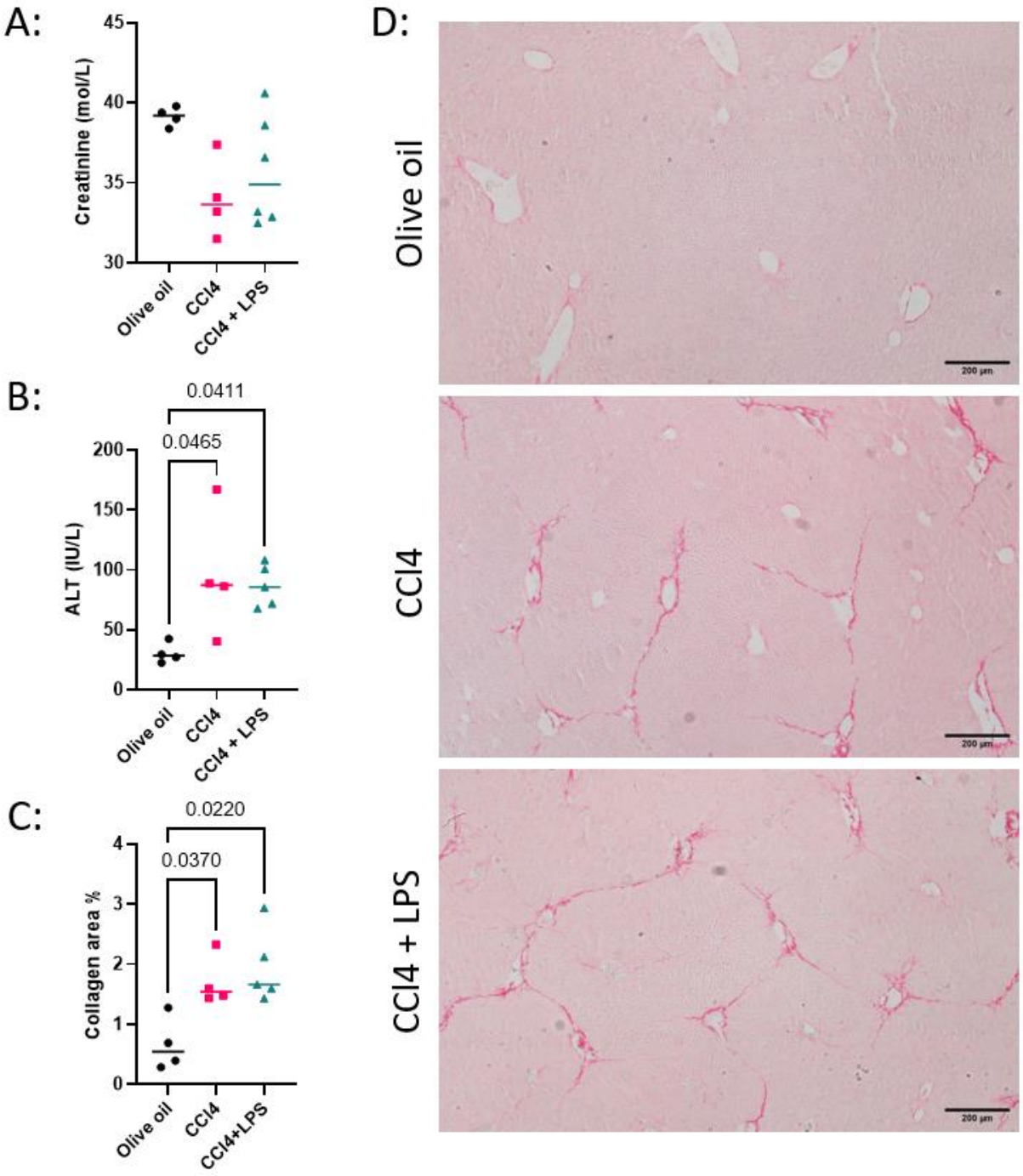

Figure 25: Subcutaneous CCl4 cirrhosis mice validation. *A: Serum creatinine and B: ALT levels, as well as C: liver collagen area % by picrosirius red stain was measured. D: Picrosirius red stained liver of representative samples from olive oil, CCl4, CCl4 + LPS groups. CCl4 (n=4) and CCl4 + LPS (n=6) groups were compared to olive oil (control, n=4); one-way ANOVA with Tukey's post hoc test; significance $p<0.05$.*

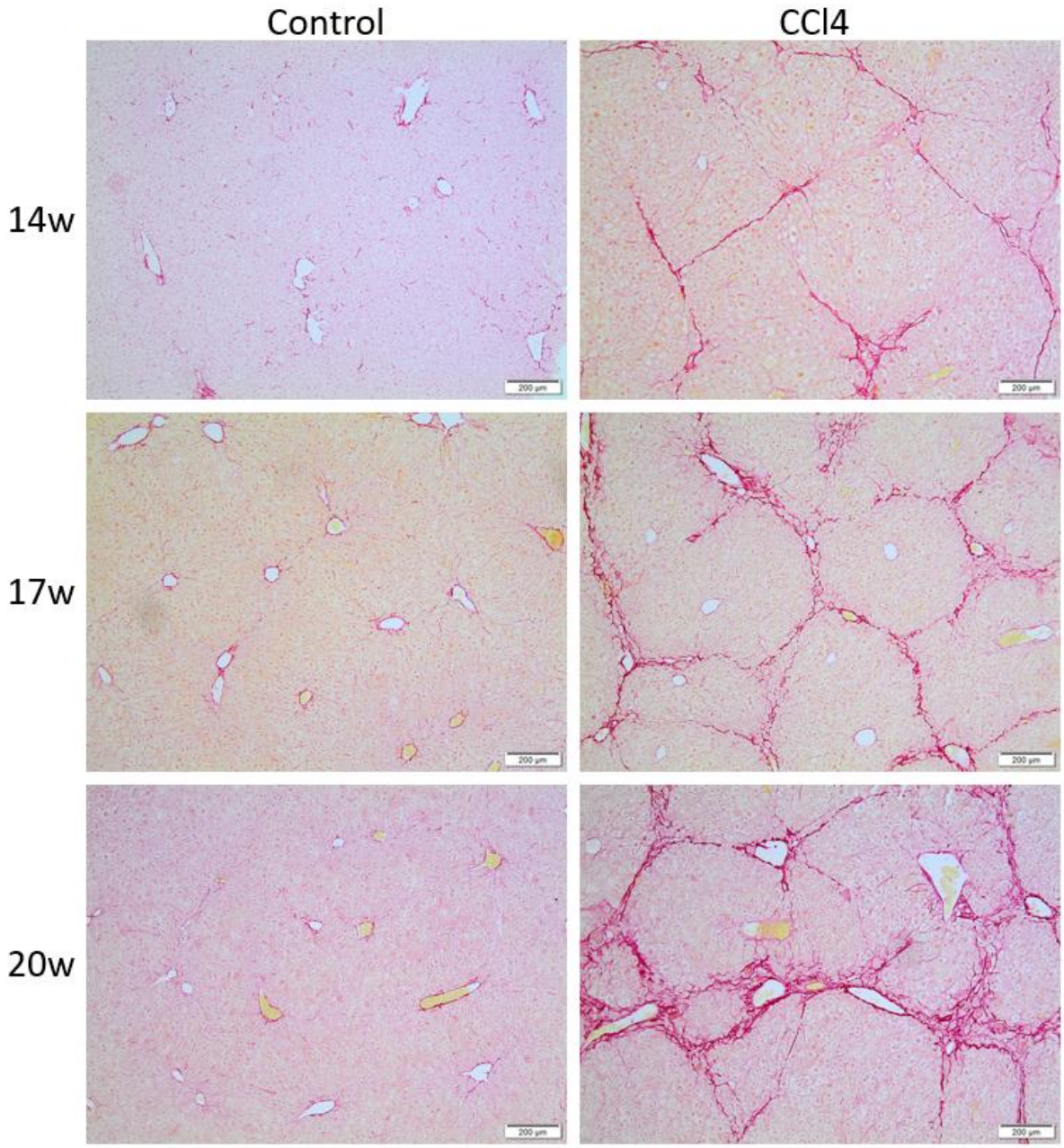

Figure 26: Subcutaneous CCl4 cirrhosis mice validation 14, 17 and 20 weeks administration, liver collagen stain.

Representative images of liver sections stained for collagen with sirius red stain of control and CCl4 treated mice 14, 17 and 20 week administration, by Lena Smets (Laboratory of Hepatology - KU Leuven, Schalk van der Merwe).

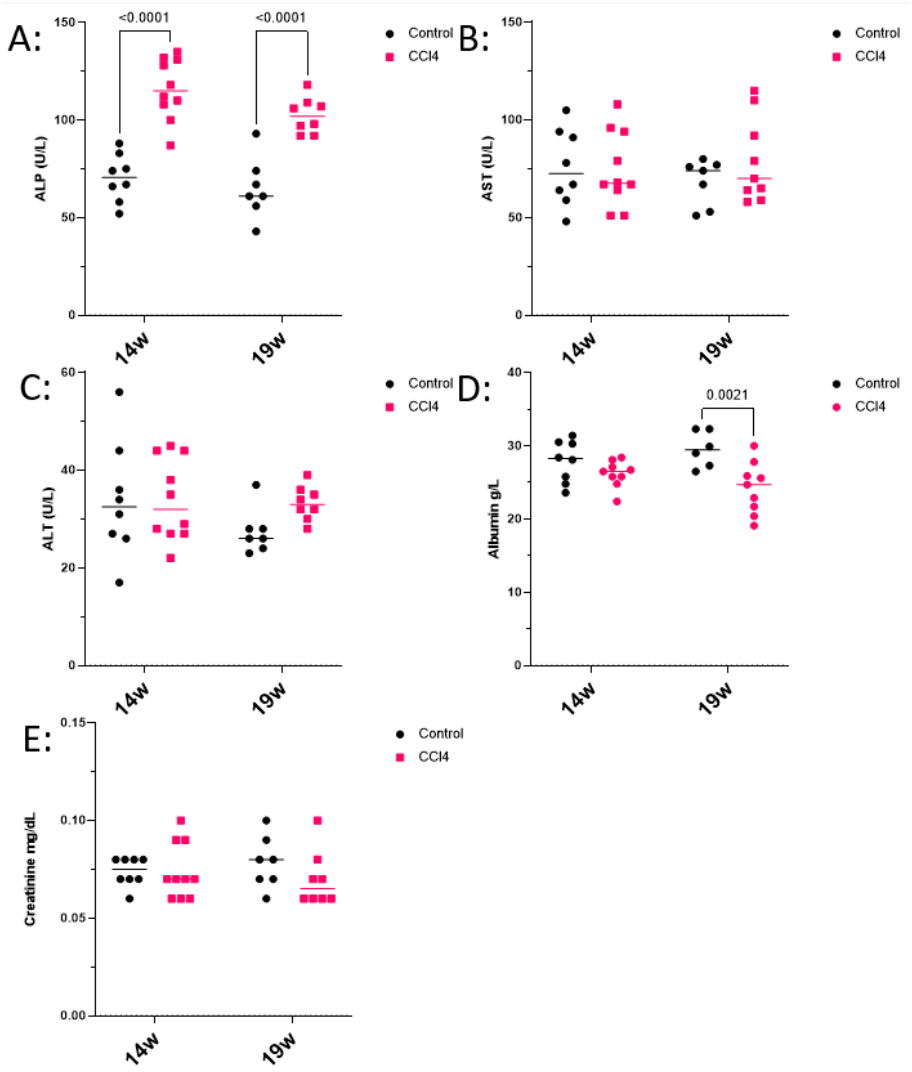

Figure 27: Subcutaneous CCl4 cirrhosis mice validation 14, 17 and 20 weeks administration, serum ALP, AST, ALT, Albumin, Creatinine levels. *A: Serum ALP, B: AST, C: ALT, D: Albumin, E: Creatinine levels was measured. 14w control (n=8), 14w CCl4 (n=10), 19w control (n=7), 19w CCl4 (n=9). CCl4 groups (14w and 19w) were compared to control groups, respectively, ordinary two-way ANOVA with Sidak's test, significance p<0.05.*

In order to examine ER stress, I firstly performed experiments to identify a suitable housekeeping gene that showed stable expression in our colon samples. I tested a battery of housekeeping genes with qPCR and western blot for gene and protein expression, respectively. I examined gene expression of Beta-actin (ACTB), Cyclooxygenase (COX), Histone H3 (H3), TATA box binding protein (TBP), Glyceraldehyde-3-phosphate dehydrogenase (GAPDH), and Cyclophilin B (PPIB), **Figure 28**. PPIB had the highest R^2 (goodness of fit, simple linear regression) value of 0.6970, the second most straight slope of -0.4316, lowest slope standard error of 0.08998, and lowest standard deviation of 0.11, **Figure 28**. For protein expression I examined alpha-Tubulin (Tub), GAPDH, PPIB, TBP, H3, and COX IV housekeeping genes. Western blot bands for TBP, H3, and COX IV were not detected, but was detected for Tub, GAPDH, and PPIB, **Figure 29**. Tub and PPIB both showed high variation between

samples, and GAPDH was most stable across the samples with the highest R^2 of 0.06234, the second most straight slope of 26982, and the lowest slope standard error of 30207, **Figure 29**.

A:

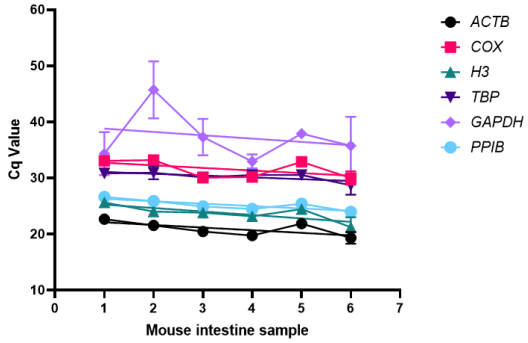

B:

Sample	ACTB Mean	ACTB SD	COX Mean	COX SD	H3 Mean	H3 SD	TBP Mean	TBP SD	GAPDH Mean	GAPDH SD	PPIB Mean	PPIB SD
1	22.66	0.08	33.06	0.08	25.66	0.06	30.82	0.08	34.33	3.83	26.62	0.12
2	21.55	0.22	33.20	0.14	24.03	0.18	30.92	1.17	45.72	5.08	25.88	0.23
3	20.46	0.10	30.07	0.16	23.82	0.16	30.11	0.23	37.28	3.25	24.93	0.01
4	19.73	0.17	30.20	0.24	23.17	0.04	30.54	0.07	32.94	1.27	24.47	0.05
5	21.86	0.03	32.87	0.04	24.44	0.35	30.54	0.01	37.89	0.33	25.40	0.03
6	19.31	1.03	30.00	1.20	21.22	1.77	28.71	1.68	35.74	5.16	23.98	0.22
Average	20.93	0.27	31.56	0.31	23.72	0.43	30.27	0.54	37.32	3.15	25.21	0.11
Slope	-0.4717		-0.462		-0.6174		-0.3213		-0.5941		-0.4316	
Std Error	0.1722		0.2414		0.1836		0.1445		0.8784		0.08998	
R squared	0.4287		0.2681		0.5308		0.3308		0.04375		0.697	

Figure 28: Gene expression of housekeeping genes on mouse colon samples. *RNA was isolated from mouse colon samples, synthesised into cDNA. cDNA from these colon samples was used to perform qPCR on housekeeping genes, ACTB, COX, H3, TBP, GAPDH, and PPIB. A: Cq values with nonlinear regression (curve fit) analysis, B: Mean Cq values, SD, average Cq, average SD, slope, and R^2 values from nonlinear regression (curve fit).*

A:

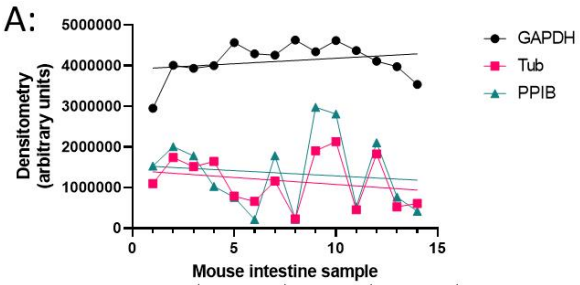

	GAPDH	Tub	PPIB
Slope	26982	-34519	-25949
Std Error	30207	42050	63287
R squared	0.06234	0.05317	0.01382

B:

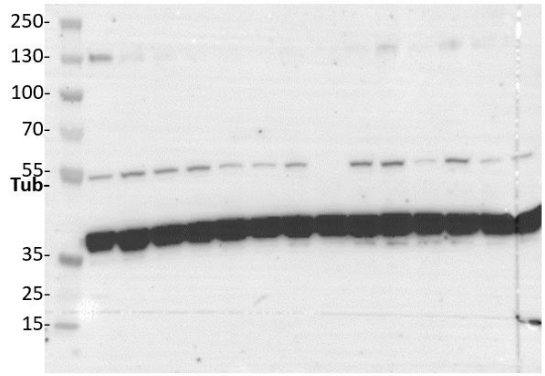

C:

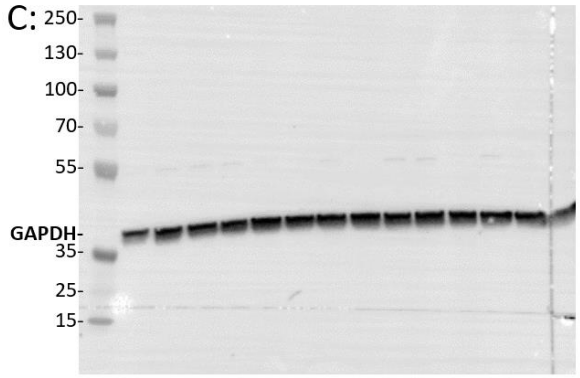

D:

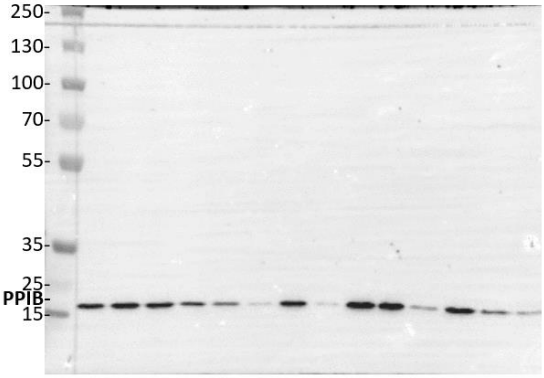

Figure 29: Protein expression of housekeeping genes on mouse colon samples. *Densitometry values were measured from GAPDH, Tub, and PPIB from western blots with proteins extracted from mouse colon samples. Western blot were imaged with Bio-Rad ChemiDoc and analysed with Image Lab. A: Densitometry data of GAPDH, Tub, PPIB from western blots with mouse colon protein extracts, B: western blot image with Tub bands, C: GAPDH, D: PPIB.*

3.4.1 Characterise intestinal inflammasome activation in cirrhosis mice models.

To examine intestinal inflammasome activation in cirrhosis, I determined gene and protein expression levels of inflammasome pathway genes in colon samples of olive oil, CCl4, and CCl4 + LPS treated mice for 12 weeks, as well as control and CCl4 treated mice for 14, 17 and 20 weeks. No significant differences were found in our 12 weeks mice, or the 14, 17 and 20 weeks mice, but NLRP3, Caspase-1, Caspase-11, IL-1beta, IL-18 and GSDMD showed a upward trend in our 12 weeks CCl4 + LPS treated mice, **Figure 30**, **Figure 31**.

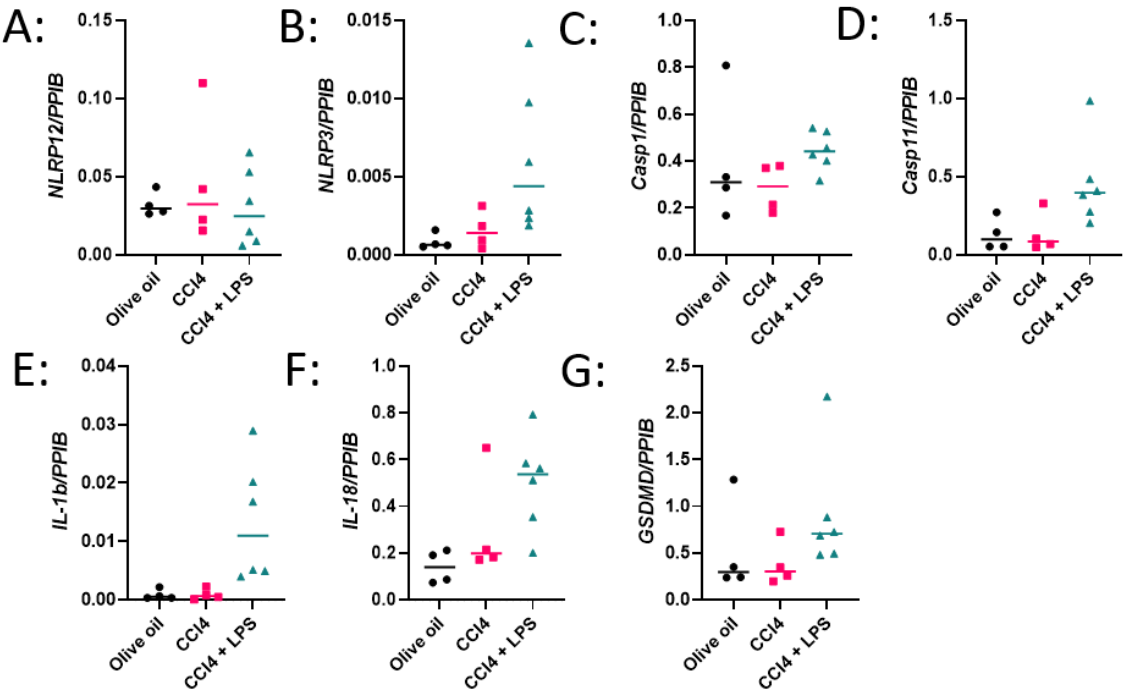

Figure 30: Gene expression of inflammasome pathway genes of mouse colon samples. *Gene expression was measured with qPCR on cDNA synthesised from RNA isolates of mouse colon samples. A: NLRP12, B: NLRP3, C: Caspase-1, D: Caspase-11, E: IL-1beta, F: IL-18, G: GSDMD. Olive oil (n=4), CCl4 (n=4), CCl4 + LPS (n=6) groups were compared with one-way ANOVA with Tukey's post hoc test; significance p<0.05.*

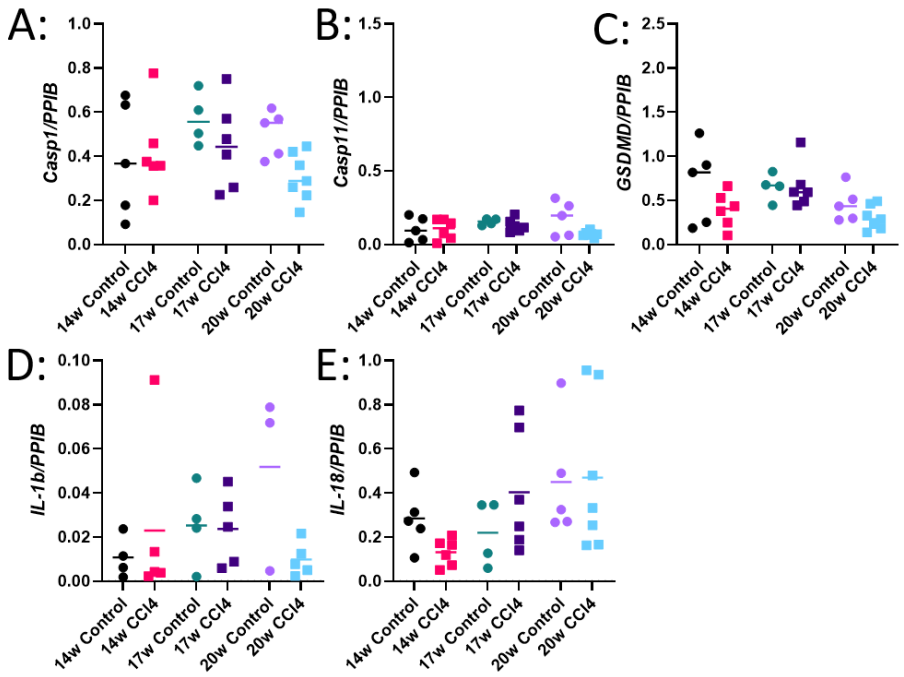

Figure 31: Gene expression of inflammasome pathway genes of mouse colon samples. *Gene expression was measured with qPCR on cDNA synthesised from RNA isolates of mouse colon samples. A: Caspase-1, B: Caspase-11, C: GSDMD, D: IL-1beta, E: IL-18. 14w control (n=5), 14w CCl4 (n=6), 17w control (n=4), 17w CCl4 (n=6), 20w control (n=5), 20w CCl4 (n=7) groups were compared with one-way ANOVA with Tukey's post hoc test; significance p<0.05.*

I examined protein expression of full length and cleaved caspase-1, caspase-11, GSDMD, IL-1beta, and IL-18 in colon samples of our 12 weeks treated mice to determine if the trend of increased expression of these genes resulted in increased protein and increased activation (cleaved to full length ratio). Full length caspase-1, GSDMD, IL-1beta, and IL-18, as well as cleaved IL-18 protein expression did not show any difference between treated and control groups, **Figure 32**. Cleaved caspase-1 and cleaved IL-1beta showed a trend downward in the treated groups compared to the olive oil group. Cleaved to full length ratio of caspase-1, GSDMD, IL-1beta and IL-18 did not show any difference between groups. Protein expression levels of full length, cleaved, and cleaved to full length ratio of caspase-11 protein expression shows a trend upward in the CCl4 + LPS group compared to the olive oil and CCl4 groups, but did not reach significance. In the 14, 17 and 20 weeks treat mice, cleaved caspase-1 and cleaved GSDMD were not detected and there was no difference in protein expression of full length caspase-1, caspase-11 and GSDMD, and cleaved caspase-11 or cleaved to full length caspase-11 ratio in treated mice compared to control, **Figure 33**.

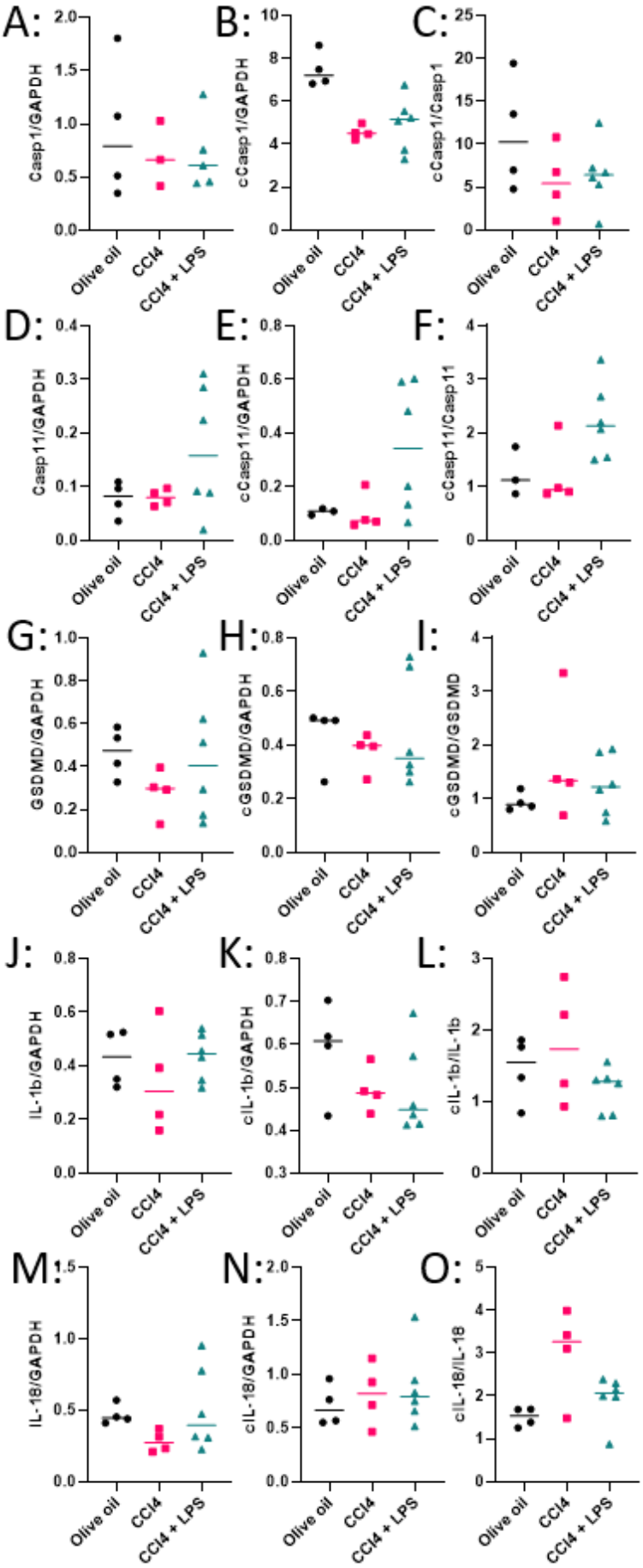
A:
Casp1/GAPDH
B:
cCasp1/GAPDH
C:
cCasp1/Casp1
D:
Casp11/GAPDH
E:
cCasp11/GAPDH
F:
cCasp11/Casp11
G:
GSDMD/GAPDH
H:
cGSDMD/GAPDH
I:
cGSDMD/GSDMD
J:
IL-1b/GAPDH
K:
cIL-1b/GAPDH
L:
cIL-1b/IL-1b
M:
IL-18/GAPDH
N:
cIL-18/GAPDH
O:
cIL-18/IL-18
Olive oil
CCl4
CCl4 + LPS

Figure 32: Protein expression of inflammasome pathway genes of mouse colon samples. *Protein expression was measured with western blot on protein extracts from mouse colon samples. A-C: Caspase-1, D-F: Caspase-11, G-I: GSDMD, J-L: IL-1beta, M-O IL-18. A, D, G, J, M: full length protein normalised to GAPDH, B, E, H, K, N: cleaved protein normalised to GAPDH, C, F, I, L, O: cleaved protein to full length protein ratio. Olive oil (n=4), CCl4 (n=4), CCl4 + LPS (n=6) groups were compared with one-way ANOVA with Tukey's post hoc test; significance p<0.05.*

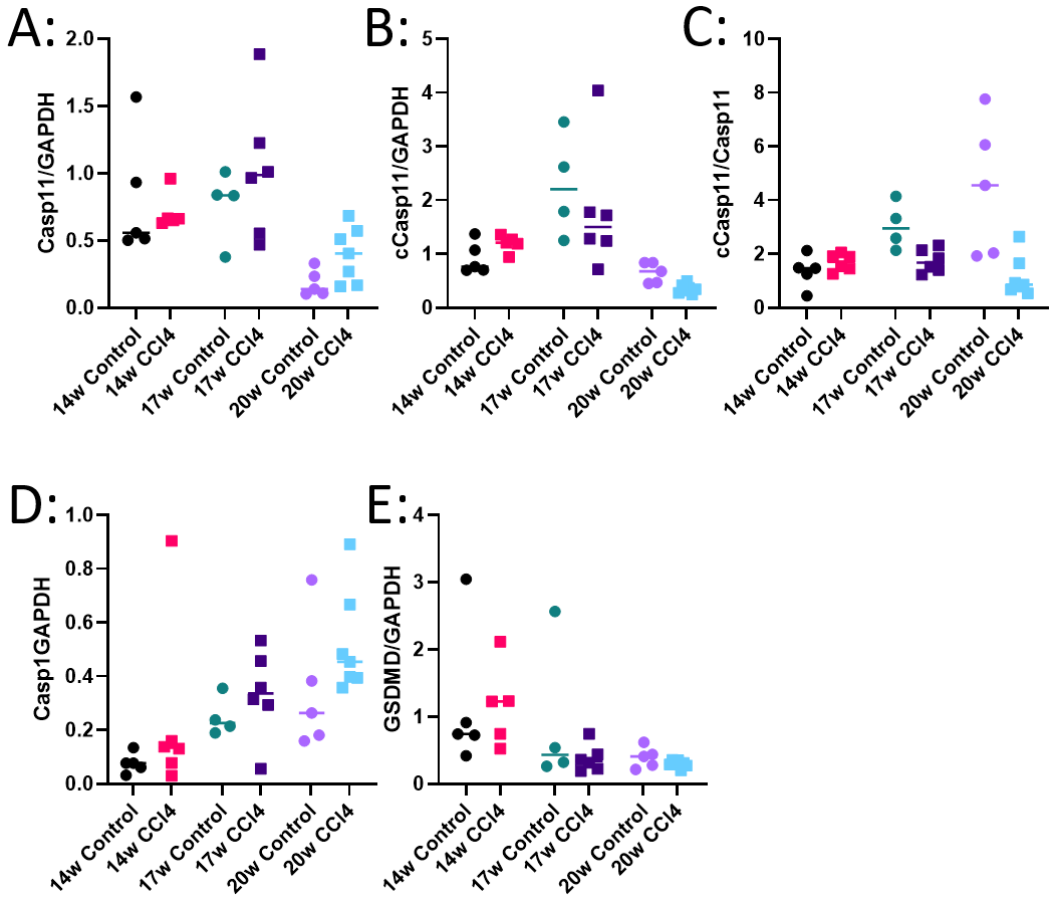

Figure 33: Protein expression of inflammasome pathway genes of mouse colon samples. *Protein expression was measured with western blot on protein extracts from mouse colon samples. A: full length Caspase-11, B: cleaved Caspase-11, C: cleaved Caspase-11 to full length Caspase-11 ratio, D: full length Caspase-1, E: full length GSDMD. 14 control (n=5), 14w CCl4 (n=6), 17w control (n=4), 17w CCl4 (n=6), 20w control (n=5), 20w CCl4 (n=7) groups were compared with on e-way ANOVA with Tukey's post hoc test; significance p<0.05.*

3.4.2 Characterise intestinal ER stress induction (UPR activation) in cirrhosis mouse models.

To examine intestinal ER stress in cirrhosis, I determined gene expression of UPR genes in colon samples of the 12 weeks mice model. GRP78, spliced XBP1, and CHOP gene expressions were used to determine UPR activation. GRP78 gene expression was significantly increased in the CCl4 + LPS group compared to the olive oil group, **Figure 34**. However, XBP1 splicing was significantly decreased in the CCl4 and CCl4 + LPS groups compared to the olive oil group. No difference was found in CHOP expression between the groups.

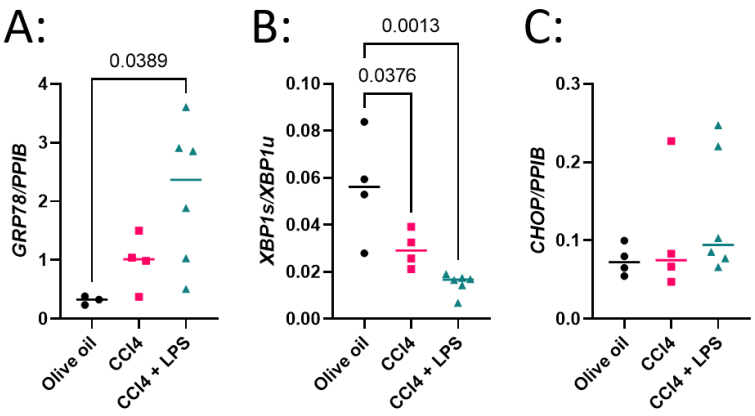

Figure 34: Gene expression of unfolded protein response genes of mouse colon samples. *Gene expression was measured with qPCR on cDNA synthesised from RNA isolates of mouse colon samples. A: GRP78, B: XBP1 splicing, C: CHOP. Control (n=4), CCl4 (n=4), CCl4 + LPS (n=6) groups were compared with one-way ANOVA with Tukey's post hoc test; significance p<0.05.*

3.4.3 Determine synergy between ER stress and non-canonical inflammasome activation on intestinal cell death.

To examine whether UPR and non-canonical inflammasome activation can have synergistic effect on intestinal epithelial cell death, I used an *in vitro* model. I first optimised ER stress induction with tunicamycin on intestinal epithelial cell lines before combination treatment targeting UPR and non-canonical inflammasome activation. I treated Caco-2 and HCT-116 with 1µM and 10µM tunicamycin for 6 and 24 hours.

GRP78 expression and XBP1 splicing were significantly increased by 1µM and 10µM tunicamycin treatment after 6 hours in caco-2 cells, **Figure 35**. CHOP expression did not show a significant difference by 1µM and 10µM tunicamycin treatment after 6 hours, but showed an upward trend. Tunicamycin treatment for 24 hours at 1µM significantly increased GRP78 expression and XBP1 splicing, but did not significantly increase CHOP expression in caco-2 cells. 10µM tunicamycin treatment in caco-2 cells for 24 hours significantly increased XBP1 splicing and CHOP expression, but did not significantly alter GRP78 expression.

6 hours treatment with 1µM and 10µM on HCT-116 cells significantly increased GRP78 and CHOP expression and XBP1 splicing, **Figure 36**. 24 hour treatment of 1µM and 10µM tunicamycin on HCT-116 cells significantly increased GRP78 and CHOP expression, but did not increase XBP1 splicing.

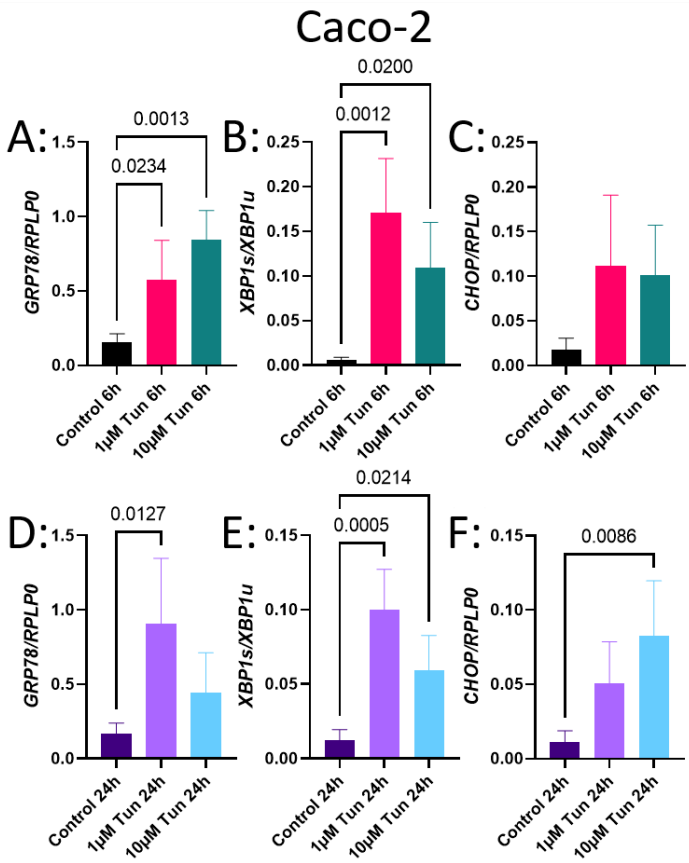

Figure 35: Gene expression of unfolded protein response genes of tunicamycin treated caco-2 cells. *Gene expression was measured with qPCR on cDNA synthesised from tunicamycin treated cells. A: GRP78, B: XBP1 splicing, C: CHOP. Control, 1µM and 10µM tunicamycin treated caco-2 cells for 6 and 24 hours (n=4), groups were compared with one-way ANOVA with Tukey's post hoc test; significance $p<0.05$.*

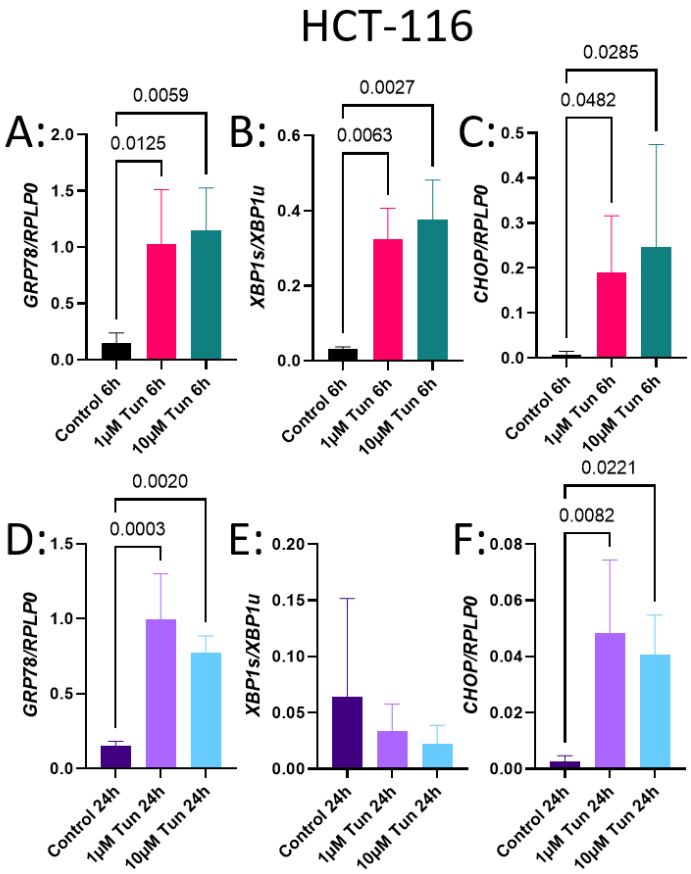

Figure 36: Gene expression of unfolded protein response genes of tunicamycin treated HCT-116 cells. *Gene expression was measured with qPCR on cDNA synthesised from tunicamycin treated cells. A: GRP78, B: XBP1 splicing, C: CHOP. Control, 1µM and 10µM tunicamycin treated HCT-116 cells for 6 hours (A,B,C) and 24 hours (D,E,F) (n=4), groups were compared with one-way ANOVA with Tukey's post hoc test; significance p<0.05.*

To examine "short" and "long" ER stress synergy with non-canonical inflammasome activation on intestinal cell death, I treated Caco-2 and HCT-116 cells with 1µM tunicamycin for 6 hours and 24 hours. This was based on similar UPR activation between 1µM and 10µM tunicamycin treatment, and to minimise toxicity of tunicamycin alone. Combination treatment of 1µM tunicamycin for 6 hours with 10,30,60 and 100µg/ml LPS treatment for 3 hours did not show synergistic effect on cell death (LDH release) in Caco-2 and HCT-116 cells, **Figure 37**. Combination treatment of 1µM tunicamycin for 24 hours with and without 1µg/ml LPS for 24 hours followed with 10,30 and 100µg/ml LPS for 3 hours also did not show a synergistic effect on cell death in Caco-2 and HCT-116 cells, **Figure 37**.

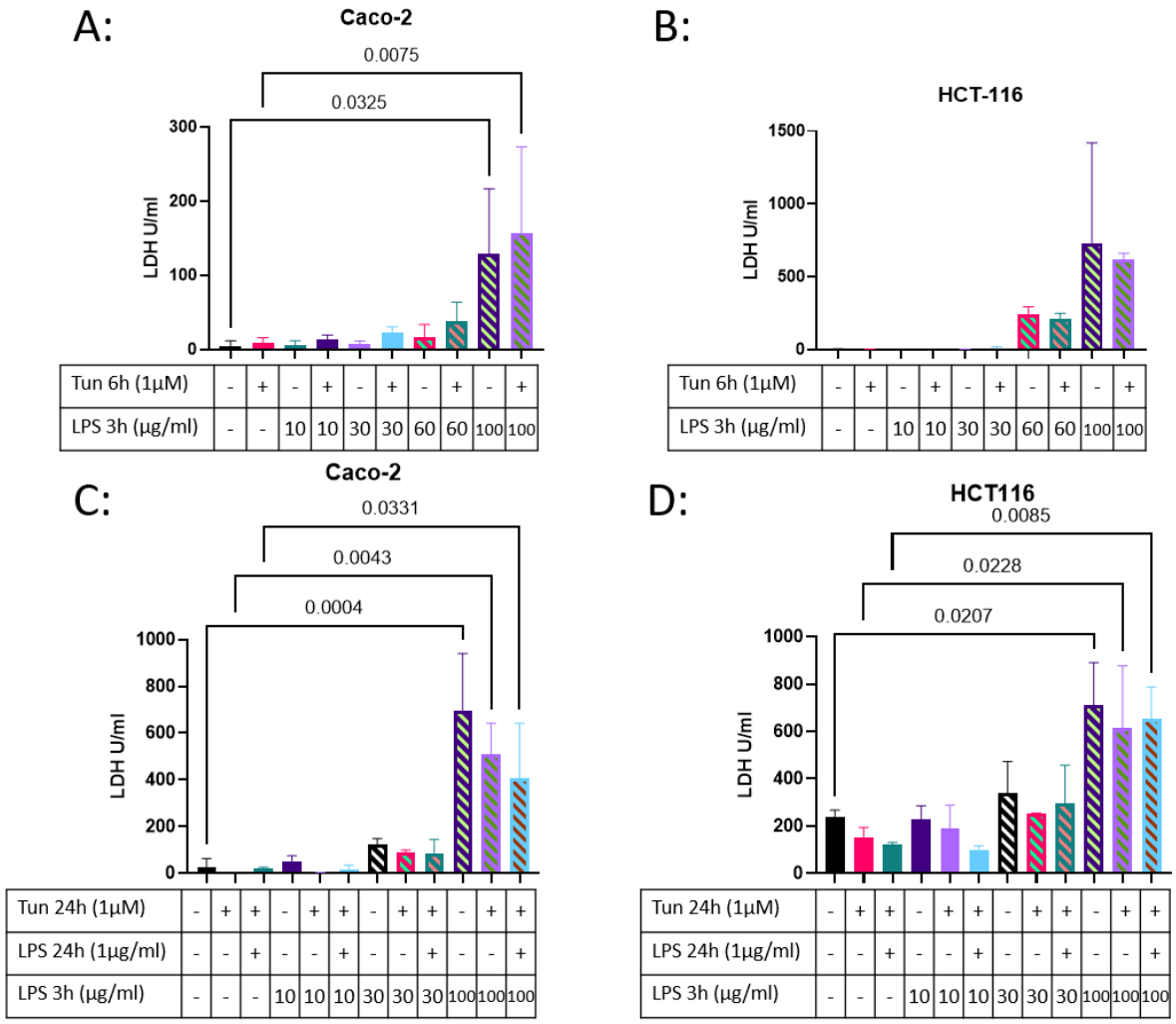

Figure 37: LDH release of tunicamycin and LPS treated caco-2 and HCT-116 cells. *LDH was measured using LDH-Glo assay on conditioned media of tunicamycin and LPS treated caco-2 and HCT-116 cells. A: Caco-2 and B: HCT-116 cells were treated with and without 1µM tunicamycin for 6 hours, with and without 10, 30, 60 and 100µg/ml LPS for 3 hours. C: Caco-2 and D: HCT-116 cells were treated with and without 1µM tunicamycin for 24 hours, with and without 1µg/ml LPS for 24 hours, with and without 10,30 and 100µg/ml LPS for 3 hours. n=2, groups were compared with one-way ANOVA with Tukey's post hoc test; significance p<0.05.*

I suspected the negative results of lack of synergy between ER stress and non-canonical inflammasome activation on intestinal cell death could have been attributed to the limitation of 2D cell culture and the derivation of the cell lines from cancer cells, which selects for decreased cell death properties. Therefore, to model the intestinal epithelium more physiologically I derived mouse intestinal organoids from small intestinal crypts, which cell renewal does not rely on cancer cell's characteristics. The first step was to validate the organoid model by verifying the presence of Paneth cells, Goblet cells, Enteroendocrine cells, Enterocytes, and stem cells. To examine the presence of intestinal epithelial cell types I determined the gene expression of intestinal epithelial cell type markers: Lysozyme 1 (Paneth cells), Sucrase-isomaltase (Enterocytes), Keratin 20 (Enterocytes),

Mucin 2 (Goblet cells), Chromogranin A (Enteroendocrine cells), Ki-67 (proliferating cells), Leucine Rich Repeat Containing G Protein-Coupled Receptor 5 (Stem cells), and Olfactomedin 4 (Stem cells). Gene expression of these intestinal epithelial cell type markers showed the presence of Paneth cells, Enterocytes, Goblet cells, Enteroendocrine cells, and proliferating/stem cells in the mouse intestinal organoids, as well as the intestine samples where the organoids were derived from, **Figure 38**. Furthermore, we stained intestinal organoids for Actin, to determine polarity, and Ki67 (proliferating cells), Villin (Enterocytes), Lysozyme (Paneth cells), Mucin 2 (Goblet cells) and CHGA (Enteroendocrine cells). Intestinal organoids stained for these markers confirmed the presence of Enterocytes, Paneth cells, Goblet cells, Enteroendocrine cells, and proliferating stem cells, as well as the polarity with the lumen inside the organoid **Figure 39**.

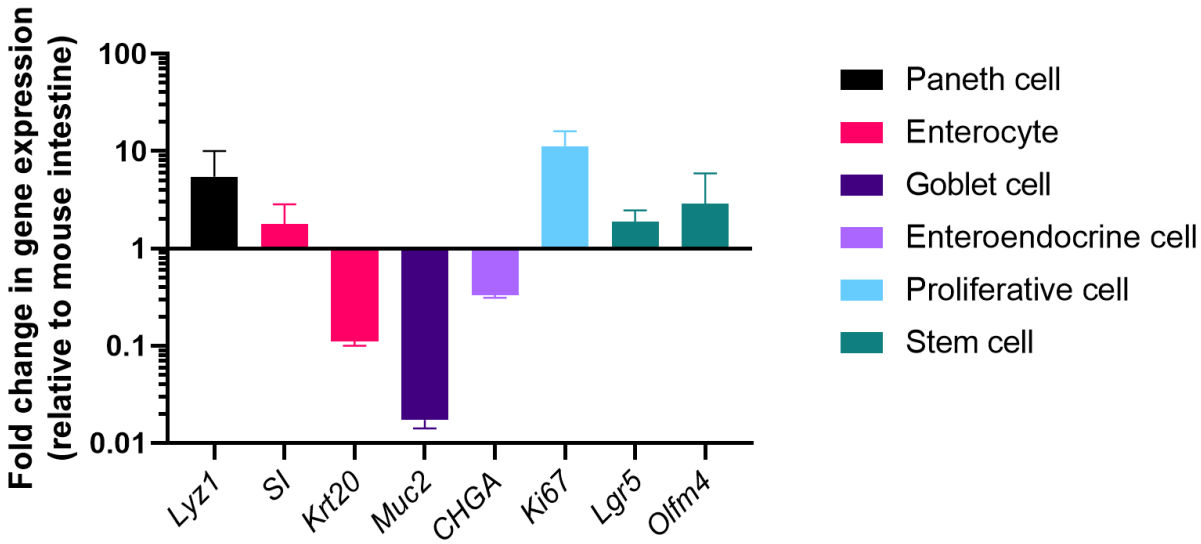

Figure 38: Gene expression of intestinal cell type markers in mouse intestinal organoids. *Gene expression was measured with qPCR on cDNA synthesised from RNA isolated from mouse intestinal organoids and mouse intestine samples. Gene expression was measured from Lysozyme 1, Sucrase-isomaltase, Keratin 20, Mucin 2, Chromogranin A, Ki-67, Leucine Rich Repeat Containing G Protein-Coupled Receptor 5, and Olfactomedin 4, n=2.*

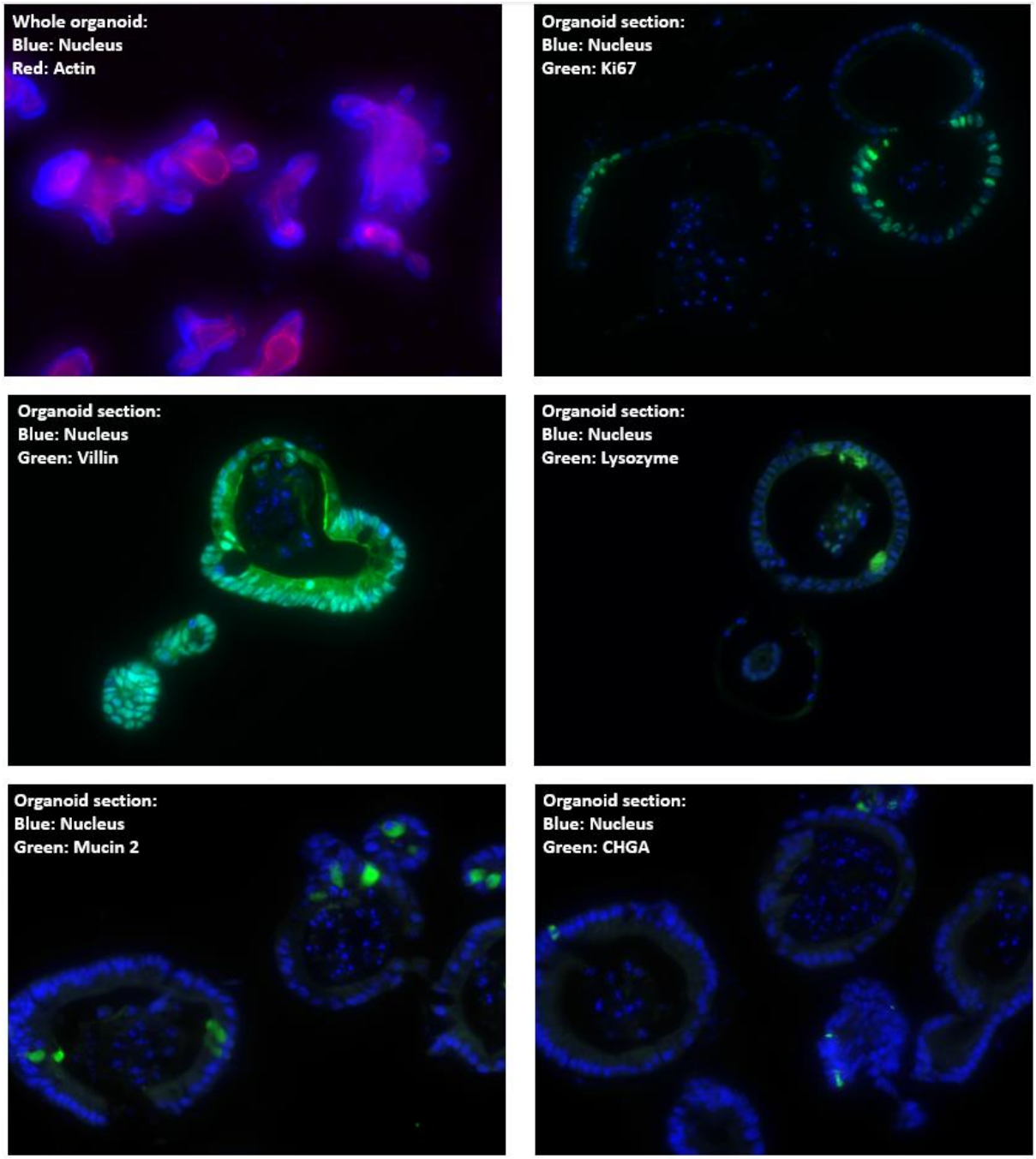

Figure 39: Whole and sectioned intestinal organoids cell stains. *Whole mouse intestinal organoids were fixed, permeabilised, and stained with HOECHST (Nucleus) and Phalloidin (Actin), top left. Whole mouse intestinal organoids were fixed, paraffin embeddded, and sectioned for antibody staining on glass slides. Sectioned organoids were stained with DAPI (Nucleus) and antibodies for Ki67 (top right), Villin (mid left), Lysozyme (mid right), Mucin 2 (bottom left), and CHGA (bottom right).*

Once the organoid model was validated to contain several epithelial cells, I treated mouse intestinal organoids with 10nM and 100nM tunicamycin for 6 or 24 hours to find the best conditions to induce ER stress and elicit an UPR in the organoids without inducing cell death. I analysed LDH release, XBP1

splicing and caspase-1, caspase-11, GRP78 and CHOP gene expression in the tunicamycin treated intestinal organoids.

10nM tunicamycin treatment for 6 hours did not affect cell death, caspase-1, caspase-11, GRP78 and CHOP expression, or XBP1 splicing, **Figure 40**. 100nM tunicamycin treatment for 6 hours significantly increased GRP78 expression and XBP1 splicing. 100nM tunicamycin treatment for 6 hours did not significantly affect cell death, and caspase-1, caspase-11 and CHOP expression, but did show an upward trend in CHOP expression.

10nM tunicamycin treatment for 24 hours significantly increased GRP78 expression, did not significantly affect cell death, caspase-1, caspase-11 and CHOP expression or XBP1 splicing, but cell death showed a trend upward. 100nM tunicamycin treatment for 24 hours significantly increased GRP78 expression and XBP1 splicing, significantly decreased caspase-1 expression, and significantly increased cell death, but did not significantly affect caspase-11 and CHOP expression.

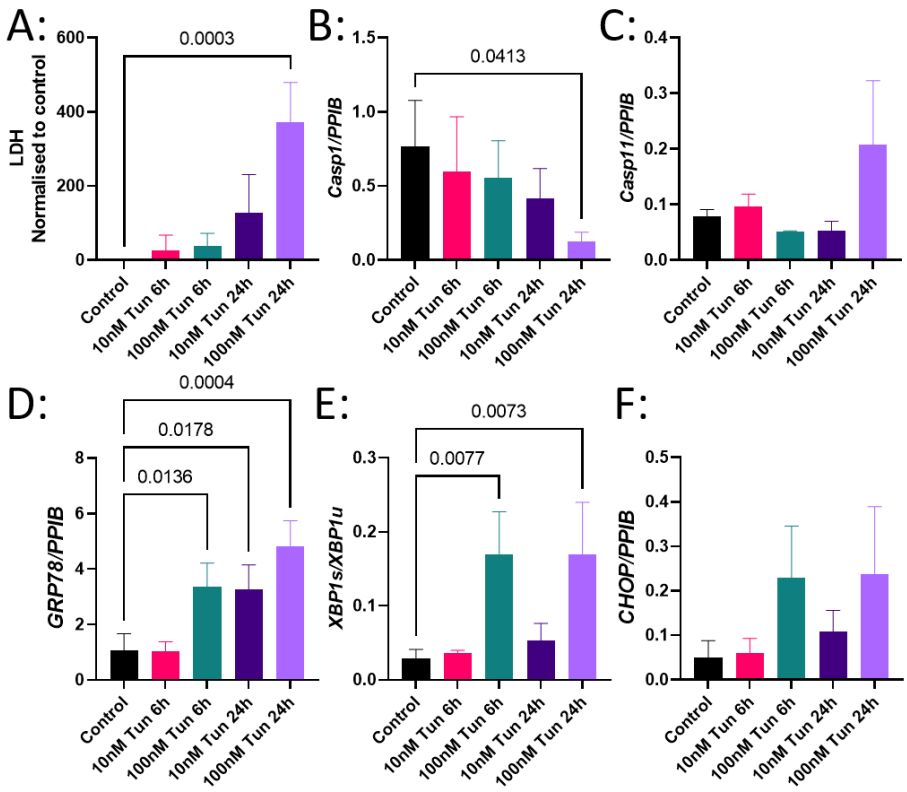

Figure 40: LDH release and gene expression of tunicamycin treated mouse intestinal organoids. *Mouse intestinal organoids were treated with or without 10nM and 100nM tunicamycin for 6 and 24 hours. LDH was measured using LDH-Glo assay on conditioned media and gene expression was measured with qPCR on cDNA synthesised from RNA isolated from mouse intestinal organoids. A: LDH release, and gene expression of B: Caspase-1, C: Caspase-11, D: GRP78, E: XBP1 splicing, and F: CHOP. n=3, groups were compared with one-way ANOVA with Tukey's post hoc test; significance p<0.05.*

To study the synergistic effect of ER stress and non-canonical inflammasome activation on intestinal cell death, I aimed to induce ER stress with UPR activation in intestinal organoids by tunicamycin treatment without causing cell death. I showed that 10nM tunicamycin treatment for 24 hours induced UPR with increased GRP78 expression, but also showed a trend in increased cell death. Therefore, I treated intestinal organoids with half of the dose (5nM) for 16 hours to attempt to limit cell death, while still inducing the UPR. Control and treated organoids were then further incubated for 3 hours with or without 100µg/ml LPS. Control organoids treated with 100µg/ml LPS for hours showed no increase in cell death, however treatment with 5nM tunicamycin caused a significant increase in the release of LDH, albeit to a lower extent than the one observed in organoids treated with 10nM for 24 hours, **Figure 41**. LPS treatment after 5nM tunicamycin treatment also significantly increased cell death compared to untreated organoids, but LPS and tunicamycin did not synergistically increase cell death. I then examined GRP78 and CHOP expression to determine the UPR activation, but 5nM tunicamycin for 16 hours with or without LPS treatment did not significantly affect the expression of either gene.

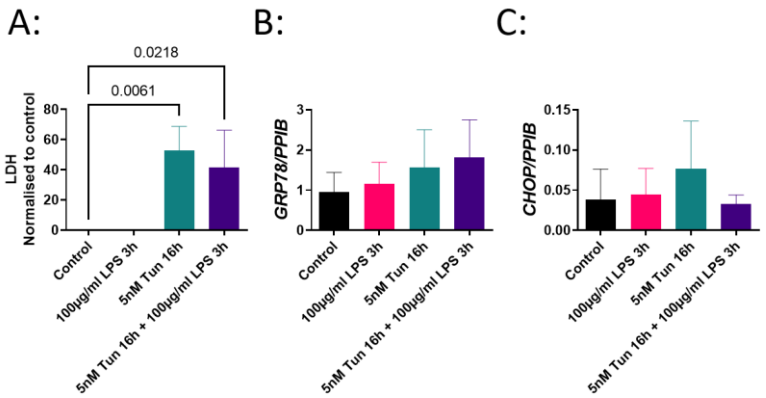

Figure 41: LDH release, and gene expression of tunicamycin and LPS treated mouse intestinal organoids. *Mouse intestinal organoids were treated with and without 5nM tunicamycin for 16 hours, with and without LPS for 3hours. LDH was measured using LDH-Glo assay on conditioned media, and gene expression was measured with qPCR on cDNA synthesised from RNA isolated from mouse intestinal organoids. A: LDH release, and gene expression of C: GRP78, D: CHOP. n=3, groups were compared with one-way ANOVA with Tukey's post hoc test; significance p<0.05.*

To determine whether ER stress could sensitise cell death in intestinal epithelial cells to bacterial products, mouse intestinal organoids were treated with tunicamycin and LPS. Additionally, mouse intestinal organoids were derived from inflammasome pathway genes KO mice (Caspase-11, Caspase-1+11) and treated to determine the dependency on inflammasome activation on the cell death.

WT, Casp-11 KO, and Casp-1+11 KO intestinal organoids were treated with 10nM tunicamycin for 24 hours, 100µg/ml LPS for 6 hours, a combination of 10nM tunicamycin treatment for 24 hours with

100µg/ml LPS, and 100nM tunicamycin for 6 hours. After treatment the conditioned media was collected, and the mouse intestinal organoids were incubated for another 24 hours with fresh media. In the first conditioned media (after treatment) there was no difference in cell death between any of the treatment groups of all the mouse intestinal organoid groups (WT, Casp-11 KO, Casp1+11 KO), **Figure 42**. In the conditioned media after 24 hours with fresh media only 100nM tunicamycin treatment for 6 hours showed significantly increased cell death from WT, and Casp-1+11 KO mouse intestinal organoids. 100nM tunicamycin treatment for 6 hours did not significantly affect cell death in Casp-11 KO mouse intestinal organoids 24 hours after treatment, but showed a trend of increased cell death.

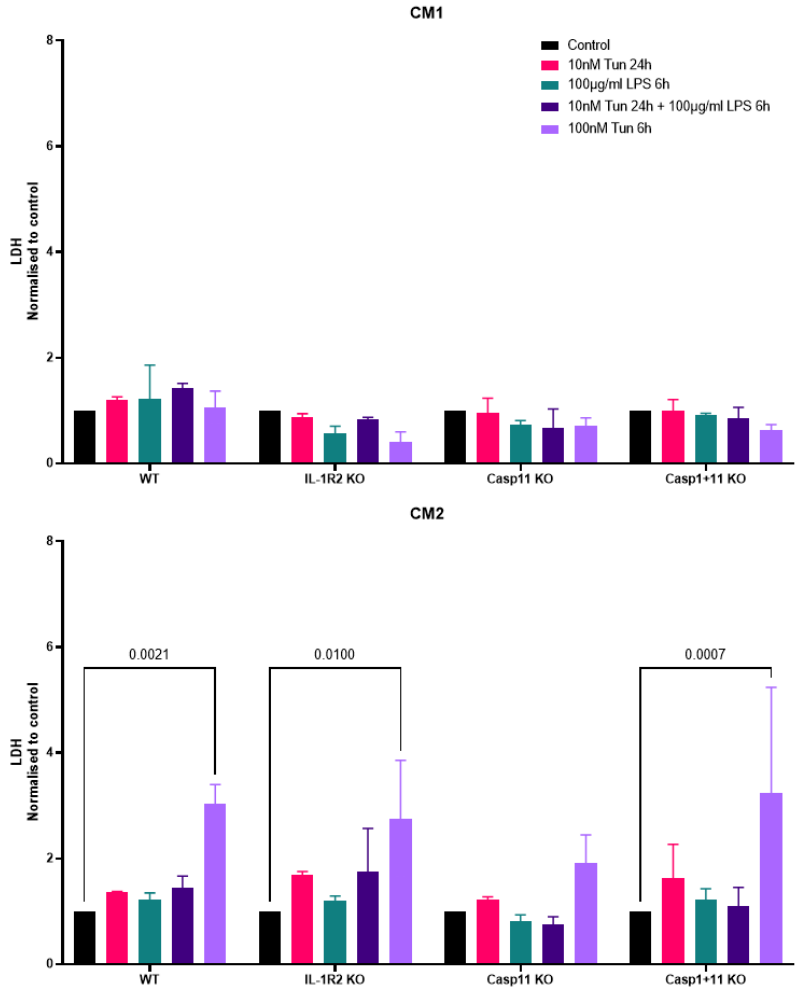

Figure 42: LDH release of tunicamycin and LPS treated mouse intestinal organoids. *Mouse intestinal organoids of WT, Caspase-11 and Caspase-1+11 KO mice were treated with and without 10nM tunicmycin, with and without 100µg/ml LPS, or 100nM Tunicamycin for 6 hours. Media was replaced after treatment with fresh media for 24 hours. LDH was measured using LDH-Glo assay on conditioned media from treated mouse intestinal organoids. A: LDH release in conditioned media after treatment and B: LDH release in conditioned media after 24 hours with fresh media. n=3, groups were compared with one-way ANOVA with Tukey's post hoc test; significance p<0.05.*

3.4.4 Characterise intestinal ER stress induction (UPR activation) in cirrhosis patients.

To examine whether ER stress is induced in the intestine of cirrhosis patients, I analysed the gene expression of GRP78, CHOP and XBP1 splicing in intestinal biopsies (colon and duodenum). Most of the colon biopsy donors were males in both the healthy control (average age 56) and cirrhosis group (average age 58), with the majority of cirrhosis patients with ALD aetiology, **Table 5**. Most of the duodenum biopsy donors were females in both the healthy control (average age 48) and cirrhosis group (average age 63), with the most cirrhosis patients with ALD aetiology. Age did not significantly differ between healthy control and cirrhosis donors for either colon and duodenum biopsies (Mann-Whitney t-test). GRP78 and CHOP expression, and XBP1 splicing did not show any difference in the cirrhosis group of colon and duodenum biopsies compared to the healthy control group, **Figure 43**.

Table 5: Patient characteristics and clinical presentation (%) with MELD and MELD-Na scores of intestine biopsy donors (Laboratory of Hepatology - KU Leuven (Schalk van der Merwe)).

Intestine	Donor	Age	Female	NAFLD	ALD	NAFLD/ALD	Ascites	HE	Varices	MELD-Na	MELD
Colon	HC	56±19	25%								
	Cirrhosis	58±6	17%	8%	77%	15%	60%	60%	50%	15.6±5.4	13.7±4.4
Duodenum	HC	48±17	57%								
	Cirrhosis	63±6	60%	20%	50%	30%	38%	0%	38%	16.1±8.2	14.6±8.4

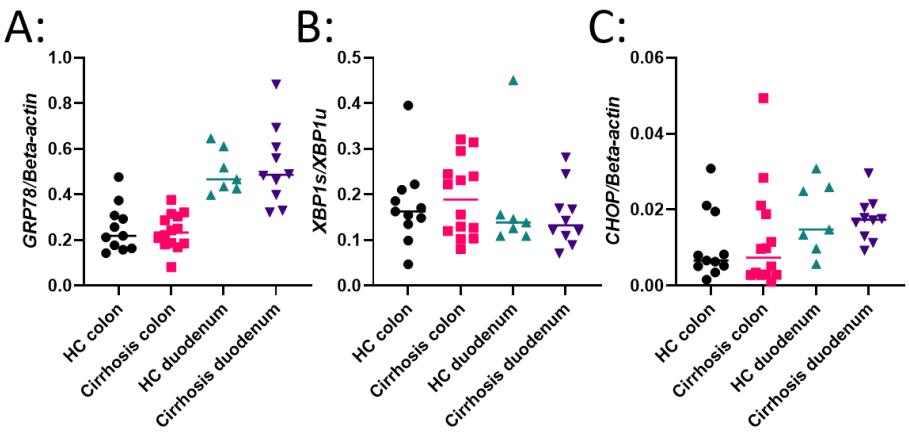

Figure 43: Gene expression of unfolded protein response genes of healthy control and cirrhosis patient intestinal biopsies. *Gene expression was measured with qPCR on cDNA synthesised from RNA isolates of healthy control and cirrhosis patient intestinal biopsies. A: GRP78, B: XBP1 splicing, C: CHOP. HC colon (n=11), Cirrhosis colon (n=14), HC duodenum (n=7) and Cirrhosis duodenum (n=10), Cirrhosis groups were compared to HC with unpaired t-test; significance p<0.05.*

3.5 Discussion

I hypothesised that ER stress mediated intestinal inflammasome activation and pyroptotic cell death are associated with cirrhosis. My aims were to 1: characterise intestinal inflammasome activation in

cirrhosis mouse models, 2: characterise intestinal ER stress induction (UPR activation) in cirrhosis mouse models, 3: determine synergy between ER stress and non-canonical inflammasome activation on intestinal cell death, and 4: characterise intestinal ER stress induction (UPR activation) in cirrhosis patients.

To study intestinal ER stress and inflammasome activation in cirrhosis, I used a 12-week subcutaneous CCl4 model. Literature has shown that subcutaneous administration of CCl4 leads to cirrhosis with portal hypertension, sodium retention, and development of ascites after 13 weeks in mice [238]. Importantly, subcutaneous administration reduces confounding effects on the gastrointestinal tract compared to conventional intraperitoneal injection of CCl4, which could directly affect the development of ER stress and inflammasome activation in the intestine [238]. In our and Schalk van der Merwe's models, there was increased liver injury and scar formation similar to the development of cirrhosis in patients. However, classification of cirrhosis, e.g. advanced fibrosis, compensated cirrhosis, decompensated cirrhosis, in these mice was not performed due to the established cirrhosis classification of the subcutaneous CCl4 model [238]. Extended CCl4 treatment in the mice from Schalk van der Merwe showed more severe liver collagen deposition, as would be expected with longer duration of liver insult.

The first aim, to characterise intestinal inflammasome activation in cirrhosis mouse models, I quantified gene and protein expression of key genes of the canonical and non-canonical inflammasome pathways in our cirrhosis models. These proved to be largely unaltered in the colon of CCl4 treated mice, with NLRP3, caspase-1, caspase-11, IL-1beta, IL-18 and GSDMD only showing trends towards upregulation in the CCl4 + LPS group. No differences were detected between our mice and those provided by Schalk van der Merwe's group. Similarly, no differences were found in protein expression, with unaltered levels of caspase-1, IL-1beta, IL-18, and GSDMD. However, the observed trend of increased colonic capsase-11 gene expression was accompanied by a similar trend at the protein level in the CCl4 + LPS group. Importantly, our study lacked a LPS control group, and therefore it cannot be determined whether the trend of colonic caspase-11 activation was caused by the LPS and not the cirrhosis with a decompensation event. Caspase-11 is activated directly by LPS without any pattern recognition receptors, and thus it is possible that LPS injection caused the trend of non-canonical inflammasome activation in the colon of CCl4 + LPS mice [251]. Additionally, large variations between groups suggests the study might have been underpowered, and thus unable to adequately detect significant results.

The second aim, to characterise intestinal ER stress induction (UPR activation) in cirrhosis mouse models, I quantified gene expression of the UPR in our subcutaneous CCl4 mice model. I showed a

significant increase in colonic GRP78 expression, the initiator of the UPR, in the CCl4 + LPS group. However, XBP1 splicing ratio, activation marker of the IRE1 pathway in the UPR, was significantly decreased in both the CCl4 and CCl4 + LPS groups. One possible explanation for these contradictory results is that the activation of the UPR reduced the ER stress and inhibited the UPR with a decrease of XBP1 splicing. This could show a decrease in XBP1 splicing and lagging behind GRP78 expression regulation.

The third aim, to determine synergy between ER stress and non-canonical inflammasome activation on intestinal cell death, I used Caco-2 and HCT-116 cells as models in which I induced ER stress with tunicamycin followed by non-canonical inflammasome activation with LPS. First, I optimised the tunicamycin treatment to induce ER stress and UPR. Tunicamycin induces ER stress by inhibiting N-linked glycosylation in the ER [252]. Tunicamycin treatment effectively induced ER stress as measured by GRP78, XBP1 splicing, and/or CHOP expression. "Short" ER stress induction by tunicamycin treatment with LPS at different doses did no show synergistic effect on cell death in either Caco-2 or HCT-116 cells. Additionally, "long" ER stress induction, exposure to low LPS, followed by high dose LPS treatment combinations also did not show synergistic effect on cell death in Caco-2 and HCT-116 cells. Caco-2 and HCT-116 cells are widely used as intestinal epithelial cells lines, however Caco-2 is derived from a human colorectal adenocarcinoma and HCT-116 from a human colon carcinoma, which are selected to survive conditions that would induce cell death in healthy epithelial cells because of their cancer cell characteristics [253]. These cells have increased expression of anti-apoptotic genes and decreased expression of pro-apoptotic genes, i.e. HCT-116 cells do not express RIP3 and therefore cannot activate necroptosis [254]. This can interfere with determining synergy between ER stress and non-canonical inflammasome activation on intestinal cell death [253].

To better model the intestinal epithelium than intestinal cancer/cancer-like cell lines, I derived intestinal organoids, which can maintain stem cell pluripotency and proliferation with the use of supplements in the media that activate stem cell pathways. Intestinal organoids are derived from intestinal crypts and are thereby not selected to survive harsh environments like cancer cells [244]. Additionally, intestinal organoids possess the villi-crypt structure, cell type composition, self-renewal capabilities similar to the intestine, and can be cryopreserved and re-cultured [244][253]. I only derived intestinal organoids from mice and not from human, as human intestinal biopsies would have required additional ethics and approval, which was not granted in time for this project.

The first thing after deriving intestinal organoids was to compare the cell type composition. I measured gene expressions of cell type markers for Paneth cells (Lyz1), Enterocytes (SI and Krt20),

Goblet cells (Muc2), Enteroendocrine cells (CHGA), proliferating cells (Ki67), and stem cells (Lgr5 and Olfm4) in mouse intestinal organoids and mouse intestine samples. All these cell type markers were expressed in both mouse intestinal organoids and mouse intestine samples, albeit at varying levels. Furthermore, the mouse intestinal organoids showed villi-crypt structures with the intestinal lumen in the organoids and proliferating cells, Enterocytes, Paneth cells, Goblet cells, and Enteroendocrine cells as identified by cell marker staining.

To further examine the third aim, to determine synergy between ER stress and non-canonical inflammasome activation on intestinal cell death, I used mouse intestinal organoids as a model in which I induced ER stress with tunicamycin followed by non-canonical inflammasome activation with LPS. First, I optimised the tunicamycin treatment to induce ER stress and UPR. 10nM tunicamycin treatment for 24 hours effectively induced UPR activation, but these organoids also showed a non-significant trend in increased cell death. Therefore, I opted for a milder treatment, consisting of 5nM tunicamycin for 16 hours to reduce the effect on tunicamycin induced cell death. I exposed mouse intestinal organoids to "long" ER stress by 5nM tunicamycin treatment for 16 hours with non-canonical inflammasome activation by 100µg/ml LPS treatment for 3 hours. However, GRP78 and CHOP expression was unaffected by 5nM tunicamycin treatment for 16 hours, which showed that this dose and duration was unsuited to induce ER stress. Thus, this combination treatment did not determine whether ER stress and non-canonical inflammasome activation synergistically affect epithelial cell death.

I determined whether ER stress could sensitise cell death in intestinal epithelial cells in response to these bacterial products. I treated intestinal organoids from control, caspase-11 and caspase-1+11 KO mice with 10nM tunicamycin for 24 hours, and LPS for 6 hours to analyse synergistic effect on cell death and inflammasome pathway dependency. The treatment combinations examined, besides 100nM tunicamycin, did not induce cell death in the organoids after treatment or 24 hours post treatment. This indicates that ER stress has little/no effect on epithelial cell death sensitisation to bacterial products or toxins in the intestinal lumen.

The fourth aim, characterise intestinal ER stress induction (UPR activation) in cirrhosis patients, I quantified gene expression of GRP78, XBP1 splicing, and CHOP in duodenum and colon biopsies from healthy control and cirrhosis patients. I showed that GRP78 and CHOP expression, and XBP1 splicing did not differ between cirrhosis patients and healthy controls in the duodenum and colon. This contradict previous findings that showed a significant increase of GRP78 and CHOP expression in duodenal biopsies from cirrhosis patients compared to healthy controls [194]. However, Liu *et al.* showed relative mRNA levels normalised to HPRT1, which could explain the different results [194].

Additionally, differences in aetiology and disease stage of the cirrhosis patients can explain the contradicting results. The cirrhosis patients from Liu *et al.,* all had active hepatitis C as the aetiology, whereas our samples came from cirrhosis patients from ALD and/or NAFLD aetiology [194]. Furthermore, our cirrhosis patients had higher MELD scores (14.6±8.4) compared to the cirrhosis from Liu *et al.,* (9.4±4), which shows their patients had less severe cirrhosis. This could indicate that earlier in cirrhosis development ER stress is induced in the intestine, but is no longer present in worse/progressed cirrhosis [194].

I did not show significant differences of intestinal ER stress (UPR activation) or inflammasome activation in our cirrhosis mice models. However, the whole lysate of the intestine sample contains cells from the mucosa, submucosa, muscularis, and serosa, which could have obscured specific cellular processes of the epithelial cells and immune cells. FACS or cell staining can be used in future studies examining these cellular processes to specifically characterise the UPR and inflammasome activation in epithelial cells, immune cells, etc. Additionally, cirrhosis mice models deficient for specific inflammasome genes or UPR genes in the intestine can help delineate the role of these pathways on intestinal cell death and barrier disruption.

3.6 Conclusion

My results showed that ER stress and non-canonical inflammasome activation did not synergistically affect intestinal epithelial cell death in our intestinal epithelial models. I showed no proof of intestinal inflammasome activation in our cirrhosis model. Furthermore, I did not show ER stress induction in intestinal samples from our cirrhosis mice model or intestinal biopsies from cirrhosis patients.

4 Development of a permeability assay for mouse intestinal organoids.

4.1 Introduction

4.1.1 Transport across the intestine epithelium

Regulating permeability in the intestine is essential for the absorption and transportation of nutrients and metabolites across the epithelium, while limiting translocation of toxins and bacteria [139]. Compounds in the lumen can cross the epithelium via two routes, between the cells, the paracellular route, or across the epithelial cell, the transcellular route [255][256].

The paracellular route is regulated via junctions, i.e. tight junctions, adherens junctions and desmosomes, in the intercellular space between cells [256][257]. This route facilitates the translocation of "medium" (<600 Da) sized hydrophilic molecules, with easier transport of ions and positively charged molecules, and under healthy conditions is impermeable to protein-sized molecules [256][257]. Tight junctions in particular are key in the epithelial bidirectional transport of compounds to and from the intestinal lumen, and regulates polarity of the epithelial cells in the monolayer [257].

The transcellular route allows for both the passive diffusion across the cell membrane of lipid soluble and "small" hydrophilic compounds, and for the active transport via endocytosis of "large" (>600 Da) molecules that cannot be transported via the paracellular route or diffuse through the cell membrane [256][257]. The transport of PAMPs and bacteria via endocytosis is essential for mounting an appropriate an immune response, but can also offer a route for pathogenic bacteria to gain entry into the host [257].

4.1.2 Intestinal permeability and disease

Disrupting any of the processes described above, can lead to increased permeability across the intestine epithelium [253]. Increased intestinal permeability has been linked to Crohn's disease, ulcerative colitis, coeliac disease, graft-vs-host disease, sepsis, irritable bowel syndrome, and extra-intestinal diseases such as cirrhosis [253][256]. Toxins and pathogenic bacteria from the lumen, but also DAMPs from immune responses in the lamina propria, can cause epithelial injury resulting in increased permeability [253]. The increased permeability allows for PAMPs and other toxins from the lumen to cross the epithelium unimpeded, further exacerbating inflammation and intestinal injury [253].

4.1.3 Importance of measuring intestinal permeability

Examination on intestinal biopsies from patients help to understand the cellular processes that are associated with the disease; however, this cannot help to determine causality between toxins, cellular processes, and intestinal permeability [258]. Therefore, *in vitro* and *in vivo* models have been developed, which can help distinguish between association and causality [253], [257], [258]. These models are used to explore the mechanisms involved that lead to increased intestinal permeability and disease progression, which is important to understand disease development [257]. Furthermore, therapeutic drugs can be examined on their effect to remedy increased intestinal permeability [259]. Additionally, orally administered drugs are investigated on their abilities to cross the epithelium to be absorbed into the systemic circulation using permeability models for the biopharmaceutics classification system used by the FDA and EMA [260].

4.1.4 Intestinal permeability assays

Current intestinal permeability markers can be categorised as *in vivo* with either functional or biomarker assays, and *in vitro* functional tests.

In vivo functional permeability assays work by administration of labelled compounds to the gastrointestinal tract of the host and measuring translocation into the blood/urine/tissue [256][261]. Alternatively, i*n situ* functional tests work similar by admiration of labelled compounds to an isolated segments of the intestine and measuring the translocation [256]. The benefit of these permeability models is that all the aspects of the intestine that regulate translocation (host-microbe interactions, intestinal barriers, cell absorption, blood circulation, etc) are examined [256]. Biomarkers can measure permeability by the translocation of bacteria/bacterial products to the other organs or blood circulation [256]. Additionally, epithelial junction gene and protein expression can be measured in samples as a marker of permeability [256], [262], [263]. These biomarkers can be easily measured but alterations in the junction expression does not necessarily equate to increased permeability [256][262]. Confounding factors can affect results of the *in vivo* functional and biomarker assays, they limit delineation of the effect on the epithelium specifically, are time consuming, costly, and come with ethical considerations [253][256].

In vitro functional permeability assays using 2D epithelial monolayers (most notably Caco-2 cells) can measure epithelial permeability directly. Caco-2 cells are plated and differentiated on a semi-permeable membrane, commonly Transwell, and trans epithelial electrical resistance (TEER) or the diffusion of labelled compounds (FITC-Dextran) across the monolayer is measured [255][260]. Caco-2 cells when differentiated create a polarised monolayer with microvilli, efflux transporters and junctions similar to the intestine epithelium [260]. Caco-2 cells plated on a Transwell semi-

permeable membrane has also been applied in a microfluidic device to provide fluidic and mechanical forces [264]. The FDA and EMA approved caco-2 TEER assays for the measurement of permeability of oral drugs across the epithelium [260]. However, due to differences in expression of efflux and uptake transporters in caco-2 cells the sole data from Caco-2 permeability assays of permeability for biopharmaceutics classification system is limited to passive transported drugs and thus not used for actively transported drugs by the FDA and EMA [260]. Caco-2 cells are derived from a colon adenocarcinoma, which select to survive harsh environments, high expression of anti-apoptotic genes, and low expression of pro-apoptotic genes, which can increase drug and toxin resistance [253].

In vitro functional permeability tests have recently been developed for intestinal organoids [265]–[271]. Intestinal organoids have been plated on a Transwell as a 2D monolayer, and measured TEER to quantify permeability [270]. However, other permeability assays have also been developed for 3D intestinal organoids. Labelled compounds can be microinjected into the intestinal organoids and the diffusion out of the organoid quantified to measure permeability [265]. Similarly, labelled compounds can be added to the media surrounding intestinal organoids and the diffusion into the organoids quantified to measure permeability [266]–[269]. Additionally, the cell polarity can be reversed to create apical-out organoids, where labelled compounds can be added to the surrounding media "lumen side" and the diffusion into the organoids quantified to measure permeability [271][272].

Table 6: Methods to measure intestinal permeability.

	Method:	Measurement:	Sample:
In vivo / in situ	Labelled compounds	Translocation of compounds	Blood/urine/tissue
	Bacterial biomarkers	Translocation of bacteria/PAMPs	Blood/tissue
	Epithelial biomarkers	Epithelial junction expression	Tissue
***In vitro* (2D)**	Transwell with TEER	Electrical resistance	Live resistance
	Transwell with labelled compounds	Diffusion of compounds	Conditioned media
***In vitro* (3D)**	Labelled compounds	Diffusion of compounds	Live imaging

4.1.5 Characteristics of intestinal organoids to model the intestine epithelium

Intestinal organoids derived from intestinal samples/biopsies contain the cell types from the epithelium and not only enterocytes (Caco-2) [244]. Additionally, supplements added to the intestinal organoids media are similar to the stem cell niche *in vivo*, therefore intestinal organoids do not need to be derived from cancer cells [244][253]. Furthermore, intestinal organoids can be derived from knock-out mice to create intestinal organoids deficient for a specific gene. *In vivo* functional intestinal organoid permeability tests thus facilitate the direct assessment of toxins and drugs on the permeability of the epithelium.

For the above-mentioned benefits of examining intestinal epithelial permeability using intestinal organoids, I examine the feasibility of using *in vitro* functional intestinal organoid permeability assays with the equipment available to us. I hypothesise that mouse intestinal organoids can be used to quantify intestinal epithelial permeability. To examine this, I aim to measure intestinal organoid permeability using established protocols. Alternatively, I aim to develop a permeability assay for mouse intestinal organoids.

4.2 Hypothesis and aims

Hypothesis: Mouse intestinal organoids can be used to quantify intestinal epithelial permeability.

Aim 1: Measure intestinal organoid permeability using established protocols.
Aim 2: Develop a permeability assay for mouse intestinal organoids.

4.3 Materials and Methods

4.3.1 2D mouse intestinal organoid monolayer

To plate mouse intestinal organoids as a 2D monolayer I derived intestinal organoids from mice, according to **2.2.2 Organoid derivation and culture**. Organoids were cultured for a week. Coat wells from a 24-well plate with 100µl collagen and incubate for 1 hour at RT [270]. Excess collagen was removed and the wells washed with PBS once. Media was removed from 4 mouse intestinal organoid domes (50-100 organoids per dome) and organoid dome disrupted by resuspending vigorously with ice cold PBS. The suspension was transferred to a falcon tube and the well rinsed once with fresh ice cold PBS and transferred to the falcon tube to collect residual organoids. The falcon tube was centrifuged at 500g for 3 minutes and supernatant discarded. Organoid pellet was resuspended in 2ml TrypLE and incubate at 37C for 10 minutes to dissociate cells. 10ml PBS was added, centrifuged at 500g for 3 minutes and supernatant discarded. Cell pellet was resuspended in 500µl mouse intestinal organoid media with Rock inhibitor and cell suspension added to collagen coated well. This was Incubated at 37C with 5% CO_2 for 3 days, afterwards media was replaced with

fresh media, and incubated for another 4 days at 37C with 5% CO_2. HOECHST 33342 was added to the media to a final concentration of 5µg/ml, incubated for 30 minutes at 37C with 5% CO_2, and organoids imaged with the Cytation 5 at bright field and DAPI channels.

4.3.2 3D mouse intestinal organoids permeability with FITC-Dextran

Intestinal organoids were derived from mice, according to **2.2.2 Organoid derivation and culture**. Organoids were cultured for a week, and then plated in 30µl domes on a 24 well plate with 500µl intestinal organoid media. Intestinal organoids were incubated at 37C with 5% CO_2 for 3 days. EDTA was added to the media of an organoid well (EDTA) at a final concentration of 2mM and left an organoid well untreated (control). The organoids were incubated for 2 hours at 37C with 5% CO_2, and afterwards added FITC-Dextran 4k.Da to the organoid media at a final concentration of 20µg/ml. Organoids were imaged with the Cytation 5 at bright field and GFP channels.

4.3.3 A permeability assay for mouse intestinal organoids

Intestinal organoid were derived and cultured according to **2.2.2 Organoid derivation and culture**. Intestinal organoids were plated at a density to allow individual organoids to be imaged without overlapping organoids (~50-100 organoids per dome). A single 30 µL Matrigel dome with intestinal organoids was plated in a 24-well plate with 500 µL medium to measure permeability. Additional wells with organoids were used as a negative control, positive permeable control (EDTA), and positive cell death control (Triton X-100).

Table 7: Key resources table.

REAGENT or RESOURCE	SOURCE	IDENTIFIER
Chemicals, peptides, and recombinant proteins		
HOECHST 33342	ThermoFisher	H1399
Propidium Iodide Solution	Merck	P4864
Corning Matrigel Growth Factor Reduced Basement Membrane Matrix, phenol red-free	VWR	734-1101
Gibco DMEM/F12, HEPES	ThermoFisher	11330032
N-2 Supplement (100X)	ThermoFisher	17502048
B27 Supplement (50X)	ThermoFisher	17504044
N-Acetyl-L-cysteine	Merck	A9165
Recombinant murine EGF	PeproTech	315-09
Recombinant murine Noggin	PeproTech	250-38
Recombinant human R-Spondin-1	PeproTech	120-38
Penicillin Streptomycin	ThermoFisher	15140122

EDTA	Merck	ED2SS
Triton X-100	Merck	X100
Experimental models: Organisms/strains		
Mouse: C57BL/6J	The Jackson Laboratory	JAX: 000664
Critical commercial assays		
LDH-Glo Cytotoxicity assay	Promega	J2380
Software and algorithms		
Fiji (or ImageJ)	ImageJ	https://imagej.net/software/fiji/
Other		
Cytation 5	Agilent (BioTek)	https://www.biotek.com/products/imaging-microscopy-cell-imaging-multi-mode-readers/cytation-5-cell-imaging-multi-mode-reader/overview/

Table 8: Mouse intestinal organoid growth media.

Reagent	**Final concentration**	**Amount**
Gibco DMEM/F12, HEPES (2/8°C)	n/a	480 mL
N-2 Supplement (100X) (-5/-20°C)	1X	5 mL
B27 Supplement (50X) (-5/-20°C)	1X	10 mL
N-Acetyl-L-cysteine (2-8°C)	1 mM	81.5 mg
Recombinant murine EGF (-20°C)	50 ng/mL	25 µg
Recombinant murine Noggin (-20°C)	100 ng/mL	50 µg
Recombinant human R-Spondin-1 (-20°C)	1 µg/mL	500 µg
Penicillin (10.000 U/ml), Streptomycin (10.000 µg/ml) (-5/-20°C)	100 U/mL, 100 µg/mL	5 mL
Total	**n/a**	**500 mL**

Intestinal organoid growth medium was stored between 2°C and 8°C. Some components have a short shelf life at 4°C, therefore stock solutions was aliquoted in order to produce fresh medium every week.

Organoid cell staining:

Propidium iodide (PI) is cell impermeable and therefore only stains dead cells. Dead cells within the intestinal organoid lumen are shielded from PI by the intestinal monolayer, and thus will not be stained by PI without an increase in organoid permeability [246].

PI solution (5 mg/ml stock) was mixed in pre-warmed intestinal organoid growth media with a final concentration of 5 µg/mL PI. Existing media in the organoid well was replaced with media with PI, and incubated at 37°C for 20 minutes.

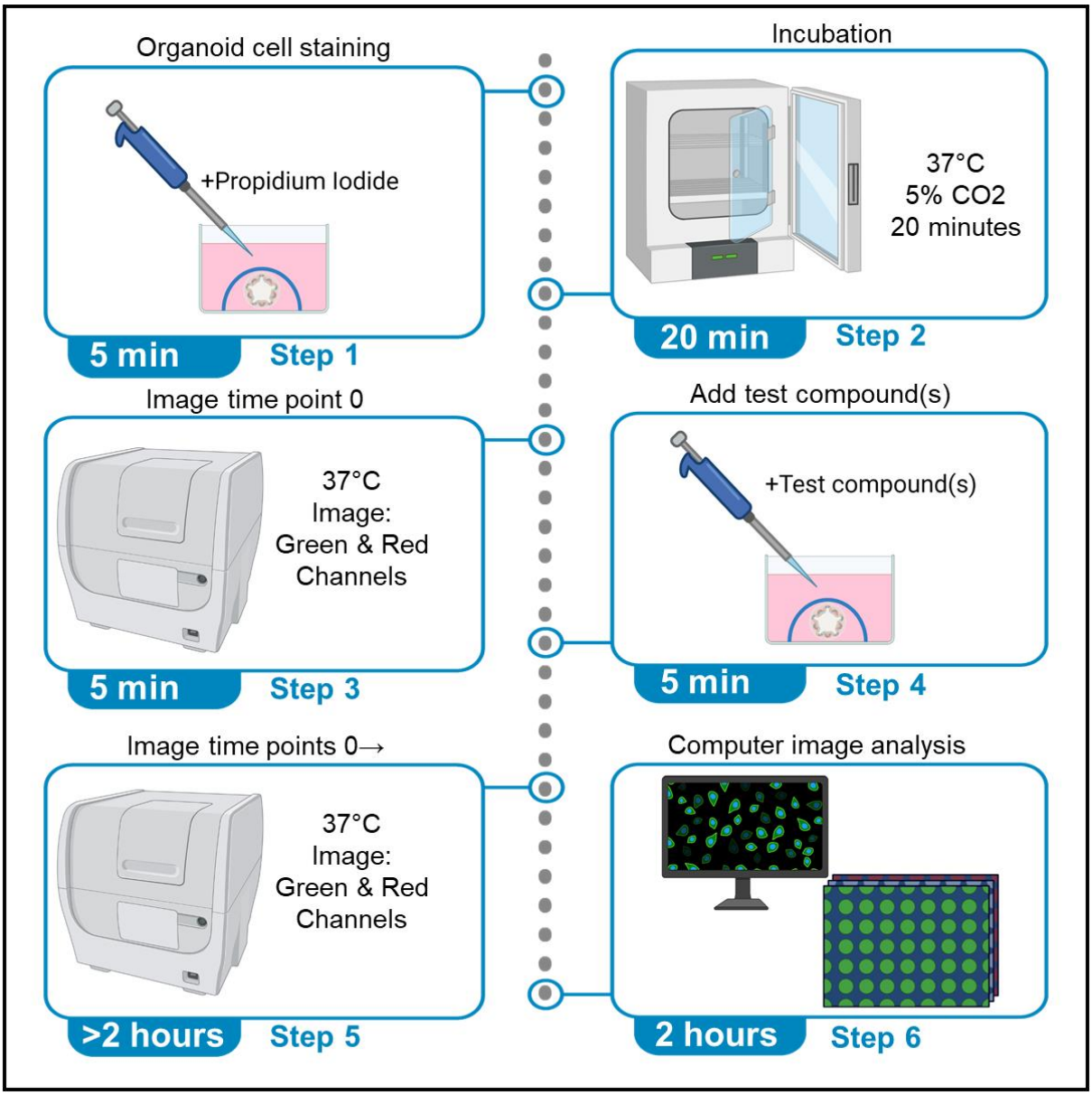

Figure 44: Summary of the steps to measure mouse intestinal organoids using "A permeability assay for mouse intestinal organoids".

Organoid imaging and permeability analysis:

Green background autofluorescence, that is found in the intestinal organoid lumen, is in the green (469-525 nm) channel, and PI is emits in the red (531-593 nm) channel. Measuring PI stain within the organoid lumen at the same position can measure the permeability of the organoid for PI. The

lumen of intestinal organoids can be defined by the green background AF of dead cells and other debris inside the organoid lumen [269].

The stained intestinal organoid plate was added to the Cytation 5 and imaged in the green and red channels for time point 0 as a Z-stack at 4x magnification with most/all organoids in focus.

EDTA and Triton X-100 were added to the organoids for a final concentration of 2mM and 0.5%, respectively. 2 µL media was collected for the LDH assay before taking each image. Control, EDTA, and Triton X-100 treated organoids were imaged with the Cytation 5 every half hour for 150 minutes. LDH was measured, as previously described **2.3.3 Promega LDH-Glo cytotoxicity assay**.

Permeability was measured as follows:

1. Open the green channel image of time point 0 as a stack in Fiji.
    a. "Z Project" the stack to get all organoids of the stack in focus (Image, Stacks, Z Project…, Max Intensity).
    b. Set the "Threshold" (Image, Adjust, Threshold) so that only green background AF of dead cell debris in the organoid lumen is selected.
    c. Select this region of the binary image by "Create Selection" (Edit, Selection, Create Selection).
2. Open the red channel image of time point 0 as a stack in Fiji.
    a. "Z Project" the stack to get all organoids of the stack in focus (Image, Stacks, Z Project…, Max Intensity).
    b. Paste the previously selected region into this image (Control + Shift +E)
    c. Measure the mean intensity of PI in this region by "Measure" (Analyse, Measure).

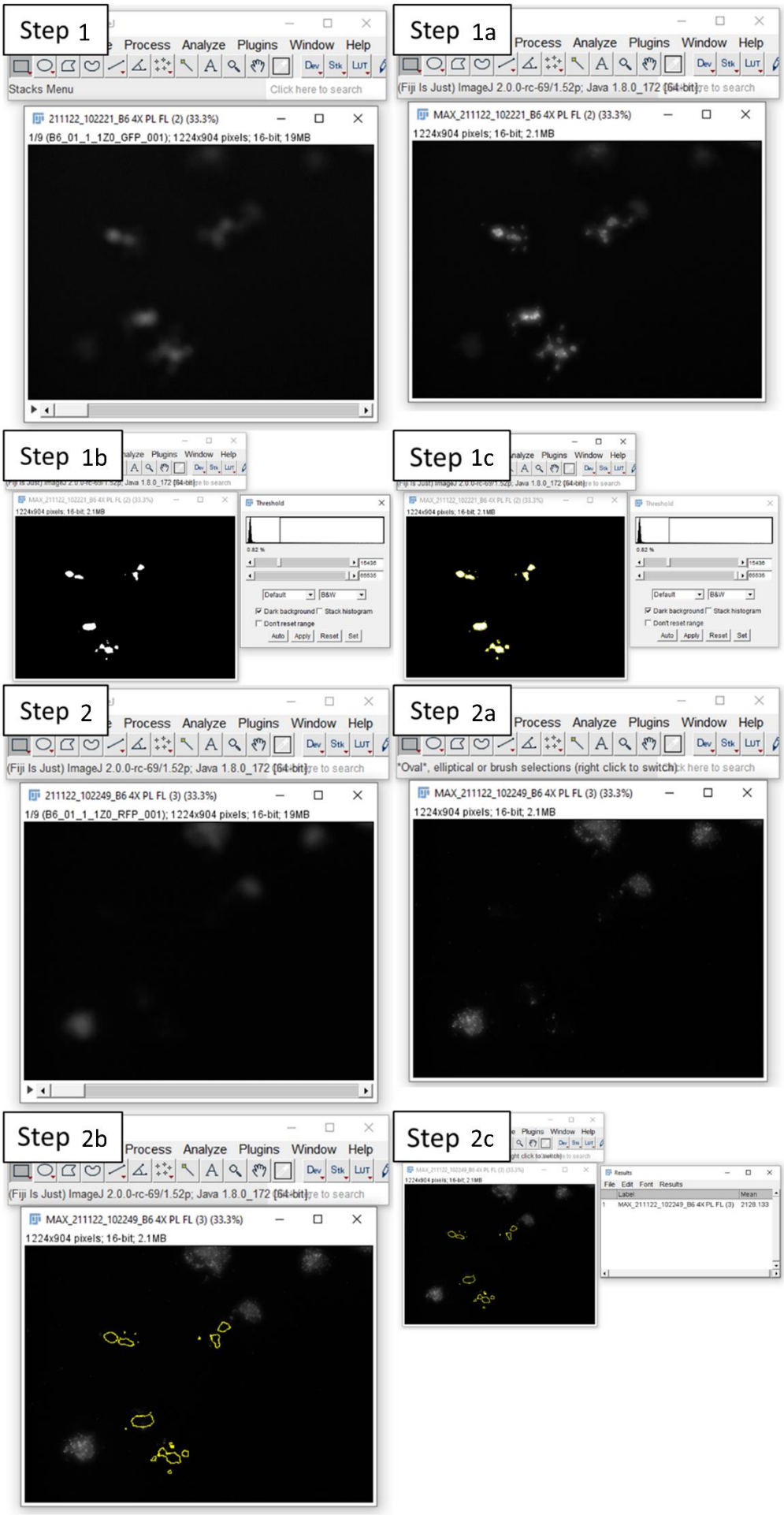
Step 1
Process Analyze Plugins Window Help
Stacks Menu
Click here to search
211122_102221_B6 4X PL FL (2) (33.3%)
1/9 (B6_01_1_1Z0_GFP_001); 1224x904 pixels; 16-bit; 19MB
Step 1a
Process Analyze Plugins Window Help
(Fiji Is Just) ImageJ 2.0.0-rc-69/1.52p; Java 1.8.0_172 (64-bit)
MAX_211122_102221_B6 4X PL FL (2) (33.3%)
1224x904 pixels; 16-bit; 2.1MB
Step 1b
Threshold
Default
B&W
Dark background
Stack histogram
Don't reset range
Auto
Apply
Reset
Set
Step 1c
Threshold
Default
B&W
Dark background
Stack histogram
Don't reset range
Auto
Apply
Reset
Set
Step 2
Process Analyze Plugins Window Help
(Fiji Is Just) ImageJ 2.0.0-rc-69/1.52p; Java 1.8.0_172 (64-bit)
211122_102249_B6 4X PL FL (3) (33.3%)
1/9 (B6_01_1_1Z0_RFP_001); 1224x904 pixels; 16-bit; 19MB
Step 2a
Process Analyze Plugins Window Help
"Oval", elliptical or brush selections (right click to switch)
MAX_211122_102249_B6 4X PL FL (3) (33.3%)
1224x904 pixels; 16-bit; 2.1MB
Step 2b
Process Analyze Plugins Window Help
(Fiji Is Just) ImageJ 2.0.0-rc-69/1.52p; Java 1.8.0_172 (64-bit)
MAX_211122_102249_B6 4X PL FL (3) (33.3%)
1224x904 pixels; 16-bit; 2.1MB
Step 2c
Results
File Edit Font Results
Label
Mean
1 MAX_211122_102249_B6 4X PL FL (3) 2128.133

Figure 45: Fiji screenshots of steps 8-9.

3. Open the other time points of the red channel and repeat step 2.
4. Compare the mean intensity of PI stain of dead cells inside the selected organoid lumen of treated organoids to control (untreated) organoids. By measuring mean PI intensity inside the selected organoid lumens at time point 0 the size and number of organoids are normalised and are equalised at time point 0. By comparing treated to control luminal mean PI intensity after treatment time any change in background fluorescence is accounted for. When analysing data after a pre-selected time point a parametric/non-parametric test can be used, e.g. t-test or ANOVA.

4.4 Results

4.4.1 Measure intestinal organoid permeability using established protocols.

I examined two permeability methods for intestinal organoids with in house equipment for the feasibility of measuring mouse intestinal organoids permeability in response to insults and drugs. Transepithelial electrical resistance (TEER) can be used to measure permeability across a 2D epithelial monolayer. Mouse intestinal organoids were grown on coated wells to grow 2D mouse intestinal organoid monolayers. Mouse intestinal organoids grown on coated wells formed 2D monolayer clusters, but did not form an intact 2D epithelial monolayer, which is needed to measure permeability with TEER, **Figure 46**.

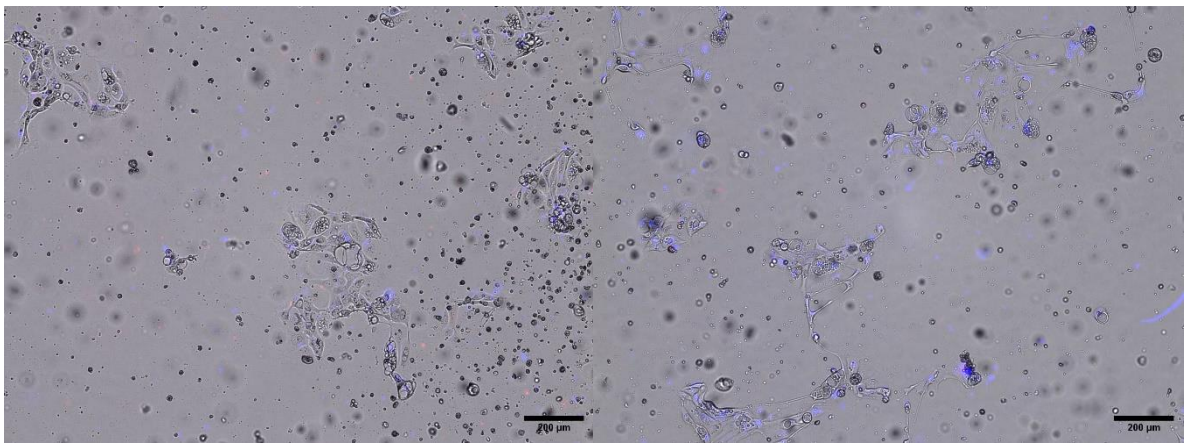

Figure 46: Brightfield and HOECHST stained 2D mouse intestinal organoid monolayer images.

FITC labelled 4k.Da dextran can be used to measure permeability in the intestinal organoids by assessing the fluorescence inside and outside the organoid, after addition of FITC labelled 4.Da dextran to the media. Mouse intestinal organoids were treated with and without 2mM EDTA, which disrupt cell-cell junctions, and FITC labelled 4.Da dextran added to the media. The Cytation 5 automated fluorescence microscope (not confocal) was used to image the 2mM EDTA treated and

untreated mouse intestinal organoids with FITC labelled 4.Da dextran media. FITC labelled 4k.Da dextran fluorescence difference between in and outside the intestinal organoid in control and 2mM EDTA treated organoids could not be determined due to the fluorescence bleeding from the out of focus planes, **Figure 47**.

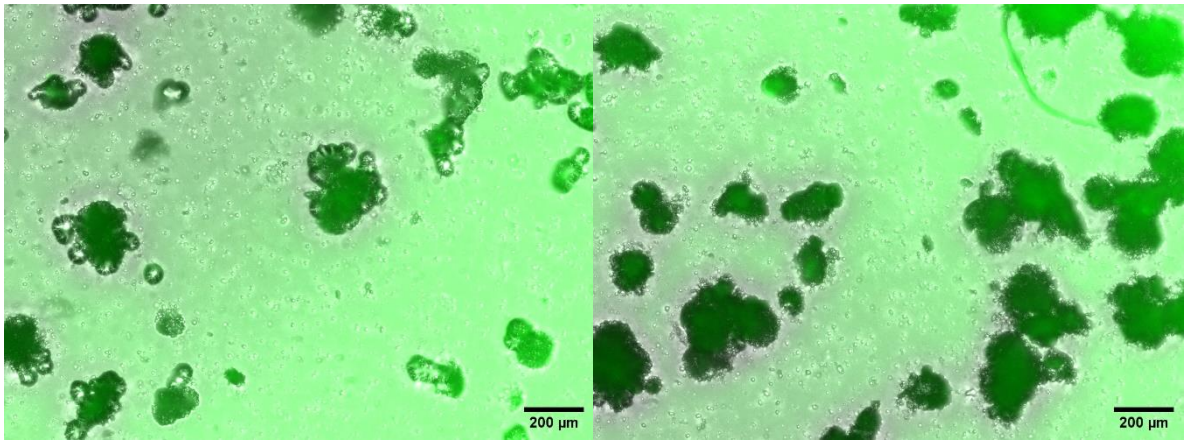

Figure 47: Mouse intestinal organoids permeability assay with FITC labelled dextran. *Mouse intestinal organoid permeability assay using FITC labelled dextran 4 k.Da to measure dextran diffusion across organoid membranes. Left: untreated, Right: 2mM EDTA treated for 2 hours.*

4.4.2 Develop a permeability assay for mouse intestinal organoids.

I developed this permeability assay for mouse intestinal organoids on two observations. Intact mouse intestinal organoids showed a high green background autofluorescence in lumen, which is originated by dead cell debris and mucus [269]. Propidium Iodide, did not penetrate the intestinal organoid lumen to stain extruded dead cells inside intact intestinal organoids, however is able to diffuse into the intestinal organoid and stain the extruded dead cells in the lumen if the organoid is made permeable [246][253].

Untreated mouse intestinal organoids (timepoint 0) showed a clearly defined intestinal organoid lumen in the green channel (excitation 469, emission 525), **Figure 48**. 150 minutes after 2mM EDTA treatment the green background autofluorescence inside of the organoid lumen was less prominent. The lumen region at timepoint 0 was selected and overlayed on the red channel with propidium iodide stained cells. At timepoint 0 no propidium iodide stained cells are visible in the lumen region, but 150 minutes after 2mM EDTA treatment, propidium iodide is able to stain the dead cells inside the organoid lumen.

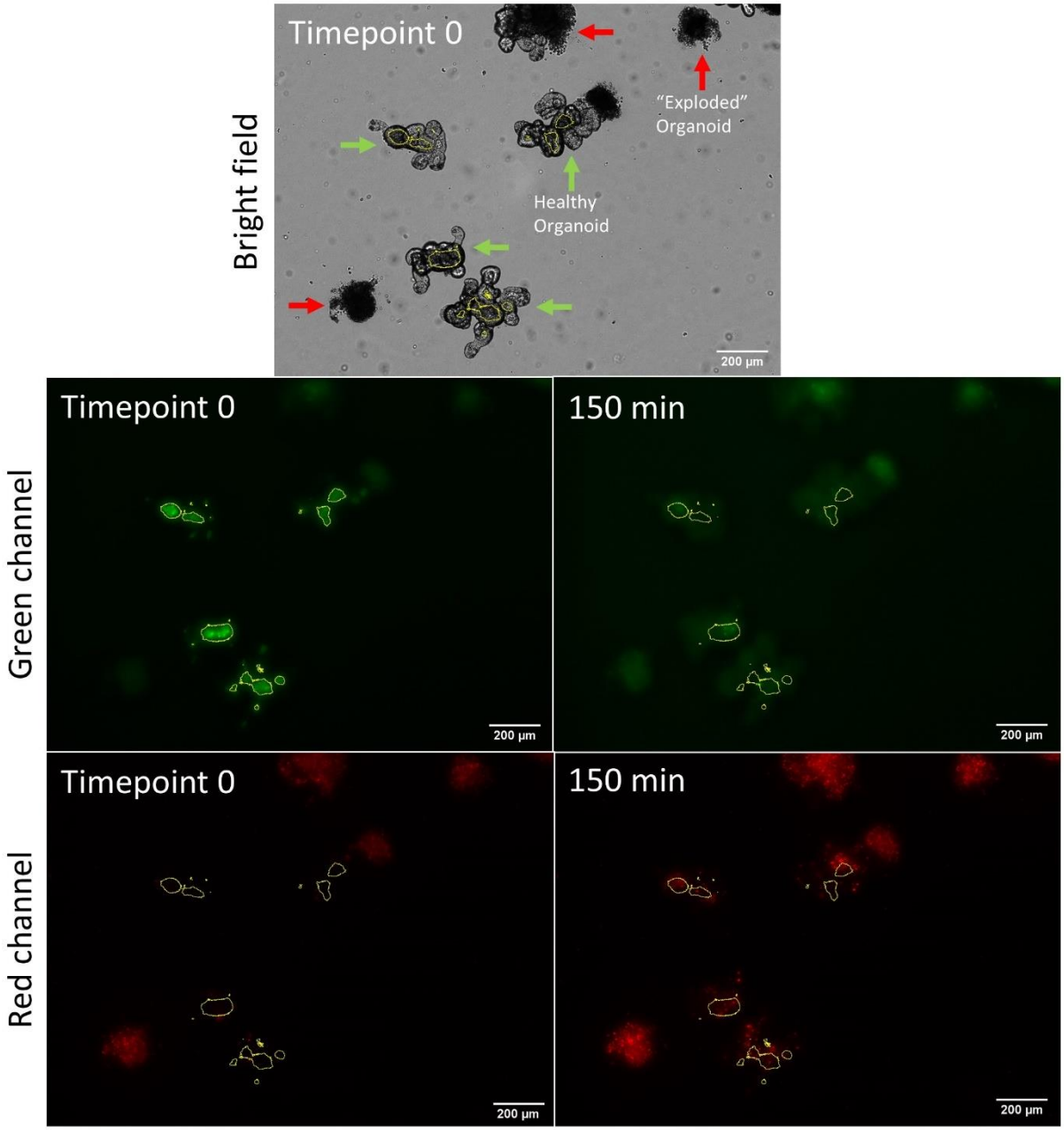

Figure 48: Intestinal organoids treated with EDTA. *Mouse intestinal organoids were treated with 2 mM EDTA and imaged at time point 0 and every 30 minutes for 150 minutes. A bright field image at time point 0, green channel images of time point 0 and after 150 minutes, and red channel images from time point 0 and after 150 minutes are shown with luminal region selected from the green channel from time point 0.*

To quantify intestinal organoid permeability with this technique, the luminal propidium iodide intensity inside the lumen was measured of control, EDTA (to permeabilise), and Triton-X (to cause cell death) treated mouse intestinal organoids every 30 minutes for 150 minutes total, as well as cell death determined with LDH release into the conditioned media. Control mouse intestinal organoids showed a low background and level luminal propidium iodide intensity over 150 minutes, as well as low and level LDH in the conditioned media. Mouse intestinal organoids treated with 2mM EDTA

started at the same low background luminal propidium iodide intensity at 0 minutes, but the signal increased over time, becoming significantly different at 90 minutes, after which it plateaued and remained constant for the duration of the assay. However, LDH in the conditioned media of 2mM EDTA treated organoids was similar to control and did not increase over time.

Mouse intestinal organoids treated with 0.5% Triton-X started at the same low background luminal propidium iodide intensity at 0 minutes, which significantly increased over time already after the first 30 minutes. Triton-X treatment also increased LDH in the conditioned media with a significant increase after 150 minutes.

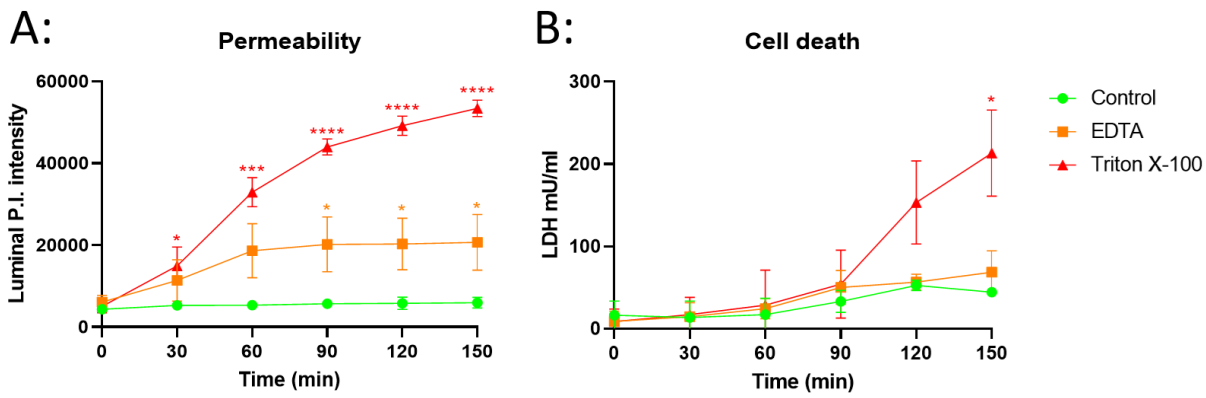

Figure 49: Results of luminal propidium iodide and LDH measurements of intestinal organoids. *Luminal propidium iodide stain and LDH release of intestinal organoids treated with 2mM EDTA, and 0.5% Triton X-100 were measured over time using this intestinal organoid permeability assay and compared to control. Statistics calculated using two-way ANOVA with post-hoc Tukey test, *p<0.05, **p<0.01,***p<0.005, ****p<0.0001, n=4.*

4.5 Discussion

I hypothesised that mouse intestinal organoids can be used to quantify intestinal epithelial permeability. My aims were to 1: measure intestinal organoid permeability using established protocols, 2: develop a permeability assay for mouse intestinal organoids.

Other groups have successfully used intestinal organoids plated as an intact 2D monolayer on Transwells to measure permeability with TEER and FITC-Dextran 4k.Da [270]. Alternatively, FITC-Dextran 4k.Da can be added to the media apical side and diffusion to the basolateral side can be measured for permeability [270]. I show a proof of principle that intestinal organoids can be plated as a 2D monolayer, but I did not grew an intact monolayer, which is required to measure permeability on Transwells via TEER or FITC-Dextran 4k.Da diffusion. This was likely due to too few starting cells from the number of organoids, and with more organoids full coverage might have been

accomplished. However, because of the large quantity of intestinal organoids required to grow an intact 2D monolayer, this method of measuring permeability in 2D intestinal organoids on Transwell would not be feasible for the planned experiments in the next chapter: **5 Are increased intestinal cell death and reduced stemness associated with cirrhosis?**.

Other groups have successfully used FITC-Dextran 4k.Da diffusion into mouse intestinal organoids to measure permeability with a confocal fluorescence microscope. My images were taken with the Cytation 5, which lacks the optical resolution and contrast of a confocal fluorescence microscope, which uses a spatial pinhole to block out-of-focus fluorescence from planes above and below the focus point. By using a confocal fluorescence microscope the high background fluorescence of FITC-Dextran 4k.Da in the media would be eliminated, which allows for quantification of fluorescence inside and outside the intestinal organoid to determine permeability. However, the requirement of a confocal fluorescence microscope limited the feasibility and through-put of this permeability method to quantify intestinal organoid permeability for my experiments for the next chapter: **5 Are increased intestinal cell death and reduced stemness associated with cirrhosis?**.

I developed this permeability assay for mouse intestinal organoids based on these two observations. Healthy intact intestinal organoids emit green background autofluorescence inside the organoid lumen by dead cell debris and mucus [269]. Additionally, I observed that propidium iodide that stains dead cells, did not penetrate into the intestinal organoid lumen, and did not stain the luminal extruded dead cells inside the intact intestinal organoids. However, propidium iodide was able to penetrate and stain dead cells in the lumen of permeable intestinal organoids and can be used to measure cell death in intestinal organoids in response to insults [246][253].

In vitro experiments have shown that EDTA disrupts tight junctions and induces paracellular pores that facilitate transport exclusively through the paracellular pathway in cell monolayers [262]. In intestinal epithelial adenocarcinoma cells (Caco-2), the mechanism of EDTA disruption of tight junctions has been shown to be through calcium chelation, leading to an increase in paracellular transport [255]. Consequently, EDTA has been used to loosen crypt cells from isolated intestines for organoid derival, and also to increase organoid permeability [254][274].

Using this protocol, the effect of a toxin or compound on intestinal organoid permeability can be measured over time. Untreated intestinal organoids are not expected to show an increase in organoid permeability and will show a horizontal line of luminal PI accumulation over time. EDTA treated intestinal organoids showed an increase in luminal propidium iodide intensity in the absence of cell death. Therefore, luminal propidium iodide intensity can be used to measure permeability. Triton-X treated intestinal organoids also showed an increase in luminal propidium iodide intensity

but accompanied by an increase in cell death. Triton X-100 induces a loss of inter- and intra-cellular integrity through detergent action, leading to increased cell permeability and cell death, which results in propidium iodide staining of all organoid cells.

My permeability assay has limitations that can restrict its use for certain experiments. This protocol determines the lumen by green background autofluorescence at time point 0 and measures propidium iodide intensity within that region pre and post treatment. Since the lumen will grow as the organoids is growing and expending, over time the lumen will be different from time point 0. Therefore, this exact protocol is not suitable to measure permeability after treatment with toxin/compound's that take more than 24 hours.

Compounds with a fluorophore that falls within the same emission wavelength as PI cannot be administered as this will interfere with the measurement of dead cells inside the organoid lumen. However, compounds with different fluorophores can be administrated to intestinal organoids to determine their effect on organoid permeability.

To measure propidium iodide stained cells inside the organoid lumen, it is essential to image on the same spot as time point 0, as the lumen areas are defined at that time point. I utilise the Cytation 5, which can image at precise locations in a repeated manner over time; other automated fluorescence microscopes can be used as well, provided that the image location can be repeated.

In this protocol the intestinal organoid lumen is defined by the green background autofluorescence of dead cell debris and mucus within the lumen of intact organoids. This automatically excludes dead and/or damaged organoids which lack an intact lumen, since they do not show green background autofluorescence. Intestinal organoids that are newly-plated may lack the green background autofluorescence of dead cell debris and mucus within the lumen since insufficient dead cell debris and mucus may have been extruded into the lumen or insufficient dead cells to be stained; these organoids are thereby excluded from this protocol.

This protocol can in principle also be used to measure permeability of intestinal organoids derived from other species, if healthy and proliferating intestinal organoids are used. Sato *et al.,* has described deriving and culturing of organoids from mice samples and human biopsies of the small intestine and colon into differentiated budding intestinal organoids and colon organoids [244]. It is important to notice that this assay requires green background autofluorescence of dead cell debris and mucus inside the organoid lumen, which excludes analysing permeability on other types of organoids that do not extrude dead cells into the organoid lumen. For example, intestinal organoids with the polarity reversed, as demonstrated by Co *et al.*, cannot be analysed with this assay [272].

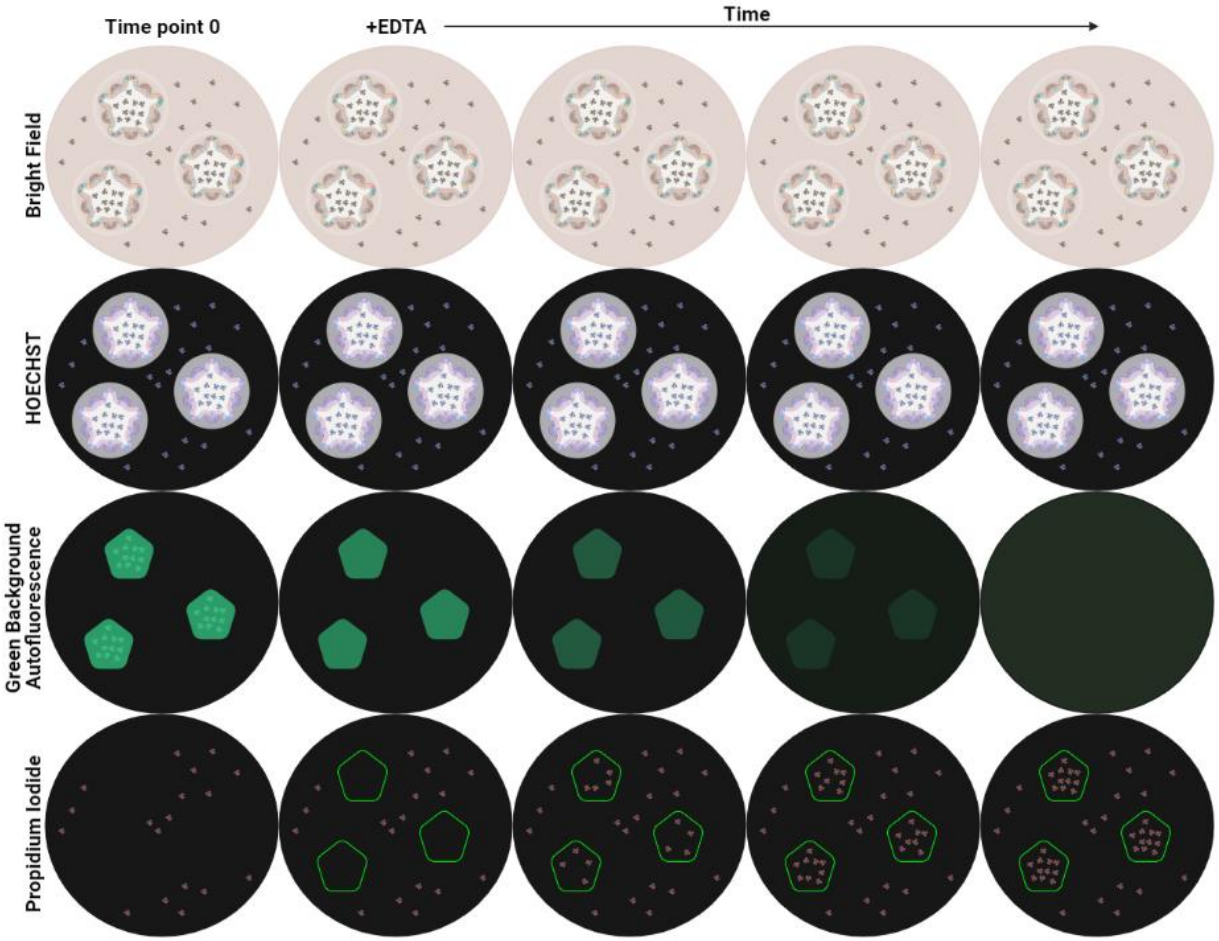

Figure 50: Illustrations of expected EDTA treated intestinal organoids images. *Illustrations of bright field, HOECHST, green background autofluorescence (AF), and propidium iodide (PI) images of intestinal organoids treated with EDTA over time. In the PI images, the luminal areas of intestinal organoids are highlighted, which are made by selecting the luminal region in the green background AF. Analysing PI stain over time in these luminal regions are indicative of organoid permeability.*

4.6 Conclusion

Intestinal permeability is increasingly recognised as an important process in the progression of liver disease and neuropsychiatric disorders. I was unable to grow mouse intestinal organoids as an intact 2D monolayer, which is required to measure permeability on Transwells via TEER or FITC-Dextran 4k.Da diffusion. Furthermore, FITC-Dextran diffusion across whole intestinal organoids could not be used to measure permeability, due to high background fluorescence by FITC-Dextran 4k.Da in the media. Herein, I described a novel, reproducible and scalable assay to assess intestinal permeability in intestinal organoids. Propidium iodide staining of dead cells inside the organoid lumen increased over time when intestinal organoids were permeabilised by EDTA compared to untreated organoids, which did not increase cell death (LDH release). Thus, luminal propidium iodide intensity can be used to measure permeability in mouse intestinal organoids.

5 Are increased intestinal cell death and reduced stemness associated with cirrhosis?

5.1 Introduction

As described in the chapters above, cell renewal and cell death are key factors to maintain intestinal epithelial monolayer homeostasis. Newly proliferated cells from stem cells in the intestinal crypt differentiate and migrate up the villi [150]. However, certain cells: stem cells, Paneth cells in the small intestine, and deep secretory cells/Goblet-like cells in the colon, maintain their position in the crypts [147], [151]–[153]. Cells at the end of their life at the top of the villi are extruded from the epithelial monolayer. Anoikis and apoptosis, in combination with cytoskeletal remodelling, regulates the turn-over of cells in the epithelium while maintaining monolayer integrity [150]. Conversely, necroptosis and pyroptosis, although essential for the host defence with lytic cell death and pro-inflammatory cell signalling, also contributes to increasing epithelial permeability [254][273]. The balance between cell renewal and cell death in the epithelial monolayer is thus essential for maintaining intestinal permeability.

The intestinal epithelium has been extensively investigated for its role in the systemic inflammatory response during intestinal disease such as ischemia/reperfusion, sepsis, and inflammatory bowel. Excessive intestinal cell death has been linked to barrier disruption and increased inflammation during inflammatory bowel disease [274]. Excessive colonic necroptosis contributes to damage to the epithelial integrity as well as the mucosal barrier in IBD, and reducing necroptosis has shown beneficial effects in colitis (inflammatory colon) [254][273]. Additionally, reducing ER stress mediated colonic cell death mediates inflammation and permeability with beneficial effects on survival in mice colitis models [275][276]. The role of pyroptosis in intestinal disease is less clear, with some studies showing beneficial effects of inflammasome deficiency for colitis development, while other studies showing increased susceptibility to loss of epithelial integrity and colitis [163], [165], [181], [183], [277].

Increased intestinal permeability is a known feature of cirrhosis but the underlaying mechanisms remain ill-defined. However, Du Plessis *et al.,* showed an increased of amount of activated macrophages in cirrhosis, which were a source of pro-inflammatory cytokines in the intestinal mucosa [154]. These pro-inflammatory cytokines were also detected in the serum of cirrhosis patients [154]. Furthermore, intestinal permeability was increased in cirrhosis, but no difference in inter-epithelial junction gene and protein expressions was found [154]. These findings indicate that the pro-inflammatory intestinal macrophage response could contribute to the systemic

inflammation in cirrhosis, but a potential role of intestinal macrophage activation on intestinal permeability remains unknown.

The role of intestinal crypt pluripotent stem cells is to replenish the cells removed by cell death in the epithelial monolayer, while maintaining pluripotency [150]. LeBlond's crypt base columnar cells are located in the crypt bottom and actively proliferate into progenitors, which differentiate into enterocytes, goblet cells, Paneth cells, etc. [147], [151], [153]. Potten's quiescent label-retaining stem cells are located at the +4 position and function to replenish CBC cells [151][152]. Additionally, in response to injury revival stem cells from progenitors have been described that can replenish CBC to repair damaged crypts [259][278].

The stem cells in the intestinal crypt require ligands to maintain pluripotency, which are secreted by neighbouring cells in the stem cell niche. Secreted R-spondin in the niche binds to the Lgr5 receptor of stem cells, which leads to binding of RNF43 to the receptor [279]. Additionally, secreted Wnt in the niche binds to Frizzled, which facilitates Frizzled-Axin complex formation [280], [281]. Binding of RNF43 with Lgr5 restricts RNF43 from inhibiting Frizzled-Axin formation [279]. Active Wnt-Frizzled-Axin complex leads to beta-catenin signalling of transcriptional targets of Wnt signalling, including Lgr5, Olfm4 and Axin2, but also the negative regulator RNF43 [279][282]. Inactive Wnt signalling leads to degradation of beta-catenin by the proteasome facilitated by Axin-YAP/TAZ complex [279][282]. Alternatively, YAP can induce gene expression of Ly6a, Clu, Anxa1, etc. that contributes to revival stem cell formation with fetal gene activation to replenish stem cells in response to injury [278][283]. Furthermore, the AHR pathway is a self-regulating negative regulator of the Wnt pathway [284]. Activated AHR leads to expression of RNF43, but also leads to the expression of CYP1, which inhibits the AHR pathway [284].

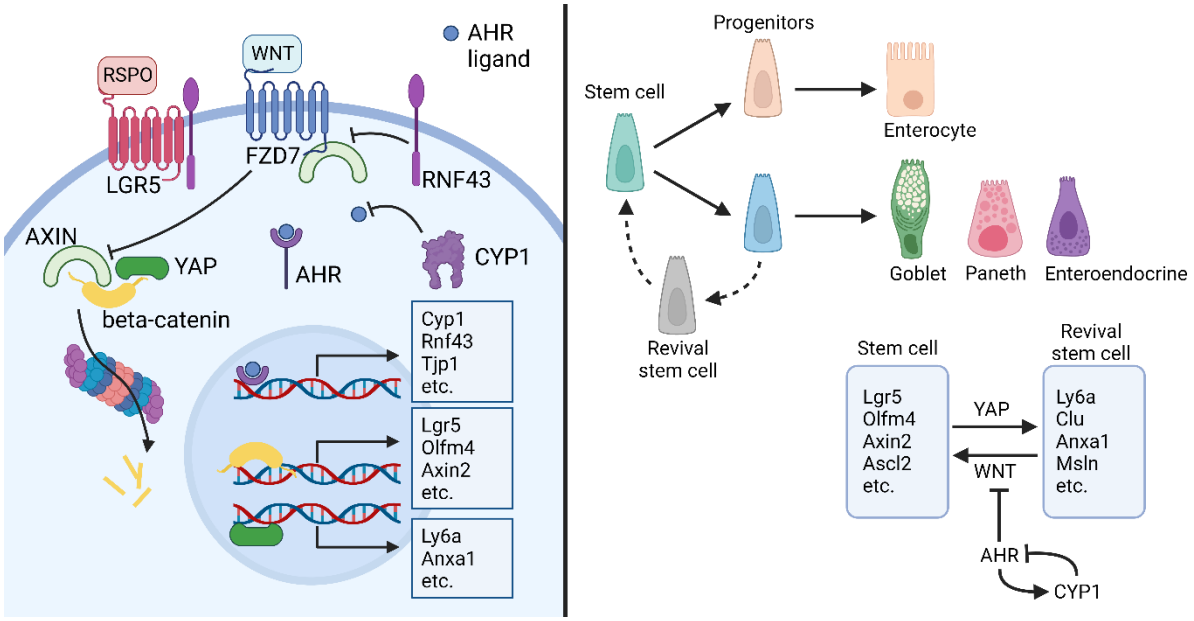

Figure 51: Intestinal crypt base columnar stem cell regulation. *Crypt base columnar stem cell regulation is facilitated by the WNT pathway. WNT and YAP signalling regulates the stem cell and revival stem cell balance in healthy conditions or in response to injury.*

To maintain pluripotency and to grow intestinal organoids in culture, stem cells in isolated intestinal crypts require supplements (e.g. R-spondin, epidermal growth factor, Noggin, etc.) including Wnt for undifferentiated colon organoids of human and mice, and without Wnt differentiating small intestinal organoids [244]. Dysregulation of the pathways that regulate pluripotency can result in a loss of stem cells, or lead to tumorigenesis. For example, AHR deficiency or inhibition reduces the negative regulator of Wnt signalling (RNF43), leading to overstimulation of the Wnt pathway, which results in uncontrolled stem cell proliferation and impaired differentiation (tumorigenesis) in intestinal organoids [167]. AHR ligand can restore epithelial homeostasis by regulating the Wnt signalling in stem cells, and additionally restore inter-epithelial junction expression [167][285]. Furthermore, absence of R-spondin in the intestinal organoid media inhibits growth and decreases survival of the organoids [247]. The proportional response to stem cell receptor ligands and accurate regulation of the stem cell pathway in intestinal organoids, contrary to cancel cell lines, make intestinal organoids a more relevant model to study the cell death and survival response to injury or other manipulations [253].

The Wnt and AHR pathways are affected amongst others by alcohol, fatty diets, and bacterial products, which are drivers of cirrhosis development. Chronic alcohol consumption increases intestinal permeability and induces stem cell injury by dysregulating the Wnt pathway and cell renewal capabilities of intestinal stem cells [286][287]. Additionally, epithelial specific dysregulation of the AHR pathway enhances injury to alcohol, resulting in increased bacterial translocation, which

is protected against by supplementing with AHR agonist to correct AHR pathway activation [288]. Conversely, high fat diet in mice increases the number of intestinal stem cells resulting in increased cell renewal capabilities, which in turn compromises epithelial barrier function and contributes to tumorigenesis [289][290]. Furthermore, LPS induces gut injury by decreasing tight junction, increasing intestinal permeability, disrupting the brush border, and causes excessive crypt cell death resulting in decreased number of Paneth cells, Lgr5+ cells, and overall decreased Olfm4 expression [259]. Increased crypt cell death and depleted Lgr5+ cells induces revival stem cells, but does not alleviate gut injury [259]. Enhancing Lgr5 viability and epithelial regeneration capabilities independent of Wnt/Notch pathways reduced these negative effects by LPS [259]. Additionally, *in vitro* culture of bacteria with intestinal organoids reduces the stem cell population, and results in reduced budding rate and increased mortality [291]. Targeting stem cell regulation for epithelial barrier regeneration and reducing inflammation for gut injury recovery is therefore being investigated for inflammatory bowel disease, but could also be applicable for cirrhosis [146][169].

As previously highlighted, Liu *et al.* showed a role of unfolded protein response mediated intestinal cell death in a BDL cirrhosis mice model and cirrhosis patient intestinal biopsies [194]. ER stress induced by thapsigargin decreased Lgr5 and Ki67 expression in mouse intestinal organoids, but Lgr5 and Ki67 expression was increased in intestinal organoids derived from CHOP deficient mice in untreated and thapsigargin treated organoids [194]. They propose that intestinal ER stress causes a loss of stem cell proliferation and cell renewal, as well as CHOP mediated cell death and accompanied loss of tight junctions during cirrhosis development [194]. This loss of barrier function leads to increased bacterial translocation, contributing to the inflammation and fibrosis in the liver [194]. Furthermore, they showed an unfolded protein response mediated reduction of the villi length in their BDL model, as well as reduced markers of stemness in their BDL model and cirrhosis patient intestinal biopsies [194]. We, however, did not show increased intestinal ER stress in our mice model nor in biopsies from cirrhosis patients, as shown in chapter 3 (**3 Are ER stress mediated intestinal inflammasome activation and pyroptotic cell death associated with cirrhosis?**). However, in chapter 3 I did not investigate the inflammasome-unrelated intestinal cell death or intestinal crypt stemness in cirrhosis. Cell death and cell renewal by intestinal stem cells are essential to maintain epithelial homeostasis, and disruption cell death and stem cells can lead to a decrease of epithelial barrier function [150], [167]–[169], [190]. Therefore, I hypothesis that increased intestinal cell death and reduced stemness are associated with cirrhosis. Therefore, in this chapter I aim to characterise intestinal stemness and cell death in cirrhosis. Additionally, I aim to therapeutically treat intestinal stemness and cell death for beneficial effects in the epithelium, with AHR ligand (FICZ) to regulate

stemness, pyroptosis inhibitor (Disulfiram (DSF)), and inflammation inhibitor (Dimethyl fumarate (DMF)).

5.2 Hypothesis and aims

Hypothesis: Increased intestinal cell death and reduced stemness are associated with cirrhosis.

Aim 1: Characterise intestinal cell death in cirrhosis patients.

Aim 2: Characterise intestinal cell death in cirrhosis rodent model.

Aim 3: Characterise intestinal stemness in cirrhosis rodent models.

Aim 4: Determine effect of reduced stemness on intestinal cell death, permeability, and proliferation.

Aim 5: Characterise cell death, permeability, and proliferation in intestinal organoids derived from cirrhosis rodent models.

Aim:6 Therapeutically target cell death and stemness for beneficial effects on cell death, permeability, and proliferation in intestinal organoids derived from cirrhosis rodent models.

5.3 Materials and Methods

I used our subcutaneous CCl4 cirrhosis mice model as previously described, **2.1.3 Mouse subcutaneous CCl4**. Our 12 week CCl4 administration model (olive oil, CCl4, CCl4 + LPS) was performed at the Institute for Liver and Digestive Health – UCL. Additionally, I used our BDL cirrhosis rat model, **2.1.4 Rat bile duct ligation**. Serum creatinine, ALT, ammonia, GGT, GLUC, and AST was determined as described, **2.1.4 Rat bile duct ligation**.

RNA was isolated from colon tissue of our mice model with TRIzol as previously described, **2.4.1 RNA isolation tissue and cell culture**. cDNA was synthesised according to **2.4.2 cDNA synthesis**, and quantified stem cell markers (OLFM4, KI67, LGR5), and housekeeping (PPIB) gene expression for mice with qPCR as described in **2.4.3 qPCR**. RNA was isolated from Caecum tissue of our rat model with TRIzol as previously described, **2.4.1 RNA isolation tissue and cell culture**. cDNA was synthesised according to **2.4.2 cDNA synthesis**, and quantified stem cell marker (LGR5), AHR pathway (AHR, CYP1A1, CYP1B1), goblet cell marker (MUC2), and housekeeping (RPLP0) gene expression for rat with qPCR as described in **2.4.3 qPCR**.

Intestine tissues from our BDL rat model were formalin fixed, paraffin embedded, and sectioned according to **2.5.3 Tissue formalin fixation, paraffin-embedding, and sectioning**. Human biobank healthy control, cirrhosis, and IBD patient samples came FFPE, which was sectioned according to **2.5.3 Tissue formalin fixation, paraffin-embedding, and sectioning**. Cell death was analysed by TUNEL staining as described by **2.5.5 Abcam TUNEL Assay Kit – BrdU-Red**.

Intestinal organoids were derived from mice, **2.2.2 Organoid derivation and culture**. For the experiments mouse intestinal organoids were plated and cultured immediately with the treatment (LPS, depletion of R-spondin, CH223191, FICZ). Intestinal mouse organoid media was replaced with fresh media with treatment after 2 days. I stained organoids with HOECHST and Propidium Iodide after treatment, according to **2.2.3 Organoid cell death, permeability, and size assay** and quantified cell death, permeability and size. Afterwards, the conditioned media and organoid cell pellet was collected for RNA isolation, **2.4.1 RNA isolation tissue and cell culture**, cDNA synthesis, **2.4.2 cDNA synthesis**, and quantification of inter-epithelial junction proteins (OCL, CLA, TJP), AHR pathway (AHR, CYP1A1, CYP1B1), stem cell markers (KI67, LGR5, AXIN2, YAP1, LY6A, FZD7), and housekeeping (PPIB) gene expression for mice with qPCR, **2.4.3 qPCR**.

Intestinal organoids were derived from another cohort of 20w subcutaneous CCl4 treated and control mice from Schalk van der Merwe's group, **2.2.2 Organoid derivation and culture**. After 6/7 days of culture from deriving, organoid cells were stained by adding HOECHST and Propidium Iodide with an end concentration of 5µg/ml, and added FITC-Dextran 4k.Da with an end concentration of 20µg/ml and incubated for 90 minutes prior to imaging. The stained intestinal organoids were imaged using an inverted confocal fluorescence microscope, measuring green fluorescence inside the organoids normalised to the fluorescence outside the organoids for permeability, and cell death and size as described previously, **2.2.3 Organoid cell death, permeability, and size assay**. Unstained organoids were cryopreserved from control and cirrhosis mice after 6/7 days of culture [292].

Cryopreserved organoids from control and cirrhosis mice were thawed and culture for treatment experiments and isolated organoid cell pellet for RNA isolation, **2.4.1 RNA isolation tissue and cell culture**, cDNA synthesis, **2.4.2 cDNA synthesis**, and quantification of stem cell markers (KI67, LGR5, AXIN2, YAP1, LY6A, FZD7), AHR pathway (AHR, CYP1A1, CYP1B1), and housekeeping (PPIB) gene expression for mice with qPCR, **2.4.3 qPCR**. The thawed cryopreserved organoids (1st passage) were plated and immediately treated with and without 5nM FICZ for 3 days, and organoids were stained with HOECHST and Propidium Iodide after treatment, according to **2.2.3 Organoid cell death, permeability, and size assay** and quantified cell death, permeability, and size. For 2nd, 3rd, 4th, and 5th passaged organoids, they were plated and immediately treated with and without 25µM DSF, 500nM FICZ, 25µM DMF, 500nM FICZ, respectively, for 3 days, and organoids were stained with HOECHST and Propidium Iodide after treatment, according to **2.2.3 Organoid cell death, permeability, and size assay** and quantified cell death, permeability, and size.

5.4 Results:

For this chapter I used our CCl4 cirrhosis mice model from chapter 3 (**3 Are ER stress mediated intestinal inflammasome activation and pyroptotic cell death associated with cirrhosis?**), but due to colon sample collection limitations, I also used a BDL cirrhosis rat model. Serum creatinine, ALT, ammonia, GGT, GLUC and AST were measured from sham, BDL, BDL+LPS and BDL+LPS+DSF treated rats to validate the cirrhosis rat model. Serum creatinine was significantly increased in the BDL+LPS treated rats compared to sham, but not in any of the other groups **Figure 52**. Serum ALT and ammonia, however, were significantly increased in all groups (BDL, BDL+LPS, BDL+LPS+DSF) compared to sham. Serum GGT and AST were both significantly increased in BDL+LPS and BDL+LPS+DSF groups compared to sham (BDL not determined), and serum GLUC significantly decreased in BDL+LPS and BDL+LPS+DSF compared to sham (BDL not determined).

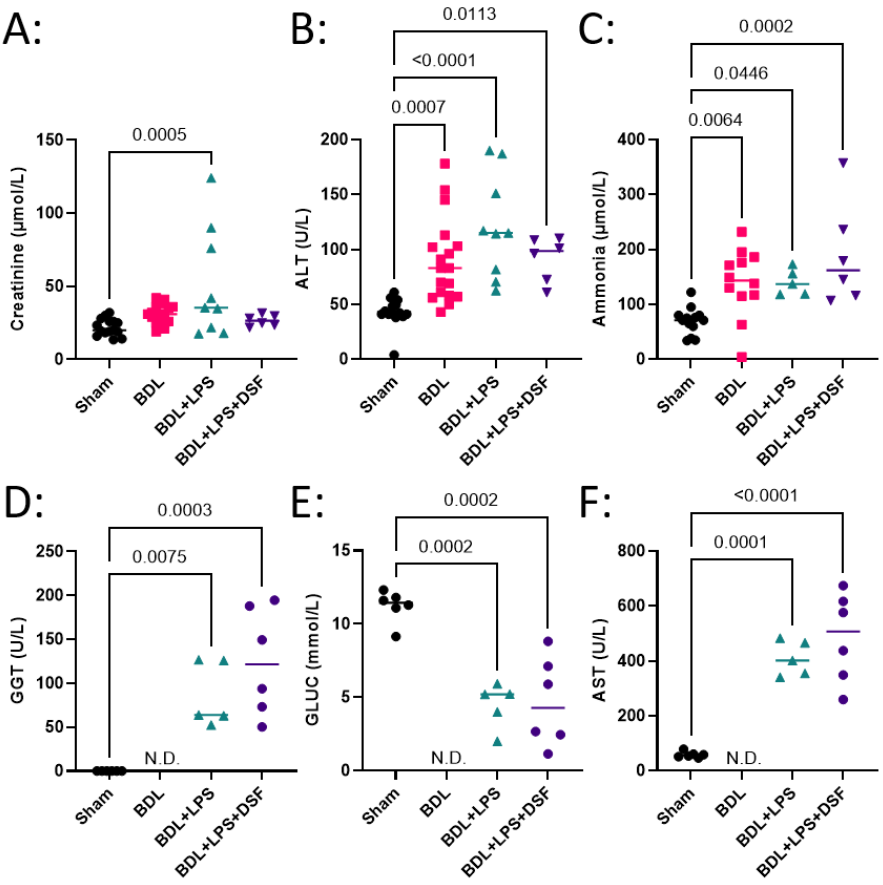

Figure 52: Bile duct ligated cirrhosis rats validation, serum ALP, AST, ALT, Albumin, Creatinine levels. *A: Serum creatinine, B: ALT, C: Ammonia, D: GGT, E: GLUC, F: AST. A-C: Sham (n=15), BDL (n=18), BDL+LPS (n=9), BDL+LPS+DSF (n=6). D-F: Sham (n=6), BDL (n=0), BDL+LPS (n=5), BDL+LPS+DSF (n=6). Groups were compared with one-way ANOVA with Tukey's post hoc test; significance p<0.05.*

5.4.1 Characterise intestinal cell death in cirrhosis patients.

To examine intestinal epithelial cell death in cirrhosis, we acquired biobank FFPE intestinal samples of healthy control, inflammatory bowel disease (IBD), and cirrhosis patients for TUNEL staining. TUNEL staining of ascending colon samples showed a significant increase of epithelial dead cells in cirrhosis patients compared to healthy control, but not in IBD patients, **Figure 53**.

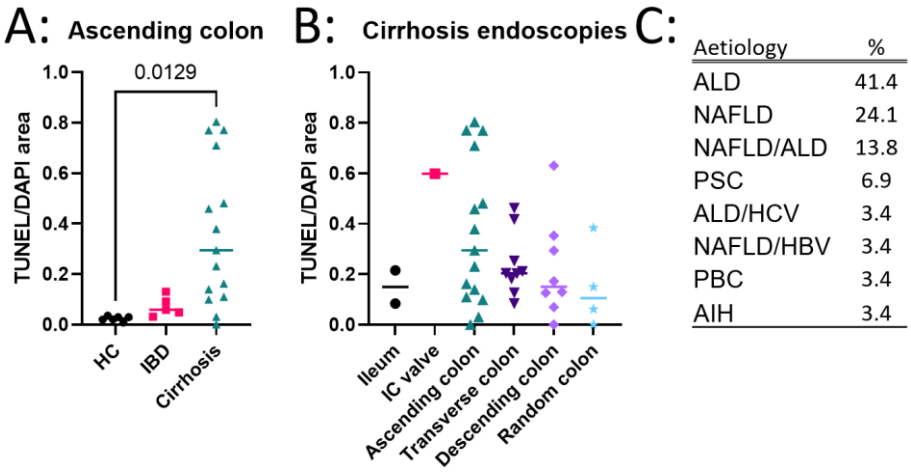

Figure 53: TUNEL cell death staining of human healthy control, IBD, and cirrhosis patient intestinal biobank biopsies. *TUNEL positive cells was measured on FFPE sectioned ileum, IC valve, ascending colon, transverse colon, descending colon, and random colon location biopsies of cirrhosis patients, and ascending colon biopsies of healthy control and IBD patients. A: HC (n=6), IBD (n=5), and cirrhosis ascending colon (n=15) TUNEL stain. B: Cirrhosis ileum (n=2), IC valve (n=1), ascindin g colon (n=15), transverse colon (n=9), descending colon (n=8), and random colon (n=4) biospie TUNEL stain. C: aetiology of cirrhosis patients. Groups were compared with one-way ANOVA with Tukey's post hoc test; significance p<0.05.*

5.4.2 Characterise intestinal cell death in cirrhosis rodent model.

To further determine the effect of cirrhosis on intestinal epithelial cell death, I TUNEL stained epithelial dead cells in intestinal samples from our BDL rat model. I stained the epithelium of ileum, caecum, and colon samples from sham, BDL, BDL+LPS, and BDL+LPS+DSF treated rats. TUNEL staining showed no difference in the ileum and colon across any groups, **Figure 54**. However, in the caecum I observed a significant increase of dead epithelial cells in the BDL+LPS group compared to sham. Interestingly, treatment with DSF in the BDL+LPS group significantly decreased the epithelial cell death to baseline levels.

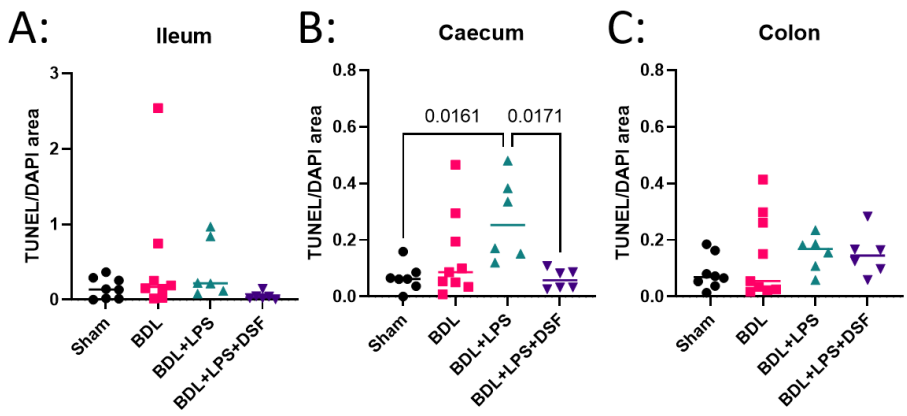

Figure 54: TUNEL cell death staining of rat ileum, caecum, and colon samples. *TUNEL positive cells was measured on FFPE sectioned ileum, caecum, and colon samples from rats. A: Ileum, B: Caecum, C: Colon. Sham (n=8), BDL (n=8), BDL+LPS (n=6), BDL+LPS+DSF (n=6), groups were compared with one-way ANOVA with Tukey's post hoc test; significance p<0.05.*

5.4.3 Characterise intestinal stemness in cirrhosis rodent models.

To determine the effect of cirrhosis on the intestinal epithelial crypt stemness, I measured the gene expression of stem cell markers in colon samples. OLFM4 and Ki67 expression showed no difference across groups of the CCl4 mice models, while Lgr5 was significantly decreased in the colon of CCl4 + LPS mice compared to olive oil and CCl4 groups, **Figure 55**. Furthermore, Lgr5 expression was unchanged in 12-, 14-, 17-, and 20-week CCl4 treated groups.

I determined Lgr5, intestinal crypt stemness genes in the aryl hydrocarbon receptor pathway (AHR, Cyp1a1, Cyp1b1), and Muc2 expression in caecum samples from sham, BDL, BDL+LPS, and BDL+LPS+DSF treated rats to further examine stemness and cell markers in cirrhosis. Caecum Lgr5 expression was significantly decreased in all groups (BDL, BDL+LPS, and BDL+LPS+DSF) compared to sham, **Figure 56**. Caecum AHR, Cyp1a1, Cyp1b1 and Muc2 expression did not show any difference in any of the groups.

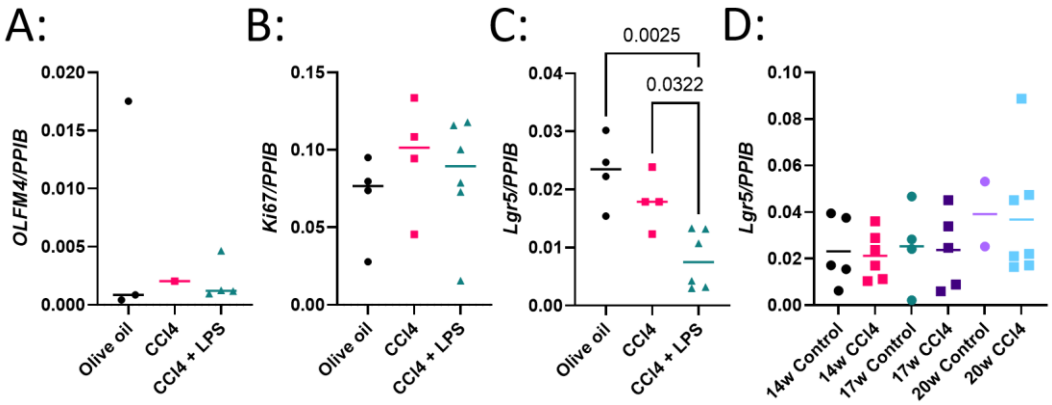

Figure 55: Gene expression of crypt stem cell markers of mouse colon samples. *Gene expression was measured by qPCR on cDNA synthesised from RNA isolates of mouse colon samples. A-C: subcutaneous CCl4 12 weeks model, D: subcutaneous CCl4 14,17,20 weeks model. A: OLFM4, B: Ki67, C-D: Lgr5. A-C: olive oil (n=4), CCl4 (n=4), CCl4+LPS (n=6), D: 14w control (n=5), 14w CCl4 (n=6), 17w control (n=4), 17w CCl4 (n=6), 20w control (n=5), 20w CCl4 (n=7). Groups were compared with one-way ANOVA with Tukey's post hoc test; significance p<0.05.*

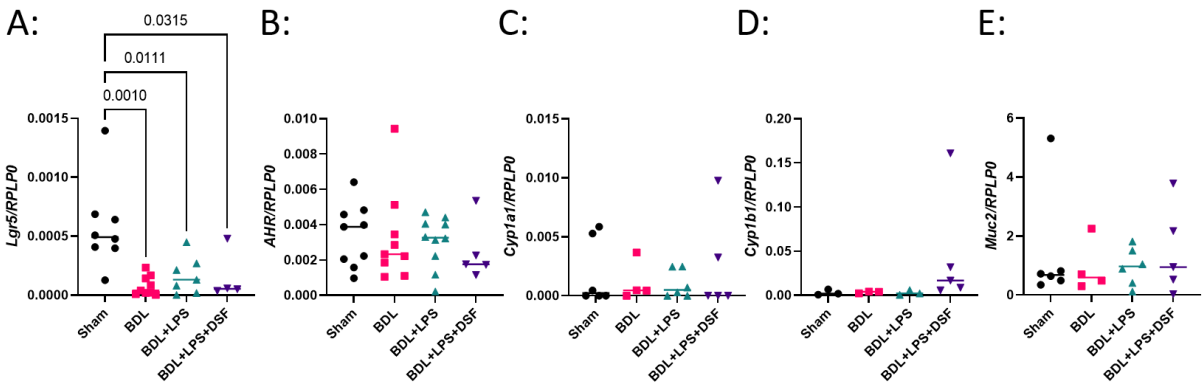

Figure 56: Gene expression of stem cell markers and goblet cell marker of rat caecum samples. *Gene expression was measured with qPCR on cDNA synthesised from RNA isolates of rat caecum samples. A: Lgr5, B: AHR, C: Cyp1a1, D: Cyp1b1, E: Muc2. A-B: Sham (n=11), BDL (n=9), BDL+LPS (n=10), BDL+LPS+DSF (n=5). C-E: Sham (n=6), BDL (n=4), BDL+LPS (n=6), BDL+LPS+DSF (n=5). Groups were compared with one-way ANOVA with Tukey's post hoc test; significance p<0.05.*

5.4.4 Determine effect of reduced stemness on intestinal cell death, permeability, and proliferation.

To examine the effect of "long" exposure to bacterial PAMPs and reduced stemness on cell death, permeability, and growth in the intestine epithelium, I treated mouse intestinal organoids with LPS, depletion of R-spondin from the media, or a combination of both for 4 days. All treatments significantly increased cell death in mouse intestinal organoids compared to control, **Figure 57**. Depletion of R-spondin with LPS significantly increased cell death compared to LPS only treatment

but did not increase cell death when compared to depletion of R-spondin alone. Permeability was unaffected by all treatments, but all treatments significantly decreased the size of the mouse intestinal organoids.

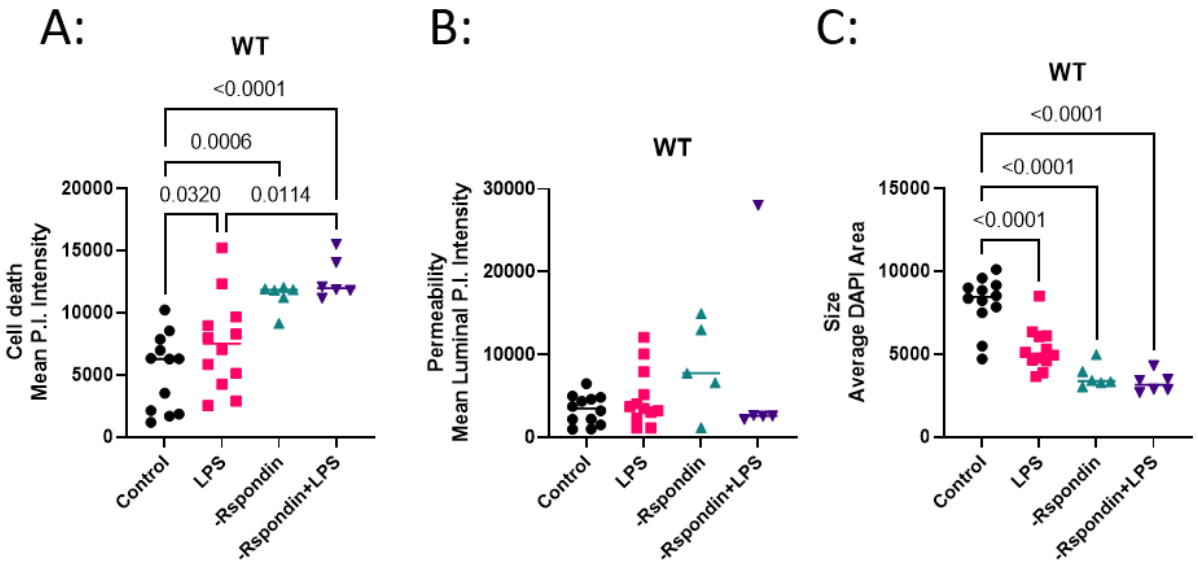

Figure 57: Mouse intestinal organoids treated with LPS with and without the depletion of R-spondin in the culture media for size, permeability, and cell death. *Mouse intestinal organoids were cultured with 100µg/ml LPS, depletion of R-spondin from the culture media, and depletion of R-spondin with 100µg/ml LPS, cultured for 4 days. Cells were stained with HOECHST and propidium iodide and fluorescent images were taken for HOECHST, green autofluorescence, and propidium iodide. A: Cell death was measured by mean propidium iodide intensity in HOECHST stained organoid areas, B: Permeability was measured by mean luminal propidium iodide intensity in green autofluorescent lumen, and C: Size was measured by mean HOECHST stained organoid areas. A-C: control (n=12), LPS (n=12), -Rspondin (n=6), -Rspondin+LPS (n=6), groups were compared with mixed-effects analysis with Hilm-Sidak's multiple comparisons test, significance p<0.05.*

In order to eliminate the confounding factor of increased cell death and focus on the effects of reduced stemness on permeability and size, I treated mouse intestinal organoids with an AHR antagonist (CH223191) and/or AHR ligand (FICZ) to manipulate stem cell maintenance. 5µM CH223191 treatment resulted in a significant increased permeability, without a difference in cell death or organoid size, **Figure 58**. Alternatively, 500nM FICZ treatment significantly increased cell death, but did not affect permeability of size. Treatment of 5µM CH223191 with 500nM FICZ or 5µM FICZ did not ameliorate the increased permeability, but combination treatment did significantly increased cell death (5µM FICZ only) and significantly decreased organoid size.

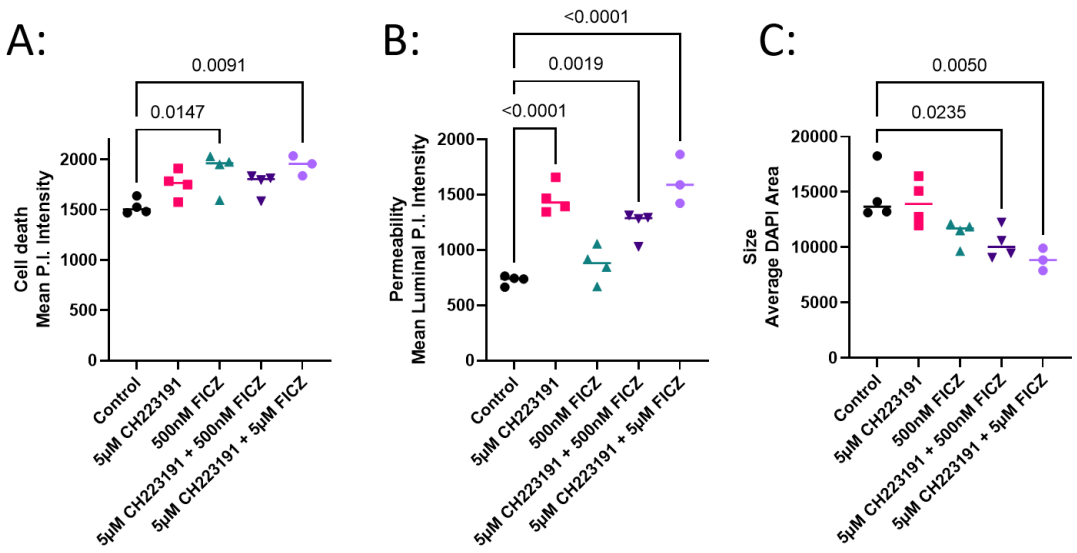

Figure 58: Mouse intestinal organoids treated with CH223191 and FICZ for size, cell death and permeability. *Mouse intestinal organoids were treated with 5µM CH223191, 500nM FICZ, and 5µM FICZ for 3 days. Cells were stained with HOECHST and propidium iodide and fluorescent images were taken for HOECHST, green autofluorescence, and propidium iodide. A: Cell death was measured by mean propidium iodide intensity in HOECHST stained organoid areas, B: Permeability was measured by mean luminal propidium iodide intensity in green autofluorescent lumen, and C: Size was measured by mean HOECHST stained organoid areas. Control (n=4), 5µM CH223191 (n=4), 500nM FICZ (n=4), 5µM CH223191 + 500nM FICZ (n=4), 5µM CH223191 + 5µM FICZ, n=3, groups were compared with one-way ANOVA with Tukey's post hoc test; significance p<0.05.*

Gene expression of epithelial junction proteins and AHR pathway genes were examined in the mouse intestinal organoids treated with CH223191 and FICZ. No significant differences in tight junction expressions, occludin, claudin, and tight junction protein 1, was found between any of the groups, but undetectable levels in several samples limited statistical power. Additionally, no significant differences was found in the markers of the AHR pathway, AHR, CYP1A1, CYP1B1, between any of the groups, but also here undetectable levels in several samples limited statistical power. However, AHR gene expression showed a small upward trend in the CH223191 treated organoids.

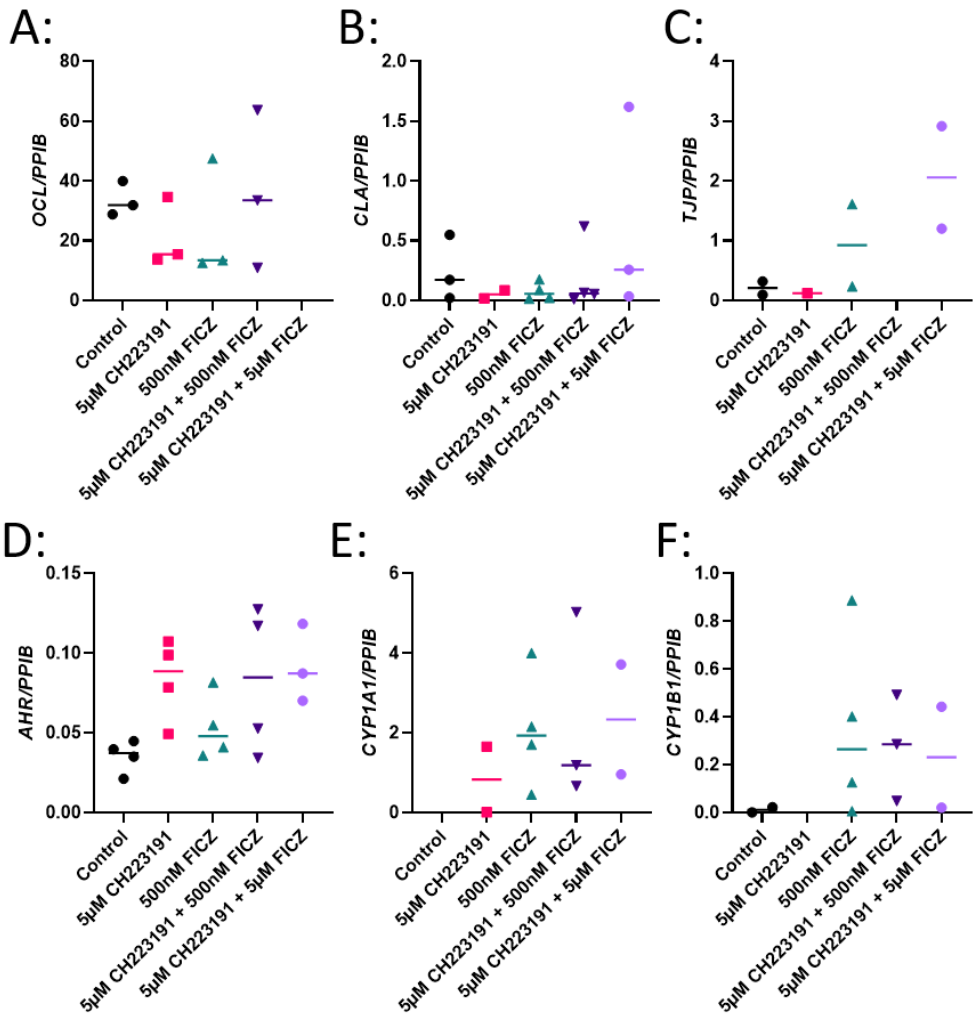

Figure 59: Gene expression of junction proteins and AHR pathway genes of mouse intestinal organoids treated with CH223191 and FICZ. *Mouse intestinal organoids were treated with 5µM CH223191, 500nM FICZ, and 5µM FICZ for 3 days. Gene expression was measured with qPCR on cDNA synthesised from RNA isolated from mouse intestinal organoids. Gene expression of A: Occludin B: Claudin, C: Tight junction protein 1, D: Aryl hydrocarbon receptor, E: Cyp1a1, and F: Cyp1b1. Control (n=4), 5µM CH223191 (n=4), 500nM FICZ (n=4), 5µM CH223191 + 500nM FICZ (n=4), 5µM CH223191 + 5µM FICZ, n=3, groups were compared with one-way ANOVA with Tukey's post hoc test; significance p<0.05.*

5.4.5 Characterise cell death, permeability, and proliferation in intestinal organoids derived from cirrhosis rodent models.

To examine whether the effect of cirrhosis on the intestine maintains its phenotype in organoids I derived organoids from control and cirrhosis mice. Mouse intestinal organoids derived from cirrhosis mice showed significantly increased cell death compared to organoids derived from control mice, **Figure 60**. Cirrhosis mice organoids did not significantly affect permeability, but did show a trend upward. Furthermore, cirrhosis mice organoids showed no significant difference in size compared to control. Additionally, gene expression markers of stem cell were analysed in these organoids. No significant differences were found of Ki67, Axin-2, Yap-1, Ly6a, Frizzled-7, AHR, Cyp1a1, Cyp1b1

between organoids derived from cirrhosis mice and control mice, **Figure 61**. However, gene expression of Lgr5 was significantly increased and expression of Frizzled-7 significantly decreased in cirrhosis organoids.

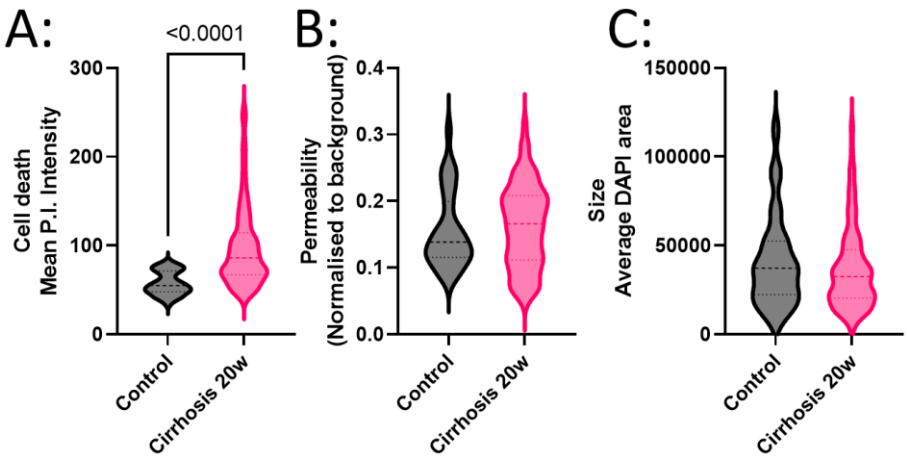

Figure 60: Mouse intestinal organoids from control and cirrhosis mice (20w CCl4). *Mouse intestinal organoids were dervived from control and 20w CCl4 subcutaneous treated mice and analysed for A: Cell death, B: Permeability, and C: Size, after a week of culture. Control (n=29), Cirrhosis 20w (n=124), groups were compared with Mann-Whitney t-test, significance p<0.05.*

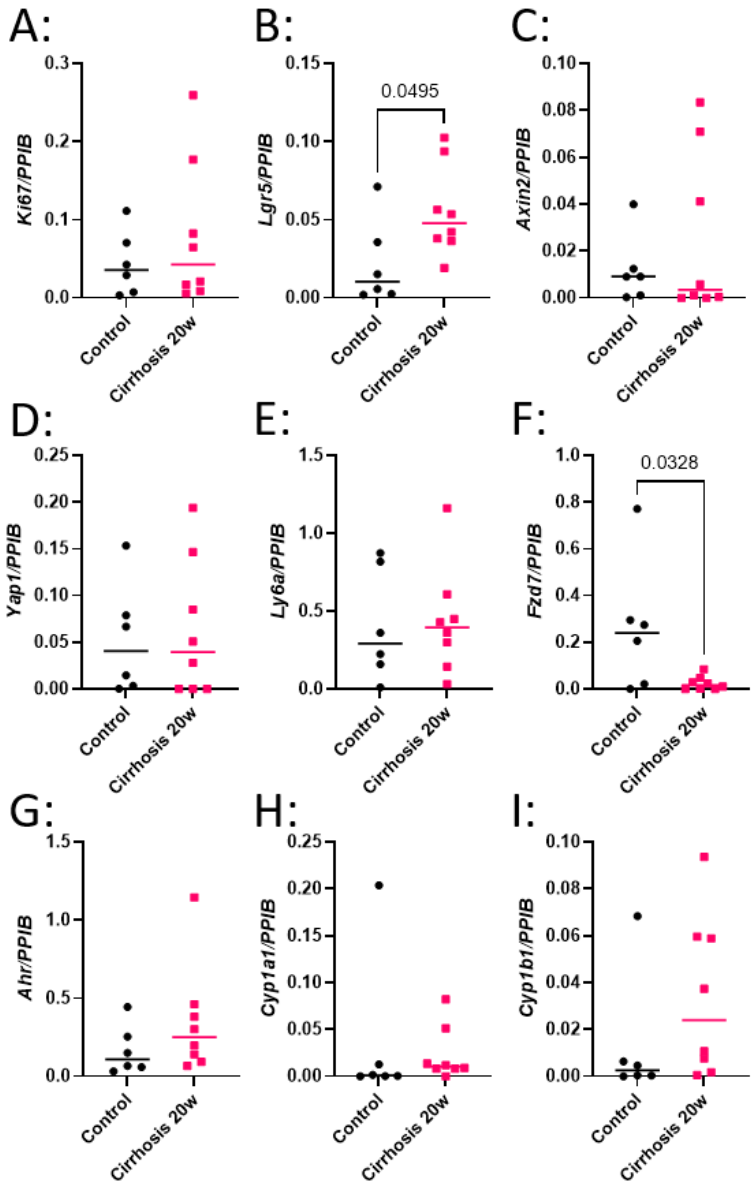

Figure 61: Gene expression of stem cell markers in intestinal organoids from control and cirrhosis mice. *Mouse intestinal organoids were derived from control and 20 week CCl4 treated mice. Gene expression was measured with qPCR on cDNA synthesised from RNA isolated from mouse intestinal organoids. Gene expression of A: Ki67 B: Lgr5, C: Axin-2, D: Yap1, E: Ly6a, F: Frizzled-7, G:AHR, H: Cyp1a1, and I: Cyp1b1. Control (n=6), cirrhosis 20w (n=8), groups were compared with Mann-Whitney t-test, significance p<0.05.*

5.4.6 Therapeutically target cell death and stemness for beneficial effects on cell death, permeability, and proliferation in intestinal organoids derived from cirrhosis rodent models.

To determine whether the phenotype of cirrhosis in intestinal organoids could be therapeutically targeted, I examined the effects of FICZ, DSF (pyroptosis inhibitor) and DMF (inflammation inhibitor) on organoid cell death, permeability, and size. Treatments were examined on the organoids from cirrhosis mice and control mice for cell death, permeability, and size with 5nM FICZ after the 1st passage, 25µM DSF 2nd passage, 500nM FICZ 3rd passage, 25µM DMF 4th passage, and 500nM FICZ 5th passage.

After 1st passage, cirrhosis organoids showed significantly increased permeability, showed no significant difference in cell death and size, but showed an upward trend cell death **Figure 62**. 5nM FICZ treatment did not significantly affect cell death or permeability in control or cirrhosis organoids but did cause a significant difference in size between control and cirrhosis organoids.

After 2nd passage, cirrhosis organoids maintained the significant increased permeability and upward trend in cell death. 25µM DSF treatment significantly increased cell death and permeability in control and cirrhosis organoids, and significantly decreased size in control organoids.

After 3rd passage, cell death and permeability were significantly increased in cirrhosis organoids. Importantly, 500nM FICZ treatment ameliorated the increased cell death and permeability, with permeability of treated cirrhosis organoids to the same level of untreated and treated control organoids.

After 4th passage, cell death was significantly increased in cirrhosis organoids. Permeability was not significantly different in the cirrhosis organoids, but showed an upward trend. Interestingly, DMF treatment negatively affected cirrhosis organoids, significantly increased cell death and permeability, but did not affected control organoids.

After 5th passage, increased cell death and permeability in cirrhosis organoids was ameliorated. 500nM FICZ treatment did not significantly affected cell death, permeability, or size in control or cirrhosis organoids.

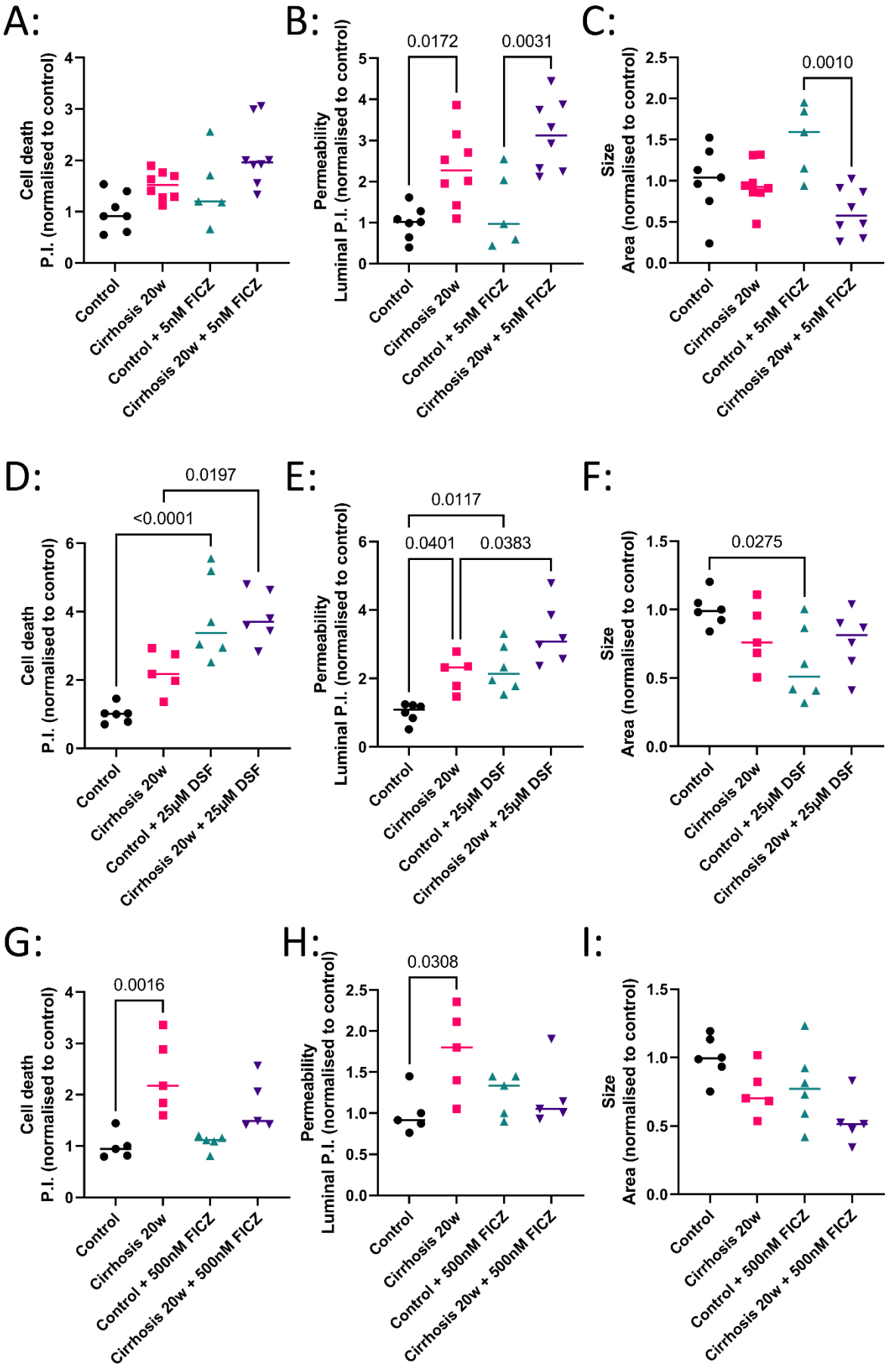
A:
Cell death
P.I. (normalised to control)
Control
Cirrhosis 20w
Control + 5nM FICZ
Cirrhosis 20w + 5nM FICZ
B:
Permeability
Luminal P.I. (normalised to control)
0.0172
0.0031
C:
Size
Area (normalised to control)
0.0010
D:
0.0197
<0.0001
Control + 25μM DSF
Cirrhosis 20w + 25μM DSF
E:
0.0117
0.0401
0.0383
F:
0.0275
G:
0.0016
Control + 500nM FICZ
Cirrhosis 20w + 500nM FICZ
H:
0.0308
I:

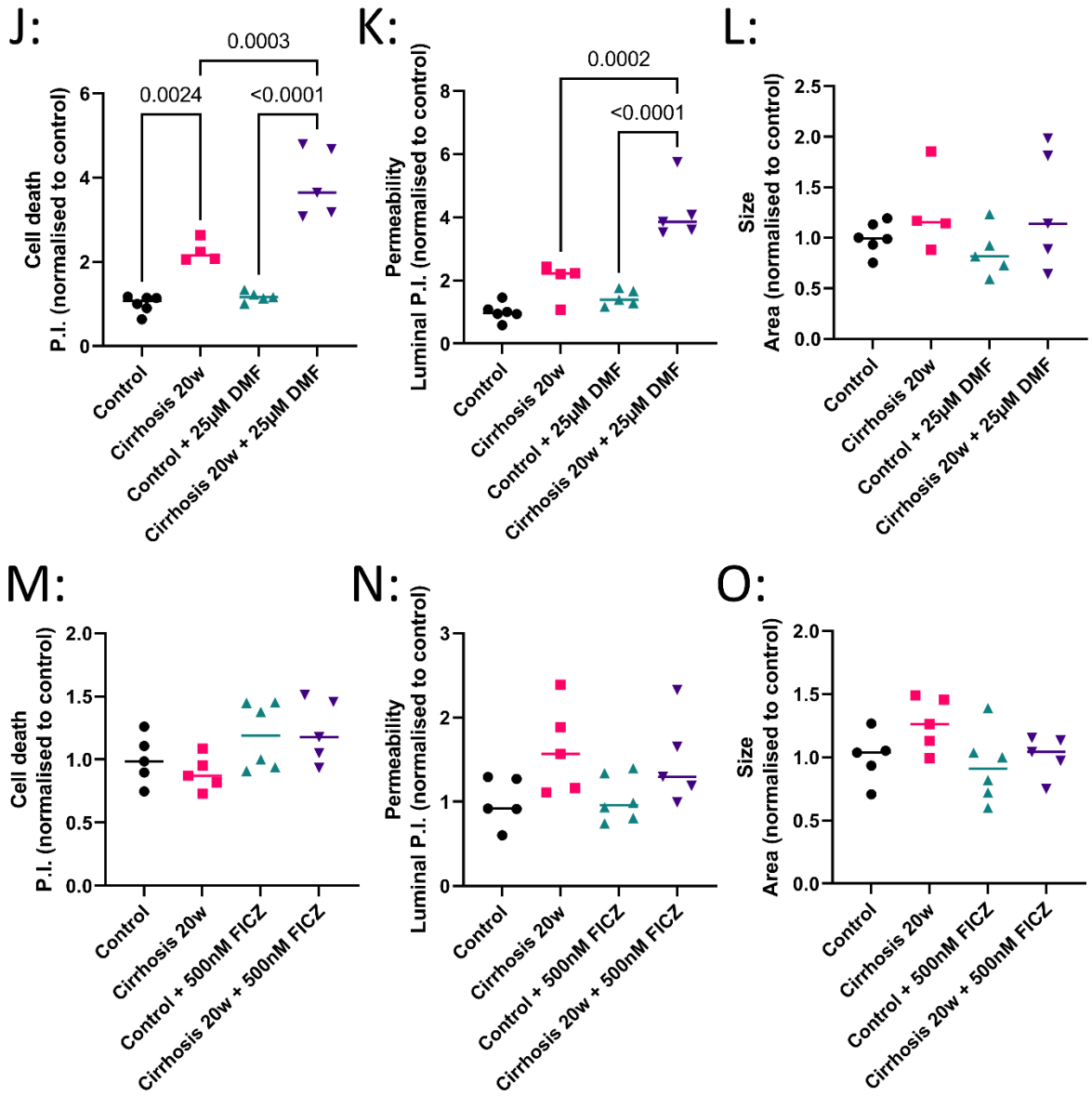

Figure 62: Mouse intestinal organoids from control and cirrhosis mice (20w CCl4) were treated with FICZ, DSF and DMF for cell death, permeability, and size. *Mouse intestinal organoids were derived from control, and 20w CCl4 subcutaneous treated mice and treated with A-C: 5nM FICZ (1st passage), D-F: 25µM DSF (2nd passage), G-I: 500nM FICZ (3rd passage), J-L: 25µM DMF (4th passage), M-O: 500nM FICZ (5th passage), for 3 days. Cells were stained with HOECHST and propidium iodide and fluorescent images were taken for HOECHST, green autofluorescence, and propidium iodide. A,D,G,J,M: Cell death was measured by mean propidium iodide intensity in HOECHST stained organoi d areas, B,E,H,K,N: Permeability was measured by mean luminal propidium iodide intensity in green autofluorescent lumen, and C,F,I,L,O: Size was measured by mean HOECHST stained organoid areas. A-C: control (n=7), Cirrhosis 20w (n=7), Control + 5nM FICZ (n=5), Cirrhosis 20w + 5nM FICZ (n=8). D-F: control (n=6), Cirrhosis 20w (n=5), Control + 5nM FICZ (n=6), Cirrhosis 20w + 5nM FICZ (n=6). G-I: control (n=5), Cirrhosis 20w (n=5), Control + 5nM FICZ (n=5), Cirrhosis 20w + 5nM FICZ (n=5). J-L: control (n=6), Cirrhosis 20w (n=4), Control + 5nM FICZ (n=5), Cirrhosis 20w + 5nM FICZ (n=5). M-O: control (n=5), Cirrhosis 20w (n=5), Control + 5nM FICZ (n=6), Cirrhosis 20w + 5nM FICZ (n=5). Groups were compared with one-way ANOVA with Tukey's post hoc test; significance p<0.05.*

5.5 Discussion

I hypothesised that intestinal cell death and reduced stemness are associated with cirrhosis. My aims were to 1: characterise intestinal cell death in cirrhosis patients, 2: characterise intestinal cell death in cirrhosis rodent model, 3: characterise intestinal stemness in cirrhosis rodent models, 4: determine effect of reduced stemness on intestinal cell death, permeability, and proliferation, 5: characterise cell death, permeability, and proliferation in intestinal organoids derived from cirrhosis rodent models, and 6: therapeutically target cell death and stemness for beneficial effects on cell death, permeability, and proliferation in intestinal organoids derived from cirrhosis rodent models.

Our cirrhosis mice model and cholestatic cirrhosis rat model showed increased liver injury similar to that observed in cirrhotic patients. Lgr5 expression was significantly decreased in colon samples of CCl4 + LPS treated mice compared to control and CCl4 treated mice from the 12-week cirrhosis model, a result that was recapitulated by our second rodent model, Lgr5 expression was significantly decreased in caecum samples of BDL treated rats. TUNEL staining on ascending colon biopsies from cirrhosis patients showed significant increased cell death in the epithelium, whereas no significant difference was found in biopsies from IBD patients. Additionally, TUNEL staining on ileum, caecum and colon samples of the rat model showed increased cell death in the caecum of BDL+LPS treated rats compared to control, which was ameliorated by DSF treatment. In *in vivo* intestinal organoid culture, depletion of R-spondin and LPS treatment increased cell death and reduced growth in organoids. Inhibiting the AHR pathway with the antagonist CH223191 increased permeability in intestinal organoids, whereas activation of the AHR pathway with the agonist FICZ increased cell death. Co-culture of intestinal macrophages from 20w CCl4 treated mice with intestinal organoids increased permeability. In general, intestinal organoids derived from cirrhosis mice showed increased cell death and permeability and no effect on growth, but after 5 passages the increased cell death and permeability was ameliorated. Lgr5 expression was increased and Frizzled 7 expression was decreased in the cirrhosis intestinal organoids. DSF and DMF treatment negatively affected intestinal organoids and increased cell death and permeability in organoids. However, FICZ treatment mitigated the increased cell death and permeability in intestinal organoids derived from cirrhosis mice.

I showed for the first time increased epithelial cell death in intestinal biopsies from cirrhosis patients. The results from TUNEL staining on different intestinal locations indicate a peak of epithelial cell death in near the ascending colon. The results in our *in vivo* rat model, corroborated the increased cell death, which showed increased cell death in the caecum of BDL+LPS treated rats. This could account for the increased cell death in the caecum of BDL+LPS treated rats, but not in the ileum or colon samples. Liu *et al.* previously showed increased cell death in the small intestine of BDL

treated mice [194]. This discrepancy could be explained by a more severe BDL model in mice compared to rats. Increased intestinal cell death contributes to intestinal barrier disruption, which is in accordance with increased permeability and bacterial translocation that occurs in cirrhosis patients. Therapeutically targeting intestinal cell death could potentially have beneficial effects on permeability, but importantly research on the cell death pathways and mechanisms that drive them are required to specifically inhibit the increased epithelial cell death.

My results showing decreased Lgr5 expression corroborate previous finding that showed decreased Lgr5 expression in the colon of BDL treated mice and duodenal biopsies of cirrhosis patients [194]. The decreased Lgr5 gene expression in our mice and rat model, indicates that the expression in Lgr5 expressing intestinal stem cells is decreased, and/or that the population of Lgr5 expressing stem cells is decreased. Both interpretations signify a disruption of stem cells in the intestinal crypts during cirrhosis development, which could explain the reduced intestinal Paneth and Goblet cells as well as shortened villi length in cirrhosis [138], [158], [194]. Alternatively to ER stress driving reduction of intestinal Lgr5 during cirrhosis development, LPS has been shown to decrease Lgr5 expression and deplete Lgr5 positive stem cells in the intestine of mice [259]. Intraperitoneal injection of LPS could account for the decreased Lgr5 expression in the CCl4 + LPS treated mice. However, BDL treated rats independent of LPS injection decreased intestinal Lgr5 expression. Increased pathogenic bacteria in the intestine during cirrhosis development can be a source of LPS and other PAMPs, which was found in caecum contents of BDL treated mice [293]. Gut dysbiosis during cirrhosis development can indirectly affect the intestine epithelium with disruptions in the production of short chain fatty acid and secondary bile acids or thus directly with an increase of luminal PAMPs that can cause epithelial injury and inflammation [37], [38], [44], [45], [259], [294]. The increase of PAMPs in the intestine could thus cause the reduction in Lgr5 expression during cirrhosis development, but further research into the mechanisms during cirrhosis development is required to confirm a direct causation.

In intestinal organoids I further show the negative effects of LPS as well as the depletion of R-spondin from the media on the intestinal epithelium. LPS and R-spondin depletion increased cell death and decreased growth in intestinal organoids. This shows that LPS can cause similar negative effects on the decreased stemness, which is in line with LPS leading to depletion of Lgr5 epithelial cells [259]. Additionally, LPS leads to reduced Ki67, which is consistent with my results of decreased growth in intestinal organoids [194]. However, LPS and depletion of R-spondin did not affect permeability, which indicates additional mechanisms are required that drive increased intestinal permeability in cirrhosis. Alternatively, by manipulating the AHR pathway with antagonist (CH223191), permeability was increased in intestinal organoids but cell death and growth was

unaffected. This indicates that dysregulating stemness, i.e. via AHR and Wnt pathways, can induce permeability. Conversely, manipulating AHR with agonist (FICZ) caused increased cell death, but did not affect permeability or growth. FICZ and CH223191 treatment did not affect gene expression of junction proteins (occludin, claudin and tight junction protein 1) or AHR pathway genes (AHR, Cyp1a1, Cyp1b1) in intestinal organoids. Liu *et al.* also found no difference in occluding and tight junction protein 1 expression while permeability was increased, which shows that permeability can be independent of junction protein expression [194]. Thus, my results manipulating the AHR pathway showed correct regulation of the AHR pathway is essential to limit excess cell death and permeability in intestinal organoids.

Intestinal organoids derived from cirrhosis at showed increased cell death and permeability for up to 4 passages. Passaging intestinal organoids would select for healthy stem cells that can grow new intestinal organoids, which is one explanation why the phenotype is lost after 5 passages. Additionally, the organoids media is supplemented with R-spondin that activates Lgr5 on the intestinal stem cells, thus helping to restore stem cell function [244]. Lgr5 expression was increased in organoids derived from cirrhosis mice, which could be a compensation mechanism after removal from a toxic environment that drove a decrease in Lgr5 expression to re-establish stemness. Conversely to Lgr5, Frizzled 7 expression is decreased in organoids derived from cirrhosis mice. The reactivation of Lgr5 by supplemented R-spondin in the organoid media could lead to reduced Frizzled 7 to regulate stemness. Alternatively, beta catenin could increase Lgr5 to attempt to combat decreased Frizzled 7 expression in cirrhosis stem cells, showing increased Lgr5 and reduced Frizzled 7.

Therapeutically targeting Lgr5 and Frizzled with R-spondin and Wnt, respectively, in intestinal organoids is complicated as R-spondin is readily present in the media and Wnt is used to grow colon organoids and inhibit differentiation into intestinal organoids. Therefore, I utilised FICZ to target the AHR pathway instead to regulate stemness. I had previously shown that FICZ increased cell death, but did not affect permeability, whereas CH223191 increased permeability, but not cell death. Intestinal organoids from cirrhosis mice showed increased cell death and permeability, which was ameliorated by FICZ treatment. Additionally, FICZ showed beneficial effects on the epithelium in IBD mice model, however off-target effects such as tumorigenic are a potential and thus requires further examination [285]. Furthermore, I attempted to therapeutically targeted cell death with DSF and DMF in organoids. However, DSF and DMF treatment did not improve cell death or permeability in intestinal organoids derived from cirrhosis or control mice, and even worsened the cell death and permeability. Targeting the increased cell death remains a potential beneficial treatment option, as our rat model showed decreased cell death in the caecum by DSF treatment. These results show that

the intestinal epithelial damage during cirrhosis development can be therapeutically targeted to reduce epithelial cell death and permeability, but further research using *in vivo* models are needed to show effectiveness of the health benefits in cirrhosis development and progression and examine toxicity.

5.6 Conclusion

Together these results indicate that gut dysbiosis with increased pathogenic bacteria and PAMPs during cirrhosis development can cause increased epithelial cell death and reduced cell renewal. Additionally, PAMPs can decrease intestinal stem cells, which are essential for sufficient cell renewal of dying epithelial cells. Organoids derived from intestinal crypts of cirrhosis mice maintain the phenotype of increased epithelial cell death and permeability, which was effectively targeted by an agonist of AHR. Increased epithelial cell death, decreased cell renewal, and increased epithelial permeability contribute to bacterial translocation, which can negatively affect cirrhosis progression. Targeting epithelial stem cells or the underlaying factors negatively affecting stemness during cirrhosis development is thus a promising therapeutic option to potentially reduce progression to AD or ACLF, but this needs to be confirmed using animal models prior to clinical trials.

6 Discussion

Systemic inflammation plays a key role in the progression from compensated to decompensated cirrhosis [23], [27], [53]. This progression to AD and ACLF severely increases the mortality rate in patients [21][22]. Translocation of PAMPs and DAMPs from the intestine are implicated as a source for the systemic inflammation [25], [53]–[55]. Therefore, I set out to investigate the effect of cirrhosis on the intestine epithelium and examine intestinal cell death that may contribute to systemic inflammation and bacterial translocation. I hypothesised that ER stress mediated intestinal inflammasome activation and pyroptotic cell death are associated with cirrhosis. I set out to develop a permeability assay for mouse intestinal organoids. And I hypothesised that intestinal cell death and reduced stemness is associated with cirrhosis.

There was no evidence of intestinal ER stress or inflammasome activation in the *in vivo* mouse models of cirrhosis and cirrhosis with decompensated event mouse models, in the first results chapter (chapter 3). Additionally, there was no significant association observed of intestinal ER stress in colon and intestinal biopsies in cirrhosis patients. This was confirmed in the *in vitro* intestinal model experiments, where no synergistic effect was observed between ER stress and inflammasome activation on cell death.

The second results chapter (chapter 4) described the development of a novel *in vitro* permeability assay for mouse intestinal organoids [1]. The main contribution to the field was to demonstrate that this model could be used to investigate the 'leaky gut'. The work revealed that the green background autofluorescence in the organoid lumen caused by cell debris and secreted mucus could be used to specifically highlight and select the lumen during imaging. The results also showed that propidium iodide did not penetrate intact intestinal organoids and thus did not stain dead cells extruded in the lumen. However, propidium iodide was able to penetrate the organoids upon permeabilization and stained the luminal dead cells. Quantification of luminal propidium iodide-stained dead cells effectively measured organoid permeability.

In the last results chapter (chapter 5) the aim was to characterise intestinal cell death and stemness in cirrhosis. The study clearly showed increased intestinal epithelial cell death in cirrhosis patients. This was further confirmed in the cirrhosis with decompensated rat model. Additionally, this study showed decreased intestinal stemness in our *in vivo* models. Furthermore, in the *in vitro* intestinal organoid model showed that LPS injury and disruption of Lgr5 activation both increased cell death and decreased organoids size without affecting permeability. This was in contrast to the observations of disrupted AHR pathway in the model, which caused increased permeability in organoids without affecting cell death or size. Intestinal organoids derived from cirrhosis mice

maintained increased cell death and permeability phenotype for 4 passages, which FICZ treatment was able to ameliorate.

To characterise intestinal ER stress in cirrhosis, no difference was shown in UPR activation in intestinal biopsies from cirrhosis patients, and no full UPR activation in the cirrhosis mouse models. This indicates that intestinal ER stress is not the driving factor behind progression. However, the mouse model showed increased GRP78, but decreased XBP1 splicing, which could indicate resolved ER stress at a stage where the UPR is no longer active. This would fit with previous findings that showed intestinal UPR activation in a BDL mice model, which is a shorter model (up to 2 weeks) compared to the CCl4 mice models used for this study (12 weeks, and 14-20 weeks) [194]. However, the study also showed increased UPR activation in duodenal biopsies of cirrhosis patients, whereas this study showed no difference in duodenal or colon biopsies of cirrhosis patient [194]. Importantly, there are key differences in the cirrhosis groups between the studies [194]. The aetiology of cirrhosis patients was active hepatitis C with MELD score of 9±4 and the aetiology of cirrhosis patients in this study was ALD/NAFLD with MELD score of 14.6±8.4 [194]. The differences in patient characteristics could account for the difference in results, but this remains speculative. Thus, the role of intestinal ER stress on cirrhosis development and progression remains undefined and requires additional studies to elaborate on these findings.

To characterise intestinal inflammasome activation in cirrhosis, this study showed no difference in intestinal inflammasome activation in the cirrhosis mouse models. This indicates that the gut dysbiosis and other factors in cirrhosis do not activate the inflammasome pathway/pyroptosis in the intestine and that these pathways do not contribute to barrier damage and increased permeability observed in the disease. To our knowledge this is the first-time showing absence of intestinal inflammasome activation in cirrhosis. However, Liu *et al.* showed increased IL-1beta and IL-18 gene expression in the BDL mice model that was alleviated by CHOP deficiency, which indicated at ER stress mediated inflammasome activation in their model [194]. Importantly, the study from Liu *et al.* did not show activation of caspase-1/11, GSDMD, or other genes of the inflammasome pathway, and used a different mouse model [194]. The role of intestinal inflammasome activation has been studied in inflammatory bowel diseases, but inhibition/deficiency of the inflammasome pathway has shown conflicting results [164], [179]–[183]. The results in this study, thus, indicate that inflammasome pathway activation/pyroptosis does not contribute to the intestinal barrier disruption in cirrhosis, but it remains unknown if other cell death mechanisms play a role.

To determine synergy between ER stress and non-canonical inflammasome activation on intestinal cell death, this study showed no synergistic effect of ER stress and inflammasome activation on cell

death in the intestinal epithelial models, unlike in liver cells [188]. This indicates that intestinal ER stress does not sensitise intestinal epithelial cells for pyroptosis in response to luminal bacterial products during cirrhosis development.

To quantify intestinal organoid permeability, this study described the development of a novel assay to measure permeability in mouse intestinal organoids. This assay functions differently than previous described organoid permeability assays, which used labelled compounds microinjected in the organoid, labelled compounds added to the media, or measure TEER on 2D intestinal organoids [265]–[271]. These techniques require specialised hardware such as a, microinjector, confocal microscope, or TEER meters that also require organoids to be plated 2D on Transwells [265]–[271]. The novel assay in this study provides an alternative for these assays, but requires a computer controlled/automated fluorescence microscope, e.g. Cytation 5. This permeability assay was demonstrated on mouse intestinal organoids. While not species-specific, this assay requires green background autofluorescence created by mucus and dead cell debris inside the organoid lumens, which limits the assay to intestinal organoids.

To characterise intestinal cell death in cirrhosis, this study showed increased cell death in cirrhosis colon biopsies and in the cirrhosis with decompensated event rat model. The results corroborates a previous study showing increased intestinal cell death in cirrhosis mice model [194]. Additionally, increased cell death is consistent with a shortened villi length found in cirrhosis rat models [295][296]. The results showed increased cell death in the epithelium but could not correspond the cell death with cell type. Therefore, this study cannot identify whether the cell death is cell specific, villi-crypt specific, or unspecific. However, DSF treatment ameliorated the increased intestinal cell death found in the cirrhosis with decompensated event rat model but did not show beneficial effects on cirrhosis. Possibly longer treatment duration, earlier administration, and/or other cell death inhibitor drug can lead to beneficial effects on cirrhosis development, however this requires future studies to further examine.

To characterise intestinal stemness in cirrhosis, this study showed decreased colon Lgr5 gene expression in our cirrhosis with decompensated event mice model and in our cirrhosis rat model. My results corroborates a previous study that showed similarly decreased intestinal Lgr5 expression in cirrhosis [194]. The decreased Lgr5 expression can be caused by decreased gene expression in intestinal stem cells, or a decreased stem cell population. Both indicate a disrupted stemness in the intestine, which can negatively affect the epithelial barrier with distorted cell renewal capabilities. This is consistent with studies that showed decreased Goblet cells and Paneth cells in cirrhosis, which could be caused by the decreased stemness [138][158]. Together, this shows a role of

intestinal stem cells in cirrhosis, which potentially could be therapeutically targeted to remedy intestinal injury. FICZ treatment was effective in ameliorating the cell death and permeability phenotype in intestinal organoids derived from cirrhosis mice, but FICZ or other stemness therapeutic options have not been tested for beneficial effects in cirrhosis animal models.

To determine the effect of reduced stemness on intestinal cell death, permeability and proliferation, this study showed increased cell death and permeability in intestinal organoids by depletion of R-spondin in the media, and similar results by LPS treatment. This indicates that R-spondin in the organoid media is essential to maintain cell viability and epithelial barrier integrity. LPS treatment induced a similar phenotype to R-spondin depletion, which is consistent with LPS leading to reduced Lgr5 stem cells [259]. Together these results indicate that the bacterial products can negatively affect epithelial barrier integrity by disrupting stem cells. However, the direct effect of LPS on intestinal stem cells and whether this occurs in the intestine during cirrhosis remains undefined. Additionally, AHR antagonist increased organoid permeability without affecting cell death or size, which indicates that the AHR pathway is essential for epithelial barrier functioning and can play a role in regulating permeability.

To characterise cell death, permeability, and proliferation in intestinal organoids from cirrhosis mice, this study showed increased cell death and permeability in organoids derived from cirrhosis mice with increased Lgr5 and decreased Fzd7 gene expression. This indicates that effect of cirrhosis on intestinal stem cells have a lasting effect and organoids derived from these crypts maintain a phenotype. This phenotype was lost after 5 passages, and FICZ treatment was able to ameliorate the increased cell death and permeability, which indicates the negative effect on crypt stem cells during cirrhosis are treatable. FICZ treatment in ALD mice model showed beneficial effects and showed increased AHR activation in the intestine, but not in hepatic cells [288]. This indicates that the FICZ treatment can effect intestinal stem cells and thereby affect ALD development, but importantly the causality remains unclear [288].

A limitation of this study is that it only includes cirrhosis patients results for intestinal cell death due to sample availability. For instance, intestinal Lgr5 expression in cirrhosis patients could not be determined due to the limited sample availability. Additionally, the rodent models lack an LPS treatment without cirrhosis, to determine the direct effect of LPS treatment on the tissue. Additionally, the results do not show cell specificity and therefore could have obscured pathway activation and gene expression in unaffected cells whereas stem cells, immune cells, etc. could have been affected. Furthermore, untargeted bulk RNA-sequencing and proteomics could have limited the biasedness in analysis of pathway activation.

Another limitation of this study is the use of intestinal models and cirrhosis rodent models, i.e. Caco-2 cells, HCT-116 cells and mouse intestinal organoids, and mouse cirrhosis models by subcutaneous administration of CCl_4 and rat cirrhosis model by BDL, with intraperitoneal injection of LPS to simulate cirrhosis with decompensated event. As mentioned before Caco-2 and HCT-116 cell lines are derived from human colorectal adenocarcinoma and human colon carcinoma cells, respectively. These cells have cancer cell characteristics that effect their responses to toxins by their increased expression of anti-apoptotic genes and decreased expression of pro-apoptotic genes [253][254]. Based on these characteristics I also used and continued with mouse derived intestinal organoids. These organoids are derived from healthy mouse intestinal tissue and maintain pluripotency from supplements in the media [244]. However, mouse cells have differences compared to human cells, e.g. caspase-11 for mice and caspase-4/5 for humans, that can contribute to a mistranslation. Additionally, the mouse intestinal organoids maintain the intestinal lumen inside the organoids, and thus the compounds such as LPS when added to the media contact the cells from the lamina propria side rather than the luminal side. Furthermore, we did not additionally use colon derived colon organoids to show results for both small intestine and colon due to technical difficulties and sample size limitations. Based on the characteristics of the various *in vivo* models of cirrhosis we used the cirrhosis mouse model by subcutaneous administration of CCl_4. The administration of CCl_4 subcutaneously reduces injection effects on the abdomen which can interfere with the results in the intestine compared to the more conventional intraperitoneal injection [238]. Furthermore, CCl_4 is a liver toxin that induces injury independent of the two most common aetiologies ALD and NAFLD. The results are therefore not limited to either aetiology, but the results show the effect of liver injury on the intestine. The other cirrhosis model, rat BDL, induces cholestatic cirrhosis by restricting the bile flow in the bile duct [237]. As mentioned before, this bile duct ligation therefore complements the subcutaneous CCl_4 cirrhosis model with a cirrhosis cholestasis model. The effects of BDL in mice is more severe compared to rats and thereby the duration of the mice model is five to seven days with a severe inflammatory response whereas the effect of BDL on rats is less severe and thereby can maintain a longer duration up to 4 weeks, therefore the rat BDL model is more appropriate to model the chronic aspect of cirrhosis [237][239]. Additionally, rats have increased intestine size compared to mice, which more easily allows for both molecular and histological sampling of the intestinal sub-compartments.

This study, thus, showed that intestinal ER stress and inflammasome activation are not associated with cirrhosis. However, intestinal cell death and decreased stemness are associated with cirrhosis. With intestinal organoids as an *in vitro* model, this study showed disruption of AHR pathway could increase organoid permeability, whereas the treatment with the ligand of AHR on intestinal

organoids from cirrhosis mice could ameliorate the increased cell death and permeability phenotype. This study showed therapeutic interventions that can target the intestinal disruptions of cell death and stemness associated with cirrhosis.

Further work leading from these studies would be to explore in detail the role of stem cells during cirrhosis development and progression to characterise the effect and causality of stem cells disruption in the disease. This project and other studies show promising results in decreasing intestinal cell death and restoring stem cell activity, both of which can be an important future therapeutic target in cirrhosis [194][288]. Whether these therapeutic interventions have beneficial effects on the disease progression remains to be investigated. The findings from this may also have implications for other gut-related conditions, such as Colitis, Crohn's disease, irritable bowel syndrome, etc. There is an urgent need for therapeutic options reducing progression from stable cirrhosis to decompensated cirrhosis. Increasing intestinal barrier integrity via restoring intestinal stem cells and decreasing cell death, could potentially reduce translocation of bacteria and PAMPs in cirrhosis patients and inhibit progression. It is important to note that whilst some of the focus of this work has been on inflammasome activation/pyroptosis in cirrhosis, other cell death pathways may also be involved in the increased cell death in cirrhosis. Further examination of which cell death pathways are involved can help more specifically target the cell death.

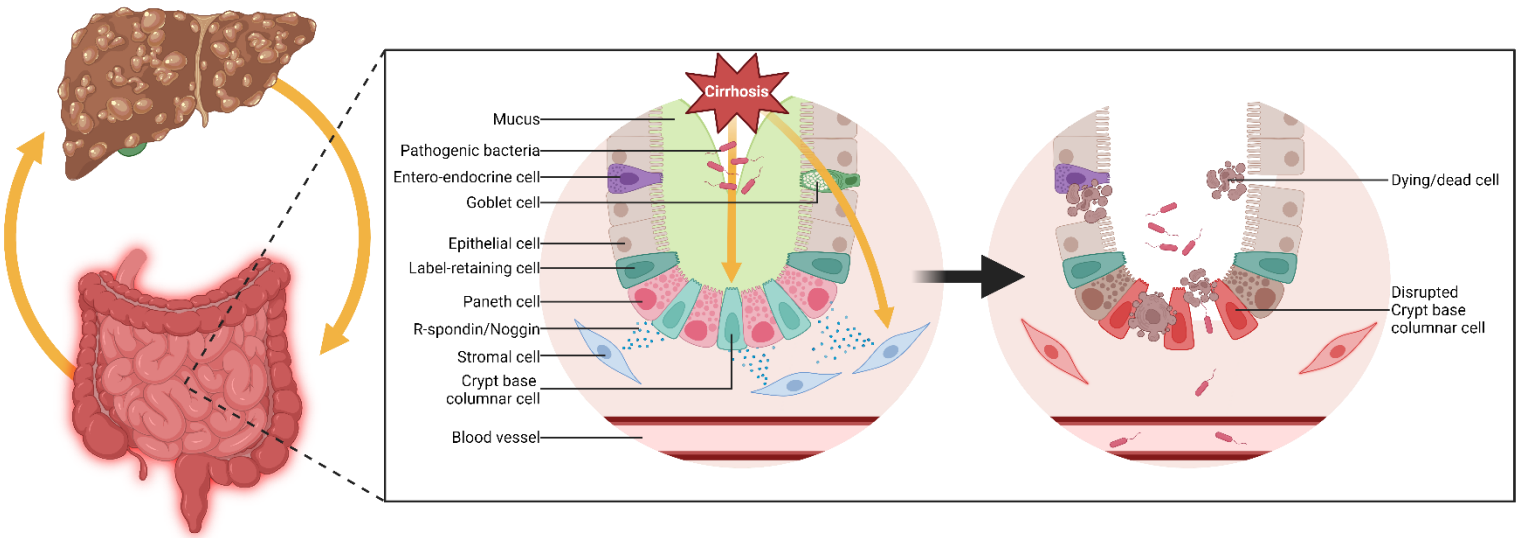

Figure 63: Results summary and conclusion.

Overall, the results from this work show that direct and/or indirect effects in the intestine during cirrhosis cause a disruption in the intestinal stem cells and an increase in intestinal epithelial cell death (independent of pyroptosis), that contributes to the increased intestinal permeability, **Figure 63**. I hypothesize that this disruption of intestinal stem cells results in the previously described reduction in Paneth cells, Goblet cells, and villi length, caused by a decrease of cell regeneration capabilities. In this project I identified potential candidate therapeutic targets and interventions that may help restore epithelial homeostasis and potentially alleviate bacterial translocation and disease progression.

7 References

[1] S. A. den Daas, U. Soffientini, S. Chokshi, and G. Mehta, "A permeability assay for mouse intestinal organoids," *STAR Protoc.*, vol. 3, no. 2, p. 101365, Jun. 2022, doi: 10.1016/j.xpro.2022.101365.

[2] A. A. Mokdad *et al.*, "Liver cirrhosis mortality in 187 countries between 1980 and 2010: A systematic analysis," *BMC Med.*, vol. 12, no. 1, pp. 1–24, 2014, doi: 10.1186/s12916-014-0145-y.

[3] S. K. Asrani, H. Devarbhavi, J. Eaton, and P. S. Kamath, "Burden of liver diseases in the world," *J. Hepatol.*, vol. 70, no. 1, pp. 151–171, 2019, doi: 10.1016/j.jhep.2018.09.014.

[4] S. G. Sepanlou *et al.*, "The global, regional, and national burden of cirrhosis by cause in 195 countries and territories, 1990–2017: a systematic analysis for the Global Burden of Disease Study 2017," *Lancet Gastroenterol. Hepatol.*, vol. 5, no. 3, pp. 245–266, 2020, doi: 10.1016/S2468-1253(19)30349-8.

[5] S. G. Sepanlou *et al.*, "The global, regional, and national burden of cirrhosis by cause in 195 countries and territories, 1990–2017: a systematic analysis for the Global Burden of Disease Study 2017," *Lancet Gastroenterol. Hepatol.*, vol. 5, no. 3, pp. 245–266, Mar. 2020, doi: 10.1016/S2468-1253(19)30349-8.

[6] L. Pimpin *et al.*, "Burden of liver disease in Europe: Epidemiology and analysis of risk factors to identify prevention policies," *J. Hepatol.*, vol. 69, no. 3, pp. 718–735, 2018, doi: 10.1016/j.jhep.2018.05.011.

[7] "Liver disease: applying All Our Health," *UK Office for Health Improvements & Disparities*, 2022. [Online]. Available: https://www.gov.uk/government/publications/liver-disease-applying-all-our-health/liver-disease-applying-all-our-health#fnref:3. [Accessed: 25-Oct-2022].

[8] M. Blachier, H. Leleu, M. Peck-Radosavljevic, D. C. Valla, and F. Roudot-Thoraval, "The burden of liver disease in Europe: A review of available epidemiological data," *J. Hepatol.*, vol. 58, no. 3, pp. 593–608, 2013, doi: 10.1016/j.jhep.2012.12.005.

[9] A. K. Singal and B. S. Anand, "Mechanisms of Synergy Between Alcohol and Hepatitis C Virus," *J. Clin. Gastroenterol.*, vol. 41, no. 8, pp. 761–772, Sep. 2007, doi: 10.1097/MCG.0b013e3180381584.

[10] C. L. Hart, D. S. Morrison, G. D. Batty, R. J. Mitchell, and G. Davey Smith, "Effect of body mass index and alcohol consumption on liver disease: analysis of data from two prospective cohort studies," *BMJ*, vol. 340, no. mar11 1, pp. c1240–c1240, Mar. 2010, doi: 10.1136/bmj.c1240.

[11] R. Loomba, H.-I. Yang, J. Su, D. Brenner, U. Iloeje, and C.-J. Chen, "Obesity and Alcohol Synergize to Increase the Risk of Incident Hepatocellular Carcinoma in Men," *Clin. Gastroenterol. Hepatol.*, vol. 8, no. 10, pp. 891-898.e2, Oct. 2010, doi: 10.1016/j.cgh.2010.06.027.

[12] R. Loomba *et al.*, "Synergism between obesity and alcohol in increasing the risk of hepatocellular carcinoma: A prospective cohort study," *Am. J. Epidemiol.*, vol. 177, no. 4, pp. 333–342, 2013, doi: 10.1093/aje/kws252.

[13] A. Baiocchini *et al.*, "Extracellular Matrix Molecular Remodeling in Human Liver Fibrosis Evolution," 2016, doi: 10.1371/journal.pone.0151736.

[14] R. Bataller and D. A. Brenner, "Liver fibrosis," *J. Clin. Invest.*, vol. 115, 2005, doi: 10.1172/JCI200524282.

[15] P. Ginès, A. Krag, J. G. Abraldes, E. Solà, N. Fabrellas, and P. S. Kamath, "Liver cirrhosis," *Lancet*, vol. 398, no. 10308, pp. 1359–1376, 2021, doi: 10.1016/S0140-6736(21)01374-X.

[16] G. D'Amico *et al.*, "Competing risks and prognostic stages of cirrhosis: A 25-year inception cohort study of 494 patients," *Aliment. Pharmacol. Ther.*, vol. 39, no. 10, pp. 1180–1193, 2014, doi: 10.1111/apt.12721.

[17] A. Smith, K. Baumgartner, and C. Bositis, "Cirrhosis: Diagnosis and management," *Am. Fam. Physician*, vol. 100, no. 12, pp. 759–770, 2019.

[18] G. D'Amico, M. Bernardi, and P. Angeli, "Towards a new definition of decompensated cirrhosis," *J. Hepatol.*, vol. 76, no. 1, pp. 202–207, 2022, doi: 10.1016/j.jhep.2021.06.018.

[19] H. B. Lefton, A. Rosa, and M. Cohen, "Diagnosis and Epidemiology of Cirrhosis," *Med. Clin. North Am.*, vol. 93, no. 4, pp. 787–799, 2009, doi: 10.1016/j.mcna.2009.03.002.

[20] H. Ohnishi, J. Sugihara, H. Moriwaki, and Y. Muto, "Acute-on-chronic liver failure," *Ryōikibetsu shōkōgun shirīzu*, no. 7. Ryoikibetsu Shokogun Shirizu, pp. 217–219, 1995.

[21] R. Jalan *et al.*, "The CLIF Consortium Acute Decompensation score (CLIF-C ADs) for prognosis of hospitalised cirrhotic patients without acute-on-chronic liver failure," *J. Hepatol.*, vol. 62, no. 4, pp. 831–840, 2015, doi: 10.1016/j.jhep.2014.11.012.

[22] R. Moreau *et al.*, "Acute-on-chronic liver failure is a distinct syndrome that develops in patients with acute decompensation of cirrhosis," *Gastroenterology*, vol. 144, no. 7, pp. 1426–1437, 2013, doi: 10.1053/j.gastro.2013.02.042.

[23] J. Trebicka *et al.*, "The PREDICT study uncovers three clinical courses of acutely decompensated cirrhosis that have distinct pathophysiology," *J. Hepatol.*, vol. 73, no. 4, pp. 842–854, Oct. 2020, doi: 10.1016/j.jhep.2020.06.013.

[24] J. Trebicka *et al.*, "PREDICT identifies precipitating events associated with the clinical course of acutely decompensated cirrhosis," *J. Hepatol.*, vol. 74, no. 5, pp. 1097–1108, May 2021, doi: 10.1016/j.jhep.2020.11.019.

[25] S. Macdonald *et al.*, "Cell death markers in patients with cirrhosis and acute decompensation," *Hepatology*, vol. 67, no. 3, pp. 989–1002, 2018, doi: 10.1002/hep.29581.

[26] M. Bernardi, R. Moreau, P. Angeli, B. Schnabl, and V. Arroyo, "Mechanisms of decompensation and organ failure in cirrhosis: From peripheral arterial vasodilation to systemic inflammation hypothesis," *J. Hepatol.*, vol. 63, no. 5, pp. 1272–1284, 2015, doi: 10.1016/j.jhep.2015.07.004.

[27] R. Jalan, V. Stadlbauer, S. Sen, L. Cheshire, Y. M. Chang, and R. P. Mookerjee, "Role of predisposition, injury, response and organ failure in the prognosis of patients with acute-on-chronic liver failure: A prospective cohort study," *Crit. Care*, vol. 16, no. 6, 2012, doi: 10.1186/cc11882.

[28] A. T. Blei, "Portal hypertension and its complications," *Curr. Opin. Gastroenterol.*, vol. 23, no. 3, pp. 275–282, 2007, doi: 10.1097/MOG.0b013e3280b0841f.

[29] Y. Iwakiri, "Pathophysiology of portal hypertension," *Clin. Liver Dis.*, vol. 18, no. 2, pp. 281–291, 2014, doi: 10.1016/j.cld.2013.12.001.

[30] B. Simbrunner, M. Mandorfer, M. Trauner, and T. Reiberger, "Gut-liver axis signaling in portal hypertension," *World J. Gastroenterol.*, vol. 25, no. 39, pp. 5897–5917, 2019, doi: 10.3748/wjg.v25.i39.5897.

[31] A. Gilbert and P. Carnot, *Les fonctions hepatiques*. Paris: C.Naud, 1902.

[32] L. S. Gunarathne, H. Rajapaksha, N. Shackel, P. W. Angus, and C. B. Herath, "Cirrhotic portal hypertension: From pathophysiology to novel therapeutics," *World J. Gastroenterol.*, vol. 26, no. 40, pp. 6111–6140, 2020, doi: 10.3748/wjg.v26.i40.6111.

[33] E. H. Starling, “On the Absorption of Fluids from the Connective Tissue Spaces,” *J. Physiol.*, vol. 19, no. 4, pp. 312–326, May 1896, doi: 10.1113/jphysiol.1896.sp000596.

[34] V. Hernández-Gea *et al.*, “Development of ascites in compensated cirrhosis with severe portal hypertension treated with β-blockers,” *Am. J. Gastroenterol.*, vol. 107, no. 3, pp. 418–427, 2012, doi: 10.1038/ajg.2011.456.

[35] J. G. Abraldes, I. Tarantino, J. Turnes, J. C. Garcia-Pagan, J. Rodés, and J. Bosch, “Hemodynamic response to pharmacological treatment of portal hypertension and long-term prognosis of cirrhosis,” *Hepatology*, vol. 37, no. 4, pp. 902–908, 2003, doi: 10.1053/jhep.2003.50133.

[36] J. S. Bajaj *et al.*, “Colonic mucosal microbiome differs from stool microbiome in cirrhosis and hepatic encephalopathy and is linked to cognition and inflammation,” *Am. J. Physiol. - Gastrointest. Liver Physiol.*, vol. 303, no. 6, pp. 675–685, 2012, doi: 10.1152/ajpgi.00152.2012.

[37] J. S. Bajaj *et al.*, “Altered profile of human gut microbiome is associated with cirrhosis and its complications,” *J. Hepatol.*, vol. 60, no. 5, pp. 940–947, May 2014, doi: 10.1016/j.jhep.2013.12.019.

[38] N. Qin *et al.*, “Alterations of the human gut microbiome in liver cirrhosis.,” *Nature*, vol. 513, no. 7516, pp. 59–64, 2014, doi: 10.1038/nature13568.

[39] E. K. Kwong and P. Puri, “Gut microbiome changes in nonalcoholic fatty liver disease & alcoholic liver disease,” *Transl. Gastroenterol. Hepatol.*, vol. 6, no. 8, 2021, doi: 10.21037/TGH.2020.02.18.

[40] T. G. Oh *et al.*, “A Universal Gut-Microbiome-Derived Signature Predicts Cirrhosis,” *Cell Metab.*, vol. 32, no. 5, pp. 878-888.e6, Nov. 2020, doi: 10.1016/j.cmet.2020.06.005.

[41] J. Chesta, C. Defilippi, and C. Defilippi, “Abnormalities in proximal small bowel motility in patients with cirrhosis,” *Hepatology*, vol. 17, no. 5, pp. 828–832, May 1993, doi: 10.1002/hep.1840170513.

[42] A. M. Madrid, F. Cumsille, and C. Defilippi, “Altered small bowel motility in patients with liver cirrhosis depends on severity of liver disease,” *Dig. Dis. Sci.*, vol. 42, no. 4, pp. 738–742, 1997, doi: 10.1023/A:1018899611006.

[43] S. Gunnarsdottir, “Small intestinal motility disturbances and bacterial overgrowth in patients with liver cirrhosis and portal hypertension,” *Am. J. Gastroenterol.*, vol. 98, no. 6, pp. 1362–

1370, Jun. 2003, doi: 10.1016/S0002-9270(03)00250-8.

[44] C. Solé *et al.*, "Alterations in Gut Microbiome in Cirrhosis as Assessed by Quantitative Metagenomics: Relationship With Acute-on-Chronic Liver Failure and Prognosis," *Gastroenterology*, vol. 160, no. 1, pp. 206-218.e13, 2021, doi: 10.1053/j.gastro.2020.08.054.

[45] Y. Chen *et al.*, "Characterization of fecal microbial communities in patients with liver cirrhosis," *Hepatology*, vol. 54, no. 2, pp. 562–572, Aug. 2011, doi: 10.1002/hep.24423.

[46] E. Kalaitzakis, J. E. Johansson, I. Bjarnason, and E. Björnsson, "Intestinal permeability in cirrhotic patients with and without ascites," *Scand. J. Gastroenterol.*, vol. 41, no. 3, pp. 326–330, 2006, doi: 10.1080/00365520510024278.

[47] R. Wiest, M. Lawson, and M. Geuking, "Pathological bacterial translocation in liver cirrhosis," *J. Hepatol.*, vol. 60, no. 1, pp. 197–209, 2014, doi: 10.1016/j.jhep.2013.07.044.

[48] J. Traub, L. Reiss, B. Aliwa, and V. Stadlbauer, "Malnutrition in patients with liver cirrhosis," *Nutrients*, vol. 13, no. 2, pp. 1–19, 2021, doi: 10.3390/nu13020540.

[49] R. Maslennikov *et al.*, "Gut dysbiosis and body composition in cirrhosis," *World J. Hepatol.*, vol. 14, no. 6, pp. 1210–1225, 2022, doi: 10.4254/wjh.v14.i6.1210.

[50] D. Costa *et al.*, "Systemic inflammation increases across distinct stages of advanced chronic liver disease and correlates with decompensation and mortality," *J. Hepatol.*, vol. 74, no. 4, pp. 819–828, 2021, doi: 10.1016/j.jhep.2020.10.004.

[51] B. Simbrunner *et al.*, "Systemic inflammation is linked to liver fibrogenesis in patients with advanced chronic liver disease," *Liver Int.*, vol. 42, no. 11, pp. 2501–2512, 2022, doi: 10.1111/liv.15365.

[52] J. Clària *et al.*, "Systemic Inflammation in Decompensated Cirrhosis: Characterization and Role in Acute-on-Chronic Liver Failure A HE STUDY OF LIVER D I S E ASES T MERICAN ASSOCIATION FOR," *HEPATOLOGY*, vol. 64, no. 4, 2016, doi: 10.1002/hep.28740/suppinfo.

[53] V. Arroyo *et al.*, "The systemic inflammation hypothesis: Towards a new paradigm of acute decompensation and multiorgan failure in cirrhosis," *J. Hepatol.*, vol. 74, no. 3, pp. 670–685, 2021, doi: 10.1016/j.jhep.2020.11.048.

[54] J. Trebicka, J. Macnaughtan, B. Schnabl, D. L. Shawcross, and J. S. Bajaj, "The microbiota in cirrhosis and its role in hepatic decompensation," *J. Hepatol.*, vol. 75, no. Suppl 1, pp. S67–S81, 2021, doi: 10.1016/j.jhep.2020.11.013.

[55] J. Fernández *et al.*, "Effects of Albumin Treatment on Systemic and Portal Hemodynamics and Systemic Inflammation in Patients With Decompensated Cirrhosis," *Gastroenterology*, vol. 157, no. 1, pp. 149–162, 2019, doi: 10.1053/j.gastro.2019.03.021.

[56] C. Bernsmeier, S. van der Merwe, and A. Périanin, "Innate immune cells in cirrhosis," *J. Hepatol.*, vol. 73, no. 1, pp. 186–201, 2020, doi: 10.1016/j.jhep.2020.03.027.

[57] J. Michelena *et al.*, "Systemic inflammatory response and serum lipopolysaccharide levels predict multiple organ failure and death in alcoholic hepatitis," *Hepatology*, vol. 62, no. 3, pp. 762–772, 2015, doi: 10.1002/hep.27779.

[58] A. Zanetto *et al.*, "Severity of systemic inflammation is the main predictor of ACLF and bleeding in individuals with acutely decompensated cirrhosis," *J. Hepatol.*, vol. 78, no. 2, pp. 301–311, 2023, doi: 10.1016/j.jhep.2022.09.005.

[59] R. Moreau *et al.*, "Blood metabolomics uncovers inflammation-associated mitochondrial dysfunction as a potential mechanism underlying ACLF," *J. Hepatol.*, vol. 72, no. 4, pp. 688–701, 2020, doi: 10.1016/j.jhep.2019.11.009.

[60] "Treatment Cirrhosis," *Treatment Cirrhosis*, 2020. [Online]. Available: https://www.nhs.uk/conditions/cirrhosis/treatment/. [Accessed: 21-Nov-2022].

[61] D. Mansour and S. McPherson, "Management of decompensated cirrhosis," *Clin. Med. (Northfield. Il).*, vol. 18, no. Suppl 2, pp. s60–s65, Apr. 2018, doi: 10.7861/clinmedicine.18-2-s60.

[62] J. Tong *et al.*, "Granulocyte Colony-Stimulating Factor Accelerates the Recovery of Hepatitis B Virus-Related Acute-on-Chronic Liver Failure by Promoting M2-Like Transition of Monocytes," *Front. Immunol.*, vol. 13, no. May, pp. 1–13, 2022, doi: 10.3389/fimmu.2022.885829.

[63] A. De *et al.*, "Multiple Cycles of Granulocyte Colony-Stimulating Factor Increase Survival Times of Patients With Decompensated Cirrhosis in a Randomized Trial," *Clin. Gastroenterol. Hepatol.*, vol. 19, no. 2, pp. 375-383.e5, 2021, doi: 10.1016/j.cgh.2020.02.022.

[64] N. Verma *et al.*, "Outcomes after multiple courses of granulocyte colony-stimulating factor and growth hormone in decompensated cirrhosis: A randomized trial," *Hepatology*, vol. 68, no. 4, pp. 1559–1573, 2018, doi: 10.1002/hep.29763.

[65] R. Prajapati, A. Arora, P. Sharma, N. Bansal, V. Singla, and A. Kumar, "Granulocyte colony-stimulating factor improves survival of patients with decompensated cirrhosis: A randomized-controlled trial," *Eur. J. Gastroenterol. Hepatol.*, vol. 29, no. 4, pp. 448–455, 2017, doi:

10.1097/MEG.0000000000000801.

[66] P. N. Newsome *et al.*, "Granulocyte colony-stimulating factor and autologous CD133-positive stem-cell therapy in liver cirrhosis (REALISTIC): an open-label, randomised, controlled phase 2 trial," *Lancet Gastroenterol. Hepatol.*, vol. 3, no. 1, pp. 25–36, 2018, doi: 10.1016/S2468-1253(17)30326-6.

[67] C. Engelmann *et al.*, "Granulocyte-colony stimulating factor (G-CSF) to treat acute-on-chronic liver failure: A multicenter randomized trial (GRAFT study)," *J. Hepatol.*, vol. 75, no. 6, pp. 1346–1354, 2021, doi: 10.1016/j.jhep.2021.07.033.

[68] A. Venkitaraman *et al.*, "Multiple cycles of granulocyte colony-stimulating factor in decompensated cirrhosis: a double-blind RCT," *Hepatol. Int.*, vol. 16, no. 5, pp. 1127–1136, 2022, doi: 10.1007/s12072-022-10314-x.

[69] A. D. Panopoulos and S. S. Watowich, "Granulocyte colony-stimulating factor: Molecular mechanisms of action during steady state and 'emergency' hematopoiesis," *Cytokine*, vol. 42, no. 3, pp. 277–288, Jun. 2008, doi: 10.1016/j.cyto.2008.03.002.

[70] C. Villanueva *et al.*, "Development of hyperdynamic circulation and response to β-blockers in compensated cirrhosis with portal hypertension," *Hepatology*, vol. 63, no. 1, pp. 197–206, Jan. 2016, doi: 10.1002/hep.28264.

[71] L. Bossen, A. Krag, H. Vilstrup, H. Watson, and P. Jepsen, "Nonselective β-blockers do not affect mortality in cirrhosis patients with ascites: Post Hoc analysis of three randomized controlled trials with 1198 patients," *Hepatology*, vol. 63, no. 6, pp. 1968–1976, 2016, doi: 10.1002/hep.28352.

[72] R. J. Groszmann *et al.*, "Beta-Blockers to Prevent Gastroesophageal Varices in Patients with Cirrhosis," *N. Engl. J. Med.*, vol. 353, no. 21, pp. 2254–2261, Nov. 2005, doi: 10.1056/NEJMoa044456.

[73] C. Villanueva *et al.*, "β blockers to prevent decompensation of cirrhosis in patients with clinically significant portal hypertension (PREDESCI): a randomised, double-blind, placebo-controlled, multicentre trial," *Lancet*, vol. 393, no. 10181, pp. 1597–1608, 2019, doi: 10.1016/S0140-6736(18)31875-0.

[74] T. Tittanegro *et al.*, "Use of non-selective B-blockers is safe in hospitalised decompensated cirrhosis patients and exerts a potential anti-inflammatory effect: Data from the ATTIRE trial," *eClinicalMedicine*, vol. 55, p. 101716, 2023, doi: 10.1016/j.eclinm.2022.101716.

[75] G. N. Kalambokis *et al.*, "Conversion of Propranolol to Carvedilol Improves Renal Perfusion and Outcome in Patients with Cirrhosis and Ascites," *J. Clin. Gastroenterol.*, vol. 55, no. 8, pp. 721–729, 2021, doi: 10.1097/MCG.0000000000001431.

[76] V. Singh, P. Kumar, N. Verma, R. Vijayvergiya, A. Singh, and A. Bhalla, "Propranolol vs. band ligation for primary prophylaxis of variceal hemorrhage in cirrhotic patients with ascites: a randomized controlled trial," *Hepatol. Int.*, vol. 16, no. 4, pp. 944–953, 2022, doi: 10.1007/s12072-022-10361-4.

[77] S. G. Rodrigues, Y. P. Mendoza, and J. Bosch, "Beta-blockers in cirrhosis: Evidence-based indications and limitations," *JHEP Reports*, vol. 2, no. 1, pp. 1–17, 2020, doi: 10.1016/j.jhepr.2019.12.001.

[78] L. Colombato, "The role of Transjugular Intrahepatic Portosystemic Shunt (TIPS) in the management of portal hypertension," *J. Clin. Gastroenterol.*, vol. 41, no. SUPPL. 3, pp. 344–351, 2007, doi: 10.1097/MCG.0b013e318157e500.

[79] M. Merli *et al.*, "Transjugular intrahepatic portosystemic shunt versus endoscopic sclerotherapy for the prevention of variceal bleeding in cirrhosis: A randomized multicenter trial," *Hepatology*, vol. 27, no. 1, pp. 48–53, 1998, doi: 10.1002/hep.510270109.

[80] À. Escorsell *et al.*, "TIPS versus drug therapy in preventing variceal rebleeding in advanced cirrhosis: A randomized controlled trial," *Hepatology*, vol. 35, no. 2, pp. 385–392, 2002, doi: 10.1053/jhep.2002.30418.

[81] G. Pomier-Layrargues *et al.*, "Transjugular intrahepatic portosystemic shunt (TIPS) versus endoscopic variceal ligation in the prevention of variceal rebleeding in patients with cirrhosis: A randomised trial," *Gut*, vol. 48, no. 3, pp. 390–396, 2001, doi: 10.1136/gut.48.3.390.

[82] X. Luo, Z. Wang, J. Tsauo, B. Zhou, H. Zhang, and X. Li, "Advanced cirrhosis combined with portal vein thrombosis: A randomized trial of TIPS versus endoscopic band ligation plus propranolol for the prevention of recurrent esophageal variceal bleeding," *Radiology*, vol. 276, no. 1, pp. 286–293, 2015, doi: 10.1148/radiol.15141252.

[83] F. Salerno *et al.*, "Randomized controlled study of TIPS versus paracentesis plus albumin in cirrhosis with severe ascites," *Hepatology*, vol. 40, no. 3, pp. 629–635, 2004, doi: 10.1002/hep.20364.

[84] J. C. García-Pagán *et al.*, "Early Use of TIPS in Patients with Cirrhosis and Variceal Bleeding," *N. Engl. J. Med.*, vol. 362, no. 25, pp. 2370–2379, Jun. 2010, doi: 10.1056/NEJMoa0910102.

[85] C. Bureau *et al.*, "Transjugular Intrahepatic Portosystemic Shunts With Covered Stents Increase Transplant-Free Survival of Patients With Cirrhosis and Recurrent Ascites," *Gastroenterology*, vol. 152, no. 1, pp. 157–163, 2017, doi: 10.1053/j.gastro.2016.09.016.

[86] Y. Lv *et al.*, "Early TIPS with covered stents versus standard treatment for acute variceal bleeding in patients with advanced cirrhosis: a randomised controlled trial," *Lancet Gastroenterol. Hepatol.*, vol. 4, no. 8, pp. 587–598, 2019, doi: 10.1016/S2468-1253(19)30090-1.

[87] M. J. Orloff, F. Vaida, K. S. Haynes, R. J. Hye, J. I. Isenberg, and H. Jinich-Brook, "Randomized Controlled Trial of Emergency Transjugular Intrahepatic Portosystemic Shunt Versus Emergency Portacaval Shunt Treatment of Acute Bleeding Esophageal Varices in Cirrhosis," *J. Gastrointest. Surg.*, vol. 16, no. 11, pp. 2094–2111, 2012, doi: 10.1007/s11605-012-2003-6.

[88] W. Zhang *et al.*, "Fecal Microbiota Transplantation (FMT) alleviates experimental colitis in mice by gut microbiota regulation," *J. Microbiol. Biotechnol.*, vol. 30, no. 8, pp. 1132–1141, 2020, doi: 10.4014/jmb.2002.02044.

[89] R. Kutmutia *et al.*, "Evaluating the role of antibiotics in patients admitted to hospital with decompensated cirrhosis: lessons from the ATTIRE trial," *Am. J. Gastroenterol.*, vol. Publish Ah, 2022, doi: 10.14309/ajg.0000000000001937.

[90] J. S. Bajaj *et al.*, "Antibiotic-Associated Disruption of Microbiota Composition and Function in Cirrhosis Is Restored by Fecal Transplant," *Hepatology*, vol. 68, no. 4, pp. 1549–1558, Oct. 2018, doi: 10.1002/hep.30037.

[91] J. S. Bajaj, A. Fagan, E. A. Gavis, Z. Kassam, M. Sikaroodi, and P. M. Gillevet, "Long-term Outcomes of Fecal Microbiota Transplantation in Patients With Cirrhosis," *Gastroenterology*, vol. 156, no. 6, pp. 1921-1923.e3, May 2019, doi: 10.1053/j.gastro.2019.01.033.

[92] J. S. Bajaj *et al.*, "Fecal Microbiota Transplant in Cirrhosis Reduces Gut Microbial Antibiotic Resistance Genes: Analysis of Two Trials," *Hepatol. Commun.*, vol. 5, no. 2, pp. 258–271, Feb. 2021, doi: 10.1002/hep4.1639.

[93] C. A. Woodhouse *et al.*, "PROFIT, a PROspective, randomised placebo controlled feasibility trial of Faecal mIcrobiota Transplantation in cirrhosis: Study protocol for a single-blinded trial," *BMJ Open*, vol. 9, no. 2, pp. 1–6, 2019, doi: 10.1136/bmjopen-2018-023518.

[94] J. Fernández *et al.*, "Efficacy of Albumin Treatment for Patients with Cirrhosis and Infections Unrelated to Spontaneous Bacterial Peritonitis," *Clin. Gastroenterol. Hepatol.*, vol. 18, no. 4,

pp. 963-973.e14, 2020, doi: 10.1016/j.cgh.2019.07.055.

[95] P. Caraceni *et al.*, "On-treatment serum albumin level can guide long-term treatment in patients with cirrhosis and uncomplicated ascites," *J. Hepatol.*, vol. 74, no. 2, pp. 340–349, 2021, doi: 10.1016/j.jhep.2020.08.021.

[96] R. Maiwall *et al.*, "A randomized-controlled trial comparing 20% albumin to plasmalyte in patients with cirrhosis and sepsis-induced hypotension [ALPS trial]," *J. Hepatol.*, vol. 77, no. 3, pp. 670–682, 2022, doi: 10.1016/j.jhep.2022.03.043.

[97] L. China *et al.*, "A Randomized Trial of Albumin Infusions in Hospitalized Patients with Cirrhosis," *N. Engl. J. Med.*, vol. 384, no. 9, pp. 808–817, 2021, doi: 10.1056/nejmoa2022166.

[98] L. China *et al.*, "Targeted Albumin Therapy Does Not Improve Short-Term Outcome in Hyponatremic Patients Hospitalized with Complications of Cirrhosis: Data from the ATTIRE Trial," *Am. J. Gastroenterol.*, vol. 116, no. 11, pp. 2292–2295, 2021, doi: 10.14309/ajg.0000000000001488.

[99] L. China, N. Becares, C. Rhead, T. Tittanegro, N. Freemantle, and A. O'Brien, "Targeted Albumin Infusions Do Not Improve Systemic Inflammation or Cardiovascular Function in Decompensated Cirrhosis," *Clin. Transl. Gastroenterol.*, vol. 13, no. 5, p. e00476, 2022, doi: 10.14309/ctg.0000000000000476.

[100] A. Eguchi *et al.*, "Emricasan, a pan-caspase inhibitor, improves survival and portal hypertension in a murine model of common bile-duct ligation," *J. Mol. Med.*, vol. 96, no. 6, pp. 575–583, Jun. 2018, doi: 10.1007/s00109-018-1642-9.

[101] J. Gracia-Sancho *et al.*, "Emricasan Ameliorates Portal Hypertension and Liver Fibrosis in Cirrhotic Rats Through a Hepatocyte-Mediated Paracrine Mechanism," *Hepatol. Commun.*, vol. 3, no. 7, pp. 987–1000, 2019, doi: 10.1002/hep4.1360.

[102] G. Garcia-Tsao *et al.*, "Emricasan (IDN-6556) Lowers Portal Pressure in Patients With Compensated Cirrhosis and Severe Portal Hypertension," *Hepatology*, vol. 69, no. 2, pp. 717–728, 2019, doi: 10.1002/hep.30199.

[103] G. Mehta *et al.*, "A Placebo-Controlled, Multicenter, Double-Blind, Phase 2 Randomized Trial of the Pan-Caspase Inhibitor Emricasan in Patients with Acutely Decompensated Cirrhosis," *J. Clin. Exp. Hepatol.*, vol. 8, no. 3, pp. 224–234, 2018, doi: 10.1016/j.jceh.2017.11.006.

[104] C. T. Frenette *et al.*, "Emricasan Improves Liver Function in Patients With Cirrhosis and High Model for End-Stage Liver Disease Scores Compared With Placebo," *Clin. Gastroenterol.*

Hepatol., vol. 17, no. 4, pp. 774-783.e4, 2019, doi: 10.1016/j.cgh.2018.06.012.

[105] G. Garcia-Tsao *et al.*, "Randomized placebo-controlled trial of emricasan for non-alcoholic steatohepatitis-related cirrhosis with severe portal hypertension," *J. Hepatol.*, vol. 72, no. 5, pp. 885–895, 2020, doi: 10.1016/j.jhep.2019.12.010.

[106] C. Frenette *et al.*, "Emricasan to prevent new decompensation in patients with NASH-related decompensated cirrhosis," *J. Hepatol.*, vol. 74, no. 2, pp. 274–282, 2021, doi: 10.1016/j.jhep.2020.09.029.

[107] L. K. Cheng, G. O'Grady, P. Du, J. U. Egbuji, J. A. Windsor, and A. J. Pullan, "Gastrointestinal system," *WIREs Syst. Biol. Med.*, vol. 2, no. 1, pp. 65–79, Jan. 2010, doi: 10.1002/wsbm.19.

[108] I. Rowland *et al.*, "Gut microbiota functions: metabolism of nutrients and other food components," *Eur. J. Nutr.*, vol. 57, no. 1, pp. 1–24, 2018, doi: 10.1007/s00394-017-1445-8.

[109] E. Trefts, M. Gannon, and D. H. Wasserman, "The liver," *Curr. Biol.*, vol. 27, no. 21, pp. R1147–R1151, Nov. 2017, doi: 10.1016/j.cub.2017.09.019.

[110] P. Kubes and C. Jenne, "Immune Responses in the Liver," *Annu. Rev. Immunol.*, vol. 36, pp. 247–277, 2018, doi: 10.1146/annurev-immunol-051116-052415.

[111] P. Kubes and W. Z. Mehal, "Sterile inflammation in the liver," *Gastroenterology*, vol. 143, no. 5. W.B. Saunders, pp. 1158–1172, 2012, doi: 10.1053/j.gastro.2012.09.008.

[112] N. S. Ghonem, D. N. Assis, and J. L. Boyer, "On fibrates and cholestasis: A review," *Hepatology*, vol. 62, no. 2, pp. 635–643, 2015, doi: 10.1002/hep.27744.On.

[113] R. Wiest, A. Albillos, M. Trauner, J. S. Bajaj, and R. Jalan, "Targeting the gut-liver axis in liver disease," *J. Hepatol.*, vol. 67, no. 5, pp. 1084–1103, 2017, doi: 10.1016/j.jhep.2017.05.007.

[114] G. Kakiyama *et al.*, "Modulation of the fecal bile acid profile by gut microbiota in cirrhosis," *J. Hepatol.*, vol. 58, no. 5, pp. 949–955, May 2013, doi: 10.1016/j.jhep.2013.01.003.

[115] P. Konturek *et al.*, "Gut–Liver Axis: How Do Gut Bacteria Influence the Liver?," *Med. Sci.*, vol. 6, no. 3, p. 79, 2018, doi: 10.3390/medsci6030079.

[116] J. N. Masse, *Petit Atlas complet d'Anatomie descriptive du Corps Humain*. Paris : J.B. Baillière, 1848.

[117] A. Albillos, A. de Gottardi, and M. Rescigno, "The gut-liver axis in liver disease: Pathophysiological basis for therapy," *J. Hepatol.*, vol. 72, no. 3, pp. 558–577, Mar. 2020, doi:

10.1016/j.jhep.2019.10.003.

[118] J. Trebicka, T. Reiberger, and W. Laleman, "Gut-Liver Axis Links Portal Hypertension to Acute-on-Chronic Liver Failure," *Visc. Med.*, vol. 34, no. 4, pp. 270–275, 2018, doi: 10.1159/000490262.

[119] I. Milosevic *et al.*, "Gut-liver axis, gut microbiota, and its modulation in the management of liver diseases: A review of the literature," *Int. J. Mol. Sci.*, vol. 20, no. 2, pp. 1–16, 2019, doi: 10.3390/ijms20020395.

[120] M. S. Roberts, B. M. Magnusson, F. J. Burczynski, and M. Weiss, "Enterohepatic circulation: Physiological, pharmacokinetic and clinical implications," *Clin. Pharmacokinet.*, vol. 41, no. 10, pp. 751–790, 2002, doi: 10.2165/00003088-200241100-00005.

[121] J. M. Ridlon, D. J. Kang, P. B. Hylemon, and J. S. Bajaj, "Bile acids and the gut microbiome," *Curr. Opin. Gastroenterol.*, vol. 30, no. 3, pp. 332–338, May 2014, doi: 10.1097/MOG.0000000000000057.

[122] M. Vancamelbeke and S. Vermeire, "The intestinal barrier: a fundamental role in health and disease," *Expert Rev. Gastroenterol. Hepatol.*, vol. 11, no. 9, pp. 821–834, 2017, doi: 10.1080/17474124.2017.1343143.

[123] L. Maccioni *et al.*, "Intestinal permeability, microbial translocation, changes in duodenal and fecal microbiota, and their associations with alcoholic liver disease progression in humans," *Gut Microbes*, vol. 12, no. 1, 2020, doi: 10.1080/19490976.2020.1782157.

[124] K. E. Pijls, G. H. Koek, E. E. Elamin, H. de Vries, A. A. M. Masclee, and D. M. A. E. Jonkers, "Large intestine permeability is increased in patients with compensated liver cirrhosis," *Am. J. Physiol. - Gastrointest. Liver Physiol.*, vol. 306, no. 2, pp. 147–153, 2014, doi: 10.1152/ajpgi.00330.2013.

[125] J. Trebicka, P. Bork, A. Krag, and M. Arumugam, "Utilizing the gut microbiome in decompensated cirrhosis and acute-on-chronic liver failure," *Nature Reviews Gastroenterology and Hepatology*, vol. 18, no. 3. Nature Research, pp. 167–180, 01-Mar-2021, doi: 10.1038/s41575-020-00376-3.

[126] S. Van der Merwe, S. Chokshi, C. Bernsmeier, and A. Albillos, "The multifactorial mechanisms of bacterial infection in decompensated cirrhosis," *J. Hepatol.*, vol. 75, pp. S82–S100, 2021, doi: 10.1016/j.jhep.2020.11.029.

[127] E. M. M. Quigley and G. Garcia-Tsao, "Bacterial translocation in acute and chronic portal

hypertension," *Hepatology*, vol. 20, no. 1, pp. 264–266, 1994, doi: 10.1002/hep.1840200145.

[128] F. B. Kasravi, L. Wang, X. D. Wang, G. Molin, S. Bengmark, and B. Jeppsson, "Bacterial translocation in acute liver injury induced by D-galactosamine," *Hepatology*, vol. 23, no. 1, pp. 97–103, 1996, doi: 10.1053/jhep.1996.v23.pm0008550055.

[129] C. Pande, A. Kumar, and S. K. Sarin, "Small-intestinal bacterial overgrowth in cirrhosis is related to the severity of liver disease," *Aliment. Pharmacol. Ther.*, vol. 29, no. 12, pp. 1273–1281, 2009, doi: 10.1111/j.1365-2036.2009.03994.x.

[130] D. W. Jun *et al.*, "Association between small intestinal bacterial overgrowth and peripheral bacterial DNA in cirrhotic patients," *Dig. Dis. Sci.*, vol. 55, no. 5, pp. 1465–1471, 2010, doi: 10.1007/s10620-009-0870-9.

[131] J. S. Bajaj *et al.*, "Altered profile of human gut microbiome is associated with cirrhosis and its complications," *J. Hepatol.*, vol. 60, no. 5, pp. 940–947, 2014, doi: 10.1016/j.jhep.2013.12.019.

[132] C. Bode, V. Kugler, and J. C. Bode, "Endotoxemia in patients with alcoholic and non-alcoholic cirrhosis and in subjects with no evidence of chronic liver disease following acute alcohol excess," *J. Hepatol.*, vol. 4, no. 1, pp. 8–14, 1987, doi: 10.1016/S0168-8278(87)80003-X.

[133] R. S. Lin *et al.*, "Endotoxemia in patients with chronic liver diseases: relationship to severity of liver diseases, presence of esophaegeal varices, and hyperdynamic circulation.," *J. Hepatol.*, vol. 22, no. 2, pp. 165–172, 1995, doi: 10.1016/0168-8278(95)80424-2.

[134] C. C. Chan *et al.*, "Prognostic value of plasma endotoxin levels in patients with cirrhosis," *Scand. J. Gastroenterol.*, vol. 32, no. 9, pp. 942–945, 1997, doi: 10.3109/00365529709011206.

[135] I. Cirera *et al.*, "Bacterial translocation of enteric organisms in patients with cirrhosis," *J. Hepatol.*, vol. 34, no. 1, pp. 32–37, 2001, doi: 10.1016/S0168-8278(00)00013-1.

[136] A. Albillos *et al.*, "Increased lipopolysaccharide binding protein in cirrhotic patients with marked immune and hemodynamic derangement," *Hepatology*, vol. 37, no. 1, pp. 208–217, 2003, doi: 10.1053/jhep.2003.50038.

[137] M. J. Zuckerman *et al.*, "Assessment of Intestinal Permeability and Absorption in Cirrhotic Patients with Ascites Using Combined Sugar Probes," *Dig. Dis. Sci.*, vol. 49, no. 4, pp. 621–626, Apr. 2004, doi: 10.1023/B:DDAS.0000026307.56909.21.

[138] Z. Teltschik *et al.*, "Intestinal bacterial translocation in rats with cirrhosis is related to

compromised paneth cell antimicrobial host defense," *Hepatology*, vol. 55, no. 4, pp. 1154–1163, 2012, doi: 10.1002/hep.24789.

[139] L. W. Peterson and D. Artis, "Intestinal epithelial cells: Regulators of barrier function and immune homeostasis," *Nature Reviews Immunology*, vol. 14, no. 3. pp. 141–153, 2014, doi: 10.1038/nri3608.

[140] N. Rolhion and B. Chassaing, "When pathogenic bacteria meet the intestinal microbiota," *Philos. Trans. R. Soc. B Biol. Sci.*, vol. 371, no. 1707, 2016, doi: 10.1098/rstb.2015.0504.

[141] A. J. Bäumler and V. Sperandio, "Interactions between the microbiota and pathogenic bacteria in the gut," *Nature*, vol. 535, no. 7610, pp. 85–93, Jul. 2016, doi: 10.1038/nature18849.

[142] S. De Schepper *et al.*, "Self-Maintaining Gut Macrophages Are Essential for Intestinal Homeostasis," *Cell*, vol. 175, no. 2, pp. 400-415.e13, 2018, doi: 10.1016/j.cell.2018.07.048.

[143] L. R. Muniz, C. Knosp, and G. Yeretssian, "Intestinal antimicrobial peptides during homeostasis, infection, and disease," *Front. Immunol.*, vol. 3, no. OCT, pp. 1–13, 2012, doi: 10.3389/fimmu.2012.00310.

[144] R. Okumura and K. Takeda, "Roles of intestinal epithelial cells in the maintenance of gut homeostasis," *Exp. Mol. Med.*, vol. 49, no. 5, pp. e338-8, 2017, doi: 10.1038/emm.2017.20.

[145] M. E. V. Johansson, M. Phillipson, J. Petersson, A. Velcich, L. Holm, and G. C. Hansson, "The inner of the two Muc2 mucin-dependent mucus layers in colon is devoid of bacteria," *Proc. Natl. Acad. Sci. U. S. A.*, vol. 105, no. 39, pp. 15064–15069, 2008, doi: 10.1073/pnas.0803124105.

[146] F. E. O. Holmberg, J. Pedersen, P. Jørgensen, C. Soendergaard, K. B. Jensen, and O. H. Nielsen, "Intestinal barrier integrity and inflammatory bowel disease: Stem cell-based approaches to regenerate the barrier," *J. Tissue Eng. Regen. Med.*, vol. 12, no. 4, pp. 923–935, 2018, doi: 10.1002/term.2506.

[147] J. R. De Mey and J. Freund, "Understanding epithelial homeostasis in the intestine," *Tissue Barriers*, vol. 1, no. 2, p. e24965, Apr. 2013, doi: 10.4161/tisb.24965.

[148] C. L. Bevins and N. H. Salzman, "Paneth cells, antimicrobial peptides and maintenance of intestinal homeostasis," *Nat. Rev. Microbiol.*, vol. 9, no. 5, pp. 356–368, 2011, doi: 10.1038/nrmicro2546.

[149] F. M. Gribble and F. Reimann, "Enteroendocrine Cells: Chemosensors in the Intestinal Epithelium," *Annu. Rev. Physiol.*, vol. 78, pp. 277–299, 2016, doi: 10.1146/annurev-physiol-021115-105439.

[150] J. V. Patankar and C. Becker, "Cell death in the gut epithelium and implications for chronic inflammation," *Nature Reviews Gastroenterology and Hepatology*, vol. 17, no. 9. Nature Research, pp. 543–556, 01-Sep-2020, doi: 10.1038/s41575-020-0326-4.

[151] A. Cairnie, L. Lamerton, and G. Steel, "Cell proliferation studies in the intestinal epithelium of the rat I. Determination of the kinetic parameters," *Exp. Cell Res.*, vol. 39, no. 2–3, pp. 528–538, Sep. 1965, doi: 10.1016/0014-4827(65)90055-8.

[152] C. S. Potten, "Extreme sensitivity of some intestinal crypt cells to X and γ irradiation," *Nature*, vol. 269, no. 5628, pp. 518–521, Oct. 1977, doi: 10.1038/269518a0.

[153] H. Cheng and C. P. Leblond, "Origin, differentiation and renewal of the four main epithelial cell types in the mouse small intestine I. Columnar cell," *Am. J. Anat.*, vol. 141, no. 4, pp. 461–479, Dec. 1974, doi: 10.1002/aja.1001410403.

[154] J. Du Plessis *et al.*, "Activated intestinal macrophages in patients with cirrhosis release NO and IL-6 that may disrupt intestinal barrier function," *J. Hepatol.*, vol. 58, no. 6, pp. 1125–1132, Jun. 2013, doi: 10.1016/j.jhep.2013.01.038.

[155] S. F. Assimakopoulos *et al.*, "Altered intestinal tight junctions' expression in patients with liver cirrhosis: A pathogenetic mechanism of intestinal hyperpermeability," *Eur. J. Clin. Invest.*, vol. 42, no. 4, pp. 439–446, 2012, doi: 10.1111/j.1365-2362.2011.02609.x.

[156] L. Muñoz *et al.*, "Intestinal Immune Dysregulation Driven by Dysbiosis Promotes Barrier Disruption and Bacterial Translocation in Rats With Cirrhosis," *Hepatology*, vol. 70, no. 3, pp. 925–938, 2019, doi: 10.1002/hep.30349.

[157] A. Isaacs-Ten *et al.*, "Intestinal Microbiome-Macrophage Crosstalk Contributes to Cholestatic Liver Disease by Promoting Intestinal Permeability in Mice," *Hepatology*, vol. 72, no. 6, pp. 2090–2108, 2020, doi: 10.1002/hep.31228.

[158] M. Sorribas *et al.*, "FXR modulates the gut-vascular barrier by regulating the entry sites for bacterial translocation in experimental cirrhosis," *J. Hepatol.*, vol. 71, no. 6, pp. 1126–1140, 2019, doi: 10.1016/j.jhep.2019.06.017.

[159] E. Marshman, C. Booth, and C. S. Potten, "The intestinal epithelial stem cell," *BioEssays*, vol. 24, no. 1, pp. 91–98, 2002, doi: 10.1002/bies.10028.

[160] M. S. D'Arcy, "Cell death: a review of the major forms of apoptosis, necrosis and autophagy," *Cell Biol. Int.*, vol. 43, no. 6, pp. 582–592, 2019, doi: 10.1002/cbin.11137.

[161] A. M. Marchiando *et al.*, "The Epithelial Barrier Is Maintained by In Vivo Tight Junction Expansion During Pathologic Intestinal Epithelial Shedding," *Gastroenterology*, vol. 140, no. 4, pp. 1208-1218.e2, Apr. 2011, doi: 10.1053/j.gastro.2011.01.004.

[162] N. Winsor, C. Krustev, J. Bruce, D. J. Philpott, and S. E. Girardin, "Canonical and noncanonical inflammasomes in intestinal epithelial cells," *Cell. Microbiol.*, no. April, pp. 1–13, 2019, doi: 10.1111/cmi.13079.

[163] E. M. Davis *et al.*, "Pyroptosis of Intestinal Epithelial Cells is Crucial to the Development of Mucosal Barrier Dysfunction and Intestinal Inflammation," *Gastroenterology*, vol. 152, no. 5, p. S967, 2017, doi: 10.1016/s0016-5085(17)33282-1.

[164] J. J. Liu *et al.*, "Epithelial cell extrusion leads to breaches in the intestinal epithelium," *Inflamm. Bowel Dis.*, vol. 19, no. 5, pp. 912–921, Apr. 2013, doi: 10.1097/MIB.0B013E3182807600.

[165] C. Bauer *et al.*, "Colitis induced in mice with dextran sulfate sodium (DSS) is mediated by the NLRP3 inflammasome," *Gut*, vol. 59, no. 9, pp. 1192–1199, 2010, doi: 10.1136/gut.2009.197822.

[166] F. Radtke and H. Clevers, "Self-renewal and cancer of the gut: Two sides of a coin," *Science*, vol. 307, no. 5717. American Association for the Advancement of Science, pp. 1904–1909, 25-Mar-2005, doi: 10.1126/science.1104815.

[167] A. Metidji *et al.*, "The Environmental Sensor AHR Protects from Inflammatory Damage by Maintaining Intestinal Stem Cell Homeostasis and Barrier Integrity," *Immunity*, vol. 49, no. 2, pp. 353-362.e5, 2018, doi: 10.1016/j.immuni.2018.07.010.

[168] H. F. Farin *et al.*, "Paneth cell extrusion and release of antimicrobial products is directly controlled by immune cell-derived IFN-γ," *J. Exp. Med.*, vol. 211, no. 7, pp. 1393–1405, 2014, doi: 10.1084/jem.20130753.

[169] Q. Hou, J. Huang, H. Ayansola, H. Masatoshi, and B. Zhang, "Intestinal Stem Cells and Immune Cell Relationships: Potential Therapeutic Targets for Inflammatory Bowel Diseases," *Front. Immunol.*, vol. 11, no. January, pp. 1–14, 2021, doi: 10.3389/fimmu.2020.623691.

[170] J. Shi *et al.*, "Cleavage of GSDMD by inflammatory caspases determines pyroptotic cell death," *Nature*, vol. 526, no. 7575, pp. 660–665, 2015, doi: 10.1038/nature15514.

[171] J. Ding *et al.*, "Pore-forming activity and structural autoinhibition of the gasdermin family," 2016, doi: 10.1038/nature18590.

[172] X. Liu *et al.*, "Inflammasome-activated gasdermin D causes pyroptosis by forming membrane pores," *Nature*, vol. 535, no. 7610, pp. 153–158, Jul. 2016, doi: 10.1038/nature18629.

[173] N. Van Opdenbosch and M. Lamkanfi, "Caspases in Cell Death, Inflammation, and Disease," *Immunity*, vol. 50, no. 6, pp. 1352–1364, 2019, doi: 10.1016/j.immuni.2019.05.020.

[174] M. Lamkanfi and V. M. Dixit, "Mechanisms and functions of inflammasomes," *Cell*, vol. 157, no. 5, pp. 1013–1022, 2014, doi: 10.1016/j.cell.2014.04.007.

[175] T. Fernandes-Alnemri *et al.*, "The pyroptosome: A supramolecular assembly of ASC dimers mediating inflammatory cell death via caspase-1 activation," *Cell Death Differ.*, vol. 14, no. 9, pp. 1590–1604, 2007, doi: 10.1038/sj.cdd.4402194.

[176] N. Kayagaki *et al.*, "Caspase-11 cleaves gasdermin D for non-canonical inflammasome signalling," *Nature*, vol. 526, no. 7575, pp. 666–671, 2015, doi: 10.1038/nature15541.

[177] J. M. Kim, L. Eckmann, T. C. Savidge, D. C. Lowe, T. Witthöft, and M. F. Kagnoff, "Apoptosis of Human Intestinal Epithelial Cells after Bacterial Invasion Salmonella • nitric oxide • pathogenesis • infection," 1998.

[178] L. A. Knodler *et al.*, "Noncanonical inflammasome activation of caspase-4/caspase-11 mediates epithelial defenses against enteric bacterial pathogens," *Cell Host Microbe*, vol. 16, no. 2, pp. 249–256, Aug. 2014, doi: 10.1016/j.chom.2014.07.002.

[179] T. Vanden Berghe *et al.*, "Simultaneous targeting of IL-1 and IL-18 is required for protection against inflammatory and septic shock," *Am. J. Respir. Crit. Care Med.*, vol. 189, no. 3, pp. 282–291, 2014, doi: 10.1164/rccm.201308-1535OC.

[180] B. Siegmund, H. A. Lehr, G. Fantuzzi, and C. A. Dinarello, "IL-1β-converting enzyme (caspase-1) in intestinal inflammation," *Proc. Natl. Acad. Sci. U. S. A.*, vol. 98, no. 23, pp. 13249–13254, Nov. 2001, doi: 10.1073/pnas.231473998.

[181] M. H. Zaki, K. L. Boyd, P. Vogel, M. B. Kastan, M. Lamkanfi, and T. D. Kanneganti, "The NLRP3 Inflammasome Protects against Loss of Epithelial Integrity and Mortality during Experimental Colitis," *Immunity*, vol. 32, no. 3, pp. 379–391, 2010, doi: 10.1016/j.immuni.2010.03.003.

[182] D. Demon, A. Kuchmiy, A. Fossoul, Q. Zhu, T. D. Kanneganti, and M. Lamkanfi, "Caspase-11 is expressed in the colonic mucosa and protects against dextran sodium sulfate-induced colitis,"

Mucosal Immunol., vol. 7, no. 6, pp. 1480–1491, 2014, doi: 10.1038/mi.2014.36.

[183] K. Bulek *et al.*, "Epithelial-derived gasdermin D mediates nonlytic IL-1β release during experimental colitis," *J. Clin. Invest.*, Jun. 2020, doi: 10.1172/jci138103.

[184] C. Lebeaupin *et al.*, "ER stress induces NLRP3 inflammasome activation and hepatocyte death," *Cell Death Dis.*, vol. 6, no. 9, 2015, doi: 10.1038/cddis.2015.248.

[185] L. Longo *et al.*, "Gut dysbiosis and increased intestinal permeability drive microrna, nlrp-3 inflammasome and liver fibrosis in a nutritional model of non-alcoholic steatohepatitis in adult male sprague dawley rats," *Clin. Exp. Gastroenterol.*, vol. 13, pp. 351–368, 2020, doi: 10.2147/CEG.S262879.

[186] I. Pierantonelli *et al.*, "Lack of NLRP3-inflammasome leads to gut-liver axis derangement, gut dysbiosis and a worsened phenotype in a mouse model of NAFLD," *Sci. Rep.*, vol. 7, no. 1, p. 12200, 2017, doi: 10.1038/s41598-017-11744-6.

[187] Y. Feng, Y. Huang, Y. Wang, P. Wang, H. Song, and F. Wang, "Antibiotics induced intestinal tight junction barrier dysfunction is associated with microbiota dysbiosis, activated NLRP3 inflammasome and autophagy," *PLoS One*, vol. 14, no. 6, 2019, doi: 10.1371/journal.pone.0218384.

[188] U. Soffientini *et al.*, "The Lipopolysaccharide-Sensing Caspase(s)-4/11 Are Activated in Cirrhosis and Are Causally Associated With Progression to Multi-Organ Injury," *Front. Cell Dev. Biol.*, vol. 0, p. 1826, 2021, doi: https://doi.org/10.3389%2Ffcell.2021.668459.

[189] O. Meir, E. Dvash, A. Werman, and M. Rubinstein, "C/EBP-β regulates endoplasmic reticulum stress-triggered cell death in mouse and human models," *PLoS One*, vol. 5, no. 3, 2010, doi: 10.1371/journal.pone.0009516.

[190] J. Heijmans *et al.*, "ER Stress Causes Rapid Loss of Intestinal Epithelial Stemness through Activation of the Unfolded Protein Response," *Cell Rep.*, vol. 3, no. 4, pp. 1128–1139, Apr. 2013, doi: 10.1016/j.celrep.2013.02.031.

[191] D. Ron and P. Walter, "Signal integration in the endoplasmic reticulum unfolded protein response," *Nature Reviews Molecular Cell Biology*, vol. 8, no. 7. pp. 519–529, 2007, doi: 10.1038/nrm2199.

[192] M. H. Smith, H. L. Ploegh, and J. S. Weissman, "Road to ruin: Targeting proteins for degradation in the endoplasmic reticulum," *Science*, vol. 334, no. 6059. American Association for the Advancement of Science, pp. 1086–1090, 25-Nov-2011, doi:

10.1126/science.1209235.

[193] A. Negroni *et al.*, "Endoplasmic reticulum stress and unfolded protein response are involved in paediatric inflammatory bowel disease," *Dig. Liver Dis.*, vol. 46, no. 9, pp. 788–794, 2014, doi: 10.1016/j.dld.2014.05.013.

[194] R. Liu *et al.*, "C/EBP homologous protein–induced loss of intestinal epithelial stemness contributes to bile duct ligation–induced cholestatic liver injury in mice," *Hepatology*, vol. 67, no. 4, pp. 1441–1457, 2018, doi: 10.1002/hep.29540.

[195] J. S. Cox, C. E. Shamu, and P. Walter, "Transcriptional induction of genes encoding endoplasmic reticulum resident proteins requires a transmembrane protein kinase," *Cell*, vol. 73, no. 6, pp. 1197–1206, 1993, doi: 10.1016/0092-8674(93)90648-A.

[196] K. Morl, W. Ma, M. J. Gething, and J. Sambrook, "A transmembrane protein with a cdc2+ CDC28-related kinase activity is required for signaling from the ER to the nucleus," *Cell*, vol. 74, no. 4, pp. 743–756, 1993, doi: 10.1016/0092-8674(93)90521-Q.

[197] X. Z. Wang, H. P. Harding, Y. Zhang, E. M. Jolicoeur, M. Kuroda, and D. Ron, "Cloning of mammalian Ire1 reveals diversity in the ER stress responses," *EMBO J.*, vol. 17, no. 19, pp. 5708–5717, 1998, doi: 10.1093/emboj/17.19.5708.

[198] W. Tirasophon, A. A. Welihinda, and R. J. Kaufman, "A stress response pathway from the endoplasmic reticulum to the nucleus requires a novel bifunctional protein kinase/endoribonuclease (Ire1p) in mammalian cells," *Genes Dev.*, vol. 12, no. 12, pp. 1812–1824, 1998, doi: 10.1101/gad.12.12.1812.

[199] C. J. Adams, M. C. Kopp, N. Larburu, P. R. Nowak, and M. M. U. Ali, "Structure and molecular mechanism of ER stress signaling by the unfolded protein response signal activator IRE1," *Frontiers in Molecular Biosciences*, vol. 6, no. MAR. p. 11, 2019, doi: 10.3389/fmolb.2019.00011.

[200] P. Walter and D. Ron, "The unfolded protein response: From stress pathway to homeostatic regulation," *Science*, vol. 334, no. 6059. American Association for the Advancement of Science, pp. 1081–1086, 25-Nov-2011, doi: 10.1126/science.1209038.

[201] H. Yoshida, T. Matsui, A. Yamamoto, T. Okada, and K. Mori, "XBP1 mRNA is induced by ATF6 and spliced by IRE1 in response to ER stress to produce a highly active transcription factor," *Cell*, vol. 107, no. 7, pp. 881–891, 2001, doi: 10.1016/S0092-8674(01)00611-0.

[202] M. Calfon *et al.*, "IRE1 couples endoplasmic reticulum load to secretory capacity by

processing the XBP-1 mRNA," *Nature*, vol. 415, no. 6867, pp. 92–96, 2002, doi: 10.1038/415092a.

[203] A.-H. Lee, N. N. Iwakoshi, and L. H. Glimcher, "XBP-1 Regulates a Subset of Endoplasmic Reticulum Resident Chaperone Genes in the Unfolded Protein Response," *Mol. Cell. Biol.*, vol. 23, no. 21, pp. 7448–7459, 2003, doi: 10.1128/mcb.23.21.7448-7459.2003.

[204] R. J. Kaufman, "Stress signaling from the lumen of the endoplasmic reticulum: coordination of gene transcriptional and translational controls," *Genes Dev.*, vol. 13, no. 10, pp. 1211–1233, May 1999, doi: 10.1101/gad.13.10.1211.

[205] H. P. Harding, Y. Zhang, and D. Ron, "Protein translation and folding are coupled by an endoplasmic- reticulum-resident kinase," *Nature*, vol. 397, no. 6716, pp. 271–274, 1999, doi: 10.1038/16729.

[206] H. P. Harding, Y. Zhang, A. Bertolotti, H. Zeng, and D. Ron, "Perk is essential for translational regulation and cell survival during the unfolded protein response," *Mol. Cell*, vol. 5, no. 5, pp. 897–904, 2000, doi: 10.1016/S1097-2765(00)80330-5.

[207] K. M. Vattem and R. C. Wek, "Reinitiation involving upstream ORFs regulates ATF4 mRNA translation in mammalian cells," *Proc. Natl. Acad. Sci. U. S. A.*, vol. 101, no. 31, pp. 11269–11274, 2004, doi: 10.1073/pnas.0400541101.

[208] P. D. Lu, H. P. Harding, and D. Ron, "Translation reinitiation at alternative open reading frames regulates gene expression in an integrated stress response," *J. Cell Biol.*, vol. 167, no. 1, pp. 27–33, 2004, doi: 10.1083/jcb.200408003.

[209] J. Shen, X. Chen, L. Hendershot, and R. Prywes, "ER stress regulation of ATF6 localization by dissociation of BiP/GRP78 binding and unmasking of golgi localization signals," *Dev. Cell*, vol. 3, no. 1, pp. 99–111, 2002, doi: 10.1016/S1534-5807(02)00203-4.

[210] H. Yoshida, K. Haze, H. Yanagi, T. Yura, and K. Mori, "Identification of the cis -Acting Endoplasmic Reticulum Stress Response Element Responsible for Transcriptional Induction of Mammalian Glucose-regulated Proteins," *J. Biol. Chem.*, vol. 273, no. 50, pp. 33741–33749, Dec. 1998, doi: 10.1074/jbc.273.50.33741.

[211] H. Hu, M. Tian, C. Ding, and S. Yu, "The C/EBP homologous protein (CHOP) transcription factor functions in endoplasmic reticulum stress-induced apoptosis and microbial infection," *Frontiers in Immunology*, vol. 10, no. JAN. Frontiers Media S.A., 2019, doi: 10.3389/fimmu.2018.03083.

[212] D. Wang, Y. Wei, and M. J. Pagliassotti, "Saturated fatty acids promote endoplasmic reticulum stress and liver injury in rats with hepatic steatosis," *Endocrinology*, vol. 147, no. 2, pp. 943–951, 2006, doi: 10.1210/en.2005-0570.

[213] F. Marra and G. Svegliati-Baroni, "Lipotoxicity and the gut-liver axis in NASH pathogenesis," *Journal of Hepatology*, vol. 68, no. 2. Elsevier B.V., pp. 280–295, 01-Feb-2018, doi: 10.1016/j.jhep.2017.11.014.

[214] K. D. Tardif, K. Mori, R. J. Kaufman, and A. Siddiqui, "Hepatitis C Virus Suppresses the IRE1-XBP1 Pathway of the Unfolded Protein Response," *J. Biol. Chem.*, vol. 279, no. 17, pp. 17158–17164, Apr. 2004, doi: 10.1074/jbc.M312144200.

[215] Y. Zheng *et al.*, "Hepatitis C virus non-structural protein NS4B can modulate an unfolded protein response," *J. Microbiol.*, vol. 43, no. 6, pp. 529–536, 2005.

[216] G. Nagy *et al.*, "Acetaminophen induces ER dependent signaling in mouse liver," *Arch. Biochem. Biophys.*, vol. 459, no. 2, pp. 273–279, Mar. 2007, doi: 10.1016/j.abb.2006.11.021.

[217] M. Sakon, H. Ariyoshi, K. Umeshita, and M. Monden, "Ischemia-reperfusion injury of the liver with special reference to calcium-dependent mechanisms," *Surgery Today*, vol. 32, no. 1. pp. 1–12, 2002, doi: 10.1007/s595-002-8105-8.

[218] C. Ji, "Dissection of endoplasmic reticulum stress signaling in alcoholic and non-alcoholic liver injury," in *Journal of Gastroenterology and Hepatology (Australia)*, 2008, vol. 23, no. SUPPL. 1, doi: 10.1111/j.1440-1746.2007.05276.x.

[219] V. Hernández-Gea *et al.*, "Endoplasmic reticulum stress induces fibrogenic activity in hepatic stellate cells through autophagy," *J. Hepatol.*, vol. 59, no. 1, pp. 98–104, Jul. 2013, doi: 10.1016/j.jhep.2013.02.016.

[220] R. S. Kim *et al.*, "The XBP1 Arm of the Unfolded Protein Response Induces Fibrogenic Activity in Hepatic Stellate Cells Through Autophagy," *Sci. Rep.*, vol. 6, 2016, doi: 10.1038/srep39342.

[221] K. A. Tazi *et al.*, "In vivo altered unfolded protein response and apoptosis in livers from lipopolysaccharide-challenged cirrhotic rats," *J. Hepatol.*, vol. 46, no. 6, pp. 1075–1088, 2007, doi: 10.1016/j.jhep.2007.01.034.

[222] G. Campos *et al.*, "The transcription factor CHOP, a central component of the transcriptional regulatory network induced upon CCl4 intoxication in mouse liver, is not a critical mediator of hepatotoxicity," *Arch. Toxicol.*, vol. 88, no. 6, pp. 1267–1280, 2014, doi: 10.1007/s00204-014-1240-8.

[223] A. Iracheta-Vellve *et al.*, "Endoplasmic reticulum stress-induced hepatocellular death pathways mediate liver injury and fibrosis via stimulator of interferon genes," *J. Biol. Chem.*, vol. 291, no. 52, pp. 26794–26805, 2016, doi: 10.1074/jbc.M116.736991.

[224] T. Jiang, L. Wang, X. Li, J. Song, X. Wu, and S. Zhou, "Inositol-requiring enzyme 1-mediated endoplasmic reticulum stress triggers apoptosis and fibrosis formation in liver cirrhosis rat models," *Mol. Med. Rep.*, vol. 11, no. 4, pp. 2941–2946, Apr. 2015, doi: 10.3892/mmr.2014.3020.

[225] S. R. Hann and R. N. Eisenman, "Proteins encoded by the human c-myc oncogene: differential expression in neoplastic cells.," *Mol. Cell. Biol.*, vol. 4, no. 11, pp. 2486–2497, 1984, doi: 10.1128/mcb.4.11.2486.

[226] G. J. Yoshida, "Emerging roles of Myc in stem cell biology and novel tumor therapies," *Journal of Experimental and Clinical Cancer Research*, vol. 37, no. 1. 2018, doi: 10.1186/s13046-018-0835-y.

[227] C. N. Spaan *et al.*, "Expression of UPR effector proteins ATF6 and XBP1 reduce colorectal cancer cell proliferation and stemness by activating PERK signaling," *Cell Death Dis.*, vol. 10, no. 7, Jul. 2019, doi: 10.1038/s41419-019-1729-4.

[228] A. Kaser *et al.*, "XBP1 Links ER Stress to Intestinal Inflammation and Confers Genetic Risk for Human Inflammatory Bowel Disease," *Cell*, vol. 134, no. 5, pp. 743–756, 2008, doi: 10.1016/j.cell.2008.07.021.

[229] A. Bashiri *et al.*, "Cellular cholesterol accumulation modulates high fat high sucrose (HFHS) diet-induced ER stress and hepatic inflammasome activation in the development of non-alcoholic steatohepatitis," *Biochim. Biophys. Acta - Mol. Cell Biol. Lipids*, vol. 1861, no. 7, pp. 594–605, Jul. 2016, doi: 10.1016/j.bbalip.2016.04.005.

[230] J. Zhang, K. Zhang, Z. Li, and B. Guo, "ER Stress-induced Inflammasome Activation Contributes to Hepatic Inflammation and Steatosis," *J. Clin. Cell. Immunol.*, vol. 7, no. 5, 2016, doi: 10.4172/2155-9899.1000457.

[231] A. G. Lerner *et al.*, "IRE1α induces thioredoxin-interacting protein to activate the NLRP3 inflammasome and promote programmed cell death under irremediable ER stress," *Cell Metab.*, vol. 16, no. 2, pp. 250–264, Aug. 2012, doi: 10.1016/j.cmet.2012.07.007.

[232] R. Sano and J. C. Reed, "ER stress-induced cell death mechanisms," *Biochimica et Biophysica Acta - Molecular Cell Research*, vol. 1833, no. 12. pp. 3460–3470, Dec-2013, doi:

10.1016/j.bbamcr.2013.06.028.

[233] U. Soffientini, N. Beaton, E. Weiss, and G. Mehta, “The Non-Canonical Inflammasome is Activated in Acute-on- Chronic Liver Failure and Causally Associated with Organ Injury,” *Hepatology*, pp. 327–331, 2019.

[234] N. Waldschmitt *et al.*, “C/EBP homologous protein inhibits tissue repair in response to gut injury and is inversely regulated with chronic inflammation,” *Mucosal Immunol.*, vol. 7, no. 6, pp. 1452–1466, 2014, doi: 10.1038/mi.2014.34.

[235] R. Garcia-Carbonell, S. J. Yao, S. Das, and M. Guma, “Dysregulation of intestinal epithelial cell RIPK pathways promotes chronic inflammation in the IBD gut,” *Front. Immunol.*, vol. 10, no. MAY, 2019, doi: 10.3389/fimmu.2019.01094.

[236] J. M. Blander, “Death in the intestinal epithelium—basic biology and implications for inflammatory bowel disease,” *FEBS J.*, vol. 283, pp. 2720–2730, 2016, doi: 10.1111/febs.13771.

[237] Y. L. Bao *et al.*, “Animal and Organoid Models of Liver Fibrosis,” *Front. Physiol.*, vol. 12, no. May, 2021, doi: 10.3389/fphys.2021.666138.

[238] M. Domenicali *et al.*, “A novel model of CCl4-induced cirrhosis with ascites in the mouse,” *J. Hepatol.*, vol. 51, no. 6, pp. 991–999, Dec. 2009, doi: 10.1016/j.jhep.2009.09.008.

[239] J. M. Seguí-Ripoll *et al.*, “Single versus double experimental bile duct ligation model for inducing bacterial translocation,” *Am. J. Surg.*, vol. 218, no. 2, pp. 380–387, 2019, doi: 10.1016/j.amjsurg.2018.09.034.

[240] B. A. Czulkies *et al.*, “Loss of LSR affects epithelial barrier integrity and tumor xenograft growth of CaCo-2 cells,” 2017.

[241] T. Zietek *et al.*, “Organoids to Study Intestinal Nutrient Transport, Drug Uptake and Metabolism – Update to the Human Model and Expansion of Applications,” *Front. Bioeng. Biotechnol.*, vol. 8, Sep. 2020, doi: 10.3389/fbioe.2020.577656.

[242] G. Linz, S. Djeljadini, L. Steinbeck, G. Köse, F. Kiessling, and M. Wessling, “Cell barrier characterization in transwell inserts by electrical impedance spectroscopy,” *Biosens. Bioelectron.*, vol. 165, no. June, p. 112345, 2020, doi: 10.1016/j.bios.2020.112345.

[243] V. Bozzetti and S. Senger, “Organoid technologies for the study of intestinal microbiota–host interactions,” *Trends Mol. Med.*, vol. 28, no. 4, pp. 290–303, 2022, doi:

10.1016/j.molmed.2022.02.001.

[244] T. Sato *et al.*, "Long-term expansion of epithelial organoids from human colon, adenoma, adenocarcinoma, and Barrett's epithelium," *Gastroenterology*, vol. 141, no. 5, pp. 1762–1772, 2011, doi: 10.1053/j.gastro.2011.07.050.

[245] I. Rauch *et al.*, "NAIP-NLRC4 inflammasomes coordinate intestinal epithelial cell expulsion with eicosanoid and IL-18 release via activation of Caspase-1 and-8 HHS Public Access," *Immunity*, vol. 46, no. 4, pp. 649–659, 2017, doi: 10.1016/j.immuni.2017.03.016.

[246] K. J. Bode, S. Mueller, M. Schweinlin, M. Metzger, and T. Brunner, "A fast and simple fluorometric method to detect cell death in 3D intestinal organoids," *Biotechniques*, vol. 67, no. 1, pp. 23–28, 2019, doi: 10.2144/btn-2019-0023.

[247] G. Levin, S. M. Zuber, A. I. Squillaro, M. C. Sogayar, T. C. Grikscheit, and A. C. O. Carreira, "R-Spondin 1 (RSPO1) Increases Mouse Intestinal Organoid Unit Size and Survival in vitro and Improves Tissue-Engineered Small Intestine Formation in vivo," *Front. Bioeng. Biotechnol.*, vol. 8, Jun. 2020, doi: 10.3389/fbioe.2020.00476.

[248] C. M. Cattaneo *et al.*, "Tumor organoid–T-cell coculture systems," *Nat. Protoc.*, vol. 15, no. 1, pp. 15–39, Jan. 2020, doi: 10.1038/s41596-019-0232-9.

[249] E. Fujii *et al.*, "A simple method for histopathological evaluation of organoids," *J. Toxicol. Pathol.*, vol. 31, no. 1, pp. 81–85, 2018, doi: 10.1293/tox.2017-0060.

[250] D. Sharma and T. D. Kanneganti, "Inflammatory cell death in intestinal pathologies," *Immunol. Rev.*, vol. 280, no. 1, pp. 57–73, 2017, doi: 10.1111/imr.12602.

[251] N. Kayagaki *et al.*, "Noncanonical Inflammasome Activation by Intracellular LPS Independent of TLR4," *Science (80-.).*, vol. 130, no. September, pp. 1246–1249, 2013, doi: 10.5061/dryad.bt51g.

[252] D. T. Rutkowski *et al.*, "Adaptation to ER stress is mediated by differential stabilities of pro-survival and pro-apoptotic mRNAs and proteins," *PLoS Biol.*, vol. 4, no. 11, pp. 2024–2041, 2006, doi: 10.1371/journal.pbio.0040374.

[253] T. Grabinger *et al.*, "Ex vivo culture of intestinal crypt organoids as a model system for assessing cell death induction in intestinal epithelial cells and enteropathy," *Cell Death Dis.*, vol. 5, no. 5, p. e1228, 2014, doi: 10.1038/CDDIS.2014.183.

[254] A. Negroni *et al.*, "RIP3 AND pMLKL promote necroptosis-induced inflammation and alter

membrane permeability in intestinal epithelial cells," *Dig. Liver Dis.*, vol. 49, no. 11, pp. 1201–1210, 2017, doi: 10.1016/j.dld.2017.08.017.

[255] M. Tomita, M. Hayashi, and S. Awazu, "Absorption-Enhancing Mechanism of EDTA, Caprate, and Decanoylcarnitine in Caco-2 Cells," 1996.

[256] H. J. Galipeau and E. F. Verdu, "The complex task of measuring intestinal permeability in basic and clinical science," *Neurogastroenterol. Motil.*, vol. 28, no. 7, pp. 957–965, 2016, doi: 10.1111/nmo.12871.

[257] I. Schoultz and Å. V. Keita, "The Intestinal Barrier and Current Techniques for the Assessment of Gut Permeability," *Cells*, vol. 9, no. 8, pp. 1–30, 2020, doi: 10.3390/cells9081909.

[258] J. Rubert, P. J. Schweiger, F. Mattivi, K. Tuohy, K. B. Jensen, and A. Lunardi, "Intestinal Organoids: A Tool for Modelling Diet–Microbiome–Host Interactions," *Trends in Endocrinology and Metabolism*, vol. 31, no. 11. Elsevier Inc., pp. 848–858, 01-Nov-2020, doi: 10.1016/j.tem.2020.02.004.

[259] S. Wang *et al.*, "Cathelicidin-WA Protects Against LPS-Induced Gut Damage Through Enhancing Survival and Function of Intestinal Stem Cells," *Front. Cell Dev. Biol.*, vol. 9, no. July, pp. 1–12, 2021, doi: 10.3389/fcell.2021.685363.

[260] B. Press and D. Di Grandi, "Permeability for Intestinal Absorption: Caco-2 Assay and Related Issues," *Curr. Drug Metab.*, vol. 9, no. 9, pp. 893–900, Nov. 2008, doi: 10.2174/138920008786485119.

[261] A. Woting and M. Blaut, "Small intestinal permeability and gut-transit time determined with low and high molecular weight fluorescein isothiocyanate-dextrans in C3H mice," *Nutrients*, vol. 10, no. 6, pp. 4–10, 2018, doi: 10.3390/nu10060685.

[262] X. Wang, N. Wang, L. Yuan, N. Li, J. Wang, and X. Yang, "Exploring tight junction alteration using double fluorescent probe combination of lanthanide complex with gold nanoclusters," *Sci. Rep.*, vol. 6, Aug. 2016, doi: 10.1038/srep32218.

[263] I. Grosheva *et al.*, "High-Throughput Screen Identifies Host and Microbiota Regulators of Intestinal Barrier Function," *Gastroenterology*, vol. 159, no. 5, pp. 1807–1823, 2020, doi: 10.1053/j.gastro.2020.07.003.

[264] Y. Sasaki *et al.*, "Intestinal Permeability of Drugs in Caco-2 Cells Cultured in Microfluidic Devices," *Biological and Pharmaceutical Bulletin*, vol. 45, no. 9. pp. 1246–1253, 2022, doi: 10.1248/bpb.b22-00092.

[265] I. A. Williamson *et al.*, "A High-Throughput Organoid Microinjection Platform to Study Gastrointestinal Microbiota and Luminal Physiology," *CMGH*, vol. 6, no. 3, pp. 301–319, Jan. 2018, doi: 10.1016/j.jcmgh.2018.05.004.

[266] P. Xu, H. Becker, M. Elizalde, A. Masclee, and D. Jonkers, "Intestinal organoid culture model is a valuable system to study epithelial barrier function in IBD," *Gut*, vol. 67, no. 10. BMJ Publishing Group, pp. 1905–1906, 05-Dec-2018, doi: 10.1136/gutjnl-2017-315685.

[267] M. Bardenbacher *et al.*, "Permeability analyses and three dimensional imaging of interferon gamma-induced barrier disintegration in intestinal organoids," *Stem Cell Res.*, vol. 35, 2019, doi: 10.1016/j.scr.2019.101383.

[268] F. Bergenheim *et al.*, "Fluorescence-based tracing of transplanted intestinal epithelial cells using confocal laser endomicroscopy," *Stem Cell Res. Ther.*, vol. 10, no. 1, p. 148, Dec. 2019, doi: 10.1186/s13287-019-1246-5.

[269] M. Bardenbacher *et al.*, "Investigating intestinal barrier breakdown in living organoids," *J. Vis. Exp.*, vol. 2020, no. 157, p. 60546, 2020, doi: 10.3791/60546.

[270] T. Roodsant *et al.*, "A Human 2D Primary Organoid-Derived Epithelial Monolayer Model to Study Host-Pathogen Interaction in the Small Intestine," *Front. Cell. Infect. Microbiol.*, vol. 10, Jun. 2020, doi: 10.3389/fcimb.2020.00272.

[271] H. Liebe *et al.*, "Determining Intestinal Permeability using Lucifer Yellow in an Apical-Out Enteroid Model," *J. Vis. Exp.*, vol. 2022 2022, no. 185, pp. 1–12, 2022, doi: 10.3791/64215.

[272] J. Y. Co *et al.*, "Controlling Epithelial Polarity: A Human Enteroid Model for Host-Pathogen Interactions," *Cell Rep.*, vol. 26, no. 9, pp. 2509-2520.e4, Feb. 2019, doi: 10.1016/j.celrep.2019.01.108.

[273] J. Zhang, H. Lei, X. Hu, and W. Dong, "Hesperetin ameliorates DSS-induced colitis by maintaining the epithelial barrier via blocking RIPK3/MLKL necroptosis signaling," *Eur. J. Pharmacol.*, vol. 873, no. January, p. 172992, 2020, doi: 10.1016/j.ejphar.2020.172992.

[274] K. J. Maloy and F. Powrie, "Intestinal homeostasis and its breakdown in inflammatory bowel disease," *Nature*, vol. 474, no. 7351, pp. 298–306, 2011, doi: 10.1038/nature10208.

[275] D. Laukens *et al.*, "Tauroursodeoxycholic acid inhibits experimental colitis by preventing early intestinal epithelial cell death," *Lab. Investig.*, vol. 94, no. 12, pp. 1419–1430, 2014, doi: 10.1038/labinvest.2014.117.

[276] P. Li, D. Fu, Q. Sheng, S. Yu, X. Bao, and Z. Lv, "TUDCA attenuates intestinal injury and inhibits endoplasmic reticulum stress-mediated intestinal cell apoptosis in necrotizing enterocolitis," *Int. Immunopharmacol.*, vol. 74, Sep. 2019, doi: 10.1016/j.intimp.2019.05.050.

[277] Y. Feng, Y. Wang, P. Wang, Y. Huang, and F. Wang, "Short-Chain Fatty Acids Manifest Stimulative and Protective Effects on Intestinal Barrier Function Through the Inhibition of NLRP3 Inflammasome and Autophagy," *Cell. Physiol. Biochem.*, vol. 49, no. 1, pp. 190–205, 2018, doi: 10.1159/000492853.

[278] S. Ouladan and A. Gregorieff, "Taking a step back: Insights into the mechanisms regulating gut epithelial dedifferentiation," *Int. J. Mol. Sci.*, vol. 22, no. 13, 2021, doi: 10.3390/ijms22137043.

[279] T. Zhan, N. Rindtorff, and M. Boutros, "Wnt signaling in cancer," *Oncogene*, vol. 36, no. 11, pp. 1461–1473, 2017, doi: 10.1038/onc.2016.304.

[280] A. Ring, Y. M. Kim, and M. Kahn, "Wnt/Catenin Signaling in Adult Stem Cell Physiology and Disease," *Stem Cell Rev. Reports*, vol. 10, no. 4, pp. 512–525, 2014, doi: 10.1007/s12015-014-9515-2.

[281] D. J. Flanagan *et al.*, "Frizzled7 functions as a Wnt receptor in intestinal epithelial Lgr5+ stem cells," *Stem Cell Reports*, vol. 4, no. 5, pp. 759–767, 2015, doi: 10.1016/j.stemcr.2015.03.003.

[282] H. W. Park *et al.*, "Alternative Wnt Signaling Activates YAP/TAZ," *Cell*, vol. 162, no. 4, pp. 780–794, 2015, doi: 10.1016/j.cell.2015.07.013.

[283] I. M. Moya and G. Halder, "Hippo–YAP/TAZ signalling in organ regeneration and regenerative medicine," *Nat. Rev. Mol. Cell Biol.*, vol. 20, no. 4, pp. 211–226, 2019, doi: 10.1038/s41580-018-0086-y.

[284] B. Stockinger, K. Shah, and E. Wincent, "AHR in the intestinal microenvironment: safeguarding barrier function," *Nat. Rev. Gastroenterol. Hepatol.*, vol. 18, no. 8, pp. 559–570, Aug. 2021, doi: 10.1038/s41575-021-00430-8.

[285] M. Yu *et al.*, "Aryl hydrocarbon receptor activation modulates intestinal epithelial barrier function by maintaining tight junction integrity," *Int. J. Biol. Sci.*, vol. 14, no. 1, pp. 69–77, 2018, doi: 10.7150/ijbs.22259.

[286] R. Lu *et al.*, "Alcohol Injury Damages Intestinal Stem Cells," *Alcohol. Clin. Exp. Res.*, vol. 41, no. 4, pp. 727–734, 2017, doi: 10.1111/acer.13351.

[287] C. B. Forsyth *et al.*, "Alcohol Feeding in Mice Promotes Colonic Hyperpermeability and Changes in Colonic Organoid Stem Cell Fate," *Alcohol. Clin. Exp. Res.*, vol. 41, no. 12, pp. 2100–2113, Dec. 2017, doi: 10.1111/acer.13519.

[288] M. Qian *et al.*, "Aryl Hydrocarbon Receptor Deficiency in Intestinal Epithelial Cells Aggravates Alcohol-Related Liver Disease," *Cmgh*, vol. 13, no. 1, pp. 233–256, 2022, doi: 10.1016/j.jcmgh.2021.08.014.

[289] S. Beyaz *et al.*, "High-fat diet enhances stemness and tumorigenicity of intestinal progenitors," *Nature*, vol. 531, no. 7592, pp. 53–58, 2016, doi: 10.1038/nature17173.

[290] Y. Xie *et al.*, "Impact of a high-fat diet on intestinal stem cells and epithelial barrier function in middle-aged female mice," *Mol. Med. Rep.*, vol. 21, no. 3, pp. 1133–1144, 2020, doi: 10.3892/mmr.2020.10932.

[291] J. Huang, C. Zhou, G. Zhou, H. Li, and K. Ye, "Effect of Listeria monocytogenes on intestinal stem cells in the co-culture model of small intestinal organoids," *Microb. Pathog.*, vol. 153, Apr. 2021, doi: 10.1016/j.micpath.2021.104776.

[292] B. E. Lee *et al.*, "A simple and efficient cryopreservation method for mouse small intestinal and colon organoids for regenerative medicine," *Biochem. Biophys. Res. Commun.*, vol. 595, pp. 14–21, 2022, doi: 10.1016/j.bbrc.2021.12.021.

[293] S. De Minicis *et al.*, "Dysbiosis contributes to fibrogenesis in the course of chronic liver injury in mice," *Hepatology*, vol. 59, no. 5, pp. 1738–1749, 2014, doi: 10.1002/hep.26695.

[294] E. Im, F. M. Riegler, C. Pothoulakis, and S. H. Rhee, "Elevated lipopolysaccharide in the colon evokes intestinal inflammation, aggravated in immune modulator-impaired mice," *Am. J. Physiol. - Gastrointest. Liver Physiol.*, vol. 303, no. 4, p. G490, Aug. 2012, doi: 10.1152/ajpgi.00120.2012.

[295] D. H. Yang *et al.*, "Salvianolate inhibits cytokine gene expression in small intestine of cirrhotic rats," *World J. Gastroenterol.*, vol. 17, no. 14, pp. 1903–1909, 2011, doi: 10.3748/wjg.v17.i14.1903.

[296] J. B. Wen *et al.*, "Oxymatrine improves intestinal epithelial barrier function involving NF-κB-mediated signaling pathway in CCl4-induced cirrhotic rats," *PLoS One*, vol. 9, no. 8, pp. 2–8, 2014, doi: 10.1371/journal.pone.0106082.